Neural signatures of conciousness abolition and recovery from coma

Brigitta Malagurski

THÈSE

En vue de l'obtention du

DOCTORAT DE L'UNIVERSITÉ DE TOULOUSE

Délivré par :

Université Toulouse 3 Paul Sabatier (UT3 Paul Sabatier)

Présentée et soutenue par :
Brigitta Malagurski

le jeudi 3 mai 2018

Titre :

Signatures neurales de l'abolition et de la récupération de conscience à partir du coma

Neural signatures of consciousness abolition and recovery from coma

---

École doctorale et discipline ou spécialité :
ED CLESCO : Neurosciences, comportement et cognition

Unité de recherche :
Toulouse NeuroImaging Center - INSERM U1214

Directeur/trice(s) de Thèse :

Dr. Stein SILVA
Dr. Patrice PERAN

Jury :

Dr. Emmanuel BARBIER	Rapporteur
Pr. Gérald CHANQUES	Rapporteur
Dr. Audrey VANHAUDENHUYSE	Examinateur
Pr. Pierre PAYOUX	Examinateur

Acknowledgments

Firstly, I would like to express my gratitude to my supervisors, Stein Silva and Patrice Péran, for their patient guidance, enthusiastic encouragement and fruitful scientific discussions. Your passion for science is truly inspirational. Patrice, thank you for guiding me through all the subtleties of neuroimaging data analysis and for providing the opportunity to collaborate on other research projects, thus allowing me to grow as a research scientist.

Besides my advisors, I would like to thank the rest of my thesis committee, for their insightful comments and encouragement, but also for their hard questions and useful critiques of this research work.

My sincere thanks also goes to Jérémie Pariente, and Emmanuel Barbeau, who provided me an opportunity to enroll in a master's program and join their research teams, here in Toulouse. Without your help, this would not have been possible.

I would like extend my gratitude to Sophie Achard, who helped oversee my training, and offered me invaluable advice and expertise regarding the application of graph theory in the field of neuroscience.

I wish to thank my fellow labmates and all of those with whom I have had the pleasure to work during this and other related projects.

Finally, I would like to express a deep sense of gratitude to my parents whose unconditional love and support are with me in whatever I pursue. Last but not the least, I wish to thank my loving partner, Daniel, for his encouragement and continual support throughout this experience, without which I would be lost. Your support keeps me going even on the toughest days.

Abstract

Recent advances in clinical care have resulted in an increasing number of patients who survive severe brain injury, however, many of these patients initially show a complete absence of arousal and awareness of one self and their surroundings. From this initial state of unarousable unresponsiveness, defined as coma, patients can fully regain consciousness or evolve into other (chronic) disorders of consciousness. The aim of the present thesis was to characterize the functional and structural neural correlates of acute consciousness abolition (i.e. coma) and identify early neural signatures of long-term neurological recovery. To do so, we studied severely brain-injured patients, recruited in the acute stage of coma, using resting-state functional and structural MRI.

We have conducted our analysis at a three-fold level: i) global level, in exploring brain's residual ability to segregate and integrate information across several high-order resting-state functional networks (RSNs) (i.e. default-mode network, executive control network and salience network), known to be involved in self-related processing and potentially critical for consciousness emergence; ii) regional level, in investigating resting-state functional interactions between the hub nodes of high-order RSNs, with a primary focus on posteromedial cortex (PMC) and the medial prefrontal cortex (mPFC) inter-connectivity; iii) multi-modal level, in exploring the association between the PMC-mPFC functional disruption and corresponding gray and white matter (i.e. cingulum) structural damage.

The global-level analysis indicated a significant topological reorganization of high-order resting-state networks in the acute stage of coma. This reorganization, assessed using graph theory, was reflected in dedifferentiated and less resilient patients' functional brain networks, accompanied with a loss of long-range fronto-parietal connections. On a regional level, we found a complex pattern of voxel-wise decrease and increase in resting-state functional connection density between the posteromedial cortex and the medial prefrontal cortex. These connection density patterns seemed to permit outcome prediction in patients, assessed three months post-coma. Furthermore, the multi-modal analysis demonstrated a significant association between the antero-posterior functional connectivity and structural integrity between/within these two regions.

In conclusion, our results imply significant heterogeneity in both functional and structural brain integrity in coma patients irrespectively of their apparent behavioral homogeneity. Regarding

functional connectivity at rest, patients' brains appear to be radically reorganized at both global and regional level, with some of these patterns seeming to be related to neurological recovery. As such, these findings hold a significant promise towards the application of neuroimaging in early outcome prediction and could inspire novel personalized therapeutic approaches aiming to promote the re-emergence of consciousness and long-term neurological recovery.

Key words: coma, brain-injury, neuroimaging, resting-state functional connectivity, structural integrity, graph theory, prognosis.

Résumé

Les progrès récents dans les soins cliniques ont entraîné un nombre croissant de patients qui survivent à une lésion cérébrale grave, cependant, beaucoup de ces patients montrent initialement une absence totale d'éveil et de conscience de soi et de leur environnement. À partir de cet état initial, défini comme un coma, les patients peuvent reprendre complètement conscience ou évoluer vers d'autres états plus chroniques d'altération de cette capacité cognitive.

L'objectif de cette thèse était de caractériser les corrélats neuronaux fonctionnels et structurels de *l'abolition* de la *conscience* dans le coma induit par une lésion cérébrale sévère et d'identifier les signatures neuronales précoces de la récupération neurologique à long-terme. Pour atteindre ce but, nous avons étudié des patients cérébrolésés, recrutés au stade aigu du coma, à l'aide de l'IRM fonctionnelle au repos et IRM structurale.

Nous avons mené notre analyse à trois niveaux: i) niveau global, en explorant la capacité résiduelle du cerveau à ségréger et à intégrer l'information à travers plusieurs réseaux fonctionnels au repos (RFR) d'ordre élevé (i.e. le réseau du mode par défaut, réseau de contrôle exécutif, réseau de saillance) connus pour être impliqués dans l'émergence de la notion de soi; ii) au niveau régional, en étudiant les interactions fonctionnelles à l'état de repos entre les nœuds centraux des RFR (cortex postéromédial (CPM) et le cortex préfrontal médian (CPFM)); iii) selon une approche multimodale, en explorant l'association entre la perturbation fonctionnelle du CPM-CPFM et les lésions structurelles. L'analyse au niveau global a indiqué une réorganisation topologique significative des réseaux d'état de repos d'ordre élevé dans le stade aigu du coma. Cette réorganisation mise en évidence par l'analyse des graphes, semble associée à une importante dédifférenciation et à une réduction de la résilience des réseaux fonctionnels au repos d'ordre élevé. Une perte de connexions fronto-pariétales à longue distance a été aussi observée.

Au niveau régional, nous avons caractérisé un schéma complexe de diminution et d'augmentation de la densité de connexion fonctionnelle à l'état de repos entre le CPM et CPFM. L'importance de ces anomalies de densité de connexion, semble liée à la récupération des patients dans le coma, à trois mois après l'agression cérébrale initiale. En outre, l'analyse IRM multimodale a permis de monter une association significative entre la connectivité fonctionnelle et l'intégrité structurelle entre/dans ces deux régions.

En conclusion, en ce qui concerne la connectivité fonctionnelle au repos, le cerveau des patients semble être radicalement réorganisé au niveau global et régional, et certaines de ces anomalies semblent liées à la récupération neurologique. En tant que tels, ces résultats représentent une promesse importante pour l'application de la neuroimagerie multimodale dans la prédiction précoce des résultats cliniques et pourraient inspirer de nouvelles approches thérapeutiques personnalisées visant à promouvoir la réémergence thérapeutique de la conscience à partir du coma.

Mots clés : coma, lésion cérébrale, neuroimagerie, connectivité fonctionnelle au repos, intégrité structurelle, théorie des graphes, pronostic.

Table of Contents

List of commonly used abbreviations

AD	Axial diffusivity
ADC	Apparent diffusion coefficient
BI	Brain injury
BOLD	Blood-oxygen-level dependent
CDN	Connection density negative correlation
CDP	Connection density positive correlation
CRS-R	Coma Recovery Scale – Revised
dDMN	Dorsal default mode network
DOC	Disorders of consciousness
DTI	Diffusion Tensor Imaging
DWI	Diffusion Weighted Imaging
ECN	Executive control network
EEG	Electroencephalography
FA	Fractional anisotropy
FC	Functional connectivity
FPN	Frontoparietal network
GCS	Glasgow Coma Scale
GM	Gray matter
HDI	Hub disruption index
ICA	Independent component analysis
LECN	Left executive control network
LIS	Locked-in syndrome
MCS	Minimally conscious state
MD	Mean diffusivity
mPFC	Medial prefrontal cortex
MRI	Magnetic Resonance Imaging
NCC	Neural correlates of consciousness
P.SAL	Posterior salience network
PCC	Posterior Cingulate cortex
PET	Positron emission tomography
PMC	Posteromedial cortex
PreCu	Precuneus
RD	Radial diffusivity
RECN	Right executive control network
ROI	Region of interest
Rs-fMRI	Resting-state functional MRI
RSN	Resting-state network
SAL/SN	Salience network
TBI	Traumatic brain injury
UWS	Unresponsive wakefulness syndrome
VBM	Voxel-based morphometry
vDMN	Ventral default mode network
WM	White matter

List of figures

List of tables

General introduction

Recent advances in clinical care have resulted in an increasing number of patients who survive severe brain injury (i.e. trauma, cardiac arrest, stroke etc.). Unfortunately, many of these patients initially show complete absence of arousal and awareness of one self and their surroundings. From this initial state of unarousable unresponsiveness, defined as coma, patients can fully regain consciousness or evolve into other disorders of consciousness such as the unresponsive wakefulness syndrome (UWS) and the minimally conscious state (MCS).

Currently, there are no objective and reliable acute-stage prognostic markers that can help predict the evolution of disorders of consciousness. Estimating the likelihood of recovery in acutely comatose patients is very difficult due to behavioral non-responsiveness, differences in nature of brain injury (i.e. traumatic versus anoxic brain injury) and potential confounding factors such as medication and metabolic disturbance. More importantly, it has been implied that the lack of a complete understanding of neural characteristics of acute stage coma and reliable prognostic markers significantly contributes to practice variation in the withdrawal of life-sustaining therapy, which can be considered as soon as few days after the initial coma-inducing brain injury.

On a more positive note, recent advances in neuro-technologies implied that structural (e.g. diffusion MRI) and functional (resting-state; rs-fMRI) neuroimaging strategies, hold a significant promise in the detection of residual neural and cognitive processes indicative of consciousness, independently of behavioral responsiveness of patients.

Following this lead, we decided to focus our analysis on the intrinsic brain "activity" in the form of functional connectivity and structural integrity of brain-injured patients in the acute stage of coma. Therefore, the aim of the present thesis was to characterize the neural correlates of acute consciousness abolition (i.e. coma) and identify early neural signatures of neurological recovery. To do so, we longitudinally studied severe brain-injured patients using multimodal MRI methodology and standardized behavioral assessment.

My education background includes a MA in Psychology from the Faculty of Philosophy, University of Novi Sad (Serbia), and a MSc in Neuropsychology and Clinical Neurosciences from the Faculty of Medicine Purpan, University of Toulouse III – Paul Sabatier.

I have joined the already ongoing *ACI-COMA* project soon after I have finished my master's degree in Toulouse. I have never worked with neuroimaging data before, so this thesis was challenging for me in the beginning, with all its difficulties related to data acquisition (and

processing) in the population of severely brain-injured patients in coma. Nevertheless, I very much appreciated the cross-domain collaboration with all its advantages and difficulties, as I worked alongside researchers with different backgrounds and clinicians who assured the safe and successful inclusion of our patients. I strongly believe that this research-clinic collaborative effort was an integral part in the evolution of the ACI-COMA project.

Outline

In chapter I we describe the behavioral profile of disorders of consciousness (DOC), various theories of consciousness, and available behavioral and neuroimaging paradigms used for the diagnostic and prognostic assessment of brain-injured patients with impairments in consciousness.

In chapter II we review previous neuroimaging studies, upon which our research draws. This section is divided into three sub-chapters, describing resting-state functional connectivity, structural integrity and structure-function association in chronic and acute stages (i.e. coma) of disorders of consciousness. In this chapter, we attempted to organize previous research based on its contribution to the domains of diagnostics, prognostics or pathology mechanisms related to different etiologies (i.e. traumatic and anoxic brain injury) in DOC.

In chapter III, we briefly describe the research design of the ACI-COMA project which served as the basis for this thesis.

In chapter IV, we present the results that we have achieved to date. This section is subdivided into three main sections, each describing a specific study conducted within the scope of this thesis.

The first study focuses on the voxel-wise resting-state functional connectivity (FC) between two regions of interest (i.e. posteromedial cortex and the medial prefrontal cortex), previously described to have a critical role in conscious processing. We also attempt to relate the identified FC changes in the acute stage of DOC – coma - to the neurological outcome registered three months after the initial inclusion.

In the second study we investigate the resting-state FC on a more global level, by applying the graph theoretical methods to analyze the topological organization of several high-order resting-state networks (i.e. DMN, SN, ECN), known to have an important role in high-level cognitive

functions including consciousness. This study was conducted in collaboration with Sophie Achard from the GIPSA-lab (CNRS) in Grenoble, France.

Finally, in the third study, we explore the association between the functional disruption and underlying structural damage, encompassing the regions of interest included in the first study.

In the chapter V, we review the contributions of the thesis and list possible directions of future research.

1 Chapter I – Conceptual framework

1.1 Theories of consciousness: neural networks and brain complexity

1.1.1 Connectionists models

The last few decades have given a myriad of philosophical and scientific theories attempting to account for the origin and nature of consciousness (Cavanna & Nani, 2014). Crucially, these theoretical frameworks have provided several concepts that could be empirically tested in physiology and pathological conditions.

The Global Neuronal Workspace (GNW) model was inspired by the theory of Baars (1988), which states that consciousness is represented within a *global workspace*, a widespread architecture of neuronal networks with the capacity to coordinate and integrate information between a set of specialized brain sites – processors. The main idea behind the GNW is that conscious access, depends on *global information availability* encompassing selection, amplification, sustainability and global broadcasting of salient information between brain-wide processors.

From the neuronal architecture standpoint, this theory proposes two main computational brain spaces (Dehaene, Changeux, & Naccache, 2011): 1) a processing network which refers to a set of functionally specialized, automatic, and non-conscious processors (i.e. visual, auditive, verbal modules) with highly specific local or medium range connection which "encapsulate" information relevant to the function of a given processor; 2) global neuronal workspace consisting of a subset of distributed cortical pyramidal neurons with long-range excitatory axons (i.e. particularly dense in prefrontal, cingulate, parietal cortices) interconnecting multiple specialized processors (Figure 1.1.1).

It is worth noting that GNW neurons are widely distributed, so there is no single brain center where the conscious information is stored and broadcasted but rather a conscious synthesis achieved when multiple brain processor "converge to a coherent metastable state" (Dehaene et al., 2011). Nevertheless, empirical data suggest that the global ignition related to conscious experience is supposedly linked to the fronto-parietal network, and the state of activation of GNW neurons is assumed to be globally regulated by vigilance signals from the ascending reticular activating system which is involved in regulating the sleep-week cycle.

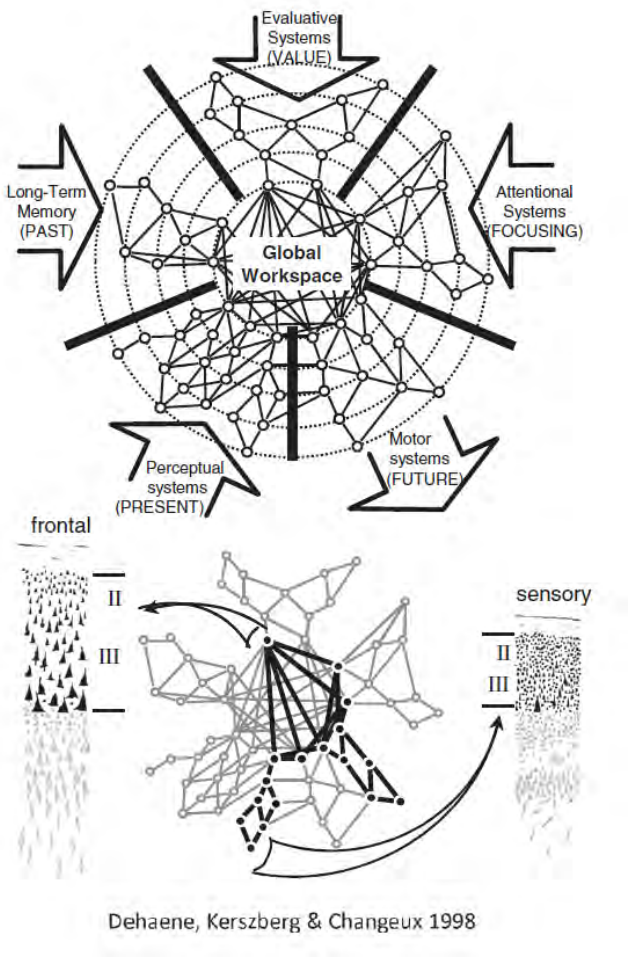

Figure 1.1.1. Schema of the global neuronal workspace (GNW) model.
The GNW model proposes that associative perceptual, motor, attention, memory and value areas interconnect to form a higher level unified space where information is broadly shared and broadcasted back to lower-level processors. Reproduced from Dehaene et al. (1998).

In 1998, Tononi and Edelman proposed an alternative model. The *dynamic core hypothesis* based on the assumption that consciousness experience is at once differentiated (i.e. isolation of one specific content out of a vast number of potential internal representations) and integrated (i.e. unified conscious representation, where whole carries more information than each part alone). In 2004, Tononi proposed the ***Integrated Information Theory of consciousness (IIT)*** which has been continuously developed over the last decade. IIT does not hypotheses about specific neural correlates underlying the conscious experience but it attempts to "explain the essential phenomenal properties of experience, or *axioms*, and infers postulates about the characteristics that are required of its physical substrate (PSC)", described below (Tononi, Boly, Massimini, & Koch, 2016):

The first axiom of IIT states that experience exists *intrinsically* and that it is *independent* of the external observer. The corresponding postulate states that the PSC must also exist intrinsically

and that it must have a cause-effect power on itself. A minimal system composed of two interconnected neurons can satisfy the criteria, because it can make a difference to itself through its reciprocal connections.

The axiom of *composition* states that consciousness is *structured*, being composed of several phenomenal distinctions which exist within it. For example, within an experience I can distinguish an olive tree, a rose flower, green grass and many other sub-elements constituting a hypothetical "garden" scene. The corresponding postulate implies that elements that constitute the PSC must also have a cause-effect power upon PSC, either alone (first-order mechanism) or in various combinations (high-order mechanism).

The axiom of *information* states that conscious experience is specific, being composed of a set of phenomenal distinctions (qualia), thereby differing from other possible experiences (*differentiation*). For example, in a "garden" scene, a content of my conscious experience might be composed of me seeing a rose flower (in opposed to not seeing it) which is red (in contrary to not being red). The corresponding postulate states the PCS must specify a cause-effect structure, a specific set of cause-effect repertoires, differing it from all other possible structure.

The axiom of *integration* states that each conscious experience is *unified* and irreducible to non-interdependent sub-sets of phenomenal distinctions. For example, my visual experience of the garden can't be subdivided into independent experience of the left and right sides of the visual field. The corresponding postulate implies that cause–effect structure specified by the PSC must also be unitary and intrinsically irreducible to non-interdependent sub-systems ($\Phi>0$). The irreducibility of a conceptual structure is measured as *integrated information* - Φ, the minimum distance between an intact and a partitioned cause–effect structure.

Finally, the axiom of *exclusion* states that an experience is *definite* in its content and spatio-temporal grain, implying that its phenomenal content and duration are definite. For example, I do not perceive the garden with more flowers than there are, nor do I perceive it in grey if it has colorful flowers. The corresponding postulate states that the cause-effect structure specified by the PCS must also be definite, with definite set of elements with definite spatio-temporal grain, maximally irreducible intrinsically (Φ^{max}), called a conceptual structure, made of maximally irreducible cause-effect repertoires (concepts).

Thus, the physical substrate of consciousness is called a *complex* and it is consisted of a set of elements in a state that satisfies all the postulates. According to IIT, the quality (content) of consciousness corresponds to the form of the conceptual structural and the quantity of consciousness refers to its irreducibility Φ^{max}.

Although both theories put an emphasis on (global) integration of information, there are some important differences between the GNW and the IIT theory.

Perhaps the most notable one is that the GNW implies underlying neuronal structure ("ignition" of fronto-parietal workspace neurons), while IIT starts from experience itself, rather than from a specific brain area or network. A comparative example between the two theories is given in an article of Tononi and colleagues (2016) (Figure 1.1.2).

In GNW, information which is relayed through sensory pathways remains unconscious until it enters the global workspace and is broadcasted to specialized processors (Figure 2– upper panel). In IIT, the information content of consciousness is specified intrinsically (by the system for the system, rater then extrinsically) and is a conceptual structure – "a form in a cause-effect space specified by the elements of the PSC" (Tononi et al., 2016; Figure 1.1.2– lower panel). Thus, in IIT neurons shape the overall form of the conceptual structure specified by the PSC, in oppose to processing, encoding or broadcasting an information as in GNW. In addition, GNW defines consciousness as all-or-none phenomenon, while IIT implies that it is graded, that it increases in accordance to a system's repertoire of available states.

Further, the association between the complexity (widespread and differentiated) of brain network activity and the state of consciousness (Koch et al., 2016) has been demonstrated in natural, pharmacological and pathological alterations of consciousness using coupled transcranial magnetic stimulation and EEG recordings (Casali et al., 2013; Casarotto et al., 2016), and dynamics of spontaneous activity measured using fMRI (Barttfeld et al., 2015; Hudetz et al., 2015; Tagliazucchi, et al., 2016). Moreover, the cerebral cortex is ideally suited for integrating information, due to a coexistence of functional specialization in form of multiple brain sub-networks (fronto-parietal) and hub-node integration (i.e. hub regions; PCC), often disrupted in brain injury and disorders in consciousness as we will see in the following chapters.

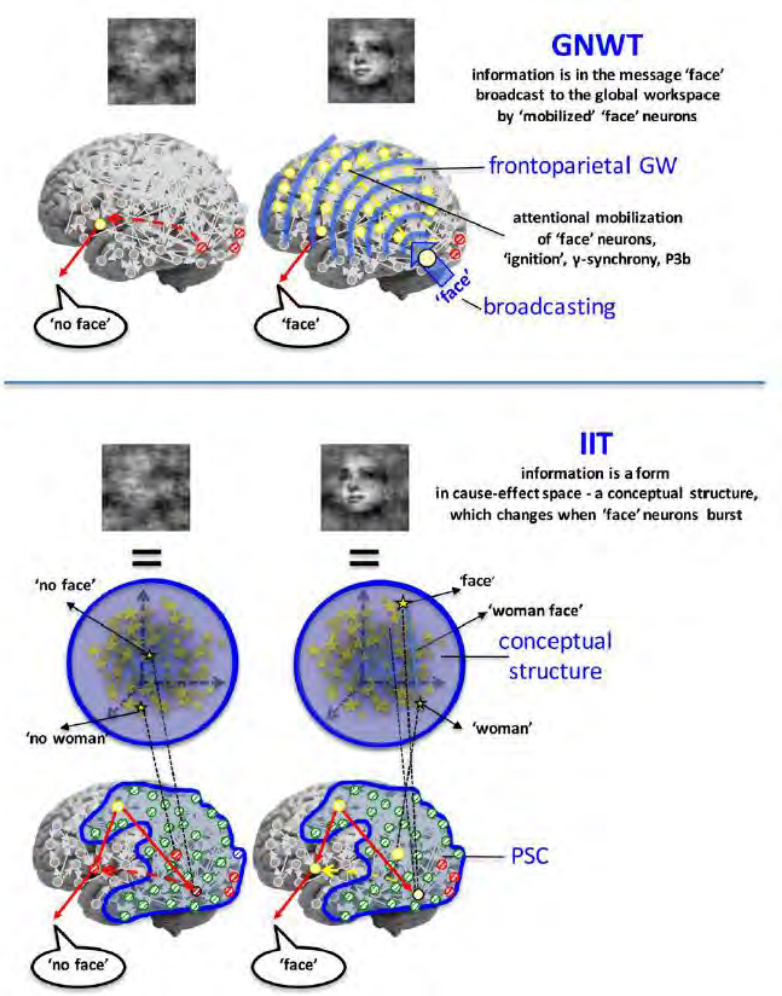

Figure 1.1.2. Seeing a face: Global Neuronal Workspace Theory (GNWT) vs. IIT.
The experience of seeing a face is contrasted with seeing visual noise following presentation of a degraded image. The top panel is a schematic rendition according to GNWT, the bottom panel according to IIT. In both panels a 'face' neuron in the fusiform gyrus turns from high firing (red) to burst firing (yellow) when the face is seen. (Top panel) In GNWT, a "piece" of information becomes conscious if it is broadcast (blue radio waves) to a broad neural audience. (Bottom panel) In IIT, when the "face" neuron within the PSC turns to burst firing it changes the form of the conceptual structure. Stars linked to the PSC by black dotted lines highlight a small subset of these concepts, and a blue line between 'face' and 'woman' indicates a relation. Here, the information content of consciousness is specified intrinsically (by the system for the system itself). Reproduced from Tononi et al. (2016).

1.1.2 Neural correlates of consciousness

The neural correlates of consciousness (NCC) are defined as the "minimum neuronal mechanisms jointly sufficient for any one specific conscious percept" (Koch, Massimini, Boly, & Tononi, 2016). The NCC can be further interpreted in two ways, depending if we refer to a specific ***content*** (i.e. transitive word use) of consciousness or the overall ***state*** (i.e. intransitive word use) of consciousness (Koch et al., 2016).

The content-specific NCC are the neural mechanisms which determine a phenomenal distinction within an experience (e.g. conscious experience of observing a rose flower in the

garden). The full NCC, are the neural substrates supporting conscious experience in its entirety, irrespective of a specific content.

The full NCC is usually investigated through such state-based comparisons, by contrasting brain activity when consciousness is present, as in healthy subjects or recovered patients, with brain activity in UWS or coma patients, in anesthesia or dreamless sleep. It is important to note, that during such states of complete consciousness abolition induced by brain injury, alterations in conscious processing occur alongside damage to multiple cognitive functions (and brain regions), frequently yielding confounding results in terms of consciousness-related neural correlates. Nevertheless, the clinical models have been proved to be indispensable in the ongoing "quest" for neural substrates of conscious processing, as we will see in the following chapter.

1.1.3 Clinical models of consciousness

The clinical definition of consciousness (e.g. as a physiopathological state) comprises two major components (Posner, Plum, & Saper, 2007): i) the arousal (the level of consciousness) implying behavioral alternation of sleep and wakefulness and the ii) awareness (content of consciousness) referring to conscious perception which includes collective thoughts and feelings of a given individual (Laureys, Owen, & Schiff, 2004; Laureys, 2005; Soddu et al., 2011). Awareness can further be subdivided into awareness of the external world (e.g., sensory perception of the environment) and of self that is the internal world (e.g., mind-wandering, mental imagery, inner speech). At a clinical level, the wakefulness or level of arousal is inferred by a prolonged period of spontaneous eye opening, while awareness is assessed by evaluating the command following and by observing non-reflex contingent behavior (i.e. eye tracking, oriented movement to pain) toward specific environmental stimuli (Demertzi, Sitt, & Sarasso, 2017).

At a neuroanatomical level, the level of arousal (and in particular of sleep-wake cycles) is controlled by the subcortical arousal systems in the brainstem, midbrain, and thalamus (Demertzi et al., 2017; Lin, 2000; Schiff, 2008). Awareness is thought to be supported by the functional integrity of the cerebral cortex and its subcortical connections, although its supporting neural correlates still need to be elucidated (Demertzi et al., 2017).

1.1.3.1 Acquired disorders of consciousness

Consciousness is not an all-or-none phenomenon but lies on a continuum of states, and it can range from normal consciousness where arousal and awareness level are high, to disorders of consciousness (DOC) where arousal can be present, while awareness is absent or fluctuating (Figure 1.1.3).

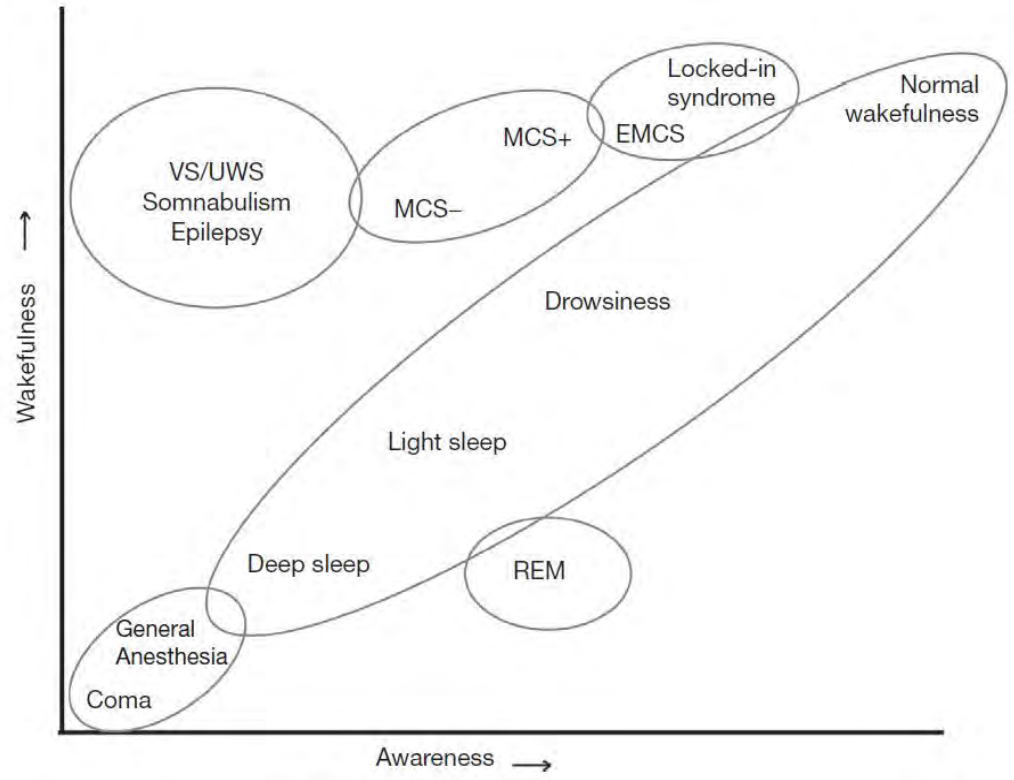

Figure 1.1.3. Interaction between arousal and awareness in different states of (un)consciousness.
REM, rapid eye movement; EMCS, emergence from a minimally conscious state; MCS+, minimally conscious state plus; MCS-, minimally conscious state minus; VS/UWS, vegetative state/unresponsive wakefulness syndrome; LIS, locked-in syndrome. Reproduced from Heine, Demertzi, Laureys, & Gosseries (2015).

We will briefly define the different states of consciousness such as coma, unresponsive wakefulness syndrome (UWS; previously known as vegetative state) and minimally conscious state (MCS), and the main causes of pathological impairment in consciousness such as traumatic and anoxic brain injury. We will also describe the locked-in syndrome (LIS), which is not a disorder of consciousness but is commonly misdiagnosed as a DOC.

1.1.3.1.1 Brain injury (BI) leading to DOC

The main etiologies of coma, and thus disorders of consciousness, are traumatic brain injury (e.g. motor vehicle accident, falling) and non-traumatic BI, such stroke, or anoxia (e.g., cardiac arrest). We will focus on two etiologies, traumatic and anoxic BI, as these were the main underlying causes of coma in our patients.

Anoxia refers to a complete reduction of oxygen supply or utilization, which is a direct result of reduced oxygen supply, reduced ambient oxygen pO2, low hemoglobin or impaired tissue utilization following poisoning of the mitochondrial cytochrome enzymes (Howard et al., 2012). **Hypoxia** is a milder form where there is available oxygen but at reduced levels for a period of time. Many anoxic comatose (i.e. post cardiac arrest) patients die or survive with severe disability after a prolonged stay in the intensive care unit (ICU) associated with important cost burden. Brain damage occurring after anoxia is related to diffuse and severe structural damage encompassing brain swelling, cortical laminar necrosis, basal ganglia necrosis, and delayed white matter degeneration and atrophy (Howard et al., 2012; Weiss, Galanaud, Carpentier, Naccache, & Puybasset, 2007). Gray matter seems to have greater vulnerability to anoxia/hypoxia in comparison to white matter, especially in brain regions that show high basal metabolic levels (Howard et al., 2012; Nolan et al., 2010).

Traumatic brain injury (**TBI**) occurs by the impact of an external force, with leading causes being falling and motor vehicle accidents (Sharp, Scott & Leech, 2014). TBI can be classified based on severity, ranging from mild trauma to severe brain injury resulting in prolonged coma or death. The primary injury can cause both focal and diffuse effects depending on the mechanism of brain injury (i.e. direct contact and acceleration–deceleration) (Sharp et al., 2014).

Focal injuries include skull fractures, hematomas, while diffuse injuries involve damage to long-distance white matter connections via diffuse axonal injury (DAI) and blood vessel damage via diffuse vascular injury (Mckee & Daneshvar, 2015; Sharp et al., 2014). Studies show that severe TBI with poor outcome and impaired consciousness, have diffuse damage to cortical, subcortical white matter and thalamic nuclei (Adams, Graham, & Jennett, 2000; Sharp et al., 2014).

Anoxic brain injury has been associated with high mortality rate in non-traumatic coma (Horsting, Franken, Meulenbelt, van Klei, & de Lange, 2015; Posner et al., 2007), and worse functional outcome following rehabilitation in comparison to traumatic brain injury (Cullen, Park, & Bayley, 2008; Cullen, Crescini, & Bayley, 2009; Cullen & Weisz, 2010). Also,

outcome (and prognostic markers) in disorders of consciousness has been shown to vary depending on etiology. Thus, brain injury mechanisms need to be taken into account during clinical management, diagnosis and prognosis of DOC patients.

1.1.3.1.2 Coma

Recent advances in clinical care have resulted in an increasing number of patients who survive severe brain injury such as trauma, cardiac arrest, stroke, infection or metabolic disruption. However, many of these patients initially show complete absence of arousal and awareness of one self and their surroundings (Laureys, 2005). This state of unarousable unresponsiveness, in which patients never open their eyes even if intensively stimulated, is defined as coma.
Autonomic functions, such as breathing and thermoregulation, are reduced, which often requires respiratory assistance. Nevertheless, coma needs to be distinguished from brain death (Wijdicks, 2001) resulting from irreversible brainstem damage. In this case neuroimaging shows "hollow skull phenomenon", indicative of the permanent loss of neuronal function in the whole brain (Laureys, 2005). In general, coma persists from 2-4 weeks. From this initial state patients can fully regain consciousness or evolve into other disorders of consciousness such as the unresponsive wakefulness syndrome (UWS) and minimally conscious states (MCS) (Figure 1.1.4).

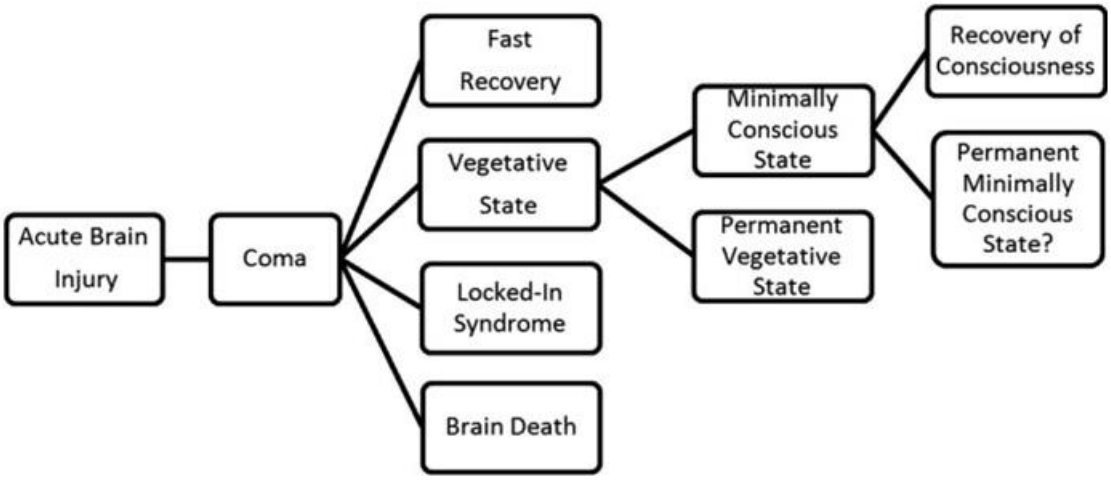

Figure 1.1.4. Different conditions that may follow acute brain injury.
The unresponsive wakefulness syndrome (UWS) was previously defined as the vegetative state. Reproduced from Gosseries et al. (2011).

1.1.3.1.3 Unresponsive wakefulness syndrome (UWS)

Unresponsive wakefulness syndrome, a revised name proposed as a more appropriate alternative to "vegetative state", refers to patients who show intermittent wakefulness (manifested as eyes-open/eyes-closed periods) but have no awareness of self or the external world (Laureys et al., 2010). Patients exhibit reflexive motor activity (i.e. grinding, swallowing, crying, smiling) devoid of any voluntary interaction with the environment and unrelated to the (emotional) context (Heine et al., 2015). Hypothalamic and brainstem autonomic functions are generally preserved, with variably preserved cranial nerve and spinal reflexes, allowing survival and prolonged medical care (Demertzi, 2017). This state can be persistent but can also transient towards minimally conscious state or recovery (The Multi-Society Task Force on PVS, 1994). When there is no recovery after 12 months after traumatic brain injury and 3 months after anoxic brain injury, the state can be declared permanent and withdrawal of hydration and nutrition may be discussed (Laureys et al., 2000, 2004), however, this point is a matter of debate. Some cases of late recovery have been described in the literature (Estraneo et al., 2010), but there are currently no prognostic biomarkers which could highlight potential recovery during the early stages when withdrawal of therapy is considered.

1.1.3.1.4 Minimally conscious state (MCS)

The minimally conscious state describes patients who regain fluctuating but reproducible non-reflexive purposeful behavior such command following, visual pursuit or sustained fixation, intelligible verbalization, emotional or motor responses relevant to the environment stimuli (Demertzi et al., 2017; Giacino et al., 2002).

A new subcategorization of the MCS into MCS+ (plus) and MCS- (minus) has been recently proposed based on the complexity of patients' behaviors (Bruno et al., 2011a). MCS+ refers to patients showing non reflexive voluntary responses such as command following, intelligible verbalization, and/or nonfunctional communication, while MCS- defines low-level behavioral responses such as visual pursuit or localization of noxious stimulation.

Patients are considered to have emerged from MCS (EMCS) when they show reliable and consistent demonstration of functional interactive communication (i.e. accurate yes/no responses to basic situational orientation questions) and/or functional object use (i.e. use of at least two different objects on two consecutive evaluations) (Giacino et al., 2002). EMCS

patients are no longer considered to suffer from DOC, however, they often have severe disability, and might continue to need full-time care. The MCS may be transitory, chronic or permanent, just like UWS. Interestingly, late recoveries have been noted, with one patient regaining reliable expressive language after 19 years in MCS (Voss et al., 2006). Importantly, the high rate of misdiagnosis in DOC has significant implication for prognosis, as it has been shown that MCS patients have significantly greater potential for recovery in comparison to UWS patients (Faugeras et al., 2017; Giacino & Kalmar, 1997; Hirschberg and Giacino, 2011; Luauté et al., 2010).

1.1.3.1.5 Locked-in syndrome (LIS)

This syndrome is not considered as a disorder of consciousness, but can be easily mistaken as a DOC due to patients' loss of voluntary motor control and thus the ability to effectively communicate with the environment (Heine et al., 2015; Laureys, 2005). However, these patients are awake and aware, with no loss of cognitive function, in most cases. The most common cause of the LIS is ventral brainstem stroke. The primary mode of interaction is eye movements and blinking, however, recent advances in brain-computer interfaces (BCI) are of great help in providing more direct and spontaneous means of communication (Chaudhary, Xia, Silvoni, Cohen, & Birbaumer, 2017).

Clinical entities	*DOC*	*Definition*	*Reference*
Brain death	No	Irreversible coma Evidence for the cause of coma Irreversible loss of all functions of the brain, including brainstem reflexes Apnea Absence of confounding factors (e.g., drugs, hypothermia, and electrolyte and endocrine disturbances)	Wijdicks (2001)
Coma	Yes	No wakefulness No awareness of self or environment Acute state (i.e., resolves in hours to maximum 4 weeks)	Posner, Saper, Schiff, et al. (2007)
Vegetative state/unresponsive wakefulness syndrome	Yes	Wakefulness No awareness of self or environment No sustained, reproducible, purposeful, or voluntary behavioral responses to visual, auditory, tactile, or noxious stimuli No language comprehension or expression Relatively preserved hypothalamic and brainstem autonomic functions (e.g., respiration, digestion, and thermoregulation) Bowel and bladder incontinence Variably preserved cranial nerve and spinal reflexes Acute and/or chronic state	The Multi-Society Task Force on PVS (1994) and Laureys, Celesia, Cohadon, et al. (2010)
Minimally conscious state	Yes	Wakefulness Awareness is inconsistent but definite Minus: Visual pursuit; Contingent behavior; Reaching for objects; Orientation to noxious stimulation Plus: Following simple commands; Intentional communication; Intelligible verbalization	Giacino, Ashwal, Childs, et al. (2002) Bruno, Vanhaudenhuyse, Thibaut, Moonen, and Laureys (2011)
Emergence from minimally conscious state	No	Functional communication Functional object use	Giacino, Ashwal, Childs, et al. (2002)
Locked-in syndrome	No	Wakefulness Awareness Aphonia or hypophonia Quadriplegia or quadriparesis Presence of communication via the eyes Preserved cognitive abilities	American Congress of Rehabilitation Medicine (1995)

Figure 1.1.5. Diagnostic criteria for DOC.
Reproduced from Heine et al. (2015).

1.2 Behavioral assessment of consciousness

There are multiple standardized behavioral scales (Bruno et al., 2011b; Seel et al., 2010) routinely used in the clinical assessment of consciousness in brain injured patients. Among them, we will describe the scales used in our study (which are also routinely used in clinical practice).

1.2.1 Behavior Rating Scales

1.2.1.1 Glasgow Coma Scale (GCS)

GCS (Teasdale & Jennett, 1974; Teasdale et al., 2014) is simple and short scale, used mainly in intensive care settings. The GCS has three subscales that measure eye opening, verbal and motor responses. Each of the scales can be communicated separately or summed to create a total score. Each level of response is assigned a number—the worse the response, the lower the number. The total score varies between 3 and 15. In acute stages, brain damage is described as

severe if the score is less than or equal to 8, moderate if the score is between 9 and 12, and mild if the score is between 13 and 15. However, there have been some concerns with the GCS. The verbal response is impossible to assess in the case of intubation or tracheotomy, and the eye opening may not be sufficient to assess brainstem function (Laureys, Majerus, & Moonen, 2002).

1.2.1.2 The Full Outline of Unresponsiveness (FOUR)

FOUR has been proposed as a replacement to the GCS as it can detect subtler neurological changes (Wijdicks, Bamlet, Maramattom, Manno, & McClelland, 2005). It consists of four subscales (eye, motor, brainstem, and respiration), and each subscale has a maximal score of 4. The scale has been translated and validated in French language (Bruno et al., 2011b). FOUR is suitable for differentiating between VS and MCS, because it assesses visual pursuit, and can diagnose LIS and brain death.

1.2.1.3 The Coma Recovery Scale-Revised (CRS-R)

CRS-R is a recently developed clinical scale (Giacino, Kalmar, & Whyte, 2004), currently considered the most reliable and sensitive test for differential diagnosis of DOC (Seel et al., 2010).

The CRS consists of 25 hierarchically arranged items that comprise 6 subscales addressing auditory, visual, motor, oromotor, communication, and arousal processes. The lowest item on each subscale represents reflexive activity, whereas the highest items represent cognitively mediated behaviors (Giacino et al., 2004). CRS has been shown to have acceptable standardized administration and scoring, excellent content validity and test-retest reliability, and good internal consistency and inter-rater reliability (Giacino, Fins, Laureys, & Schiff, 2014; Seel et al., 2010). The scale has been translated and validated in French language (Schnakers et al., 2008). However, repeated CRS-R testing is advisable to minimize the risk of misclassification (Cortese et al., 2015), with one study suggesting at least 5 assessments within a short time interval (e.g., 2 weeks) to reduce the risk of misdiagnosis (Wannez, Heine, Thonnard, Gosseries, & Laureys, 2017).

1.2.2 The challenges of diagnosis and prognosis in DOC

1.2.2.1 Limitations of behavioral-based diagnosis

Diagnostic accuracy is critical in this field, in regard to appropriate everyday medical management (e.g. pain medication) and the decision of withdrawal of life-sustaining care (Turgeon et al., 2011). In addition, it could be expected that more accurate diagnosis holds the promise for personalized medicine, including individually-targeted therapeutic pharmacological (e.g. amantadine, zolpidem; Gosseries, Zasler, & Laureys, 2014) and/or nonpharmacological (e.g., deep brain stimulation, transcranial direct current stimulation) (Schiff et al., 2007; Thibaut et al., 2014, 2015, 2017; Cavaliere et al., 2016)

Diagnostic accuracy depends on multiple factors associated with the environment, examiner and/or patient. Differential diagnosis requires repeated standardized assessment by well-experienced and trained medical staff. Nonetheless, voluntary and reflexive behavior could be difficult to distinguish, as motor responses can be very small, quickly exhaustible and inconsistent, potentially leading to diagnostic error (Schnakers, Majerus, & Laureys, 2004). Environmental factors, such as paralytic and sedative medication, can significantly constrain voluntary behavioral responses, inducing bias in the diagnostic process. Furthermore, fluctuation in level arousal, fatigue, pain, severe central and peripheral damage leading to sensory deficits (e.g., cortical blindness/deafness), motor impairment (e.g., paralysis) or cognitive deficits (e.g., aphasia, apraxia, agnosia), (Bodien & Giacino, 2016) also pose a major problem in administrating and accurately interpreting the results of current clinical tests focused on overt patient behavior.

These problems are highlighted in studies that show that around 40% of patients diagnosed as UWS have some conscious awareness (Schnakers et al., 2009; van Erp, et al., 2015). LIS patients can also easily be mistaken as unconscious (Bruno et al., 2011a).

1.2.2.2 Limitations of behavioral-based prognosis

It must be stressed that prognostic markers for accurate long-term DOC patients' assessment of recovery do not exist or are extremely limited (Haenggi, Z'Graggen, & Wiest, 2014; Weijer et al., 2016). Estimating the likelihood of recovery in acutely comatose patients is extremely difficult, due to behavioral non-responsiveness, differences in nature of brain injury (i.e. traumatic vs. anoxic BI) and potential confounding factors such as medication and metabolic disturbance. Also, patient outcome after severe brain injury is highly variable (Sharp et al.,

2014), especially in traumatic brain injury, as some patients regain independence, while others have serious cognitive deficit and are unable to function without personal care assistance.
The prediction accuracy of current prognostic markers used in the clinical setting (for brief see Weijer et al., 2016) remains generally low, and is defined according to a binary outcome (survival vs. death) without any distinction between different DOC categories or the degree of functional impairment at long-term. More importantly, the lack of objective and reliable prognostic markers might significantly contribute to practice variation in the withdrawal of life-sustaining therapy. This was highlighted in a study of Turgeon and colleagues (2011), including 720 patients with severe traumatic brain injury in six level I trauma centers. The authors found a mortality rate of 32%, with 70% of death attributable to withdrawal of life-sustaining therapy, with half occurring within the first 72 h of injury. In addition, the hospital mortality rates differed substantially, ranging from 10.8% to 44.1%, partially due to physicians' different perceptions of long-term prognosis (Turgeon et al., 2011).

Therefore, the importance of conducting coma-related research is two-fold: a) fundamental - coma presents a unique model for the research of neural correlates of consciousness; and b) clinical - there is an urgent need for acute-stage markers serving the purpose of diagnosis (e.g. brain's residual capacity for conscious processing), monitoring (e.g. changes of brain function/structure), and prognosis (e.g. identifying patients with a potential for recovery). Once these markers are identified, they can be applied in the development and application of novel personalized treatments aiming to restore consciousness and neurocognitive function.

1.3 Neuroimaging and conscious processing: (re)framing paradigms

The increasingly powerful neuroimaging technologies have been leading to a significant paradigm shift and have helped surpass some limitations posed by behavioral testing (Laureys & Schiff, 2012). Functional neuroimaging strategies (i.e. fMRI, EEG) have enabled the detection of convert awareness in patients previously thought to be in unresponsive wakefulness syndrome (i.e. fMRI-based active paradigms) (Peterson, Cruse, Naci, Weijer, & Owen, 2015; Monti et al., 2010) and permitted "non-communicative" and locked-in patients to communicate their though and interact with the environment through willfully modulated brain activity (i.e. EEG paradigms; Luauté et al., 2015).
However, due to the complexity of disorders of consciousness, as described earlier, patients may not be able to participate (via brain activity or motor/behavior responsiveness) in

neuroimaging-based tasks, and could therefore be wrongfully identified as unconscious despite preserved capacity for conscious processing. Thus, an alternative approach has been proposed to active paradigms, in the form of resting-state functional and structural neuroimaging strategies, which serve to detect residual neural and cognitive processes indicative of consciousness, independently of behavioral responsiveness of patients. These advanced (resting-state) neuroimaging techniques hold significant promise in providing diagnostic and prognostic information for DOC patients, however, much work is needed before they can be used in clinical setting. The following chapters will provide more detail on the MRI basics, current state and methodological advancement in the application of neuroimaging in DOC assessment.

1.3.1 Magnetic Resonance Imaging

Neuroimaging includes the use of various techniques to either directly or indirectly image the structure or function of the brain. Magnetic Resonance Imaging (MRI) was developed in late 1970s, by researchers including Peter Mansfield and Paul Lauterbur, and is widely used today to image the brain both in health and disease. MRI is non-invasive imaging technique that uses magnetic fields, radio waves, and field gradients to generate images of internal organs, without exposure to ionizing radiation.

1.3.1.1 Acquisition methods

The MRI scanner consists of a large, powerful magnet placed in a horizontal tube in which the patients enters. The strength of a magnet in an MRI system is rated using a unit of measure known as a tesla (T), which can range from 0.5T to 7T, with most today's scanners working at 3T. MRI is based on the magnetization properties of hydrogen nuclei (protons), mainly contained in water molecules. These protons are randomly spinning, or precessing, on their axis, around their individual magnetic fields. When the patient enters the MRI scanner a very strong magnetic field (B0) is applied to align the proton spins in the direction of the field (z direction). Next, a radio frequency (RF) pulse that is specific only to hydrogen (Larmour frequency) is applied, perturbing the alignment (or magnetization) of protons. The protons absorb the energy from the variable field and flip their spins into the xy plane, a process called excitation. When the RF pulse is turned off, the protons gradually return to their normal spin (equilibrium) releasing the energy absorbed from the RF pulses, creating a signal that is picked

up by the coils placed in the MRI tube. This process is called relaxation and occurs in different rates depending on the tissue type. There are two different relaxation times - T1 and T2. T1 is the time constant which determines the rate at which excited protons return to equilibrium, that is align with the external magnetic field in the z direction (longitudinal relaxation). T2 is the time constant which determines the rate at which excited protons reach equilibrium or go out of phase with each other in the xy plane (transverse magnetization) (external factors such as magnetic field inhomogeneity can increase the T2, as captured in T2*).

By varying several MRI sequence parameters, images can be acquired with varying contrast between different brain tissues. Some of the adjustable parameters are the: repetition time (TR) - time between successive pulse sequences - and echo time (TE) - time between the RF pulse and the sampling of the echo signal. T1-weighted images are produced by short TE and TR times. Tissues with short T1 appear bright on the image because they regain most of their longitudinal magnetization during the TR interval (such as white matter (WM)) and produce a stronger MR signal. Tissues that seem much darker on the image, therefore have longer longitudinal relaxation times (such as cerebro-spinal fluid (CSF)). T2-weighted images are produced using longer TE and TR. Therefore, tissue, such as WM, with a short T2 will appear dark on T2-weighted images, while CSF will appear bright on T2-weighted images.

1.3.2 Diffusion weighted imaging (DWI)

DWI is a variant of conventional MRI sensitive to diffusion of water protons. This technique is based on the molecular diffusion, or Brownian motion, referring to thermally driven random motion of water molecules (Soares, Marques, Alves, & Sousa, 2013; Hagmann et al., 2006). This movement is described by the diffusion coefficient, which also depends on the properties of the liquid, such as viscosity, molecular size and temperature. In an unrestricted environment, such as glass of water, the motion is completely random and only limited by the boundaries of the glass. However, biological tissue is a highly heterogeneous media, in which the random movement of molecules is impeded by compartmental boundaries and other molecular obstacles and thus restricted in various directions. The combination of these factors, produces measured signal changes that reflect the apparent diffusion coefficient (ADC) or mean diffusivity (MD) which can significantly differ from the diffusion coefficient of the unrestricted liquid (like in the glass of water).

DWI images are acquired by applying a diffusion sensitizing gradient that increases the strength of magnetic field evenly in one direction. The gradients are applied across large number of

different directions (minimum 6) to ensure a robust estimation of diffusion. For each direction, the first gradient pulse dephases the magnetization, and the second pulse rephases the magnetization. For stationary molecules, the second gradient will refocus the protons perfectly, resulting in maximally coherent magnetization and sampling of a high MRI signal. In case of a diffusion in the direction of applied gradient, the second gradient will cause a random phase shift resulting in an attenuation of the MRI signal. Thus the WM fiber tracts parallel to the gradient direction will appear dark on the DWI images in that direction (O'Donnell & Westin, 2011; Mori, & Zhang, 2006).

Diffusion tensor imaging is an extension of DWI which refers to a specific modelling of data, allowing the inference of directional dependencies of the diffusion signal, resulting in a 3D representation of the water molecule movement. The spatial dependence of the diffusion is characterized by a 3x3 matrix, called the diffusion tensor, that describes the diffusion along some combination of the 3 different spatial direction (x,y,z), assuming that the displacement distribution is Gaussian. The diffusion tensor is usually represented by an ellipsoid, where the axes represent three principal diffusion directions (eigenvectors – v1, v2, v3) and the corresponding diffusion magnitude (eigenvalues - $\lambda 1$, $\lambda 2$, $\lambda 3$). Eigenvalues are ordered $\lambda 1 > \lambda 2 > \lambda 3$, with an anisotropic diffusion (restricted diffusion) characterized by $\lambda 1 \geq \lambda 2 \geq \lambda 3$ and isotropic diffusion by $\lambda 1 \sim \lambda 2 \sim \lambda 3$ (Figure 1.3.1).

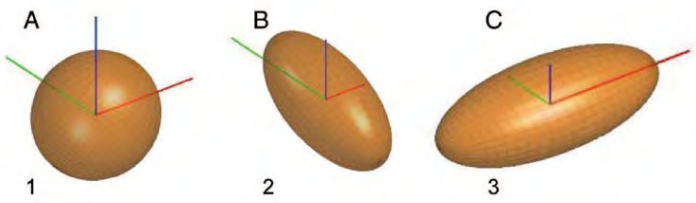

Figure 1.3.1. Three diffusion ellipsoids represent the diffusion profile of 3 different structures.
The axes represent the x- (left-right, red), y- (posterior-anterior, green), and z-(inferior-superior, blue) directions. (A) Isotropic diffusion ellipsoid, representing a region of cerebral spinal fluid. (B) Anisotropic diffusion ellipsoid, representing a white matter tract parallel to the y-axis (superior longitudinal fasciculus). (C) Anisotropic diffusion ellipsoid, representing a white matter tract parallel to the x-axis (corpus callosum. Reproduced from Feldman, Yeatman, Lee, Barde, & Gaman-Bean (2010).

The degree to which diffusion is directionally dependent can be expressed as the fractional anisotropy (FA), a parameter which is calculated comparing each eigenvalue with the mean of all the eigenvalues as in the following equation:

$$FA = \sqrt{\frac{3}{2}} \sqrt{\frac{(\lambda_1 - \langle\lambda\rangle)^2 + (\lambda_2 - \langle\lambda\rangle)^2 + (\lambda_3 - \langle\lambda\rangle)^2}{\lambda_1^2 + \lambda_2^2 + \lambda_3^2}},$$

The values of FA range from 0 (isotropic) to 1 (anisotropic). In the brain white matter, diffusion is anisotropic as it greater along the axis of the axons and not across. Thus, DTI also allows fiber tracking that is reconstruction of major white matter tracts in the brain, which are made up of densely packed myelinated axons (high values of FA). One of these major tracts is the cingulum which nestles in the WM of the cingulate gyrus and will be mentioned in following chapters (Figure 1.3.2).

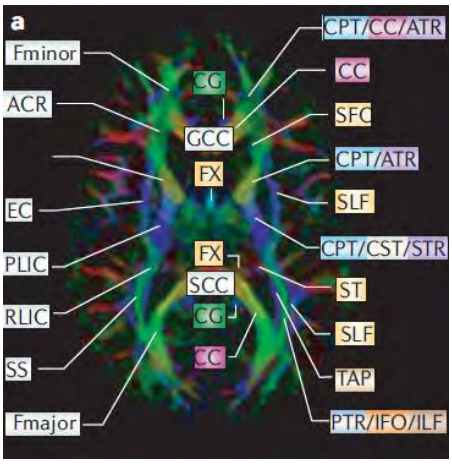

Figure 1.3.2. Major white matter structures of the human brain.
ACR, anterior corona radiata; ALIC, anterior limb of internal capsule; ATR, anterior thalamic radiation; CC, corpus callosum; CG, cingulum; CPT, corticopontine tract; CST, corticospinal tract; EC, external capsule; Fmajor, forceps major; Fminor, forceps minor; FX, fornix; GCC, genu corporis callosi; ILF, inferior longitudinal fasciculus; PLIC, posterior limb of internal capsule; PTR, posterior thalamic radiation; RLIC, retrolentricular part of internal capsule; SCC, splenium corporis callosi; SFO, superior fronto-occipital fasciculus; SLF, superior longitudinal fasciculus; SS, sagittal striatum; ST, stria terminalis; TAP, tapetum. Reproduced from Toga, Thompson, Mori, Amunts, & Zilles. (2006).

Other measures can be calculated such as mean diffusivity (λ1+λ2+λ3)/3), axial (longitudinal) diffusivity (λ1) that is the rate of diffusion in the direction that is parallel to the white matter, and radial diffusivity (λ2+λ3)/2) or perpendicular diffusivity to white matter.

More importantly, DWI/DTI is a sensitive (but non-specific) marker of neuropathology and microstructural architecture. The combination of described measures has received growing popularity in clinical diagnosis and characterization of various pathological process such as acute ischemic lesions (decrease in MD, increase in FA), inflammation and edema (increase in MD, decrease in FA), and demyelination/dysmyelination (increase MD, decrease FA, increase RD) (Alexander, Lee, Lazar, & Field, 2007).

1.3.3 Functional MRI (fMRI)

Functional magnetic resonance imaging (fMRI) measures the spontaneous (resting-state) or stimulus-driven fluctuation in the blood oxygenation level-dependent (BOLD) signal. The idea that changes in blood oxygenation could drive measurable signal changes in brain MR images was introduced by Ogawa and colleagues in 1990.

In brief, fMRI is based on the principle that an increase in neural activity in a brain region stimulates an increase in a local blood flow needed for a higher supply of oxygen and glucose. Consequently, there is a change in blood flow that exceeds the demand in the adjacent capillaries, resulting in an increase in the balance of the oxygenated arterial blood to deoxygenated venous blood (Gore, 2003). This phenomenon is called the hemodynamic response (Figure 1.3.3).

Oxygenated and deoxygenated hemoglobin present different magnetic attributes, therefore, the higher concentration of oxyhemoglobin in the venous compartment (and decreased deoxyhemoglobin) changes the paramagnetic properties of the tissue which can be detected during a T2* acquisition. An increase in blood oxygen concentration at capillary level will locally reduce magnetic field inhomogeneities leading to increased T2*-weighted signal.

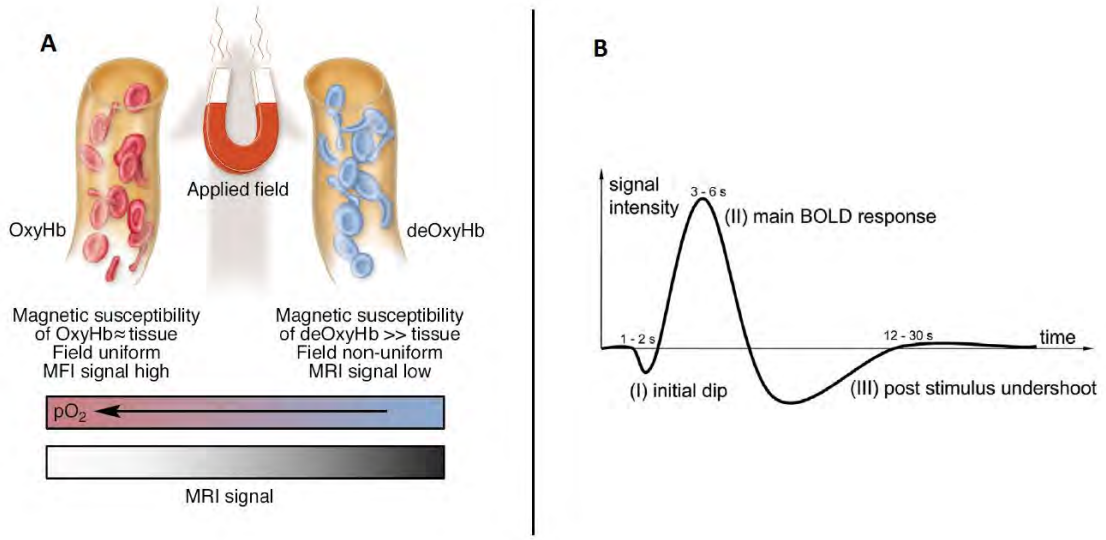

Figure 1.3.3. A. Schematic illustration of the origins of the BOLD effect in fMRI. B. Illustration of the typical BOLD hemodynamic response function.
Figure A reproduced from Gore (2003). Figure B reproduced from Siero et al. (2013).

1.3.4 Resting-state fMRI (rs-fMRI)

RS-fMRI investigates synchronous activations between regions that are spatially distinct, without applying a task or a controlled stimulus (Lee, Smyser & Shimony, 2013). Rs-fMRI focuses on spontaneous low frequency fluctuations (<0.1 Hz) in the BOLD signal (Van Dijk et al., 2010). Relative to task-based fMRI, it requires minimal patient compliance, it can be acquired under anesthesia and it is well suited for difficult clinical populations such as Alzheimer's disease or DOC patients (Fox & Greicius, 2010; Orringer, Vago, & Golbycole, 2012; Lee et al., 2013). Recently, there have been some advances in the application of rs-fMRI in prediction of individual differences (Calhoun, Lawrie, Mourao-Miranda, & Stephan, 2017; Dubois & Adolphs, 2016), which hold significant promise in obtaining diagnostic and prognostic information in a single subject, especially important in heterogeneous groups, such as the population of traumatic brain injury patients.

1.3.4.1 Rs-fMRI analysis methods

After image preprocessing steps, a number of methods can be applied in the analysis of the rs-fMRI data, each with its own inherent advantages and disadvantages.

The two main approaches to analyzing rs-fMRI are the: a) model-driven and b) the data-driven analysis (Cole, Smith, & Beckmann, 2010).

The first approach consists (Poldrack, 2007) of the a priori selection of a voxel, cluster or atlas region, from which to extract time series (i.e. BOLD signal) data which is then used to calculate whole-brain, seed-based, or voxel-wise functional connectivity maps of co-variance with the seed region (Cole et al., 2010).

The *seed-based* approach was used in the study of Biswal and colleagues (1995) in which the low-frequency coherent, spontaneous BOLD fluctuations were identified bilaterally in the somatomotor cortical regions, suggesting, for the first time, the functional importance of the resting-state activity. However, as described, this approach is hypothesis-driven, requiring a priori selection of ROIs based on the assumption of a functional dependency.

In contrast, the data-driven approach such as the *independent component analysis (ICA)* serves to estimate the component maps of maximal spatial independence (from each other) without the need for a prior selection of brain regions (Beckmann, DeLuca, Devlin, & Smith, 2005).

Importantly, the application of seed-based and ICA analysis led to the identification of several resting-state networks (RSNs) representing spatially distant but functionally connected regions,

comparable to known sensory and cognitive processing systems shown to be activated during different task-based fMRI studies (Heine et al., 2012; Rosazza, & Minati, 2011).

Another, distinct but interesting alternative to seed-based and ICA analysis is the graph theory analysis which formulates the resting-state networks as a collections of nodes connected by edges (i.e. links) (Lee et al., 2013). This approach is not so widely used as the previous ones, but is rapidly gaining interest in the neuroimaging community. The graph analysis is an advanced mathematical approach which consists of several steps of analysis, and will be explained in more detail in the following chapters.

1.3.5 Network-based analytical approach: graph theory

1.3.5.1 Graph definitions

Brain's anatomical and functional organization can be approached from the perspective of complex networks, which has led to a growing interest in the application of graph theoretical methods in the neuroscientific community (Bullmore & Sporns, 2009; Bullmore & Basset, 2011). Graph theory is a mathematical study of complex systems/networks that is graphs. Within this framework a complex system (brain) is formalized as a mathematical object consisting of a set of **vertices** (ex. neurons, brain regions, electrodes) and **edges** that is pairwise relationships between those vertices (ex. synaptic connections, interregional pathways, functional dependencies) (i.e. G = (V, E)). Using these two components, nodes and edges, graph topology can be quantitatively described by a wide variety of measures organized according to their ability to characterize large (whole network), intermediate (sub-networks) or small (nodes) topological scales (Fallani et al., 2014). Two nodes are **adjacent** if they are connected with an edge, and two adjacent nodes are called **neighbors**. A **self-loop** is an edge that connect a node to itself, and it is usually not present in simple graphs. **A cycle** is a path of edges and nodes where a node is reachable from itself. Graphs can be **unweighted** (i.e. binary), representing networks in which edges are either present or absent, or **weighted** – when each link has an assigned weight (numerical value). Graphs are **directed** when edges have a direction association with them, and **undirected** when links are symmetrical. A **signed** graph is a graph in which each edge has a positive or negative sign.

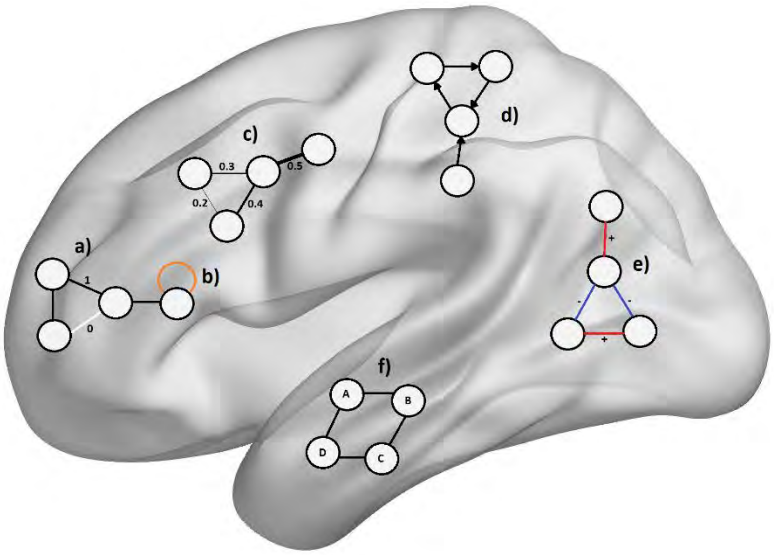

Figure 1.3.4. An example of a a) binary graph, b) self-loop, c) weighted graph, d) directed graph, e) signed graph and a f) fully connected graph.

A **fully connected** graph contains nodes that are connected with at least one edge. To generate a complete or fully connected graph, the minimum spanning tree (MST) can be applied (Alexander-Bloch et al., 2010; Prim, 1957). MST or minimum weight spanning tree consist of connecting all nodes, without any cycles and with minimum possible total edge weight (in weighted networks). The maximum number of edges are removed iteratively from a fully connected graph until all the nodes remain connected. In a graph with N nodes, the MST has N-1 edges. A graph can have many minimum spanning trees.

Graph theory offers many more concepts that will not be explored in detail, for further information please refer to a book written by Fornito, Zalesky & Bullmore (2016). In the second study (Chapter IV) we define our graphs as fully-connected, loop-less, undirected, unsigned (absolute) and unweighted.

1.3.5.2 Graph representation

Every graph is associated with an adjacency matrix – square matrix in which the elements indicate whether pairs of nodes are adjacent or not in the graph. In an undirected binary/unweighted graphs, the adjacency matrix is a symmetric (0, 1) - matrix with zeroes on its diagonal (no self-loops) (Figure 1.3.5).

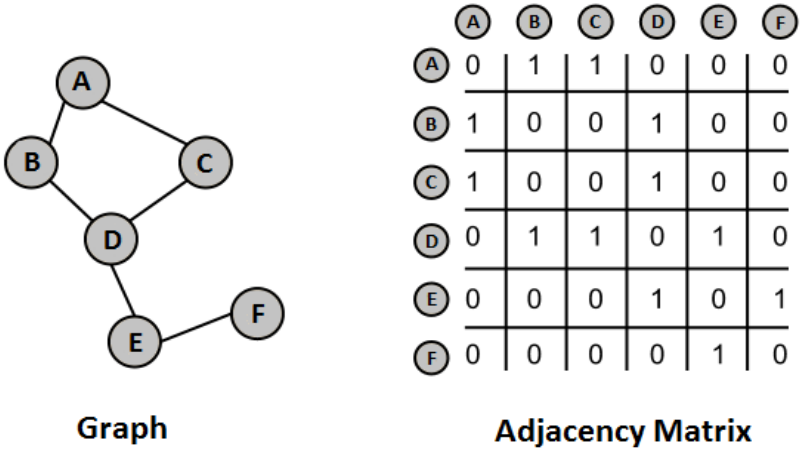

Figure 1.3.5. A simple binary graph and its representation by an adjacency matrix.

1.3.5.3 Graph analysis

The analysis of graphs entails several processing steps that need to be applied to each subject individually (Figure 1.3.6). The most important step for valid results is the accurate definition of nodes (Fornito, 2010; Fornito, Zalesky, & Breakspear, 2013; Hayasaka & Laurienti, 2010; Zalesky et al., 2010) and edges (Meskaldji et al., 2013; van Wijk, Stam & Daffertshofer, 2010), as these are the building blocks of any network and have a large impact on the extracted graph metrics (Stanley et al., 2013; Fornito et al., 2016).

In voxel-based modalities, such as fMRI, there are several ways to define brain nodes, mostly depending on the spatial scale (single voxels versus cluster of voxels) and the choice of how to combine voxels (anatomical, data-driven or hybrid parcellation) (Fornito et al., 2016). The most common approach in **rs-fMRI** is the choice of **brain regions** that are considered functionally homogeneous, as shown in task-evoked (i.e. cognitive task) or resting–state spontaneous synchronous activity (i.e. RSNs identified with ICA). **Undirected functional links** are mostly commonly defined using the Pearson correlation coefficient between the BOLD time courses extracted from different ROIs. However, the obtained functional adjacency matrix is always fully connected (except the diagonal/self-connections) and most probably contains weak and potentially spurious connections that could significantly influence the network topology. Therefore, the matrix needs to be **thresholded** before the graph metrics are calculated. To do this, we can apply a fixed cut-off value or threshold, τ, to the connectivity matrix in order to determine which connections should be retained. In the case of functional matrices, we could

set a value of the correlation coefficient to r=0.2, deciding to keep only the connection that have a higher value then r. This approach is useful in separating signal from noise, however, it usually results in a different in number of connections retained for each subject, rendering inter-individually comparison difficult. Another approach that addresses this problem is the connection density (cost) threshold. The cost (*k*) represent the ratio between the actual number of edges and the total number of possible edges in the graph. In the case of undirected graphs, the number of possible edges is divided by 2. The corresponding formula is:

$$k = \frac{E}{N(N-1)/2},$$

where E is the actual number of edges and N the number of nodes in the network (N-1 is the number of off-diagonal elements).

After applying the threshold, the remaining elements can be binarized (0, 1 matrix). Binary functional matrices assure the analysis of topological patterns of connection between nodes without the influence of variation in their weights (Fornito et al., 2016). Filtered and binarized matrices can then be used to calculate graph metrics.

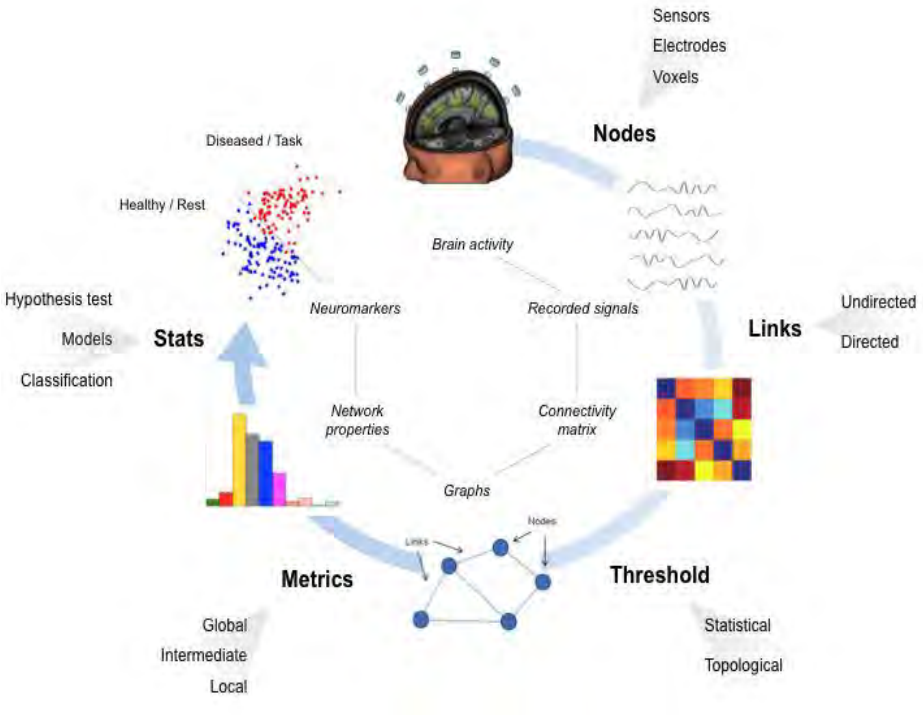

Figure 1.3.6. The processing pipeline for functional graph analysis.
Reproduced from Fallani et al. (2014).

1.3.5.4 Graph metrics

Graph theory offers a multitude of measures that can be used to explore relationships between nodes in brain networks. We will describe only the ones that we used in our second study. The metrics and corresponding formulas are integrated in the R-based libraries: brainwaver (http://cran.rproject.org/web/packages/brainwaver/index.html2) and igraph (http://cran.rproject.org/web/packages/brainwaver/index.html2http://cran.rproject.org/web/packages/igraph/index.html). For additional metrics and formulas, please see Rubinov & Sporns (2010).

1) The most basic property of a node *i* is the **degree** (k_i) that is the number of its adjacent edges that connect it to rest of the nodes in the graph. It is defined as:

$$k_i = \sum_{j \in N} a_{ij},$$

where a_{ij} is the connection status between *i* and *j*, and N is the set of all nodes in the network.

2) **Minimum path length** (distance) is the minimum number of edges that must be traversed to go from one node to another. It is a basic measure of integration within a network. It is calculated as:

$$l_{ij} = \sum_{a_{uv} \in g_{i \leftrightarrow j}} a_{uv},$$

where $g_{i \leftrightarrow j}$ is the shortest path (geodesic) between *i* and *j* ($l_{ij} = \infty$ for all disconnected pairs i, j).

3) **The global efficiency** (E) is also a metric for efficiency of integrative information transfer across the network (Latora & Marchiori, 2001). This measure is inversely related to the harmonic mean of the shortest path length (Watts & Strogatz, 1998), but is adapted to disconnected graphs. It is computed as:

$$E_{g_i} = \frac{1}{N-1} \sum_{j \in N, j \neq i} \frac{1}{l_{ij}}$$

4) **Clustering coefficient** is a measure of the degree to which nodes in a graph tend to cluster together (Watts & Strogatz, 1998). It's a basic measure of segregation within a network. It is calculated as:

$$C_i = \frac{1}{n}\sum_{i \in N} \frac{2t_i}{k_i(k_i - 1)},$$

where t_i is the number of triangles around a node i, (Ci = 0 for $k_i < 2$).

5) The **local efficiency** measures the integration capacity between immediate neighbors of a given node (Latora & Marchiori, 2001). This metric also reflects the network resilience by indicating how efficiently neighbors of a given node communicate when this node is disrupted. It is defined as:

$$E_{l_i} = \frac{1}{N_{G_i}(N_{G_i} - 1)} \sum_{j,k \in G_i} \frac{1}{l_{jk}},$$

Where, G_i is the sub-graph of G (graph) obtained from a set of nodes which are nearest neighbors (directly connected) of node i. N_{Gi} is the number of nodes in G_i.

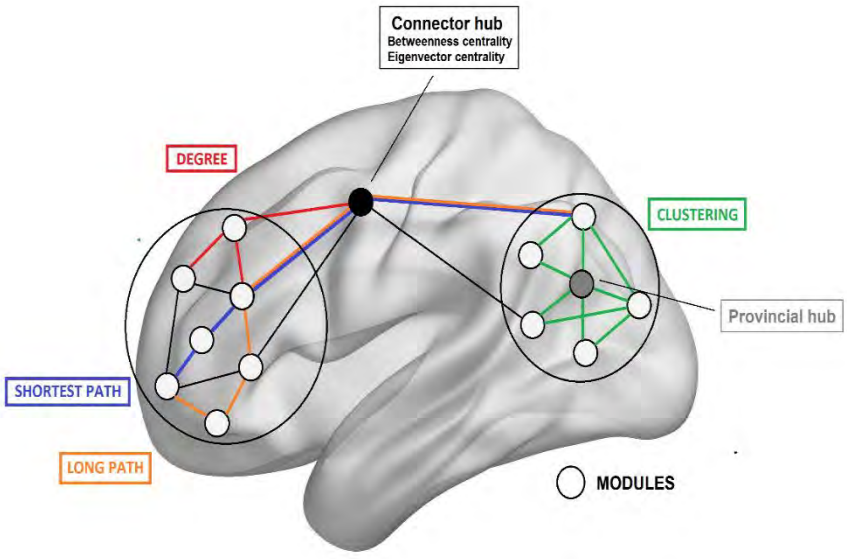

Figure 1.3.7. A graphical example of global and local metrics.

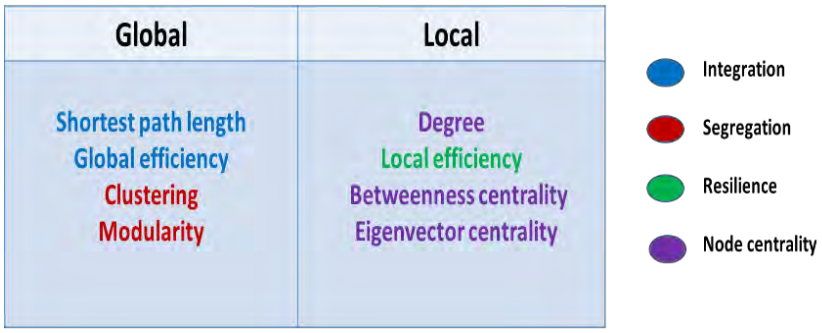

Figure 1.3.8. Table of the most basic global and local metrics and associated interpretation.

1.3.5.5 Small-word topology

Watts and Strogatz (1998) introduced a generative model for graphs which provided first evidence that neural networks have small-world (SW) properties. SW networks have high levels of clustering, like lattice (regular) networks, combined with low average path length, much like in random networks (Figure 1.3.9). The association of these two characteristics seems to provide a substrate for simultaneous segregation and integration at minimal wiring-cost (Fornito et al., 2016).

Since the Watts-Strogatz model, multiple studies have suggested that brain networks are small-world, representing functionally associated clusters with high density of local connections and few long-range connections between segregated areas supported by the integrative properties of highly connected hub nodes (Bullmore & Sporns, 2009; Collin et al., 2014).

These brain hub nodes can be defined using a range of topological measures (van den Heuvel & Hulshoff Pol, 2010; van den Heuvel & Sporns, 2013). Accordingly, the combination of different metrics, such as degree and betweenness centrality can distinguish nodes that are highly connected and have a particularly high influence on network-wide process (Fornito et al., 2016).

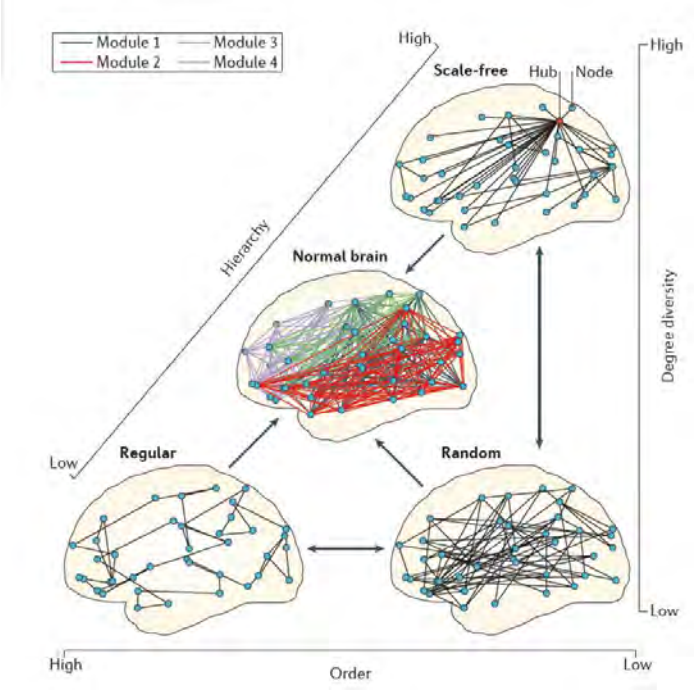

Figure 1.3.9. Graphical representation of different types of networks.
The healthy human brain has a SW organization, which consists of dense local connections (i.e. as in regular networks), short path lengths (i.e. as in random networks) and the presence of highly connected hubs (i.e. as in scale free networks). Thus, the human brain is also a hierarchical, modular network. Reproduced from Stam (2014).

Interestingly, several disorders, such as Alzheimer's disease and schizophrenia, have been associated with either more regular or random topology (Bassett & Bullmore, 2009; Bassett, Nelson, Mueller, Camchong, & Lim, 2012; Liu et al., 2008; Stam, 2014) in comparison to healthy controls who had preserved SW organization. Additionally, severe brain-injury has been shown to have a high impact on individual nodes - hubs - highly connected, central brain nodes, essential for regulating and maintaining the delicate balance between segregation and integration essential for efficient brain functioning (Fornito, Zalesky & Breakspear, 2015; Seeley et al., 2009).

1.4 The restless brain: resting-state functional brain networks (RSNs) in healthy subjects

1.4.1 Functional differentiation

The human brain is composed of a large number of regions that differ in their task and function but communicate with each other through dynamic interactions forming brain networks that

underlie complex cognitive processes. Thus, the human cerebral cortex seems to have attributes that promote modularity (differentiation) and efficient brain-wide communication (integration) (van den Heuvel & Sporns, 2013).

As previously described, rs-fMRI studies have identified multiple RSNs comprised of spatially remote but functionally connected regions underlying specialized cognitive processing. The RSNs consistently reported across studies include: the default mode network (DMN), visual networks, auditory and sensorimotor network, bilateral executive control and the salience network (Figure 1.4.1; Damoiseaux et al., 2006; Heine et al., 2012; Laird et al., 2011; Rosazza, & Minati, 2011; Shirer, Ryali, Rykhlevskaia, Menon, & Greicius, 2012; Smith et al., 2009).

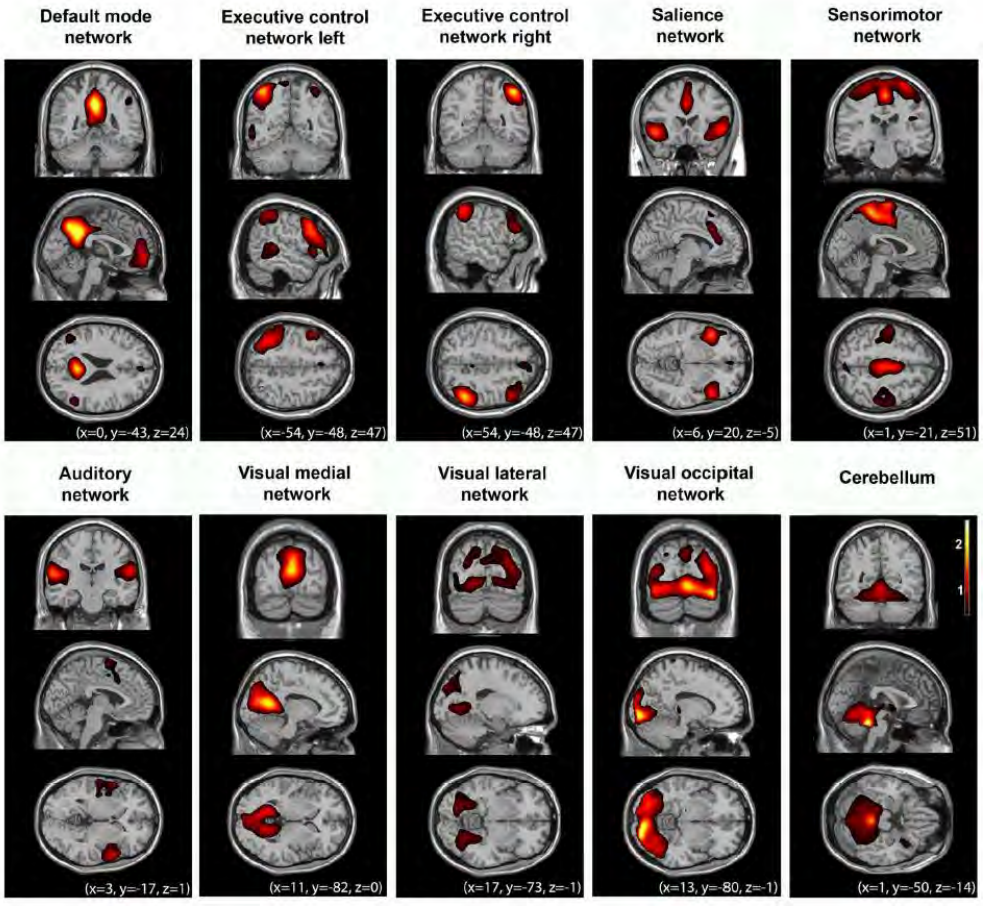

Figure 1.4.1. Multiple cerebral networks that can be identified with ICA applied on rs-fMRI.
Data acquired in healthy controls. Reproduced from Heine et al. (2012).

DMN has been studied extensively, and is the network that received the most attention in clinical and research setting (Hannawi, Lindquist, Caffo, Sair, & Stevens, 2015; Heine et al., 2012; Rosazza, & Minati, 2011). It consists of midline precuneus/posterior cingulate, lateral parietal cortex/angular gyrus and mesial prefrontal/anterior cingulate cortex. DMN was initially

identified in PET studies, which showed less activation in the corresponding regions during demanding cognitive tasks compared to resting-state condition (Mazoyer et al., 2001; Raichle et al., 2001). Since then, fMRI studies have consistently found synchronous activation in these regions (van den Heuvel & Hulshoff Pol, 2010; Lee et al., 2013), and structural MRI studies have indicated underlying anatomical connections (Figure 1.4.2; Greicius, Supekar, Menon, & Dougherty, 2009; van den Heuvel et al., 2009). Activity in the DMN has been related to self-related and internally directed cognition (Andrews-Hanna, Smallwood, & Spreng, 2014; Raichle, 2015), such as stimulus-independent (spontaneous) cognition and mind-wandering (Fox et al., 2015), autobiographical memory (Buckner, Andrews-Hanna, & Schacter, 2008) and social cognition (Andrews-Hanna & Spreng, 2015).

Multimodal rs-fMRI/DTI studies suggest that the DMN inter-regional resting-state functional connectivity is facilitated through the cingulum bundle (Wang, Dai, Gong, Zhou, & He, 2014), principally connecting the PCC/PreCu and the mPFC (Figley, Bhullar, Courtney, & Figley, 2015; Greicius, Supekar, Menon, & Dougherty, 2009; Van Den Heuvel, Mandl, Kahn, & Hulshoff Pol, 2009; Honey et al., 2009; Khalsa, Mayhew, Chechlacz, Bagary, & Bagshaw, 2014). Moreover, the microstructural organization (i.e. FA) of this white matter tract has been directly related to the level of functional connectivity between these two regions (van den Heuvel, Mandl, Luigjes, & Hulshoff Pol, 2008). In fact, structural-functional coupling seems to be highest in the regions of the DMN, especially in the posteromedial region (Collin et al., 2014; Horn, Ostwald, Reisert, & Blankenburg, 2014; Segall et al., 2012), in comparison to other brain areas.

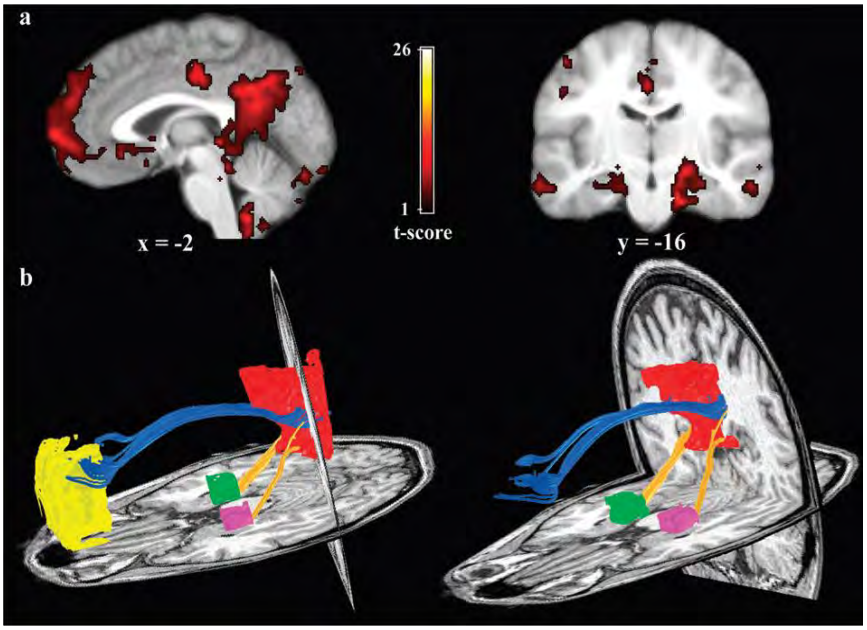

Figure 1.4.2. Functional connectivity reflects structural connectivity in the DMN.
DTI fiber tractography in a single subject demonstrates the cingulum bundle (blue tracts) connecting the PCC to the mPFC. Reproduced from Greicius et al. (2009).

The executive control network (ECN) is mainly identifiable in the medial and superior frontal gyrus, anterior cingulate and super parietal cortex. It has been related to externally-directed cognition, working memory, decision-making in goal directed behavior (Menon & Udin, 2010), with left ECN being more involved in language processing, and the right ECN in perceptual, somesthetic, and nociception processing (Smith et al., 2009; Laird et al., 2011). The salience network (SN), anchored in the anterior insula and dorsal anterior cingulate cortex is implicated in transient detection of salient stimuli, initiation of attentional control and allocation of cognitive resources towards salient stimuli (Uddin, 2014; Menon & Uddin, 2010; Menon, 2015).

During cognitively demanding tasks, executive control network usually shows an increase in activation, whereas DMN shows a decrease, resulting in negative (anticorrelation) relationship between these two networks (Greicius, Krasnow, Reiss, & Menon, 2003; Greicius & Menon, 2004). Some research even suggests that the SN mediates this 'switching' between the activation of the DMN and of the ECN to guide appropriate responses to salient stimuli (Uddin, 2014; Menon & Uddin, 2010).

1.4.2 Functional integration

The human brain sub-networks do not work in isolation but are interconnected and coordinated through a set of brain regions capable of cross-modal complex responses (Tomasi & Volkow, 2011; Wu et al., 2011) serving to distribute and converge specialized information (van den Heuvel & Sporns, 2013). These highly central hub regions maintain long-distance anatomical and functional connections and are metabolically costly, but essential for efficient brain function and cognition (Collin et al., 2014). Also, these regions seem to be more densely interconnected, forming a brain core or rich club (van den Heuvel & Sporns, 2011) serving as the backbone for functional integration across the brain.

Structural and functional "connector" hub regions have been mainly identified in parietal and frontal cortical regions, with some of them spatially overlapping with midline DMN nodes, suggesting its central role in the overall brain network structure (van den Heuvel & Sporns, 2013).

More specifically, the PCC/PreCu complex is frequently identified as a key hub node at DMN and whole brain level, with high correspondence between rs-fMRI and DTI fiber-tracking studies (Hagmann et al., 2008; Horn, Ostwald, Reisert, & Blankenburg, 2014; Van Oort, van Cappellen van Walsum, & Norris, 2014). The importance of posteromedial cortex in the overall brain network interaction was also demonstrated in a lesion stimulation study, where lesions along the cortical midline caused large and widely distributed changes in functional connectivity, in opposed to lesions of primary sensory or motor regions whose effects remained more localized (Alstott, Breakspear, Hagmann, Cammoun, & Sporns, 2009).

1.4.2.1 Key hubs for consciousness emergence: PMC-PCC/PreCu complex

The posteromedial cortex (PMC) has been recently termed as a posterior "hot zone" zone and a good candidate for both full and content-specific NCC (Koch et al., 2016; Tononi et al., 2016). This architectonically discrete region, has been recognized as a critical site integrating an important range of multimodal information (Dehaene & Changeux, 2011). This highly dynamic functional core seems to participate in multiple transitional connectivity networks seemingly playing a critical role in internally/externally directed high-level cognition (Cavanna & Trimble, 2006; Leech & Sharp, 2014). Converging data from physiological, pharmacological (Heine et al., 2012; Siclari et al., 2017) and pathological models (Hannawi et al., 2015), suggest the implication of PMC and its long-range functional connections in conscious processing.

Interestingly, a growing body of literature on animal and human studies, suggests a significant heterogeneity in cytoarchitectonic (Vogt & Laureys, 2005; Vogt, Vogt, & Laureys, 2006), structural (Parvizi, Van Hoesen, Buckwalter, & Damasio, 2006; Zhang et al., 2014) and functional connectivity maps characterizing different sub-region of the PMC (Bzdok et al., 2015; Zhang and Li, 2013). Recent studies highlighted that the "metastable" functional connectivity detected in this region follows a complex ventral/dorsal and anterior/posterior gradient, partially overlapped across anatomically defined sub-regions (i.e. precuneus (PreCu) and posterior cingulate cortex (PCC)) (Bzdok et al., 2015; Cauda et al., 2010; Margulies et al., 2009; Zhang & Li., 2012).

On the other hand, findings in human and non-human primates also suggest functional unity within the PMC given the strong local interconnections among its components and their shared connections with other neural structures (Cauda et al., 2010; Parvizi et al., 2006).

In healthy subjects, most rs-fMRI studies suggest a subdivision of PMC on dorsal and ventral portions, the dorsal corresponding to the PreCu and further divided into anterior, central and posterior subareas (Cauda et al., 2010; Margulies et al., 2009). A rs-fMRI study with 225 healthy individuals showed three functional subdivisions of the PreCu, the dorsal-anterior, dorsal-posterior, and the ventral PreCu shown to connect to other regions of the DMN (Figure 1.4.3; Zhang & Li, 2012). Multiple studies also indicate that the anterior and posterior portions of the PreCu are differentially associated with several cognitive functions such as visuo-spatially guided behavior, mental imagery and episodic memory retrieval (Cavanna & Trimble, 2006).

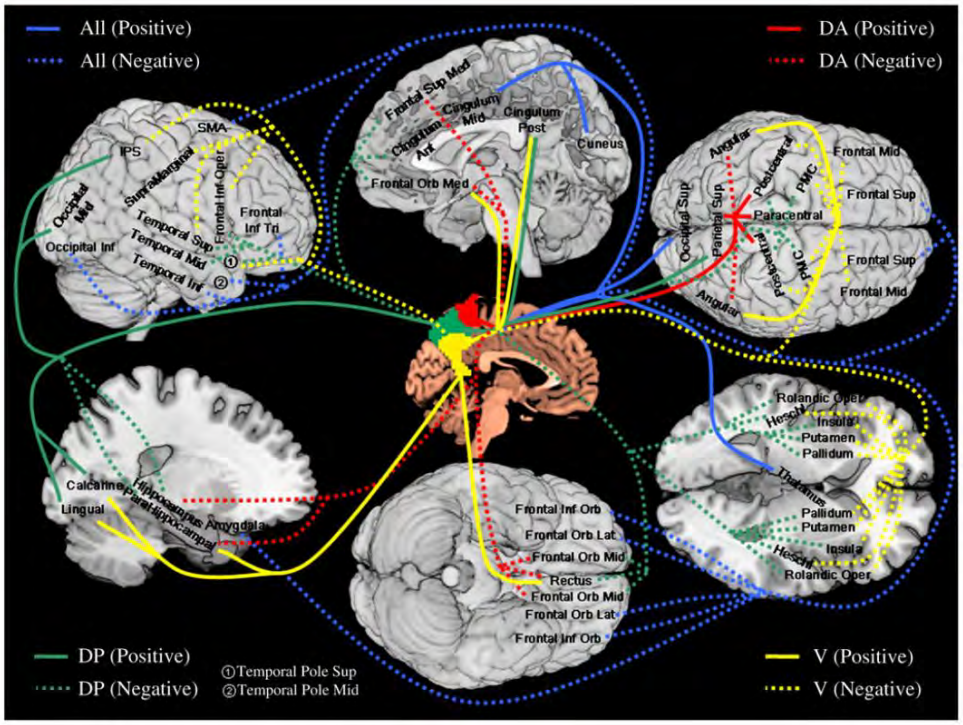

Figure 1.4.3. A summary of functional connectivity of different sub-areas of the precuneus.
Connectivity of the dorsal-anterior (DA, red), dorsal-posterior (DP, green), and ventral (V, yellow) precuneus, with blue indicating connectivity with all three regions. Positive and negative connectivities are each indicated by solid and dashed line. Reproduced from Zhang & Li (2012).

The ventral PMC most often corresponds to the PCC (Cauda et al., 2010; Margulies et al., 2009) and is further segregated into dorsal (dPCC) and ventral portions (vPCC) (Vogt et al., 2006; Yu et al., 2011; Zhang & Li, 2012). Recent study (Cha, Gibson, & Lee, 2017) suggested that PCC could be separated into two sub-regions (i.e. dPCC and vPCC) based on global functional connectivity, or four sub-regions based on local functional connections and hierarchical clustering. As the PreCu, the PCC also shows a complex pattern of connectivity with other intrinsic networks (Leech & Sharp, 2014; Figure 1.4.4), with the ventral PCC showing strong functional connectivity with the DMN, and the dorsal PCC exhibiting a more transitional connectivity, linking and coordinating the activity across multiple resting state networks such as the frontoparietal control network, dorsal attentional network, sensorimotor and salience network (Leech, Braga, & Sharp, 2012).

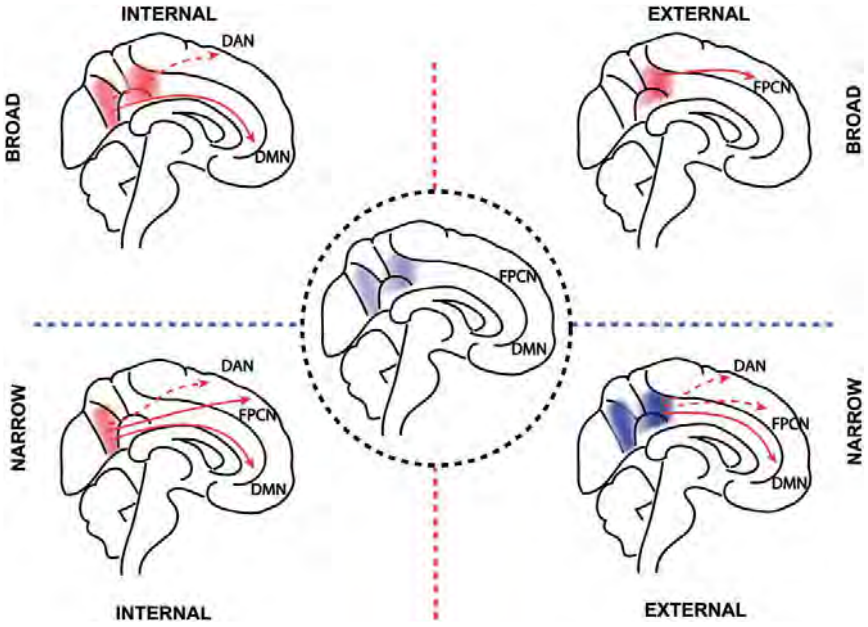

Figure 1.4.4. Illustration of the proposed theoretical account of the PCC, combining the three dimensions of (i) arousal; (ii) internal/external focus; and (iii) breadth of attentional focus.
Solid arrows signify increased functional connectivity, broken arrows greater anticorrelation. Red areas within the PCC signify relatively increased neural activity, blue areas relatively decreased activity. DAN = dorsal attention network, FPCN = frontoparietal control network. Reproduced from Leech & Sharp (2014).

Interestingly, the potential consciousness-related role of the dPCC was recently supported by the study of Herbet and colleagues (2014, 2015) who applied cortical and white matter electrical stimulations throughout the surgical procedure of patients with slow growing tumor situated in the PMC. It was concluded that the transient breakdown of the posterior cingulate cortex, particularly dorsal PCC, and its underlying anatomical connectivity in both hemispheres, impacts conscious information processing (i.e. inducing a dream-like state, confusion and behavioral unresponsiveness).

Thus, all of these functional PMC sub-regions have been differentially associated with several intrinsic brain networks and consequently have been implicated in a variety of cognitive functions (Cavanna & Trimble, 2006; Leech & Sharp, 2014). Nevertheless, it must be noted that the DOC neuroimaging literature traditionally explored PMC as a homogenous structure and failed to describe such a functional segregation in pathological conditions (Norton et al., 2012; Silva et al., 2010; Vanhaudenhuyse et al., 2010).

2 Chapter II – State of the art

2.1 Resting-state functional connectivity in acquired disorders of consciousness

2.1.1 DOC neuroimaging-based diagnosis

Rs-fMRI studies with DOC patients most frequently indicate a decrease in activity and connectivity within the midline and subcortical regions associated with the default mode network (Table 2.1.1; Hannawi et al., 2015; Heine et al., 2012). Importantly, the magnitude of reduction in DMN functional connectivity (FC) seems related to the degree of consciousness impairment, with a greatest decrease in coma and UWS compared to MCS (Demertzi et al., 2015; Rosazza et al., 2016; Roquet et al., 2016; Soddu et al., 2011, 2012; Vanhaudenhuyse et al., 2010).

Reduced functional connectivity within other RSNs has also been associated with the loss of consciousness. These include the left and right executive control, frontoparietal, auditory, attention and salience networks (Demertzi et al., 2014, 2015; Qin et al., 2015; Ovadia-Caro et al., 2012; Kirsch et al., 2017; Roquet et al., 2016; Soddu et al., 2016; Tsai et al., 2014). It has recently been implied that the FC within the salience network (supragenual anterior cingulate cortex, left anterior insula) correlates with the current level of consciousness (UWS vs. MCS), whereas DMN (PCC, left lateral parietal cortex) connectivity predicts recovery of consciousness (Qin et al., 2015).

Additionally, several fMRI studies with passive speech processing tasks, suggested that patients with higher consciousness levels and better recovery have a larger response in the language-related brain network coupled with a deactivation in the DMN (Crone et al. 2011; Tomaiuolo et al., 2016; Wang et al., 2015).

There results imply that interactions within a single RSN cannot be regarded independently from the functional dynamics in other networks. Accordingly, a recent study has shown that UWS and MCS patients don't only have a decrease in positive correlation within the DMN, but also in negative correlation between the external (task-positive) network and DMN, which seems to reappear in EMCS patients (di Perri et al., 2016). The importance of network

interaction and balance between positive and negative connectivity within RSNs was also demonstrated in the study of Amico and colleagues (2017). They showed that patients with lower levels of consciousness and higher functional disability exhibit a reduction in positive visual-sensory motor connectivity and a decrease in DMN-FPN negative connectivity (Amico et al., 2017).

In addition to hypoconnectivity, pathological hyperconnectivity in UWS and coma patients has been found in regions involved in externally directed cognition (di Perri et al., 2016; He et al., 2014a; Wu et al., 2015). Hyperconnectivity may be related to compensatory brain plasticity processes (di Perri et al., 2014; Fornito, Zalesky, & Breakspear, 2015; Hillary et al., 2015), however, the significance of pathology-related increase in functional connectivity is still under debate (Hillary et al., 2015). In addition, cross-hemispheric integration of information seems to play an important role, as some studies implied a loss of inter-hemispheric connections in extrinsic and DMN networks in DOC patients, irrespective of the etiology (Amico et al., 2017; Ovadia-Caro et al., 2012; Zhang et al., 2017).

Finally, the study of Achard and colleagues (2012), has been the first and only rs-fMRI study to investigate the global and local network topology in the acute DOC patients. Their findings showed conserved global network properties (e.g. efficiency, clustering, small-worldness, modularity), but a radical reorganization of high degree or highly efficient hub nodes. Cortical regions (i.e. fusiform gyrus and precuneus) that were hubs in controls were non-hubs in comatose patients, and non-hub regions (i.e. angular gyrus) in controls displayed hub-like properties in patients (Figure 2.1.1). These findings suggested that whole-brain global properties may be homeostatically conserved under severe brain injury, and that consciousness likely depends on the anatomical location of hub nodes in human brain networks.

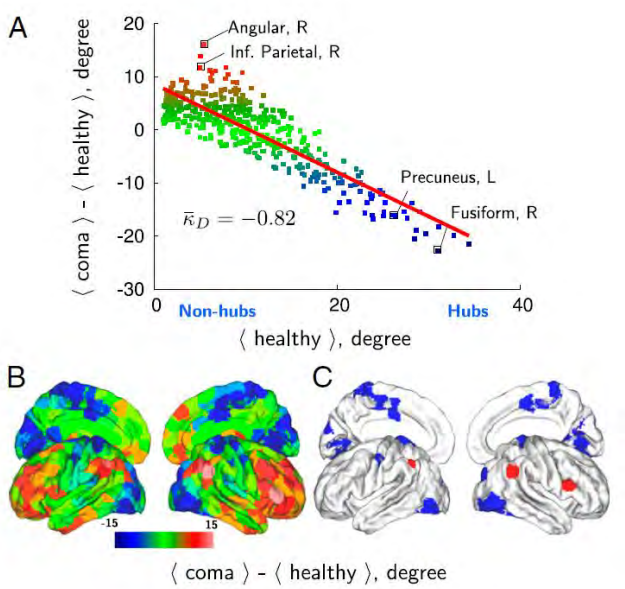

Figure 2.1.1. Hub disruption of functional networks in comatose patients.
The mean degree of each node in the healthy volunteer group (healthy (x axis)) is plotted versus the difference between groups in mean degree of each node (coma−healthy (y axis)). Reproduced from Achard et al. (2012).

Table 2.1.1. Resting-state functional connectivity in DOC.

Author	Method	Type of DOC	Etiology	Delay injury(DOC)/imaging (Mean±SD)	Findings
Cauda et al. (2009)	ICA	3 UWS	2 TBI; 1 mixed	20 months	Dysfunctional DMN, reduced right-hemisphere connectivity.
Vanhaudenhuyse et al. (2010)	ICA	5 coma; 4 UWS; 4 MCS; 1 LIS	2 TBI; 1 anoxia; 11 other	159.8±473.8 days	Reduced DMN connectivity in proportion to severity of consciousness impairment. PreCu connectivity stronger in MCS in comparison to UWS and coma.
Achard et al. (2012)	Seed; Graph theory	17 DOC	12 anoxia; 5 other	3 – 32 days	No significant abnormality of global metrics, but radical reorganization of hub nodes and abnormal variability in modular structure between comatose patients.
Ovadia-Caro et al. (2012)	Seed	1 BI; 2 coma; 2 VS; 2 MCS; 1 LIS	1 TBI; 2 anoxia; 5 other	207±542 days; coma: 13-14 days	Reduced inter-hemispheric extrinsic network connectivity in subjects with impaired versus intact consciousness.
Soddu et al. (2012)	ICA	8 UWS; 1 MCS; 2 LIS	5 TBI; 3 anoxia; 3 other	349.8±462.1 days;	Fewer connections in the DMN regions in UWS in comparison to controls and LIS; Intact right lateralized DMN connectivity in MCS.
He et al. (2014)	ICA; ALFF	9 UWS; 3 MCS	4 TBI; 3 anoxia; 5 other	2 – 7 months	ICA – diminished activity in the DMN, mainly in the MPFC. ALFF – decrease in PCC/PreCu, ACC, parahippocampal areas (DMN); increase in the insula, lingual gyrus and paracentral gyri (external network).

Crone et al. (2014)	Seed; Graph theory	34 UWS; 25 MCS	10 TBI; 6 anoxia; 5 SAH; 3 mixed; 6 hemorrhage; 13 CPR; 16 other	7 - 9900 days	Reduced modularity in DOC compared to healthy controls. Reduced degree in the medial FR regions and bilateral thalamus. Increased degree in left superior and inferior FR gyrus. Reduced CC in PCC and right insular cortex. LE of the PMC (PreCu) differed between the UWS and MCS patients. CC in the right middle FR gyrus and the FR pole correlated with the CRS-R score.
Huang et al. (2014)	Voxel-wise; Seed	6 UWS; 5 MCS	6 TBI; 5 non-TBI	90±42.4 days	FCS and ALFF decreased in ACC, MPFC and PCC.
Tsai et al. (2014)	ICA; ReHo; ALFF	3 coma patients; 12 not classified	7 ischemic stroke; 8 hemorrhagic stroke	Within 24h	Lower ALFF and ReHo in PCC and PreCu, respectively. Decrease in DMN FCS, correlated with level of consciousness. Lower FCS in executive and attention networks.
Liu et al. (2014)	Graph theory	5 UWS; 8 healthy controls undergoing propofol anesthesia	2 TBI; 3 other	42 - 66 days	Scale-free distributions of node size and node degree were present across wakefulness, propofol sedation, and recovery, despite FC changes. In UWS, the scale-free distribution of node degree was absent, suggesting absent self-organizing processes underlying adaptive reconfiguration of functional interaction.
He et al. (2015)	ICA and Seed	7 UWS ; 2 MCS	2 TBI; 2 anoxia; 5 other	3 – 7 months	Decrease in FCS between the mediodorsal thalamus and DMN regions, predominantly in mPFC and PCC/PreCu.
Demertzi et al. (2014)	ICA	5 Coma ; 24 VS; 24 MCS	17 TBI; 11 anoxia; 30 other; Coma - 4 CVA; 1 TBI	816.8±1783 days; coma: 5-38 days	More neuronal components in RSNs in healthy compared to UWS and coma patients.

Demertzi et al. (2015)	ICA	6 Coma; 19 UWS; 26 MCS	Coma – 2 TBI; 3 SAH; 1 Stroke	2 - 7814 days; coma: 2 -38 days	Reduced to absent connectivity in six RSNs (DMN, FPN, SAL, AUD, SM, VIS) in coma patients.
DiPerri et al. (2016)	Seed	21 UWS; 24 MCS; 13 EMCS	29 TBI; 14 anoxia; 7 mixed; 8 other	1-312 months	Lower positive DMN connectivity in DOC compared to controls. Negative DMN connectivity present only in healthy and EMCS. UWS and MCS showed pathological between-network positive connectivity.
Roquet et al. (2016)	ICA	12 UWS; 5 LIS	2 TBI; 9 anoxia; 1 ischemia; 5 other	3-180 days	Number of RSNs, total RSNs and high-level cognitive RSNs differentiated controls and LIS from UWS. DMN had the highest accuracy, FPN had maximum specificity but more limited sensitivity.
Amico et al. (2017)	connICA	2 coma; 17 UWS; 21 MCS; 13 EMCS; 4 LIS	28 TBI; 29 non-TBI	>28 days	Decrease in positive visual- sensorimotor network connectivity and DMN-FPN negative connectivity, associated with lower levels of consciousness.
Kirsch et al. (2017)	Seed	6 UWS; 2 MCS	2 TBI; 6 other	23–693 days	Decreased FC in DMN, salience, left and right ECN, auditory, sensorimotor RSNs. Lower connectivity between thalamus and RSNs.

ACC – anterior cingulate cortex; ALFF - amplitude of low-frequency fluctuation; AUD – auditory network; CC – clustering coefficient; CPL – characteristic path length; CPR - cardiopulmonary resuscitation; CVA – cardiovascular accident; DMN – default mode network; FCS – functional connectivity strength; FPN – frontoparietal network; FR – frontal; HBI – hypoxic-ischemic brain injury; LE – local efficiency; PC – participation coefficient; ReHo - regional voxel homogeneity; SAH - subarachnoid hemorrhage; SAL – salience network; SM – sensorimotor network; TPJ – temporoparietal junction; VIS – visual network.

The potential consciousness-related hub nodes have been identified in a recent coordinate-based meta-analysis (13 studies: 272 patients, 259 healthy controls), which pointed to the medial dorsal thalamus (mDor) and the PCC/PreCu complex as most frequently affected in DOC (Hannawi et al., 2015), with the FC of the latter correlating with the magnitude of impairment of consciousness (Soddu et al., 2012; Vanhaudenhuyse et al., 2010). Other regions with disrupted functional connectivity included the left cingulate gyrus, medial temporal lobe, middle frontal lobe, and bilateral medial dorsal nuclei of the thalamus. In fact, all DOC patients showed a disruption in the cingulate gyrus, whereas UWS patients showed impairment in bilateral mDor thalamus compared with the right mDor thalamus in MCS. In a separate study, He and colleagues (2015) found a significant reduction in DOC in the functional connectivity between the mDor thalamus and the regions within the DMN, including PCC/PreCu and mPFC, illustrating the potential role of cortico-thalamic circuits in conscious processing. In addition, fMRI studies imply low frequency fluctuations (ALFF) or regional voxel homogeneity (ReHo) (He et al., 2014; Tsai et al., 2014; Huang et al., 2014) in the PreCu/PCC complex, suggesting low activity in these sub-regions. This is supported by PET studies showing a significant reduction in DMN-PCC/PreCu metabolism, related to clinical severity (Kim, Kim, An, & Im, 2010; Silva et al., 2010; Thibaut et al., 2012).

Anticorrelation in rs-fMRI

Although there has been an overwhelming number of studies investigating resting-state functional connectivity, negative correlation or anticorrelation has frequently been ignored or not assessed properly. This is partially due to some studies showing that these anticorrelation can be artificially induced by conventional fMRI preprocessing methods like global signal regression (Murphy et al., 2009; Weissenbacher et al., 2009). Other studies emphasized greater between-subject variability, higher temporal fluctuations (dynamic changes) and a weaker connectivity strength of negative in comparison to positive correlations, therefore making them harder to interpret (Chang & Glover, 2010; Cole et al., 2010).

Chai and colleagues (2012) compared the two preprocessing methods, the global signal regression and the component base noise reduction method (CompCor, Behzadi et al., 2007) and showed robust anticorrelation between the default and task-positive network regions independently of the choice of the preprocessing method. Specificity of negative correlations was equal or higher under the CompCor method, and the sensitivity and the specificity of positive correlations detection was better when combining this method with band-pass filtering and the movement parameter regression (Chai et al., 2012).

Furthermore, anticorrelation between individual brain hubs and resting state networks has consistently been reported in healthy subjects with and without global signal regression (Chang & Glover, 2009; Fox et al., 2009; Fox & Greicius, 2010; Fransson, 2005; Gopinath et al., 2015; Liu et al., 2015; Parente et al., 2017; Uddin et al., 2009) and it has been shown to increase with age (Chai et al., 2014). These findings suggest a potential biological origin of negative correlations, as further implicated in studies showing anticorrelated electrophysiological fluctuations (Keller et al., 2013; Popa et al., 2009) and structural connections between regions shown to be functionally anticorrelated (Fox et al., 2009; Honey et al., 2009; Skudlarski et al, 2008).

A recent study suggested (Chen et al., 2017) that the inconsistency regarding DMN anticorrelation across different studies, might be due to differences in seed-coordinates used in the analysis, in addition to differences in preprocessing steps. The same authors showed that the ventral branch of the DMN (vDMN) yielded significantly weaker anticorrelations in opposed to the dorsal branch of the DMN (dDMN).

Nevertheless, there is an ongoing debate on the qualitative interpretation of these anticorrelations as there has not yet been a consensus on their exact significance in the whole-brain organization.

2.1.2 Prognostic value of resting-state functional connectivity in DOC

The association between functional neuroimaging data and outcome in disorders of consciousness was assessed in a small number of studies (Table 2.1.2) (Table 2.1.3).

Studies with chronic DOC implied a relatively preserved DMN connectivity in patients who recovered as opposed to patients who remained in UWS (Rosazza et al., 2016; Kondziella et al., 2017), with an emphasis on PCC/PreCu connectivity (Qin et al., 2015; Wu et al., 2015).

In another graph theoretical project, a group of recovered patients exhibited significantly increased connectivity degree in the mPFC, as compared to patients who had not recovered consciousness 3 months after the initial MRI scan (Liu et al., 2017), suggesting a potential beneficial compensatory role of functional hyperconnectivity.

To our knowledge, there have only been four rs-fMRI studies aiming to assess the prognostic value of FC changes in the acute stage of DOC (i.e. coma) (Table 2.1.3).

Two of these studies indicated preserved DMN connectivity (Norton et al., 2012), with a greater PCC/PreCu connectivity strength in anoxic BI patients who eventually regained consciousness as opposed to those who did not (Koenig et al., 2014). Another study, including anoxic and TBI patients, concluded that comatose patients who went to recover had a stronger connection between the PCC-centered seed (not the PreCu-centered seed) and the mPFC as opposed to patients who had an unfavorable outcome (Silva et al., 2015; Figure 2.1.2).

Finally, the most recent study, including cardiac arrest coma patients, showed higher within-DMN connectivity and greater anticorrelation between the salience network (SN) and DMN, and SN and the executive control network in patients with a 1-year favorable outcome compared to patients who did not regain consciousness (Sair et al., 2017).

Table 2.1.2. Prognostic value of resting-state FC in chronic DOC patients.

Author	Method	Type of DOC	Etiology	Delay injury/imaging (Mean±SD)	Delay inclusion/ outcome	Outcome assessment	Reported outcome	Findings
Qin et al. (2015)	Seed	56 UWS; 29 MCS; 48 BI	109 TBI; 24 non-TBI	UWS – 96d; MCS – 119d; BI -149 days	3 months	GOS	23 emerged from UWS (UWS-E; GOS >3); 30 remained in UWS (UWS-R; GOS ≤3).	Higher PCC-left lateral parietal cortex FCS in UWS-E in comparison to UWS-R.
Wu et al. (2015)	Voxel	14 coma; 18 UWS; 27 MCS; 40 BI with communicative abilities	82 TBI; 17 non-TBI	coma –38.6d; UWS – 85.6d; MCS – 80.1d; BI - 104.1 days	3 month	GOS	GOS in subgroups: BI (4.3±0.9); MCS (3.0±0.8); UWS (2.4±0.6); coma (2.6±0.8)	Higher FCS in DMN and SN/ECN during baseline predicts better recovery; FCS in PCC/PreCu predicts whether UWS/VS and coma patients would regain consciousness (accuracy 81.25%).
Rosazza et al. (2016)	Seed; ICA	72 UWS; 36 MCS; 11 severe disability	36 TBI; 42 anoxia; 41 vascular	26 months (2–252 months)	12 - 24 months	CRS-R	2 UWS patients evolved to MCS	Preserved DMN connectivity in 2 UWS patients who evolved to MCS.
Kondziella et al. (2017)	Seed	2 Coma; 1 UWS; 3 MCS-; 1 MCS+	1 TBI; 6 non-TBI	5 – 25 days	3 months	mRS	1 death; 1 UWS; 1 MCS+; and 4 conscious states	All patients with preserved DMN regained consciousness (MCS + or better) at follow-up.
Liu et al. (2017)	Seed	17 UWS; 17 MCS	MCS: 11 TBI, 2 anoxia, 4 CH; UWS: 12 TBI, 3 anoxia, 2 CH	72.4±52.2 days	3 months	GOS	11 recovered consciousness; 18 non-recovered; 5 withdrawn	Enhanced mPFC connectivity against weakened PCC/PreCu and lateral parieto-temporal cortices, found in MCS but not in UWS. Increased mPFC connectivity significantly associated with recovery.

BI – brain injury; CH - cerebral hemorrhage; CRS-R – Coma Recovery Scale – Revised; DMN – default mode network; ECN - executive control network; FCS – functional connectivity strength; GOS – Glasgow Outcome Scale; MRS - Modified Rankin Scale; SN – salience network.

Table 2.1.3. Prognostic value of resting-state FC in coma patients.

Author	Method	Number of patients	Etiology	Delay injury/imaging	Delay inclusion/ outcome (M±SD)	Outcome assessment	Reported outcome	Findings
Norton et al. (2012)	ICA	13 coma	13 CA	~ 1 week	3 months	GOS	2 Good (GOS -5); 11 Bad (GOS -1)	DMN not observed in those who remained unconscious.
Koenig et al. (2014)	ICA	17 coma	17 CPA	4 – 7 days	36.3±41.7 days	CPC	8 Good (CPC 1-2); 9 Bad (CPC 3-5)	Higher FCS in the PCC and PreCu in patients with good outcome.
Silva et al. (2015)	Seed	27 coma	14 TBI; 13 anoxia	3 – 9 days	3 months	CRS-R	12 UWS; 11 MCS; 4 REC	Higher FCS between PCC (not PreCu) and mPFC in patients with good outcome.
Sair et al. (2017)		46 coma	46 CA	12.6±5.6 days	12 months	CPC	11 Good (CPC 1-2); 35 Bad (CPC 3-5)	Higher within-DMN connectivity and greater anticorrelation between SN and DMN and between SN and ECN, in FO compared with UFO patients.

CA – cardiac arrest; CPA – cardiopulmonary arrest; CPC - Cerebral Performance Category; CRS-R – Coma Recovery Scale – Revised; DMN – default-mode network; ECN – executive control network; FO – favorable outcome; GOS - Glasgow Outcome Scale; SN – salience network; UFO – unfavorable outcome.

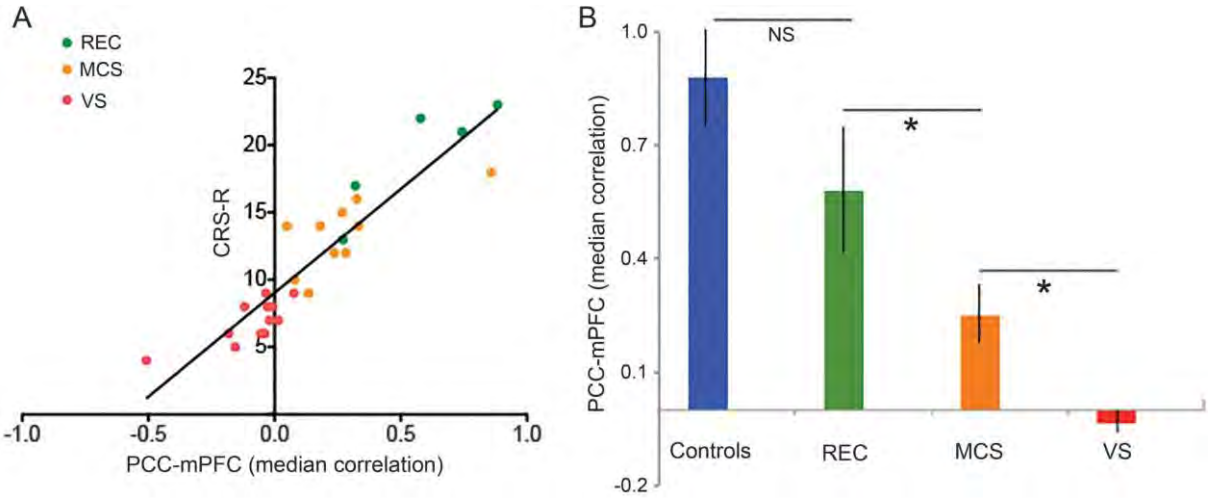

Figure 2.1.2. Predictive role of PCC-mPFC coupling measured during coma state and neurologic outcome. *Reproduced from Silva et al. (2015).*

2.1.3 Resting-state FC-related signatures of brain injury mechanisms

Most of the functional connectivity studies performed the analysis without considering the differences in DOC etiology (traumatic, anoxic or vascular brain injury) (Hannawi et al., 2015). Some studies included patients with the same etiology (Koenig et al., 2014; Norton et al., 2012) or used it as a nuisance variable in their analysis (Amico et al., 2017), in order to control for possible confounding effects of pathology-related mechanisms. In a recent multimodal study with structural MRI, FDG-PET and rs-fMRI data, the level of DMN integrity had comparable diagnostic power of impairment in consciousness irrespective of etiology (Rosazza et al., 2016). Nevertheless, the diagnostic value of rs-fMRI was consistently highest for anoxic, followed by traumatic, and then by vascular etiology. Silva and colleagues (2015) showed the prognostic value of PCC-centered functional connectivity in both TBI and anoxic BI patient groups, implying the involvement of the posteromedial cortex in conscious processing irrespectively of coma etiology.

2.2 Structural network integrity in coma, UWS and MCS

2.2.1 Diagnosis and patient's stratification

Findings from fMRI studies are supported with evidence of structural disconnections within/between midline cortical (Annen et al., 2016; Fernández-Espejo et al., 2012; Lant et al., 2016) and thalamo-cortical networks (Weng et al., 2017; Zheng et al., 2017), associated with the degree of impairment of consciousness (Di Perri et al., 2016; Fernández-Espejo et al., 2012; Lant, Gonzalez-Lara, Owen, & Fernández-Espejo, 2016) (Table 2.2.1).

Voxel based morphometry studies indicate widespread structural damage to cortical (i.e. lateral hemispheres, midline structures) and subcortical areas (i.e. brainstem, thalami, cerebellum) (Di Perri et al., 2016), with more injury to the bilateral PCC/PreCu and vmPFC in non-traumatic UWS compared to non-traumatic MCS (Guldenmund et al., 2016).

A recent DTI study, explored the structural integrity of fiber tracts connecting the nodes of the mesocircuit and the DMN in patients with DOC (Lant et al., 2016). There findings suggested extensive damage to the PreCu/PCC-related connections, but relatively spared subcortico-subcortical connections (Figure 20). According to authors, the preservation of the striato-pallidal connections and the disconnection between the PreCu and these two regions may indicate the role of the PreCu in the dysregulation in the mesocircuit system[1] and more generally in the disrupted functional brain network dynamics in DOC patients.

[1] *Anterior forebrain mesocircuit"* hypothesis (Schiff, 2010, Giacino et al., 2014) suggests that a loss of excitatory output from the central thalamus to diffuse cortical areas has a causative role in the disorders of consciousness. Such circuit dysfunction is thought to be caused by the loss of the inhibitory striatal output to the globus pallidus (interna) resulting in pallidal disinhibition and subsequent excessive inhibition of the thalamus.

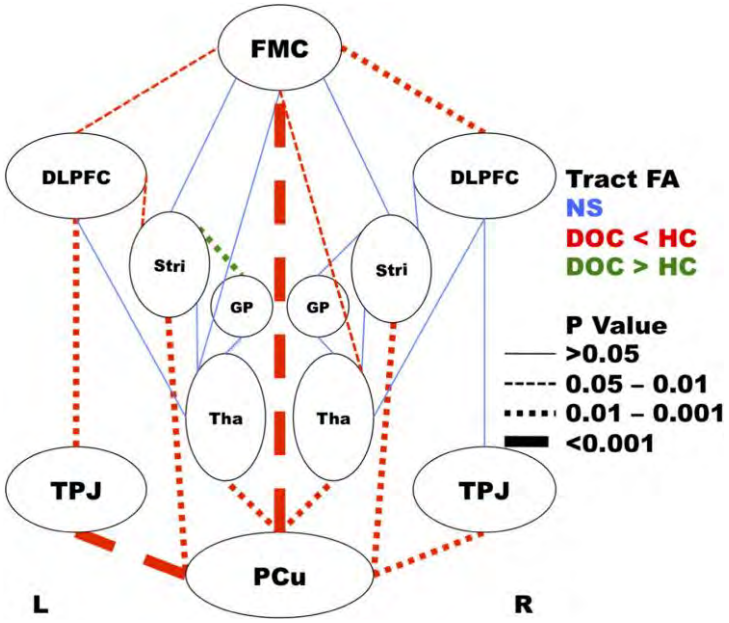

Figure 2.2.2.2.1. Individual tract analysis comparing FA values between DOC patients and healthy controls. *HC: healthy control, FMC: frontal medial cortex, DLPFC: dorsolateral prefrontal cortex, Stri: striatum, GP: globus pallidus, Tha: thalamus, TPJ: temporoparietal junction, PCu: precuneus, L: left hemisphere, R: right hemisphere. PCu–FMC tract is considered midline. Reproduced from Lant et al. (2016).*

Table 2.2.1. Structural changes in DOC.

Reference	Method	Type of DOC	Etiology	Delay injury(DOC)/imaging (M±SD)	Findings
Coma					
van der Eerden et al. (2014)	DTI/Seed-based	89 coma patients	40 TBI ; 49 CA	5–57 days	Aberrant AD and RD in TBI and CA patients compared to controls in almost all of the explored ROIs (i.e. brainstem, CP, CC). AD in cerebral hemispheres lower in CA than in TBI in 6/12 ROIs. Higher RD in TBI in 8/12 ROIs (i.e. IC, SS, SLF, EC, CR). Diffusivity values were symmetrically distributed in CA, but not in TBI.
Chronic DOC					
Newcombe et al. (2010)	DTI/Seed-based analysis; whole-brain tractography; task fMRI	12 UWS	7 TBI; 5 HBI	105-1518 days	FA significantly decreased and ADC increased in all patients compared with controls, in whole-brain WM, anterior and posterior CC. Higher ADC in whole-brain GM and thalamic ROIs. Increased ADC in brainstem regions (dorsal and ventral midbrain and pons) only in TBI. CRS-R positively correlated to central WM and negatively correlated to central ADC in all patients, irrespective of etiology.
Fernández-Espejo et al. (2012)	DTI/ROI-based fiber tracking	19 UWS; 27 MCS; 6 EMCS	32 TBI; 21 non-TBI	1–191 days	Decrease in FA in the WM pathway connecting the PCC/PreCu with the thalamus, in DOC vs. controls. FA in this pathway and other posterior WM connections (PCC/PreCu–TPJ; TPJ–thalami) correlated with the level of consciousness.
Yao et al. (2015)	DTI (TBSS); rs-fMRI	11 DAI patients with DOC	11 TBI	2 - 11 days	Lower FA in genu of the CC, right EC and SCR, left SCP and PTR. Significant positive correlation between FA in left PTR and SCP, and GCS.
Guldenmund et al. (2016)	Structural MRI - VBM	16 UWS; 45 MCS	26 TBI; 12 anoxia; 15 CVA; 4 mixed; 4 other	5 – 3342 days	TBI related to more injury in the brainstem, midbrain, thalamus, hypothalamus, basal forebrain, cerebellum, and posterior CC, in comparison to non-TBI. Bilateral PCC/PreCu and vmPFC more injured in non-TBI UWS compared to MCS. Left cerebral cortex more damaged in MCS- in comparison to MCS+.

Di Perri et al. (2016)	FDG-PET; rs-fMRI; structural MRI-VBM	21 UWS; 24 MCS; 13 EMCS	29 TBI; 14 anoxia; 7 mixed; 8 other	1 - 312 months	Consciousness-dependent increase in GM volume in almost the whole of lateral hemispheres, in the midline structures, including thalami and the cerebellum.
Lant et al. (2016)	DTI/ROI-based probabilistic tractography;	4 UWS; 3 MCS; 1 EMCS	3 TBI; 5 HBI	3523±2914 days	Lower FA in bilateral subcortico-cortical fiber tracts in DOC patients, in all tracts involving the PreCu, right hemisphere thalamus–FMC, bilateral DLPFC–FMC, left DLPFC–TPJ, and left striatum–DLPFC. Higher FA in left striatum–globus tract. Significant correlation between FA in left subcortico-cortical, bilateral cortico-cortical fiber tracts and CRS-R scores.
Weng et al. (2017)	DTI/ROI-based probabilistic tractography; Graph theory/NBS	6 UWS; 7 MCS	4 TBI; 7 HBI	3 – 40 weeks	Reduced connectivity between the BG, thalamus, and frontal cortex; Reduced FA and increased RD in WM of the DOC patients - decreased FA in the bilateral anterior and posterior limbs of the IC and the bilateral superior, anterior, and posterior CR; Decreased nodal efficiency in BG and left amygdala. Decreased degree in the BG, left frontal, temporal, parietal, and occipital cortex. Nodal degree in the right angular gyrus negatively correlated with the CRS-R score.
Zheng et al. (2017)	DTI/ROI-based probabilistic tractography	10 UWS; 7 MCS-; 8 MCS+	17 TBI; 8 non-TBI	3 - 30 months	UWS patients had reduced WM connectivity in thalamocortical circuits (frontal, temporal, sensorimotor), as compared to MCS+, but more pulvinar-occipital connections when compared to MCS-. MCS- had less thalamo-premotor and thalamo-temporal connectivity than MCS+. Thalamo-cortical tracts (frontal, parietal, temporal) had 100% accuracy in DOC group discrimination.

M – mean; SD – standard deviation; BG – basal ganglia; HBI- hypoxic ischemic BI; NBS – network-based statistics; AD – axial diffusivity; RD – radial diffusivity; MD – mean diffusivity; ADC – apparent diffusion coefficient; FA – fractional anisotropy; TBSS - Tract-Based Spatial Statistics; GM – gray matter; WM – white matter; CC – corpus callosum; EC - external capsule; SCR - superior corona radiate; SCP - superior cerebellar peduncle; PTR - posterior thalamic radiation; IC – internal capsule; EC – external capsule, CR – corona radiate; SLF- superior longitudinal fasciculus, BG – basal ganglia; DLPFC– dorsolateral prefrontal cortex; FMC – frontal medial cortex; TPJ - temporo-parietal junction; IP – inferoparietal.

2.2.2 DOC patient's neuroprognostication

Despite the growing number of studies and some recent advances in structural MRI, we are still lacking a complete understanding of structural substrates of loss and recovery of consciousness. The first study that raised the possibility of DTI being able to detect axonal regrowth and neuronal plasticity potentially underlying late recovery, was the one of Voss and colleagues (2006). Their case-report described a patient who recovered reliable expressive language after 19 years in MCS. This remarkable improvement was coupled with a notable increase in resting metabolism and anisotropy within the midline cerebral (medial parietal, occipital) white matter. One recent study implied an increase in radial diffusivity in the left superior cerebellar peduncle and a decrease in fractional anisotropy in the right sagittal stratum in coma and UWS patients who did not regain consciousness at a 3-month follow up (Wu et al., 2016).

However, not many studies have explored the prognostic value of structural integrity in DOC patients, and none have focused on the prognostic value of DMN structural connectivity (Table 2.2.2). Some research did include coma patients, but the analyses were primarily focused on predicting a dichotomized outcome (favorable neurological recovery vs. unfavorable outcome or death) without distinguishing different DOC diagnostic categories (UWS vs. MCS+/- vs. REC), with some patients exhibiting impairment in consciousness and others having normal consciousness levels with some neurocognitive difficulties.

Nevertheless, the present chapter will briefly describe the existing structural-diffusion MRI studies in coma patients, as some show promising results in terms of prognostics and better understanding of brain injury mechanisms in DOC patients (Table 2.2.3).

In recent years, there have been some interesting studies assessing whether the patterns of DWI abnormalities and quantitative regional apparent diffusion coefficient (ADC) values may have prognostic value in post cardiac arrest coma patients (Cavaliere et al., 2015; Greer & Wu, 2017; Stevens & Hannawi, 2016). Regional low diffusion values have been found in cortical (i.e. parietal and occipital cortex) and subcortical regions (i.e. thalamus and basal ganglia) in patients with poor outcome (Choi et al., 2010; Hirsch et al., 2014; Ryoo et al., 2015; Youn et al., 2015). In one study, the structural integrity in major WM tracts (i.e. internal capsule, corpus callosum) had higher predictive power in comparison to GM diffusivity coefficient in relation to 1-year functional outcome in cardiac arrest patients (Luyt et al., 2012). Finally, multiple studies have indicated a significant association between a baseline disruption in selected WM tracts (i.e. corpus callosum, cerebral peduncle, corona radiate, internal capsule, inferior longitudinal

fasciculus) and worse functional outcome at 1 year after traumatic brain injury (Dinkel et al., 2014; Galanaud et al., 2012; Perlbarg et al., 2009; Sidaros et al., 2008).

2.2.3 Structural MRI and brain injury mechanisms

A recent ROI-based DTI study showed significant white matter abnormalities in coma patients with anoxic and traumatic brain injury (van der Eerden et al., 2014). Cardiac arrest patients had changes consistent with primary axonal damage (decrease in AD) related to energy depletion from anoxic ischemia, and potential secondary myelin damage (increase in RD). Conversely, structural damage in TBI was most consistent with primary myelin damage, related to mechanical forces exerted on the brain in trauma, and axonal damage, caused either directly by trauma or secondary ischemic damage. The distribution of damage was also different between the etiologies, with anoxic injury mainly affecting the cerebral hemispheres (i.e. sagittal strata, superior longitudinal fasciculus, internal capsule, external capsule, corona radiate), and TBI mostly present in the left hemisphere and central brain (i.e. brainstem, cerebral peduncles, corpus callosum) structures. However, another study found broadly similar DTI abnormalities (diffuse reduction of FA) in the cerebral hemispheres in both TBI and ischemic hypoxic brain injury in UWS patients at minimum 3 months post-injury (Newcombe et al., 2010). Nonetheless, TBI patients had greater damage in brainstem regions (dorsal and ventral midbrain and pons), as indicated by an increase in the apparent diffusion coefficient. These results suggest that the damage in the lower brainstem (and cerebral peduncles), found in the acute stages (van der Eerden et al., 2014), may persist through chronic stages of DOC (Newcombe et al., 2010). This was also suggested in a recent VBM study (Guldenmund et al., 2016), which showed a significant association between time spent in DOC and widespread structural brain injury, with TBI related to more injury in the brainstem, midbrain, thalamus, hypothalamus, basal forebrain, cerebellum, and posterior corpus callosum, compared to non-traumatic cases.

Table 2.2.2. Prognostic value of structural changes in chronic DOC.

Author	Method	Type of DOC	Etiology	Delay injury/imaging	Delay inclusion/ outcome	Outcome assessment	Reported outcome	Findings
Voss et al. (2006)	DTI/Seed-based; PET	2 MCS	2 TBI	6 and 19 years	18 months	Motor, oculomotor, language, verbal fluency	Neurological improvement in one patient	Increased FA within midline cerebral (medial parietal, occipital) WM was correlated with improvement in motor function and an increase in PET resting metabolism in one MCS patient (19y).
Wu et al. (2016)	DTI/Seed-based	8 Coma; 8 UWS; 14 MCS;	Coma - 8 TBI; UWS - 6 TBI, 2 non-TBI; MCS - 13 TBI, 1 non-TBI	10-182 days	3 months	GOS	8 regained consciousness (GOS > 2); 8 did not regain consciousness	Increased RD of left superior CP and decreased FA of right SS in patients who did not regain consciousness.

CP- cerebellar peduncle; FA – fractional anisotropy; GOS – Glasgow Outcome Scale; RD – radial diffusivity; SS – sagittal stratum; WM – white mater.

Table 2.2.3. Prognostic value of structural changes in coma.

Author	Method	Type of DOC	Etiology	Delay injury/imaging (M±SD)	Delay inclusion/outcome	Outcome assessment	Reported outcome	Findings
Perlbarg et al. (2009)	DTI/Voxel-based; TBSS	30 patients; 24 with GCS ≤ 8;	TBI	23 days (5–53 days)	1 year	GOS	15 FO (GOS>3); 15 UFO (GOS≤3)	Decreased FA in ILF, CP, posterior limb of the IC, and posterior CC in UFO compared to FO group.
Luyt et al. (2012)	DTI/ROI-based	57 coma patients	CA	Median=11 (7–17) days	1 year	GOS-E	8 FO (GOS-E ≥5); 49 UFO (GOS-E ≤4)	The prognostic model based on FA values in selected WM tracts (20 ROIs) predicts accurately UFO (94% sensitivity, 100% specificity).

Galanaud et al. (2012)	DTI/ROI-based	105 severe TBI patients who remained in coma ≥7 days	TBI	21 ± 9 days	1 year	GOS-E	65 FO (GOS-E ≥5); 40 UFO (GOS-E ≤4) of which: 21 D, 5 with UWS, 14 MCS	A composite DTI score increased the accuracy of outcome prediction compared with available clinical/radiographic prognostic score.
Silva et al. (2017)	Structural MRI/ROI-based	126 coma patients; additional testing sample of 18 coma patients	CA	16 ± 8 days	1 year	GOS-E	37 survivors; FO: GOS-E ≥5; UFO: GOS-E ≤4)	Decrease of cortical thickness in the frontal cortex and the volume in the thalamus, putamen, and pallidum in patients with UFO. Significant discriminative power of volume changes in frontal cortex, posterior cingulate cortex, thalamus, putamen, pallidum, caudate, hippocampus, and brain stem.

FA – fractional anisotropy; FO – favorable outcome; GOS-E - Glasgow Outcome Scale Extended; TBSS - Tract-Based Spatial Statistics; UFO – unfavorable outcome.

2.3 Neural structure-function relationship in DOC – multimodal neuroimaging studies

Little is known about how structural integrity allows the emergence of functional connectivity in brain-injured patients, as not many multimodal studies have attempted to directly investigate this function-structure relationship in disorders of consciousness (Table 2.3.1). Bruno and colleagues (2011c) showed a highly asymmetrical pattern in FDG-PET and fMRI in two patients, with mostly left lateralized changes, which were complemented with DTI results.

Another study indicated a decline in regional metabolism and WM integrity in the DMN, but preserved function–structure relationship within most regions from this network in DOC, which was even stronger in the thalamus (i.e. thalamo-inferoparietal tract) of those who emerged from the MCS (Annen et al., 2016). The structural integrity of PreCu/PCC-thalamic pathway, as well as that of those connecting the posterior areas of the network, was previously found to be higher in EMCS patients in opposed to MCS and UWS patients (Fernández-Espejo, et al., 2012).

The implication that abnormal brain function may be the consequence to white matter injury, was also demonstrated in a study showing positive correlation between the dysfunction in the postcentral gyrus and structural damage of the left posterior thalamic radiation tract (Yao et al., 2015).

Finally, a recent study found an association between the decrease in effective functional connectivity and global white matter damage in brain-injured patients, and this structure-function relationship was proposed as a potential mechanisms preventing the emergence of consciousness in chronic DOC (Bodart et al., 2017).

Table 2.3.1. Multimodal studies – structure-function association in DOC.

Author	Method	Type of DOC	Etiology	Delay injury(DOC)/imaging	Findings
Bruno et al. (2011c)	DTI (whole-brain tractography); resting-state FDG-PET, fMRI, and EEG	Case report with 1 UWS and 1 MCS patient	2 TBI	6 months and 3 months	Residual right-lateralized hemispheric function on FDG-PET, fMRI, and EEG measurements. Reduction in the number of identified WM tracts in the left hemisphere for UWS patient and a much more symmetrical image for MCS patient.
Yao et al. (2015)	DTI (TBSS); rs-fMRI	11 DAI patients with DOC	11 TBI	2 - 11 days	ALFF of the amygdala and postcentral gyrus correlated with FA of the right EC and left PTR, respectively.
Annen et al. (2016)	FDG-PET; MRI-DWI	7 UWS; 12 MCS; 6 EMCS	12 TBI; 11 anoxia; 1 mixed; 1 infection	31 - 2424 days	FA and metabolic function (standardized metabolic rates) significantly diminished in DMN, in DOC compared with controls. Sig. association between functional metabolism of IP, PreCu, and frontal regions and structural integrity of the frontal-IP, PreCu-IP, thalamo-IP, and thalamo-frontal tracts. Stronger relationship between thalamo-IP tract and thalamic metabolism in EMCS compared with DOC.
Di Perri et al. (2016)	FDG-PET; rs-fMRI; structural MRI-VBM	21 UWS; 24 MCS; 13 EMCS	29 TBI; 14 anoxia; 7 mixed; 8 other	1 - 312 months	Significant positive correlation between the positive DMN connectivity in the PCC/PreCu, and the brain metabolism. Significant negative correlation between negative DMN connectivity in the PCC/PreCu and the brain metabolism. Only UWS patients had decreased metabolism coupled with pathological between-network hyperconnectivity.

Bodart et al. (2017)	DWI (whole brain FA); TMS/EEG	9 UWS; 11 MCS; 2 EMCS; 2 LIS	12 TBI; 10 non-TBI; 2 mixed	5 -1371 weeks	Negative correlation between structural integrity (i.e. global FA) and effective functional connectivity. Global FA could predict 56% of PCI variance in the patients' group.

ALFF - amplitude of low-frequency fluctuation; DAI - diffuse axonal injury; EC – external capsule; FA – fractional anisotropy; IP – inferoparietal; PCI - perturbational complexity index - a transcranial magnetic stimulation (TMS) derived marker of effective connectivity; PTR - posterior thalamic radiation; TBSS - Tract-Based Spatial Statistics.

2.4 Summary of neuroimaging findings

The review of neuroimaging studies demonstrated functional and structural disruption in DOC patients most consistently observed within (and between) high-order resting-state networks (i.e. DMN, SN, ECN), mainly encompassing midline cortical brain regions (i.e. PMC, mPFC) and their corresponding white matter connections (i.e. corpus callosum, cingulum).

These findings were observed across a range of DOC etiologies and imaging modalities with more severe alterations in coma and UWS as opposed to MCS patients.

A few studies that investigated the relationship between neuroimaging data and patients' prognosis showed reduced functional connectivity in the DMN and PCC/PreCu, and damaged structural integrity in some of the major white matter tracts (i.e. corpus callosum, cerebral peduncle), in coma patients with poor outcome. The importance of cortical hub nodes ensuring efficient global brain functioning was also highlighted in a few graph theoretical studies. Several multimodal neuroimaging studies indicated the potential role of the structure-function relationship in the emergence of consciousness, however, further research is required in order to better understand this association in the context of disorders of consciousness.

Nonetheless, there haven't been many cases with acquired data in early stages of coma, which is urgently needed in order to find reliable markers serving to predict coma emergence and potential for long-term recovery. Early identification of patients who have a high chance of recovery is important, to avoid withdrawal of life sustaining treatment and ensure the administration of pharmacologic and non-pharmacological therapies aimed at restoring consciousness. Also, better understanding of etiology differences may prove to be essential in early prediction and understanding of patient's outcomes, as the identification of etiology-related factors may ameliorate the predictive value of consciousness-related markers, and help guide more effective therapy adapted to individual patient needs.

In summary, the reviewed results imply great potential in clinical application of (multimodal) neuroimaging data in early prediction of long-term outcome in coma and chronic DOC patients and in increasing our knowledge about the neural correlates of consciousness.

3 Chapter III – The ACI-COMA project

3.1 ACI-COMA

This thesis is based on the data acquired for the ACI-COMA project. This project was approved by the ethics committee of the University Hospital of Toulouse, France ("Comite Consultatif pour la Protection des Personnes," CHU Toulouse, ID-RCB: 2012-A00009-34). Written informed consent was obtained directly from the healthy volunteers and from the legal surrogate of the patients. Clinical trials identifier: NCT01620957. Funding has been obtained from the University Teaching Hospital of Toulouse and the French Society of Intensive Care.

3.1.1 Project design

This is an observational, longitudinal and multicenter project. It consisted of two neuroimaging sessions (Figure 3.1.1) both executed during coma (≤30 days after the brain-injury). The goal of this repeated acquisition was to explore potential functional or structural brain connectivity changes independent of behavioral amelioration/worsening, which could potentially serve as a valid prognostic marker of neurological recovery.

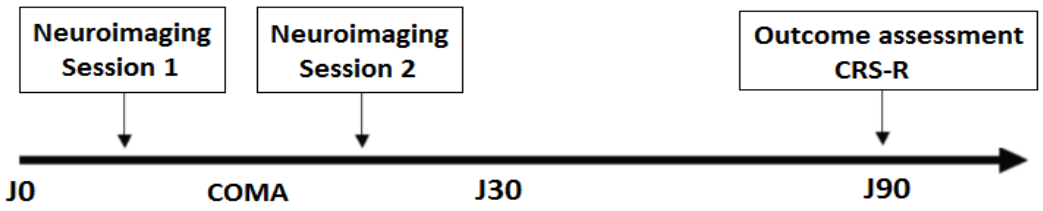

Figure 3.1.1. ACI-COMA project design.

The initial evaluation was done as soon as possible after clinical stabilization of patients, but to avoid confounding effects of anesthesia and hypothermia (Kirsch et al., 2017), patients underwent MRI scanning at least 2 days (4 +/- 2 days) after complete withdrawal of sedation and under normothermic condition.

Behavioral assessment. The level of consciousness was assessed at admission to hospital and on the day of the MRI scanning using Glasgow Coma Scale (GCS) (Teasdale & Jennett, 1974).

and Full Outline of Unresponsiveness (FOUR) (Wijdicks et al., 2005). The outcome (neurological recovery) was assessed 3-months post coma using the Coma Recovery Scale-Revised (CRS-R) (Schnakers et al., 2008). The standardized clinical examination was performed by raters blinded to neuroimaging data. The behavioral tests were translated and validated in French language.

Neuroimaging. This is a multimodal neuroimaging project. The MRI machine used for the acquisition of data was MRI 3T Philips ACHIEVA scanner. Functional and structural imaging sequences and their order of acquisition are presented in Figure 3.1.2.

The instructions for the rs-fMRI were: "Close your eyes, try to move as little as possible and let your thoughts run freely". The passive-movement task consisted of the passive movement of the wrist extension between 0° and 30° from the right hand index finger with a frequency of 1 Hz. The total duration of the MRI exam was around 60 minutes.

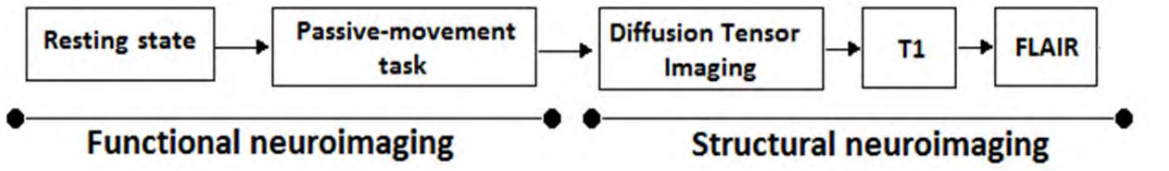

Figure 3.1.2. The MRI sequences.

3.1.2 MRI data acquisition parameters

T1

A high-resolution structural image was acquired for each subject using three-dimensional MRI sequences with following parameters: 170 contiguous slices; TR=8.1 ms, TE = 3.7 ms, FOV= 220x232x170mm, flip angle = 8°, resolution= 1mm3 isovoxel.

Rs-fMRI

In all participants, 11 min resting state fMRI was obtained. Two hundred and fifty multislice T2*- weighted images were retrieved with a gradient echo-planar sequence using axial slice orientation: 37 slices; voxel size: 2 x 2 x 3.5 mm; TR = 2,600 ms; TE = 30 ms; flip angle = 90°; FOV = 240 mm.

DTI

DTI data was collected using a gradient echo planar imaging sequence with the following parameters: 32 gradient orientations, TE=76ms, TR=12000ms, flip angle= 90°, FOV = 230x188x143, image matrix = 152 x 124, slice thickness = 1.5mm, and b value=1000 s/mm2.

3.1.3 The recruited participants

The patients were recruited (Table 3.1.1) at 4 Intensive Critical Care Units affiliated with the University Teaching Hospital (CHU de Toulouse, France) in Toulouse. The inclusion of patients started in the early 2013 and finished in August 2016.

Table 3.1.1. Criteria for patient recruitment.

Criteria of inclusion	Criteria of exclusion
• Men or woman between 18 and 80 years; • Diagnosis of coma (GCS at the admission to hospital < 8, with motor responses < 6; FOUR score < 10); • Etiology - traumatic or anoxic BI; • Acute stage – first 30 days after initial BI; • Informed consent from the legal surrogate of the patients; • Interruption of administration of any sedative or hypnotic agent from >24h (propofol/ketamine/clonidine/morphine) or > 72h (benzodiazepines). The administration of non-morphine analgesic drugs is compatible with inclusion (i.e. absence of sedative effect).	• History of neurological or psychiatric illness; • Subject not affiliated to a social security scheme; • Subject under legal protection; • Pregnant or nursing women; • Subjects with pacemakers or metallic and other electrically conductive medical devices may interfere with the magnetic field of the MRI; • Subjects susceptible to attacks of claustrophobia.

To this day, we have included 58 comatose patients in total. We have also included 34 healthy subjects serving as controls. Demographic and clinical characteristics of all the subjects are reported in Table 3.1.2

Table 3.1.2. Demographic and clinical characteristics of participants.

		Patients (N=58)	Controls (N=34)
Age	Mean=49y (18-81y); STD=18y		Mean=50y (22-74y); STD=20y
Sex	39M; 19F		13M; 21F
Etiology	Traumatic	19	/
	Anoxic	35	
	Mixed (TBI + Anoxic)	4	
Outcome	Death	11	/
	UWS/Vegetative state	22	
	Minimally conscious state	18	
	Recovery	7	
Sessions	Session 1	N = 58	/
	Session 2	N = 19	

3.1.4 Main goals and objectives

This thesis is centered on the analysis of intrinsic brain "activity" in the form of functional connectivity and structural brain integrity of brain-injured patients in the acute stage of coma. The aim of the present thesis is to characterize the neural correlates of acute consciousness abolition (i.e. coma) and identify early neural signatures of neurological recovery. To do so, we longitudinally studied severe brain-injured patients using multimodal MRI methodology and standardized behavioral assessment.

The outcome of this project will hopefully contribute to: (i) a development of reliable multimodal neuroimaging battery of tests serving to improve severely brain injured patient's early diagnosis and prognosis (ii) the assessment of the impact of novel pharmacological and non-pharmacological therapeutic interventions in future studies.

4 Chapter IV – Methods and Results

4.1 Neural signature of coma revealed by posteromedial cortex connection density analysis

Based on the article: "Neural signature of coma revealed by posteromedial cortex connection density analysis". Malagurski. B, Péran, P., Sarton, B., Riu, B., Gonzalez, L.,…Silva, S. (2017). *NeuroImage: Clinical, 15,* 315–324. **(**Paper I**)**

4.1.1 Scientific justification

Converging data from physiological, pharmacological (Heine et al., 2012) and pathological models (Hannawi et al., 2015), suggest the implication of the posteromedial cortex (PMC) and its long-range functional connections in conscious processing. Patients with disorders of consciousness consistently demonstrate a reduced activity (He et al., 2014; Silva et al., 2010; Tsai et al., 2014) and/or diminished connectivity between this posterior brain structure and other cortical hubs (Hannawi et al., 2015; Vanhaudenhuyse et al., 2010; Qin et al., 2015; Wu et al., 2015), in particular the medial prefrontal cortex (mPFC) (Lant et al., 2016; Silva et al., 2015). As we have seen in the chapter titled: "Key hubs for consciousness emergence: PMC-PCC/PreCu complex", the posteromedial cortex (PMC) is considered as a heteromodal cortical region, as its sub-regions have been differentially functionally associated with several intrinsic brain networks and consequently have been implicated in a variety of cognitive processes (Cavanna & Trimble, 2006; Leech & Sharp, 2014).

Nevertheless, the DOC neuroimaging literature traditionally explored PMC as a homogenous structure and failed to describe such a functional segregation in pathological conditions (Norton et al., 2012; Silva et al., 2010; Vanhaudenhuyse et al., 2010). This important issue is probably due to (anatomical) seed-based approaches that are currently used in this setting to evaluate the functional connectivity among non-parcelled brain regions, by using correlation analyses of spontaneous fluctuations of brain activity in resting state conditions (Hannawi et al., 2015).

4.1.2 Objectives and hypotheses

We suggest that a better understanding of intrinsic PMC functional topology (Silva et al., 2015) could significantly expand our understanding of how this cortical hub contributes to the generation and the maintenance of conscious awareness and might considerably improve DOC patient's clinical management. To explore this, we used a recently developed voxel-based unbiased approach that does not rely on a priori selection of the seed regions, named functional connectivity density (CD) (Tomasi & Volkow, 2010). This voxel-based method, accurately enables the identification of functional connectivity hubs and permits to specifically investigate within brain regions parcellation, in both healthy and pathological conditions. Thus, we aimed to investigated the functional impact of acute brain injures responsible of coma at the level of PMC and intended to study in this setting: (i) the specific interactions of the PMC anatomical (PCC and PreCu) or functional (ventral/dorsal gradient) sub-regions, with a distant cortical hub (medial prefrontal cortex; mPFC) in resting state conditions (ii) a complete assessment of the whole range of increase/decrease of both positive/negative, i.e. corresponding to positive/negative correlation, connection patterns that could theoretically be detected by this approach, (iii) the impact of injury mechanisms (i.e. traumatic or anoxic), on brain functional connectivity patterns (iv) the prognostic value of functional connection density data for neurological recovery.

4.1.3 Materials and methods

4.1.3.1 Participants

We compared 27 patients, 15 with traumatic and 12 with anoxic brain injury, who met the clinical definition of coma (Glasgow Coma Scale score (Teasdale & Jennett, 1974) at the admission to hospital< 8, with motor responses< 6; age range: 19–70 years) to 14 approximately age-matched healthy controls (age range: 22–37 years). Patients underwent rs-fMRI scanning at least 2 days (4 ± 2days) after complete withdrawal of sedation and under normothermic condition. Standardized clinical examination was performed on the day of the scanning using the Glasgow Coma Scale and the Full Outline of Unresponsiveness (Wijdicks et al., 2005) and 3 months later using Coma Recovery Scale-Revised (Schnakers et al., 2008).

4.1.3.2 Pre-processing

The rs-fMRI data was preprocessed using SPM 8 (http://www.fil.ion.ucl.ac.uk/spm/) and CONN toolbox ver. 13f (http://www.nitrc.org/projects/conn) (Whitfield-Gabrieli & Nieto-Castanon, 2012). In order to reduce the motion effects on our data, we only included subjects characterized by motion parameters smaller than 3 mm translation and 3° rotation. First, the echo-planar images were realigned (motion corrected), slice-time corrected and normalized to the Montreal Neurological Institute echo-planar imaging template. Second, non-neuronal sources of noise were estimated and removed using the anatomical CompCor method (aCompCor) integrated in the CONN toolbox. Principal components of the signals from the white matter and the CSF voxels, alongside the motion parameters estimated during realignment were removed with regression. Finally, a temporal band-pass filter was applied to the residual blood oxygen level–dependent (BOLD) time course in order to obtain a low-frequency range of interest (0.008-0.09 Hz).

4.1.3.3 Region of interest selection

Using a home-made MATLAB (MATLAB and Statistics Toolbox Release 2011a, The MathWorks Inc., Natick, Massachusetts, United States) script, the BOLD time series was extracted from voxels in two main regions of interest (ROI), the Posterior Medial Cortex (PMC) and the Medial Prefrontal Cortex (mPFC), defined by the Automated Anatomical Labeling atlas (Tzourio-Mazoyer et al., 2002) (voxel size 2× 2× 2 mm). The PMC (size = 12,862 voxels) consisted of the Precuneus L/R (size = 11,222 voxels) and the Posterior Cingulate Cortex L/R (size =1640 voxels), and the mPFC (size = 13,389 voxels) comprised the Frontal Superior Medial L/R (size =8373 voxels) and the Anterior Cingulate Cortex L/R (5016 voxels). As preliminary step, T2* mean images were used the extract the mean value of voxels in the PMC region, and a two-sample t-test was performed to compare values between the control and the patient group. Additionally, to investigate if the potential changes in connection density are specific to the PMC-mPFC interactions, we have also included the bilateral Calcarine L/R (size = 7134 voxels; part of the primary visual cortex) as a control region, currently not considered to be relevant for conscious awareness.

4.1.3.4 Voxel-based connection density

The data analysis pipeline is presented in Figure 4.1.1. Pearson correlation coefficients were computed between the BOLD time course of all the possible pairs of voxels from PMC and mPFC. Correlation coefficients were then normalized using Fisher's r-to-z transformation. A subject-specific threshold of $p<0.05$ was applied to each correlation coefficient in order to retain only a subset of connections with higher in further analysis. We labelled the obtained connections as positive and negative depending on the sign of the obtained z coefficients and we treated them separately. Importantly, to avoid the artificial induction of negative correlations (anticorrelations) by the global signal regression (Murphy et al., 2009; Weissenbacher et al., 2009) we adopted the CompCor method in the preprocessing step, which has been reported as a reliable approach for the exploration of both positive and negative correlations (Chai et al., 2012, 2014). The resulting z coefficients were binarized and then summed to obtain the density of connections between every voxel belonging to PMC and every voxel within the mPFC. These would represent the number of significant positive and negative connections from PMC to mPFC. The number of significant connections obtained for a single PMC voxel was then used to compute a Z-score for every voxel in the patient group using the mean (M) and the standard deviation (SD) of the healthy control group. This will represent the significant deviation of each voxel from the corresponding control. Thus, the number of PMC voxels with a Z-score higher or equal to 2 SD or less or equal to −2 SD (for positive and negative connections) were counted for each patient individually and further used to investigate the changes (significant deviations) in functional connectivity between the PMC to the mPFC. The same analysis was repeated for the control pathway (i.e. representing the connections between the bilateral calcarine and the mPFC). Furthermore, in order to facilitate the discussion of our results (Fig. 1), a significant decrease (Patients < Controls, Z-score≤ -2) in connection densities is designated as “hypo” connection density or hypo-CDP and hypo-CDN, for positive and negative correlation based connection densities, respectively. The opposite - increase in connection densities (Patients > Controls, Z-score ≥ 2) is denoted by “hyper” connection density e.g. hyper-CDP and hyper-CDN for positive and negative correlation based connections, respectively. Lastly, to allow an easier description of our findings and to test our hypothesis on the differences in functional connectivity changes between the PreCu and PCC, we present the results from these two ROIs separately.

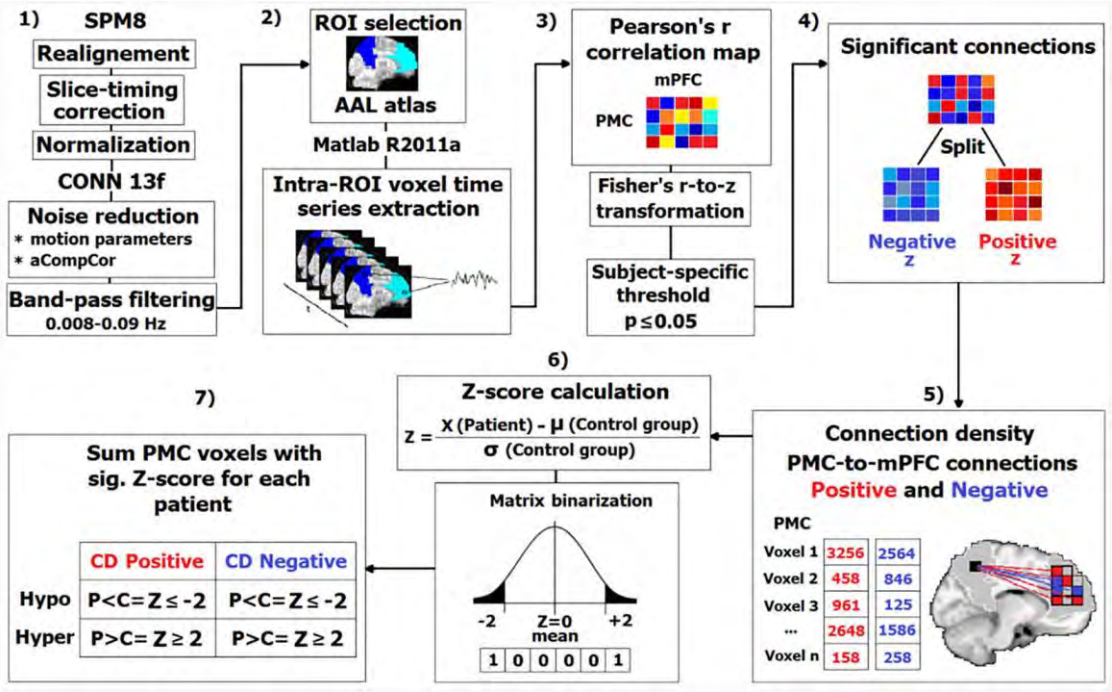

Figure 4.1.1. Overview of the data analysis pipeline.
1) First, the rs-fMRI data was pre-processed using SPM8 and CONN13f, respectively. 2) Using a home-made MATLAB script, the BOLD time series was extracted from voxels in two main regions of interest then used in 3) calculation of Pearson correlation coefficients between the BOLD time course of all the possible pairs of voxels from PMC and mPFC. Then, a subject-specific threshold of $p \leq 0.05$ was applied to include only the significant connections in further analysis. 4) The obtained significant connections were split on positive and negative (based on the sign of the normalized z coefficients), binarized and used to 5) obtain the density of connection between PMC and mPFC voxels. 6) A Z-score was calculated for each single PMC voxel as explained in the figure. 7) Voxels with a significant Z score were summed and characterized as hypo/hyper-CDP and hypo/hyper- CDN as presented in the figure.

4.1.3.5 Spatial homogeneity

In addition to the individual results, we were interested in the spatial similarity (overlap) of these changes between patients within groups (intra-group) and between different coma etiology groups (inter-group). This allowed us to investigate if these changes were spatially scattered thus highly heterogeneous between subjects or if they were organized in functional clusters shared among multiple participants within/between the two etiology groups. The intra-group spatial congruity of single voxel Z-score results was explored at two thresholds: a criterion of 33% and 67% was used to define the total number of disconnected voxels spatially shared between 1/3 and 2/3 of the patient group, respectively. This was explored in the group with all the patients and with two coma etiology groups separately. To explore the inter-group similarity, we have calculated the Jaccard similarity coefficient (index) to further test the spatial overlap in connectivity changes between these two groups. The Jaccard index (JI) is defined as the intersection divided by the union of the number of voxels representing significant changes

in PMC-mPFC connection density in given groups. The values of JI range from 0 (0%), indicating no overlap, to 1 (100%) suggesting full spatial overlap.

4.1.3.6 Statistical analysis

We have conducted the Mann-Whitney U test to investigate the differences in PMC-to-mPFC connection density changes between the PreCu and PCC. The same test was used to compare the changes in functional connectivity between our two coma etiology groups – traumatic and anoxic brain injury patients. This analysis was also repeated for the control pathways. The resulting p values were corrected for multiple comparison using a false discovery rate at the level of $p = 0.05$. We have also calculated the effect size for the Mann-Whitney U test by dividing the z value (test statistic) by the square root of N (sample size). This is analogous to Cohen's d for parametric group testing. Spearman's correlation analysis was performed to explore the link between the number of PMC voxels with significant changes in connection density and the CRS-R score. The same correlation analysis was done to test the association between the connection density changes in the control pathway - Calcarine-mPFC - and the CRS-R score. The resulting p values were corrected for multiple comparison using a false discovery rate. Additionally, in order to explore the non-linear association between the outcome and the significant changes in PMC-mPFC connection density, and thus the predictive value of these changes in relation to recovery, we have conducted the binary/logistic regression analysis. Patients were divided into two outcome groups (based on the CRS-R score): good outcome - comprising patients who had recovered or progressed to minimally conscious state (MCS) ($N = 12$); and the bad outcome – incorporating patients with unresponsive wakefulness syndrome/vegetative state (UWS/VS) ($N = 15$). This analysis was not done separately for the two etiologies due to small sample size. All of the above mentioned analyses were performed using the IBM SPSS (IBM SPSS Statistics for Windows, Version 20.0. Armonk, NY: IBM Corp.) statistical package.

4.1.4 Results

4.1.4.1 Induced functional topological changes in the PMC

4.1.4.1.1 Anatomical sub-regions — precuneus and posterior cingulate cortex

In Figure 4.1.2 we report the induced changes in functional connectivity of the entire PMC and the differences between its anatomical sub-regions, the PreCu and PCC, between the patient and the control group. The changes in connection density are presented as the percentage of voxels more or less connected within a given region/sub-region in order to take into account the differences in size (total number of voxels) of different ROIs.

The PCC exhibited significantly more voxels with hypo-CDP ($U = 202$, $p = .004$; $r=0.38$; Figure 4.1.2 – subpanel A-1) in comparison to PreCu, which is in accordance to previous research. The PreCu showed a tendency toward a higher number of voxels with hyper-CDP (Figure 4.1.2 - subpanel A-2) in comparison to PCC, but these results were not statistically significant ($p= .074$). There were no statistically significant differences in the number of hyper-CDN and hypo-CDN voxels between these two sub-regions, after the multiple comparisons correction (fdr corrected $p=.005$) (Figure 4.1.2- subpanel A-3).

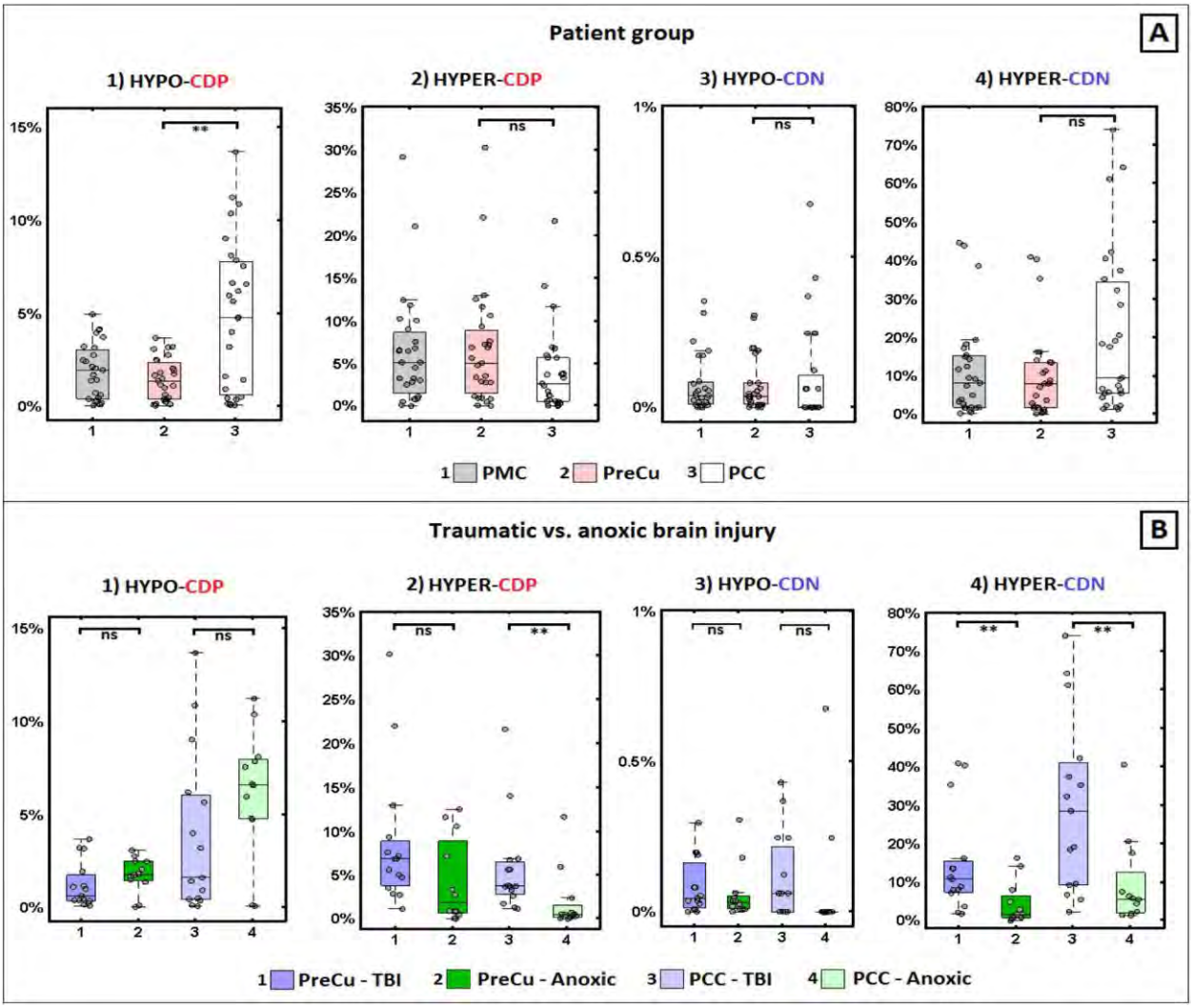

Figure 4.1.2. Differences in changes in connection density between PreCu and PCC and between traumatic and anoxic brain injury.
*Panel A) PCC showed significantly more hypo-CDP (subpanel 1) in comparison with the PreCu. Panel B) Traumatic BI patients had more hyper-CDP (sub-panel 2) within the PCC and hyper-CDN voxels in both PreCu and PCC (sub-panel 4) in comparison to anoxic BI patients; Boxplots represent medians with interquartile range and whiskers signify minimum and maximum values (excluding the outliers) (*p < 0.05, (**p < 0.005, ns: non-significant).*

4.1.4.1.2 Functional sub-regions — ventral/dorsal segregation of the PMC

In order to investigate the spatial architecture of the observed changes in the density of connections, in Figure 4.1.3 we report the spatial topography of the obtained connections. This figure represents the group-wise changes in functional connectedness. The individual spatial topography maps of these changes (with etiology and prognostic information) are presented in the supplementary Figure 6.3.1 and Figure 6.3.2. It can be noted that: (i) the ventral PCC and the ventral PreCu form a functional cluster of hypo-CDP voxels (Figure 4.1.3 A), (ii) the hyper-CDP voxels are primarily located in the dorsal PreCu and dorsal PCC, alongside a portion of the ventral PCC (Figure 4.1.3 B), (ii) the hyper-CDN voxels are widespread (suggesting high inter-

individual variability) and cover large portions of both PMC sub-regions (Figure 4.1.3. D), including almost the entire PCC, (iv) finally, the hypo-CDN PMC voxels are barely present and are mostly found in the posterior ventral PreCu (Figure 4.1.3. C). There is a significant spatial overlap between voxels with hypo-CDP and hyper-CDN, equivalent to almost the total number of hypo-CDP voxels (see Table 1.) in the entire patient group. However, this overlap is not homogeneous between patients and is characterized by important inter-individual differences, as demonstrated in the supplementary Table 6.3.1. Individual patient results – the total number of hypo/hyper-CDP and hypo/hyper-CDN voxels for PMC (Panel A), PreCu (Panel B) and PCC (Panel B).

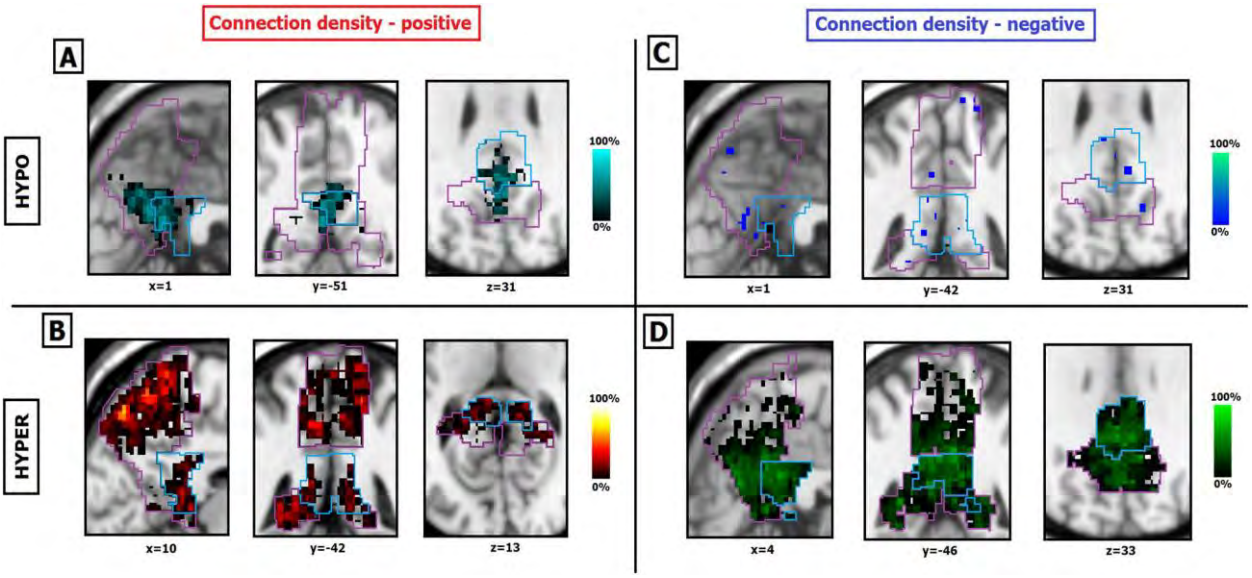

Figure 4.1.3. Spatial maps of changes in PMC-to-mPFC connection density in the patient group.
Patients seem to show significant hypo-CDP changes in the ventral portions of both PreCu and PCC (panel A). Hyper-CDP voxels are more specific to the dorsal sub regions of the PreCu and PCC, and slightly border on the ventral PCC (panel B). Hypo-CDN changes are barely noticeable (panel C), and hyper-CDN voxels seem wide-spread and highly heterogeneous between patients (panel D). Individual results of patients are summed and presented in a single image; Purple and blue outlines reflect the borders of the anatomical PreCu and PCC respectively. Gradient bars (%) reflect the percentage of patients sharing the same voxel with a sig. Z-score (hypo/hyper CDP/CDN) at given anatomical location (spatial homogeneity).

4.1.4.2 Control pathways — Calcarine-mPFC

The changes in the control pathway connection density are fully presented in the supplementary Figure 6.3.3. Differences in Calcarine-mPFC connection density changes between traumatic and anoxic brain injury. The results showed only a small percentage of Calcarine hypo-CDP voxels in patients, representing reduced connectivity between this region and the mPFC (Mdn=0.04%, range 0-0.7%). The same result was found for the hypo-CDN voxels (Mdn=0, range 0-0.2%). In contrary to these result, hyper-CDN (Mdn=22%, range 0.08-63) and hyper CDP (Mdn=4%, range 0.04-22%) voxels were present in this control pathway.

4.1.4.3 Impact of brain injury mechanisms

4.1.4.3.1 PMC-mPFC connection density changes

The impact of the patients' etiology on the observed changes is reported in Figure 4.1.2 – subpanel B. The group-level statistical analysis showed significant differences between the two etiologies in the percentage of PMC voxels with hyper-CDN (U = 32, p= .004; r=.55).
There were no significant differences in hypo-CDP (U= 63, p = .200 r= .25), hyper-CDP (U= 49, p = .045 r= .39) and hypo-CDN voxels (U= 66, p= .249; r= .23).
These significantly higher percentage of PMC hyper-CDN voxels, was present in both PreCu (U =32, p= .004; r=.55) and PCC (U = 33.5, p = .005; r=.53) sub-regions, in TBI in comparison to the anoxic BI patient group (Figure 4.1.2 – subpanel B-4). Additionally, the results showed a higher percentage of hyper-CDP voxels in the PCC sub-region (but not in the PreCu) in the TBI group (U = 27, p = .001; r=.59) (Figure 4.1.2 - subpanel B-2).

4.1.4.3.2 Connection density changes in control pathways

We wanted to test if the hyper-CDP and hyper-CDN voxels, found in the control pathways, were more specific to one of the etiologies. The group-level statistical analysis showed a significantly higher percentage of Calcarine-mPFC hyper-CDP (U =37, p = .009; r =.5), and hyper-CDN voxels (U = 33, p = .004; r= .54) voxels in traumatic in comparison to anoxic brain injury patients (Supplementary Figure 6.3.3 and Figure 6.3.4).

4.1.4.4 Spatial homogeneity

The intra-group spatial similarity in voxels with changes in connection density are presented in Table 4.4.1.1. The hypo-CDN voxels were not included in the analysis, because there were no significant differences between the control and patient group. The results are reported without a threshold and with the threshold of 33% and 67% of patients having the same voxel changes. First, there seemed to be a lower spatial congruity in the entire group of patients, as opposed to the groups of same etiology. Second, in comparison with traumatic patients, anoxic brain injury patients seem to have a slightly higher spatial homogeneity in PMC voxels with hypo-CDP. Third, TBI patients showed a higher intra-group similarity in hyper-CDP and hyper-CDN in comparison to anoxic patients.

The Jaccard index showed a similarity of 65% for hypo-CDP, 46% for hyper-CDP, and 47% for hyper-CDN spatial maps between traumatic and anoxic BI patients. The similarity between the spatial maps of anoxic BI and the spatial maps of all patients (including TBI) was 69% for hypo-CDP, 57% for hyper-CDP, and 49% for hyper-CDN voxel results. Finally, the comparison between the TBI and the group of all patients, suggested a similarity of 96% for hypo-CDP, 89% for hyper- CDP and 98% for hyper-CDN spatial maps. These results, along the spatial homogeneity results within different sub-groups, indicates that the results are more spatially heterogeneous and more widely distributed in the TBI group in comparison to the anoxic groups, further confirming differences in the pathological processes.

The spatial homogeneity differences between separate etiologies are visually presented in Figure 4.1.4.

Group		Hypo-CDP	Hyper-CDP	Hyper-CDN
Patients	No threshold	8% (1054)	51% (6599)	68% (8803)
N = 27	≥ 33%	3% (347)	3% (396)	9% (1138)
	≥ 67%	0% (7)	0% (9)	0% (5)
TBI	No threshold	8% (1011)	46% (5866)	67% (8668)
N = 15	≥ 33%	2% (217)	7% (942)	23% (2959)
	≥ 67%	0% (1)	0.4% (51)	0.8% (102)
ANOXIC	No threshold	6% (730)	29% (3740)	33% (4305)
N = 12	≥ 33%	4% (473)	2% (244)	3% (339)
	≥ 67%	1% (143)	0% (3)	0% (6)

Table 4.4.1.1.1. Spatial homogeneity of changes in PMC connection density in the patient group.
Threshold – at least 33% or 67% of subjects spatially share the same voxel with sig. Z-score. The percentages present the proportion of voxels with significant Z-score out of the total number of voxels in PMC spatially shared between patients.

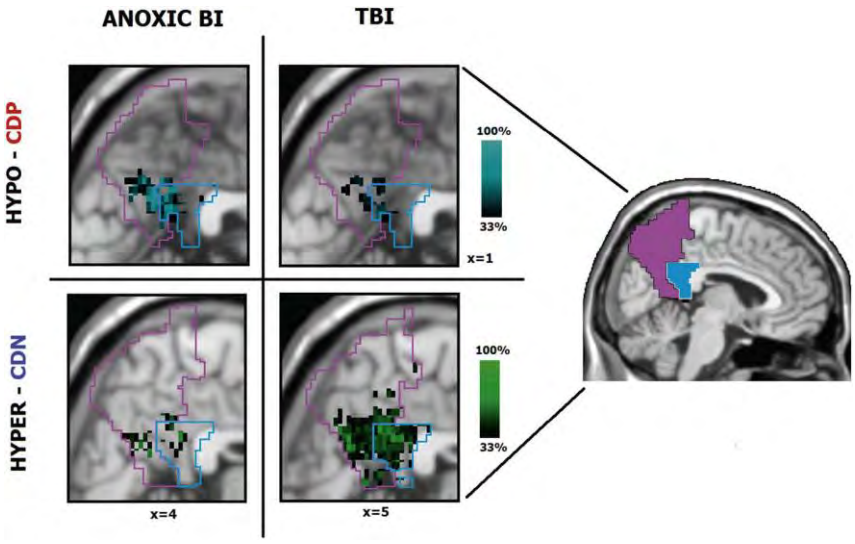

Figure 4.1.4. Intra-group spatial homogeneity differences between the traumatic and anoxic brain injury patients (threshold 33%).

Anoxic BI patients show a higher intra-group similarity in hypo-CDP in comparison to TBI patients, while TBI patients show a higher spatial congruity in hyper-CDN voxels. Purple and blue outlines reflect the borders of the anatomical PreCu and PCC respectively. Gradient bars (%) reflect the percentage of patients sharing the same voxel with a sig. Z-score (hypo/hyper CDP/CDN) at given anatomical location. The minimum spatial homogeneity is set to at least 33% of patients in a given group.

4.1.4.5 Prognostic value

4.1.4.5.1 Spearman correlation analysis with PMC-mPFC voxels

The number of PMC voxels with hypo-CDP showed a significant negative association with the CRS-R score assessed 3 months after the coma onset (r_s= −.72, p = .00002), indicating that if a patient had a higher number PMC voxels with hypo-CDP he was less likely to recover (Figure 4.1.5.). We did not find a significant correlation between hyper-CDP (r_s= .29, p =.14) and hyper-CDN (r_s= −.35, p = .07) voxels and the CRS-R score for the entire patient group.

At the etiology level, it is worth noting that in the traumatic brain injury group, we found a highly significant link between number of hypo-CDP voxels (r_s= −.80, p= .0004) and the CRS-R score (Figure 4.1.5 A).

Interestingly, a highly statistically relevant association was found between the number of hyper-CDN voxels and the CRS-R score (r_s= −.86, p= .00005). Therefore, TBI patients with a high number of hypo-CDP and hyper-CDN PMC voxels had less chance for recovery 3 months after the initial fMRI scan (Figure 4.1.5 B). Additionally, given the significant spatial overlap between voxels with hypo-CDP and hyper-CDP voxels, and the significance of these voxels in relation to the neurological recovery in TBI patients, we performed the same analysis on overlapping voxels. The results showed the same highly significant negative association between the number of spatially overlapping hypo-CDP and hyper-CDN voxels and the 3-month outcome (r_s= −.73, p =.002; Figure 4.1.5 C).

The analysis in the anoxic group did not show a significant association between the CRS-R score and the hyper-CDP (r_s= .43, p =.16), hyper-CDN (r_s= .20, p = .54) nor the hypo-CDP voxels (r_s= −.38, p = .22). However, this result should be interpreted in caution due to small sample size of anoxic BI patients.

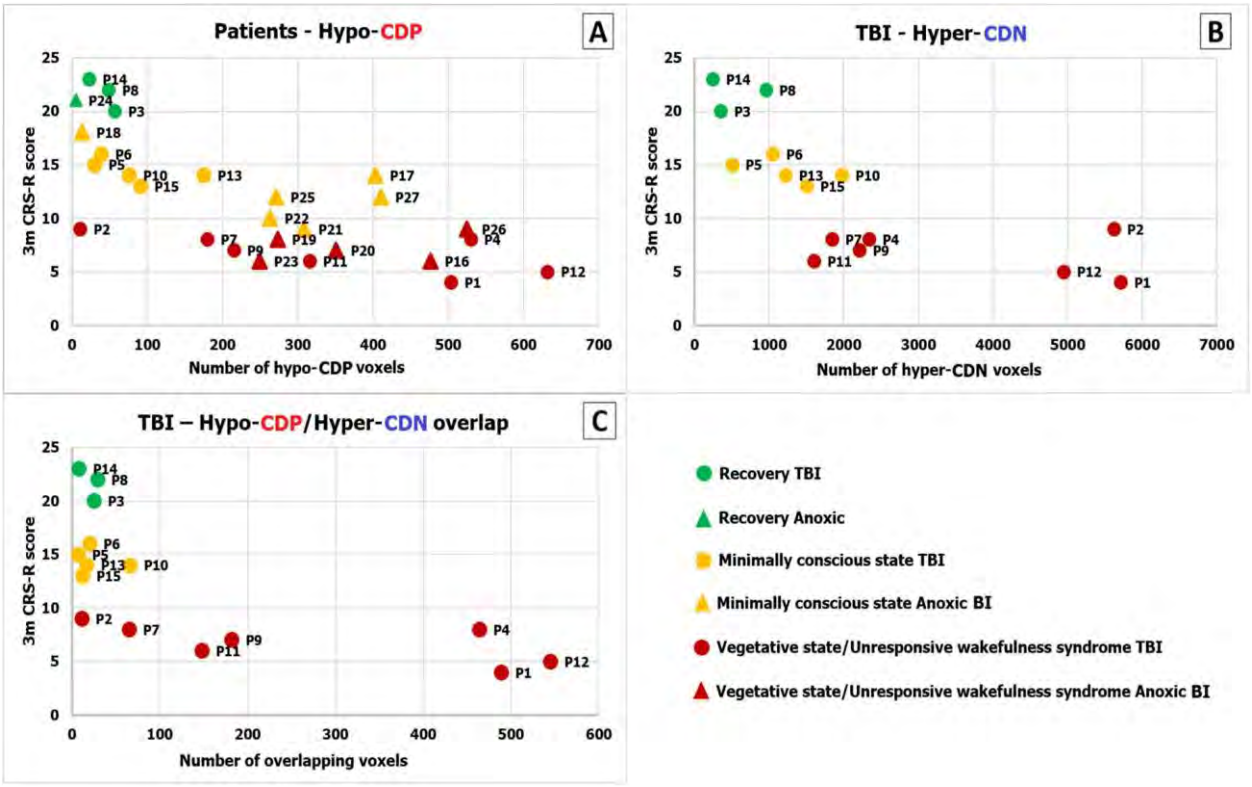

Figure 4.1.5. The prognostic value of changes in PMC-to-mPFC connection density.
Panel A) There was a sig. negative link between the number of PMC voxels with hypo-CDP and the patient outcome (rs= −0.72; p =0.00002); Panel B) TBI patients showed a significant negative association between the number of voxels with hypo-CDP (rs =−0.80; p =0.0004; panel A), hyper-CDN and the CRS-R score (rs =−0.86; p =0.00005); Panel C) In TBI patients, there was highly significant negative association between the number of spatially overlapped hypo-CDP and hyper-CDN voxels and the 3-month outcome (rs = −0.73, p =0.002; Fig. 6.C). The x axis represents the 3-month CRS-R score, the y axis represents the number of voxels with changes in connection density.

4.1.4.5.2 Spearman correlation analysis with the control pathway voxels

The Spearman correlation analysis did not show any significant association between the CRS-R score assessed 3 months after the coma onset and any of the number of voxels with significant connection density changes in the Calcarine-mPFC control pathways. This was true for the entire group of patients, and for the anoxic and traumatic BI groups separately.

4.1.4.5.3 Logistic regression analysis with PMC-mPFC voxels

A logistic regression analysis was conducted to ascertain the effects of the number of hypo-CDP, hyper-CDN and hyper-CDP PMC voxels on the likelihood that the patients had a good outcome (recovery and MCS) or bad outcome (UWS/VS). Due to significant collinearity between the hyper-CDP and hyper-NCD (r =−.91), two models were tested, the first including hypo-CDP and hyper-CDP and the second hypo-CDP and hyper-CDN as independent/predictor variables. The first model was significant (chi square = 10.204, p = .006 with df= 2), however

the number of hyper-CDP voxels did not significantly contribute to the prediction (Wald, p= .296). Thus, we decided to keep the second model, where both predictors had a significant effect on the outcome. The full model against the constant only model was statistically significant, suggesting that the predictors as a set reliably distinguished between patients with good and bad outcome (chi square =16.701, p < .001 with df= 2). The model explained 62% (Nagelkerke's R2) of the variance in outcome, and correctly classified 78% of cases (sensitivity – 80%; specificity – 75%) (Supplementary Figure 6.3.5). The Wald criterion demonstrated that both variables, hypo-CDP (p = .02) and hyper-CDN (p= .044) had a weak but significant contribution to prediction. Increase in both predictors was associated with decreased likelihood of good outcome. Accordingly, Exp (B) indicates that the for every extra unit (number of voxels) of hypo-CDP and hyper-NCD, the odds of recovery decrease by a factor of 0.988 and 0.999, respectively, all other factor being equal.

4.1.5 Discussion

Our findings demonstrate that a comparative analysis of voxel-wise connection density disruptions between the PMC and the mPFC, might constitute a reliable and fine-grained study approach, permitting to accurately address the brain functional network changes, which are critically related to consciousness abolition during coma. Crucially, built upon statistical analysis at a single subject level - a necessary condition to make reliable inferences in individual patients - this voxel-wise connection density approach, enabled the description of a novel PMC/mPFC dysconnectional taxonomy, permitting the identification of specific markers related to brain injury mechanism and useful for neuroprognostication. The current study, confirms and expands previous finding through seed-based analysis method (Silva et al., 2015), and permits: (i) a precise topological description of the PMC sub-regions (ventral PreCu and the PCC) which seems implicated in the consciousness impairment observed in this setting, (ii) identification of useful and accurate neuroimaging biomarker for prognostication in this setting, as the number of PMC voxels with hypo-CDP to mPFC, had significant predictive value in relation to patients neurological outcome assessed 3 months after the coma onset in the current study. It is worth noting that such adaptive changes, characterized by a reduction of CDP, were barely observed in the control pathway (Calcarine/mPFC). Crucially, the number of voxels with any significant connection density changes within this control pathway, was not correlated with patient's neurological outcome. These points strongly support the critical role of PMC/mPFC

functional connections in consciousness emergence, and consolidate the specific use of PMC/mPFC functional connectivity to predict coma patient's neurological outcome. Our data strongly support the concept of a significant structural and functional PMC heterogeneity, which could be implicated in the "tuning" of the whole-brain metastable status (Hellyer, Scott, Shanahan, Sharp, & Leech, 2015). Furthermore, our results are in line with the hypothesis of a dysfunctional mesocircuit (Schiff, 2010) in DOC patients, build upon anterior and posterior critical disruption of neural communication. For example, tract-tracing studies conducted in non-human primates (Vogt & Laureys, 2005) and diffusion tensor tractography in humans (Hagmann et al., 2008) have clearly identified structural connections between dorsal PCC to the mPFC along the cingulum bundle (Greicius et al., 2009). Interestingly, structural injuries within this tract have been described as related to neurological outcome of severely brain injured patients (Fernández-Espejo et al., 2012). Furthermore, our findings suggest a higher prevalence of hypo-CDP voxels in comatose patients, specifically located in the ventral subdivision of both the PCC and the PreCu. This result seems compatible with the findings of the rs-fMRI study of Silva and colleagues (2015), suggesting stronger functional connectivity between PCC-centred seed and the mPFC in patient who eventually recovered. However, our voxel-wise connection density method further elucidated the importance of the total number of PMC voxels in prediction of patient's outcome and allowed us to explore the intra-regional topological changes in connectivity which is not possible in seed based analysis. Additionally, previous resting-state fMRI (Bzdok et al., 2015; Cauda et al., 2010; Margulies et al., 2009; Vogt et al., 2006; Zhang & Li, 2012), and DTI studies (Zhang et al., 2014) indicate that both these PMC sub-regions are densely connected to other brain regions that participate to DMN network and appears to be implicated in internally directed cognition (i.e. self-referential information processing, social cognition, mind-wandering, episodic memory retrieval) (Andrews-Hanna et al., 2010; Cavanna & Trimble, 2006; Fox et al., 2015; Leech & Sharp, 2014). In contrast with this hypo-CDP restricted to ventral parts of PreCu/PCC, we demonstrated that dorsal PreCu and anterior dorsal (and a part of ventral) PCC, encompasses specific voxels with hyper-CDP in coma patients. These dorsal PMC structures are known to support and connect to other regions involved in externally directed cognitive processes (Margulies et al., 2009; Zhang & Li, 2012) such as spatially-guided behaviour, visual/motor mental imagery (Cavanna & Trimble, 2006), control of attentional focus (Leech & Sharp, 2014) and high-level sensorimotor functions (Balestrini et al., 2015; Herbet et al., 2015). Overall, the observed rostro-caudal functional segregation between increase and decrease of CDP, seems in line with the hypothesis of the central role played by an imbalance between internal and external awareness systems in the

genesis of consciousness disorders (Demertzi, Soddu, & Laureys, 2013; Di Perri et al., 2014; He et al., 2014). Actually, as described in chronic DOC patients (He et al., 2014), this imbalance could reflect overcompensation in the external network due to the loss of input from internal self-networks. Additionally, we sought for functional signatures of the brain injury mechanisms that were responsible of coma. Regarding, the hypo-CDP voxels, our findings indicate that within the PMC, hypo-CDP voxels were slightly more pronounced in anoxic patients (although not statistically significant), probably representing a neural underpinning of the overall worse prognosis of this group (Horsting et al., 2015; Koenig et al., 2014). Furthermore, in line with recent studies, suggesting that hyperconnectivity patterns are a common network response to traumatic brain injury (Bharath et al., 2015; Hillary et al., 2014, 2015; Stevens et al., 2012) we observed that hyper-CDP (in the PCC subregion) and hyper-CDN voxels were more frequently detected in the traumatic group. This was true for the PMC-mPFC connectivity patterns, but also for the control pathway, representing connections between the Calcarine and the mPFC. We hypothesize that the higher prevalence of hyperconnectivity patterns in this group could be the consequence of compensatory brain plastic processes (Di Perri et al., 2014) possibly reflecting resilient connections massively disrupted, but not totally interrupted by traumatic brain injury (i.e. diffuse axonal injury). These resilient connections might have engaged residual critical neural resources, otherwise normally distributed through efficient brain network connections, here disrupted by brain injury, resulting in impaired conscious processing (Hillary et al., 2015). Furthermore, these brain network signature of acute brain injury mechanisms was confirmed by spatial homogeneity analysis (thresholding and Jaccard index), which indicated higher spatial similarity of identified changes in voxel connection density between subjects with same etiologies in comparison to the whole patient group. However, despite higher intra-group similarity, these changes seemed more spatially scatted in the TBI patients group in comparison to anoxic patients, which is in accordance with the heterogeneity of brain lesion found in this group of patients. Finally, it is worth noting, that we specifically observed in the traumatic brain injury group, that the loss long-range connection density of positive correlations (hypo-CDP) between the PMC and the mPFC, was balanced with a spatially overlapping increase of negative coactivation (hyper-CDN). The total amount of the later was associated to patient recovery and could depict maladaptive brain plasticity processes. We hypothesize that this potentially compensatory increase of negative connection density may indicate some aberrant inhibitory processes or competitive mechanisms of information processing (Fox et al., 2009, 2012; Gee et al., 2011; Gopinath et al., 2015; Liu et al., 2015), resulting in the breakdown of more efficient network organization (i.e. PMC hypo-CDP). This is further supported by the unfavorable

outcome of our patients with a higher number of overlapping PMC voxels with decreased positive connections but yet increased negative connections with mPFC. Interestingly, the same hyper-CDP and hyper-CDN patterns in the control pathways were not associated with the outcome in TBI patients. This result indicates that despite of the more global pattern of these changes, the increase of negative connection density seems maladaptive only when present in regions critical to conscious processing.

There are several limitations in this study. First the number of patients is relatively small and our results need to be validated in larger cohorts. Second, we performed a study of density of connections between each PMC voxel and all of the mPFC voxels, aiming to explore in detail, the topology and the functional characteristics of the connections established from PMC which was assumed homogeneous. Therefore, future studies should also address the functional segregation and heterogeneity within mPFC in this setting. In future studies, brain damage in the form of lesions in traumatic brain injury should be assessed in the pre-processing step, as though not properly treated lesions can potentially give rise to artificially induced connectivity. In summary, a complex pattern of decreased and increased connections was observed, and the topography of these changes, seemed to be in agreement with the hypothesis of network imbalance between internal/external processing systems, within PMC during acquired disorders of consciousness. We report a significant link between the PMC (ventral parts of both the PCC and PreCu) and the mPFC functional connectivity and patient recovery. Actually, the number of PMC voxels with hypo-CDP showed a significant negative association with the CRSR score and a “negative” predictive value in relation to good outcome assessed 3 months after the coma onset, notwithstanding etiology. Additionally, traumatic brain injury specifically appeared to be associated with a greater prevalence of hyperconnected positively and negatively correlated voxels, and the total amount of latter, was inversely associated with patient neurological outcome. This point might reflect a maladaptive plasticity mechanism through a resilient functional network and an inefficient redistribution of remaining resources and pave the way for innovative prognosis and therapeutics methods in this challenging setting.

4.2 Topological reorganization of high-order resting state networks in coma

4.2.1 Scientific justification

Brain network graphs have small-world characteristics representing functionally associated clusters with high density of local connections (modules; i.e. resting-state networks) and few long-range connections between segregated areas supported by the integrative properties of highly connected hub nodes (Bullmore & Sporns, 2009; van den Heuvel & Sporns, 2013). In fact, connectionist theories of consciousness suggest that the brain complexity, reflected in the balance between the local (i.e. segregation) and global (i.e. integration) information processing, (i.e. hubs), may be crucial to generate and maintain conscious experience (Dehaene & Changeux, 2011; Tononi et al., 2016). Nevertheless, there have only been a few graph theoretical studies in patients with DOC (rs-fMRI - Achard et al., 2012; Crone et al., 2014; Liu et al., 2014; Liu et al. 2017), (EEG - Beudel, et al., 2014; Chennu et al., 2014, 2017), (DTI – Weng et al., 2017), and none of them have fully explored the potential contribution of such mathematical methods to specifically address the relationship between coma and the whole set of complex topological disturbances (see Table 2.1.1, Table 2.2.1. and Table 6.2.1 for review).

To our knowledge, the study of Achard and colleagues (2012) has been the first and only rs-fMRI study to investigate the global and local network topology in the acute-stage DOC patients. In this study, the authors have shown conserved global network properties, but a severe reorganization of high degree or highly efficient "hub" nodes in patient group.

4.2.2 Objectives and hypotheses

We aimed to characterize during this extreme condition of acquired consciousness abolition (i.e. coma), brain's residual ability to segregate and integrate information at a threefold level: (i) a *whole-brain* analysis, aiming to identify global neural correlates of coma (ii) a *network level* build upon multiple RSNs analysis, to enable the characterization of brain injury impact over predefined RSNs, knowns to be involved in self-related processing and potentially critical for consciousness emergence (Demertzi et al., 2014, 2015; Di Perri et al., 2016; Heine et al.,

2012; Kirsch et al., 2017; Ovadia-Caro et al., 2012; Qin et al., 2015; Roquet et al., 2016; Sair et al., 2017): the dorsal default mode network (dDMN), ventral default mode network (vDMN), salience network (SAL), posterior salience network (P.SAL), right executive control network (RECN) and the left executive control network (LECN).; (iii) and at a *nodal level*, with a special focus on network hubs reorganization (Achard et al., 2012).

In line with network-level theoretical frameworks (Dehaene & Changeux, 2011; Dehaene and Naccache, 2001; Tononi & Koch, 2008; Tononi et al. 2016), we hypothesize that the complete loss of consciousness that is observed during coma is related to the massive breakdown of whole brain functional connectivity. Despite the behavioral homogeneity which is associated to coma state, and underpinning patient's considerable neurological outcome heterogeneity, we expect to identify among patients a large repertoire of local and global information processing impairments, spanning from well-preserved to almost completely dissolute (i.e. randomized) networks, and generating less efficient and costlier functional brain configurations than small-word arrangement (Fornito et al., 2015; Stam, 2014). At a nodal level, we speculate to identify a significant functional impairment in highly connected hubs (van den Heuvel & Sporns, 2013) which have been described as involved in brain metastable dynamic (Leech & Sharp, 2014) and conscious processing (Hannawi et al., 2015). Finally, we assume that the reorganization in coma patients' brain network topology will be associated with lower resilience to targeted attack on network hubs.

4.2.3 Methods

4.2.3.1 Participants

We compared rs-fMRI data of 25 patients with anoxic brain injury, who met the clinical definition of coma (Glasgow Coma Scale score (53) at the admission to hospital < 8, with motor responses < 6; Mean=51y; STD=18y; age range=18-80y; 12M) to 25 age-matched healthy controls (Mean= 44y; STD=20y; age range=22-74y; 10M). Standardized clinical examination was performed on the day of the scanning using the Glasgow Coma Scale and the Full Outline of Unresponsiveness (Wijdicks et al., 2005).

4.2.3.2 Data preprocessing

Functional data were preprocessed using Statistical Parametric Mapping (version SPM 12; http://www.fil.ion.ucl.ac.uk/spm/). The fMRI images were realigned (motion corrected), slice-time corrected, coregistered to each subject's T1-weighted image and normalized to standard stereotaxic anatomical Montreal Neurological Institute (MNI) space. The images were not smoothed in order to minimize the spillage of the signal of the neighboring ROIs.

T1-weighted images were segmented to compute grey matter, white matter and cerebro-spinal fluid images. Rs-fMRI data was further analyzed using the CONN toolbox (v.16a; http://www.nitrc.org/projects/conn) (Whitfield-Gabrieli & Nieto-Castanon, 2012). In order to reduce the motion effects on our data, we only included subjects characterized by motion parameters smaller than 3 mm translation and 3° rotation. We have also performed ART outlier detection & scrubbing, as an additional preprocessing step to identify rapid scan-wise movement (global-signal scan-to-scan Z-value = 3, and a composite subject-motion signal mm-value = 0.5mm). In addition, using the independent sample t-test we found no significant differences between the patient (M = 0.130; SD = 0.10) and the control group (M = 0.132; SD = 0.06) in estimated composite movement parameters ($t(24) = -0.076$, $p = .94$).

We originally included 28 patients, from which three patients were excluded, one due to excessive movement (≥3 mm) and two due to preprocessing failure (ex. normalization failure). Non-neuronal sources of noise were estimated and removed using the CompCor method (Behzadi et al., 2007) integrated in the CONN toolbox. Principal components of the signals from the white matter and the CSF voxels (using normalized T1 segmented masks), alongside the motion parameters (estimated during realignment) and between-scan motion outliers (ART toolbox), were removed with regression. Finally, a temporal band-pass filter was applied to the residual blood oxygen level–dependent (BOLD) time course in order to obtain a low-frequency range of 0.01 to 0.1 Hz.

4.2.3.3 Network construction

To perform our graph theoretical analysis, we needed to construct a graph for the resting-state sessions of each of our subjects. Within this framework a brain graph consists of set of nodes that is brain regions, and edges represented by pairwise relationships between these nodes. Brain nodes were defined using a functional atlas representing temporally coherent functional networks generated using resting-state independent component analysis in an independent study with healthy controls (Shirer et al., 2012). We have used the expanded "Willard" atlas

(Richiardi et al., 2015) with more grey matter coverage but significantly overlapping with the original functional atlas published in the article of Shirer and colleagues (2012). The final nodes included in our analysis were 6 mm radius spheres defined around the center of mass coordinates of original "Willard" atlas regions. This was done in order to ensure the same number of voxels within each of the nodes, as this was not the case with the original functional atlas.

We have specifically studied six networks, given their consistent replication in other studies and established importance in relation to disorders of consciousness. These networks consisted of 82 nodes in total, reflecting the - dorsal default mode network (dDMN; 21 nodes), ventral default mode network (vDMN; 13 nodes), salience network (SAL; 12 nodes), posterior salience network (P.SAL; 13 nodes); right executive control network (RECN; 13 nodes) and the left executive control network (LECN; 10 nodes). To facilitate the presentation of results, the MNI center-mass coordinates of each of these nodes were used to identify the corresponding anatomical regions of the AAL atlas (Tzourio-Mazoyer et al., 2002). These were further used in the visualization (BrainNet; http://www.nitrc.org/projects/bnv/) (Xia, Wang, & He, 2013) and interpretation of our results. The full detailed list of brain nodes used in our study can be found in Supp. Table 6.3.2.

Graph edges were constructed by computing Pearson correlation coefficients between the average BOLD signal of all the nodes of these predefined functional networks. This resulted in 82x82 connectivity matrix for each of the subjects in each of the groups.

4.2.3.4 Graph theory analysis

4.2.3.4.1 Threshold selection

Thresholding is necessary to reduce the influence of weak and potentially spurious connections that could significantly influence the network topology. Importantly, to keep the graph fully connected, we extracted the minimum spanning tree (MST) for each subject, based on the correlation matrix with absolute weights. The remaining values of the correlation matrices were thresholded using subject-dependent connection density thresholds to obtain the same number of edges for each subject thus allowing us to compare groups with each other. Thus, the remaining top 5-50% of the strongest (absolute) connections, with an increment of 5%, were added to the MST from the MST-extracted connectivity matrix resulting in 10 binary undirected adjacency matrices per subject in each group.

4.2.3.4.2 Randomness

Lower levels of overall functional connectivity have been associated with higher degree of randomness in the individual proportionally thresholded (i.e. connection density) brain graphs. Edges with low functional strength have a higher probability of being spurious and often lead to differences in clustering and global efficiency not necessarily reflecting real changes in network organization but artificially induced differences due to low overall functional connectivity (van den Heuvel et al., 2017). In our study, the results of global metrics (global efficiency and clustering) across multiple thresholds, with the initial group of patients (N=25), indicated whole brain network randomization in coma patients compared to controls (Supp. Figure 6.3.6 - subpanels A and B). Nonetheless, the global metric results seemed highly variable within the group of patients. This "randomness" of network topology was further explored using the hub disruption index (HDI) (Achard et al., 2012) calculated using the global efficiency (GE-HDI) estimated for each node individually (Supp. Figure 6.3.6 - subpanel D; Supp. Figure 6.3.7). The GE-HDI enabled the characterization of three sub-group of patients (Supp. Figure 6.3.6 - subpanel D), with one group showing significant global network reorganization indicative of a randomization process (HDI < -0.8). The same sub-group of patients showed increased global efficiency suggesting subtle randomization (Supp. Figure 6.3.6 subpanel C). These results were supported with low values of functional connectivity in "random patients", who had lower density (<10%) of strong functional connections (Pearson's r>.2; Supp. Table 6.3.3), not sufficient to comparatively explore the network topology between groups (i.e. random configuration). Therefore, to allow meaningful interpretation of patients' global and local network topology that is not related to randomness but to node related topological changes, we decided to calculate the graph measures excluding patients (N=9) showing evidence of randomization (HDI< -0.8 and/or low functional connectivity (density <10%); Supp. Table 6.3.3), leaving a total of 16 patients for further analysis. The boxplot of pairwise functional connections (Pearson's r) in remaining patients (in comparison to controls) can be seen in Supp. Figure 6.3.8.

4.2.3.4.3 Network metrics

The network analysis was done in R (v.3.3.2; The R Project for Statistical Computing; http://www.R-project.org/) using the Brainwaver and iGraph package freely downloadable at

http://cran.r-project.org. The more detailed description of the applied graph metrics is provided in Chapter I of this thesis.

Following global metrics were calculated: clustering and global efficiency. The clustering (global average local efficiency – see description below) is a topological measure of segregated information transfer. The global efficiency (GE) is a metric for efficiency of integrative information transfer across the network. This measure is inversely related to the characteristic path length (average shortest path between nodes) but is adapted to fragmented that is disconnected graphs.

To explore the local/nodal network metrics we employed the degree and the local efficiency. Each of these measures describe different aspects of topological node centrality permitting the identification of nodes that have the highest influence on network-wide processes. The degree represents the number of links connected to the node, assuming that nodes with many connections have a higher influence on the network in comparison to low-degree nodes. The local efficiency measures the integration capacity between immediate neighbors of a given node. This metric also reflects the network resilience by indicating how efficiently neighbors of a given node communicate when this node is disrupted.

4.2.3.4.4 Network reorganization mechanism

We introduce a novel methodological approach which we labeled as the *edge probability map.* This measures presents the difference between groups in connections between specific nodes in a given network. Individual subject correlation matrices were thresholded using the connection density threshold to obtain binary undirected graphs. The individual connection density matrices were then summed for the patient and the control group separately, in order to obtain the number of subjects that had a significant connection between a given pair of nodes. These values were then normalized to a percentage of subjects having a specific connection within this network and subtracted between groups to obtain the difference in the percentage of subjects having a connection between particular nodes. This was done to identify specific disconnections driving the increase or decrease of node degree in the patient group.

To detect network reorganization in comatose patients we have also computed the *hub disruption index* (HDI) for nodal measures (Achard et al., 2012). To calculate HDI for a given metric, for example the degree, we subtract the healthy group mean degree from the degree of the corresponding node in an individual subject, and plot this individual difference against the healthy group mean. The slope of a straight line fitted to a given plot is referred to as hub

disruption index. A negative HDI close to -1, indicates a severe network reorganization, meaning that nodes with highest degree (i.e. hubness) in controls show greatest reduction in patients, whereas the nodes with lowest nodal degree in controls show the greatest increase in patients.

4.2.3.4.5 Network resilience to random failure and targeted attack

To assess the resilience of the brain network we simulated the attacks on the network by removing nodes (and its connections) in rank order of decreasing degree (targeted attack) or in random order (random failure), repeating the process until the percentage of deleted nodes was 100%. After each deletion, we re-estimated the clustering and the global efficiency in order to explore the global impact of the simulated lesion on the brain network.

4.2.3.5 Statistical analysis

Global and nodal statistics (and functional connectivity) were compared between groups with t-tests or permutation (100.000 iterations) using the package lmPerm implemented in R (v.3.3.2; The R Project for Statistical Computing; http://www.R-project.org/). To control the multiple comparisons for each nodal metric, the significance level of p-values was adjusted to 1/N (p=.012), where N represent the number of nodes included in the analysis. The results were visualized with the BrainNet Viewer (Xia et al., 2013).

4.2.4 Results

4.2.4.1 Global network topology

In comparison to controls, patients showed a decrease in clustering across multiple thresholds, as seen in Figure 4.2.1. (at cost 15%, permutation test p<.0001). However, there were no statistically significant difference in the global efficiency between the two groups (permutation test p=.198). These results seem to imply a loss of balance between segregation and integrative properties of the brain network and may reflect loss of specialized information processing and dedifferentiation within high-order resting state network included in our analysis.

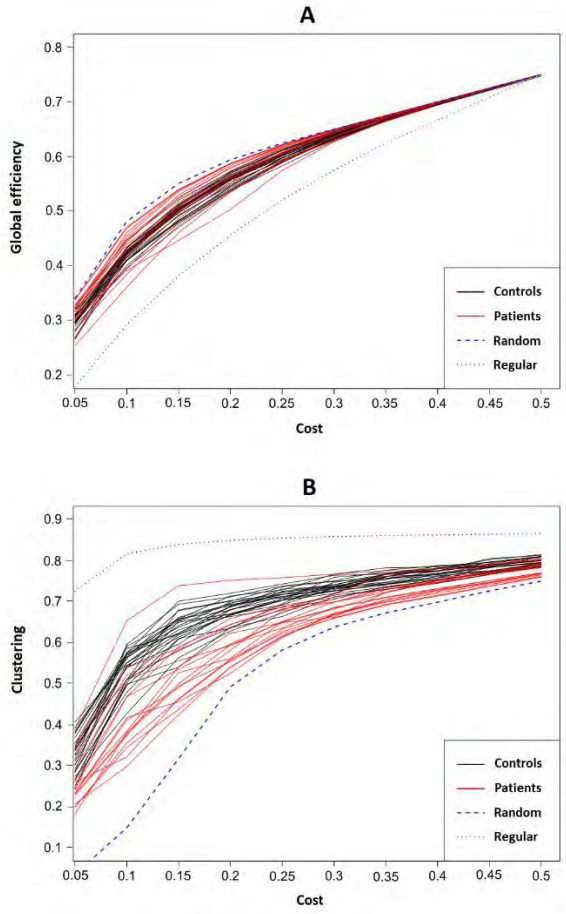

Figure 4.2.1. Global topology in controls and patients.
A) Global efficiency (GE) in controls and patients in comparison to regular and random networks, at multiple connection density thresholds (5-50%, increment 5%). B) Clustering in controls and patients in comparison to regular and random networks, at multiple connection density thresholds (5-50%, increment 5%).

4.2.4.2 Disruption of hub rank order

This hub disruption index summarizes the pattern of network reorganization, in subtracting the healthy group mean value from the value of the corresponding node in coma patients, and plotting this individual difference against the healthy group mean. The slope of a straight line fitted to a given plot is referred to as hub disruption index (Achard et al., 2012). A negative HDI close to -1, indicates a severe network reorganization, meaning that nodes with highest nodal efficiency (i.e. hubness) in controls show greatest reduction in patients, whereas the nodes with lowest nodal efficiency in controls show the greatest increase in patients. The hub disruption index calculated with the global (nodal) efficiency (permutation $p<.0001$) and local efficiency (permutation $p<.001$) implied significant brain network reorganization within the

patient group (Figure 4.2.2). Further, HDI calculated using the degree implied the same significant brain network reorganization within the patient group in comparison to control group (Figure 3A), and we found evidence of a critical reorganization of high degree nodes (i.e. hubs). Namely, cortical regions that were hubs of healthy brain networks seemed to become non-hubs of comatose brain networks and vice versa. However, there seemed to be significant heterogeneity within the coma patient group (Figure 4.2.3. - subpanel B), with some individuals showing severe reorganization at global level, while others having similar values to healthy subjects.

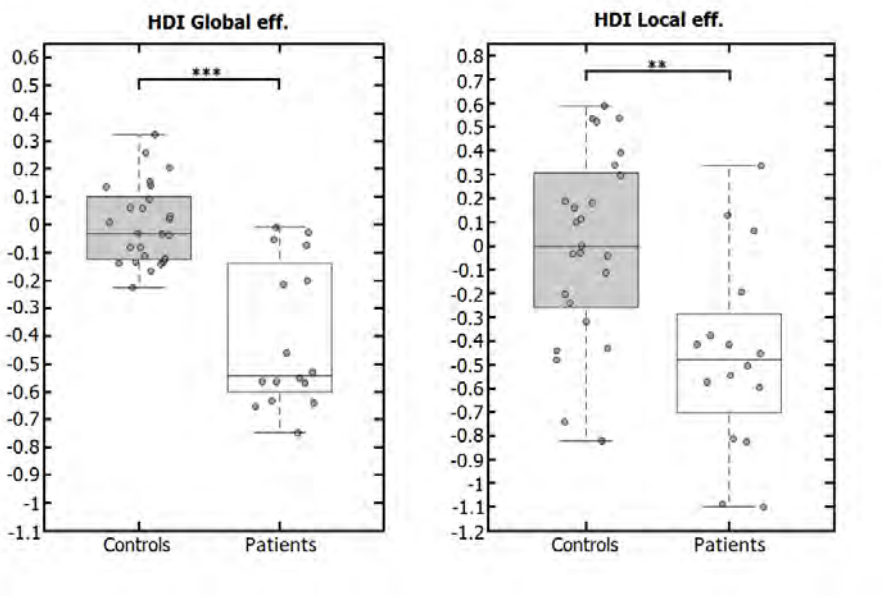

Figure 4.2.2. Brain node reorganization - the difference between groups in the HDI of global (nodal) efficiency and local efficiency.
*Boxplots represent medians with interquartile range and whiskers signify minimum and maximum values (excluding outliers); ** p< .001, *** p<.0001*

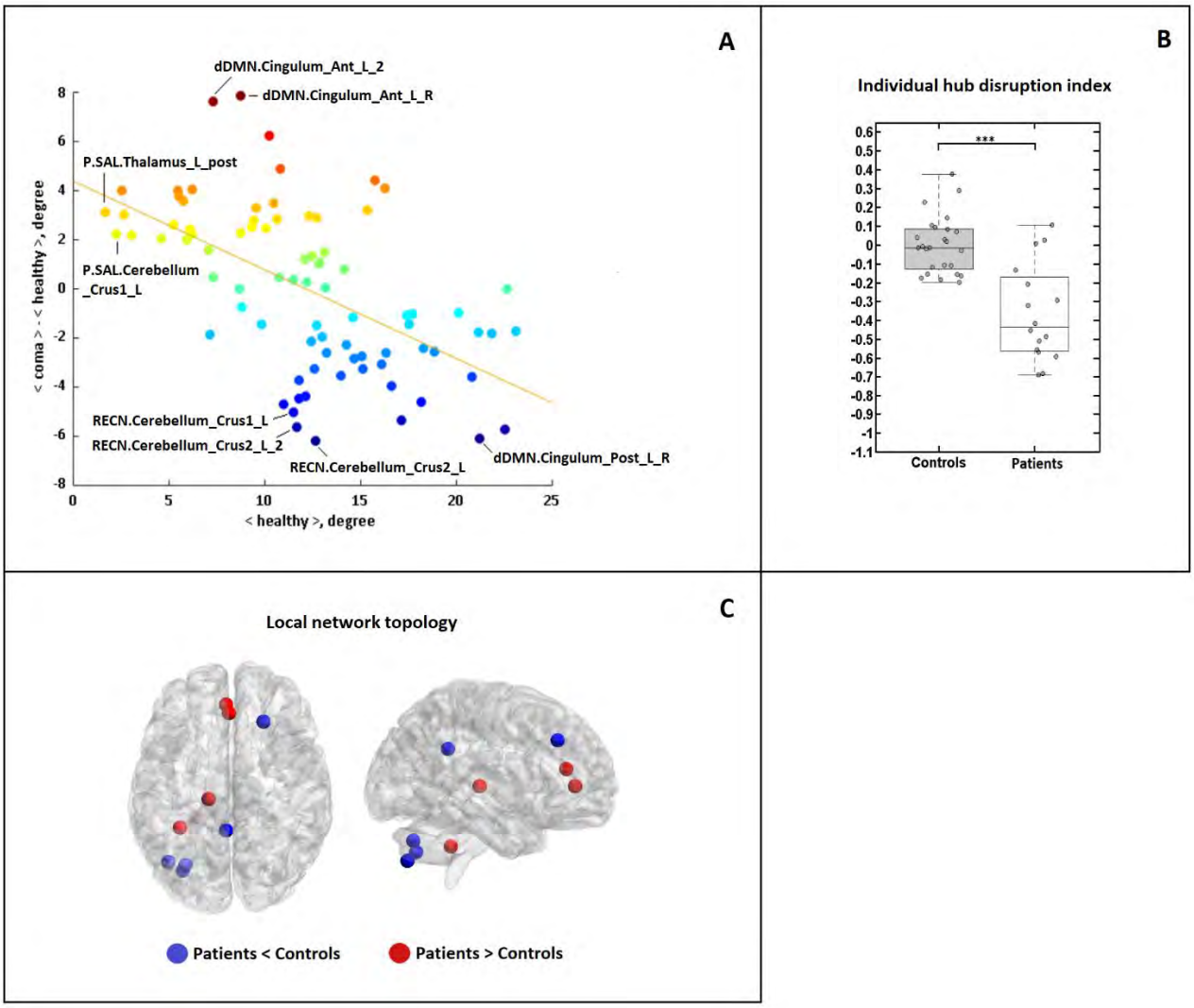

Figure 4.2.3. Local network topology.
A) Hub disruption of functional networks in comatose patients. *The mean degree of each node in the healthy control group (x axis) is plotted against the difference between the groups in mean degree of each node (y axis). Normal hub nodes with high degree in the healthy group have a reduction in degree in the comatose group (i.e. dDMN.Cingulum_Post_L_R), whereas the healthy non-hub nodes have an increase of degree in patients (i.e. dDMN.Cingulum_Ant_L_2).* ***B) Hub disruption index for each of the subjects in the control and the patient group.*** *The HDI calculated using the degree is significantly different between the groups. The boxplot represents medians with interquartile range and whiskers signify minimum and maximum values (*** p< .0001).* ***C) Brain representation of nodes that demonstrated significant between-group difference in nodal degree****; P>C – significantly higher in patients; P<C –significantly lower in patients.*

4.2.4.3 Local network topology

4.2.4.3.1 Node degree

In accordance to hub disruption index estimated using the degree (Figure 4.2.3 – subpanel A), Figure 4.2.3 (subpanel C) shows multiple regions that significantly differ between the patients and the control group at nodal level (15% threshold; see Supp. Figure 6.3.9. for other thresholds).

Overall, we can see a major disruption in brain node centrality in the patient group reflected in a combination of decrease and increase of node degree, suggesting specific regional changes in brain network organization as seen in the HDI results. The decrease of nodal degree encompassed the posterior cingulate gyrus (dDMN), the right middle frontal gyrus (vDMN) and the left crus (I and II) of cerebellar hemisphere (RECN). In contrast, the increase of nodal degree was shown in the anterior cingulate gyrus (dDMN), the left posterior thalamus (P.SAL) and a sub-region of the left crus I of cerebellar hemisphere (P.SAL).

4.2.4.3.2 Edge probability map

To identify specific disconnections driving the increase or decrease of node degree in the patient group we calculated the *edge probability map* (Figure 4.2.4 – subpanel A). This measures presents the difference in the percentage of coma patients and healthy subjects having a specific between-node pairwise connection in a given network (Figure 4.2.4 - subpanel B).

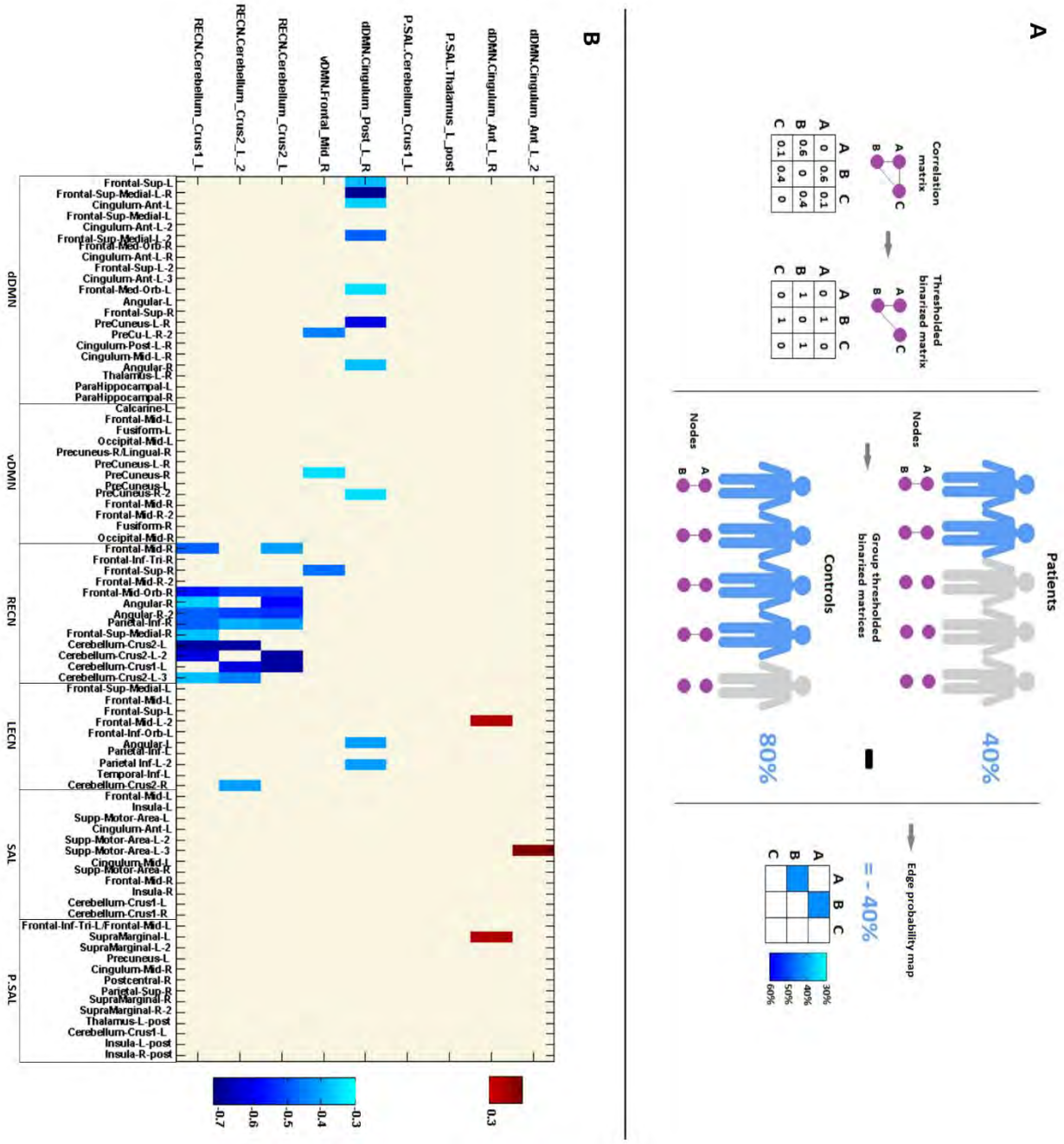

Figure 4.2.4. A) The analysis pipeline for the edge probability map.
Individual thresholded binarized adjacency matrices were summed in each subject group in order to obtain the proportion of subjects with a specific connection between a given pair of nodes. These values were then subtracted between groups in order to obtain the difference in the percentage of subjects having a particular pairwise node connection. ***B) Edge probability map.*** *X and Y axes present the nodes in a given network and the color scale reflects the difference between the percentage of patient and healthy control subjects having a particular pairwise connection. The blue color (negative values) reflects a lower percentage of patients than healthy subjects with a specific connection, while the red color shows the opposite. The map was thresholded to reflect at least 33% of more/less patients having a given between-node connection in comparison to controls.*

The posterior cingulate cortex (dDMN) seemed primarily disconnected to other regions from the predefined dDMN network, such as different sub-regions of the frontal and anterior cingulate cortex, with the most prominent disconnections with the superior medial frontal cortex and the precuneus. In addition, the posterior cingulate showed inter-network disconnections, such as lower connectivity with the left angular gyrus and the inferior parietal cortex, originally integrated in the LECN. Further, vDMN's right middle frontal gyrus (vDMN) was primarily disconnected to the sub-areas of the right precuneus and superior frontal cortex, implying mostly intra-hemispheric disruption in connectivity. Interestingly, all of these changes reflected some local but mostly long-range disconnections between posterior parietal and frontal regions. The sub-regions of the RECN's crus of the cerebellar area showed intra-network disconnections, with most other RECN regions, prominently the right medial orbitofrontal cortex, angular gyrus, inferior parietal lobule and other sub-regions of the cerebellum crus.
Increases in between-node connections found in the patient group were predominantly characterized by wide-spread mostly weak (in small percentage of patients) augmentation in connections, as present for the left posterior thalamus (P.SAL) and the cerebellum crus I (LECN). An increase in degree was more visible for dDMN's anterior cingulate cortex, with its two sub-regions showing different profiles of increase in connectivity – the left sub-portion with the left supplementary motor area (SAL), and the more medial sub-region with the left middle frontal gyrus (LECN) and the supramarginal gyrus (P.SAL).

4.2.4.4 Resilience

To assess brain network's robustness after acute brain injury, we explored both the local efficiency (i.e. measure the integration capacity between immediate neighbors of a given node) across the whole set of high-order resting state network included in our analysis, and the impact of simulated random/targeted networks attacks, aiming to have additional insights on the topological role played by brain hubs within the rearranged residual brain networks.

4.2.4.4.1 Local efficiency

The local efficiency indicates how efficiently neighbors of a given node communicate when this node is disrupted. Figure 4.2.5. shows a dramatic decrease in local efficiency, in wide range of nodes in patients, supporting the results of reduction in global clustering. This decrease was primarily seen in the precuneus, posterior cingulate, angular gyrus, cerebellum crus and the

frontal mid regions. Interestingly, these regions showed mutual disconnections (Figure 4.2.4 – subpanel B) probably underlying the lower clustering and resilience seen at global level.

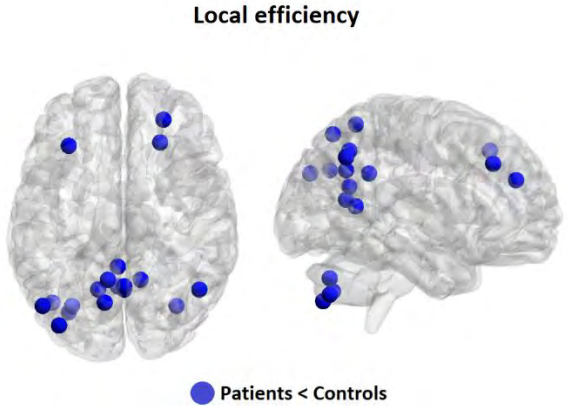

Figure 4.2.5. Brain regions with a significantly lower local efficiency in patients in comparison to controls. *The regions with lower local efficiency are predominantly localized in the posterior regions of the brain in coma patients.*

4.2.4.4.2 Node attack

To further assess the resilience of the brain network in coma patients we simulated the attacks on the network by removing nodes (and its connections) in rank order of decreasing degree (targeted attack) or in random order (random failure).

Figure 4.2.6. shows the clustering as a function of results of targeted node attack (subpanel A) or random failure (subpanel C). For example, under targeted attack after removal of 25% of nodes, the clustering decreased by 44% (median values) in controls and 64% in patients (permutation $p<.000$), indicating reduced resilience in individuals in coma. Further, we can observe that under random failure, there wasn't a large difference in resilience between the control and the patient group, with a decrease in clustering by 27% and 29% from the baseline, in the control and the patient group, respectively (permutation $p=.007$).

In contrary to these results, the global efficiency showed similar decrease in both groups (Figure 4.2.6), under targeted attack (subpanel B) and random failure (subpanel D). In other words, after targeted removal of 25% of the nodes, the GE was reduced by 57% and 54% ($p=.54$), while under random failure the global efficiency was decreased by 45% and 44% ($p=.145$), in controls and patients, respectively.

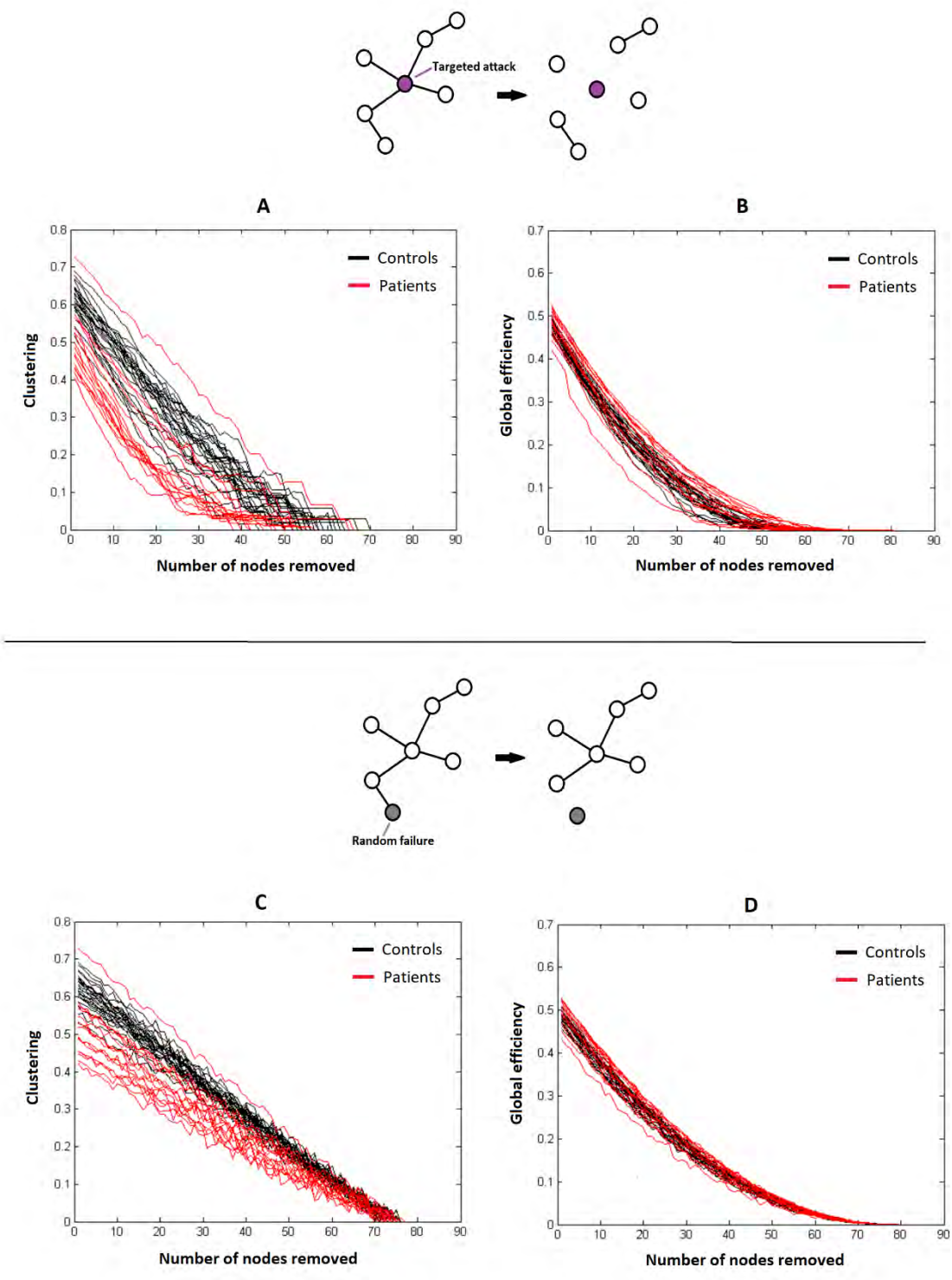

Figure 4.2.6. Network resilience. Network resilience to targeted attack (A and B) and random failure (C and D) in controls and patients.

The curves represent the clustering or global efficiency (y axis) as a function of number of nodes attacked (x axis). Under targeted attack, the clustering decreased more rapidly in patients in comparison to controls, indicating reduced resilience in individuals in coma. The global efficiency declined in a similar way after sequential removal of high-degree nodes in both groups.

4.2.5 Discussion

Our findings significantly contribute to the growing evidence of the involvement of specific high-order RSNs networks, and their critical regions, in the mechanisms during abolition of consciousness. We observed among comatose patients a large repertoire of information processing disturbances, at several levels: (i) whole brain impairments, encompassing gradual disruption in topological clustering with the most severe changes implying a loss of functional degeneracy (ii) significant disruption of hubs rank order across local networks metrics, suggesting a critical reorganization of high degree nodes, with cortical regions that were hubs of healthy brain networks becoming non-hubs of comatose brain networks and vice versa, (iii) regularly observed specific coma-related within and between high-order RSN disconnections, encompassing both losses and increases of long-range connections between connector hubs, that might be related to functional dedifferentiation and adaptive compensation processes, respectively (Fornito et al., 2015), (iv) a reduction in network resilience in coma patients as simulated damage to reorganized high-degree nodes resulted in rapid network fragmentation.
The graph theoretical analysis of rs-fMRI data in the patient group, implied less efficient local information integration and functional 'closeness' between neighboring nodes across the entire high-order RSN connectome. It must be stressed that reduced clustering and modularity were shown in previous studies on chronic DOC patients (Chennu et al., 2014; Crone et al., 2014), but have not been yet reported in the pathological setting of acute brain injured patients. In contrary to current results, a previous rs-fMRI study did not find significant changes in the global measure of functional connectivity or network topology in the acute stage of brain injured patients (Achard et al., 2012). This discrepancy may be explained by the differences in patient's neurological severity, brain injury etiologies, and network definitions, because we deliberately focused on nodes integrated in high-order RSNs considered to be implicated in consciousness-related processes (Giacino et al., 2014). The preservation of global efficiency in coma patients may be due to the homeostatic conservation of this topological property even under severe clinical conditions such as anoxic brain injury (Achard et al., 2012). However, in our case, it could be indicative of random distribution of information that is nor specialized nor integrative due to impairment in local specialized neural processing, present in our coma patients. Altogether, these results suggest a loss of small-world organization in patients, which normally ensures a balance between specialized/segregated and long-range integrated information processing (Achard, Salvador, Whitcher, Sucklig, & Bullmore, 2006; Bullmore & Sporns, 2012). These results support the hypothesis that conscious processing depends on brain

complexity, implying a fine-tuned balance between these two global topological properties (Casali et al., 2013; Chennu et al., 2017; Tononi & Koch, 2008, 2015).

At the nodal level, we found strong evidence of node centrality disruption in non-random comatose patients in comparison to the control group. The most significant decrease in centrality (i.e. degree and local efficiency) was found in the posterior cingulate of the dDMN, left cerebellum crus of RECN and frontal mid region of the vDMN network. Interestingly, the changes in nodal degree reflected some local but mostly long-range disconnections between posterior parietal and frontal hub regions, some of them related to changes in inter-modular connectivity (i.e. connector hub) as shown for the dorsal posterior cingulate of the dDMN. Previous functional connectivity studies in DOC patients, have suggested significant changes along high-order midline posterior parietal (encompassing the precuneus and the posterior cingulate cortex) and frontal regions in this setting (Achard et al., 2012; Chennu et al., 2017; Crone et al., 2014; Hannawi et al., 2015; Silva et al., 2015). In the current study, the most dramatic changes were reflected in the decrease in local efficiency in the midline posterior parietal cortex, related to a diminished integration between neighboring nodes, and consequently lower resiliency and efficiency in parallel information transfer of the network. It must be stressed that a multimodal function, underpinned by a 'rich club organization' of the posterior parietal cortex has been recently suggested (Alstott et al., 2009; van den Heuvel & Sporns, 2011; Wang et al., 2014), and its role in human attentional focus and 'tuning' of whole-brain metastability (Leech & Sharp, 2014), made of this brain region a strong candidate of the 'minimally sufficient and jointly necessary' (Crick & Koch, 2003) hubs that could constitute the neural correlate of consciousness. Our data fit well in current theoretical frameworks of conscious processing including the Global Neuronal Workspace (GNW), model according to which conscious access occurs when initially segregated specialized information processing (i.e. clustering) is made globally available to multiple brain systems through a network of neurons with long-range axons situated along the frontal and parietal brain regions (Dehaene & Changeux, 2011).

Otherwise, we found robust evidence of non-hub sub-regions of the RECN's cerebellum crus intra-network disconnections. We hypothesize that this circuit-selective significant reduction of cerebellum centrality could be linked to diaschisis phenomena caused by a reduced excitatory drive from the damaged cortex, to which cerebellum is densely connected (Herculano-Houzel, 2012) and could represent in the context of global brain severe injury, a potential useful biomarker of diffuse cortico-cortical and cortico-thalamic widespread functional disruption. From a cognitive point of view, this massive cerebellar disconnection seems in line with recent

studies which highlighted the cognitive role of this brain structure in consciousness related processes as attention, working memory and self-reference tasks (Buckner, 2013; Sokolov, Miall, & Ivry, 2017).

We concomitantly observed increases in between-node connections in the patient group, primarily characterized by wide-spread mostly weak augmentation in connections. Further analysis indicated that the regions with increased degree in patients tended to be the least central nodes in the healthy controls, implying potential compensatory brain plastic processes, reflected through reallocation of critical residual neural resources to otherwise not so central nodes (Di Perri et al. 2014; Hillary et al., 2015; Liu et al., 2017). Brain regions depicting this pathological pattern were mainly located within the salience network, which is known to be implicated in homeostatic/visceral perception (Uddin, 2014) and seems to be responsible of the critical switch between DMN and ECN throughout higher order-cognitive processes (Bonnelle et al., 2012; Menon, 2015). The functional significance of this pathological increase of connectivity remains an important topic for further investigation (Di Perri et al., 2016; Hillary et al., 2015).

Finally, we found evidence of decreased resilience in anoxic comatose patient's brain connectome reflected in a rapid deterioration of global clustering across high-order RSNs caused by a simulated high-degree node "lesioning". Nevertheless, the global efficiency of comatose patient's brain networks proved to be as resilient as those in healthy control individuals, during random and targeted deletion of nodes. Altogether, these results might imply that the coma patient's hub node reorganization may have prevented the loss of global integrative properties but did in fact lead to dedifferentiated non-specialized functional processing related to lower networks resilience and potential diffusion of network failure. In fact, strong local inter-connectivity within the modules (i.e. RSNs) is known to be closely tied to functional degeneracy which reflects the brain's capacity for resilience and recovery after injury, and seems supported by high-degree nodes embedded locally (provincial hubs) and bridge nodes serving to connect otherwise segregated processes (connector hubs), facilitating the recruitment of alternative subsystems (Fornito et al., 2015).

This study has several limitations. A recent publication (van den Heuvel et al., 2017) has implied some short-comings in applying proportional thresholding in patient-control comparison studies in which groups show differences in overall strength of functional connectivity. We have taken some measures of precaution in order to diminish this difference between our groups, however, comatose patients usually have lower global functional connectivity in contrary to healthy controls, which could induce or artificially inflate the between-group topological differences. Thus, further studies should explore different methods

of edge selection, such as weighted thresholding or the unique inclusion of statistically significant links in network construction. Different functional atlases could be used to explore the brain topology in coma patients and it would be interesting to see if differently constructed brain networks result in contrasting or comparable results with a similar clinical message. Our team is currently testing different approaches of network construction in order to define a graph-based method which could be applied to coma patients without dramatic exclusion of subjects. Additionally, further research needs to include more patients with accurate long-term longitudinal follow-up, encompassing repeated behavioral and fMRI assessment because topological organization could significantly change over the course of time (Castellanos et al., 2011; Nakamura, Hillary, & Biswal, 2009). Comatose patients with different etiologies, such as traumatic brain injury, should be also studied aiming to identify potential etiology-related pathology mechanisms.

4.3 The PMC-mPFC structure-function association in coma – an exploratory study

4.3.1 Scientific justification

A growing body of literature exists on the severe impairment in resting-state functional connectivity and white and gray matter structural damage within the midline cortical regions, primarily integrated in the default-mode network (DMN), in DOC patient (Table 2.2.1). However, most of these studies have been conducted independently, without direct investigation of the structure-function relationship in chronic DOC or acute stage coma patients (Table 2.3.1). It is important to note, that the microstructural integrity of the white matter connections between the posteromedial and medial prefrontal regions has been related to level of functional connectivity between these two regions in healthy subjects (van den Heuvel et al., 2008; Wang et al., 2014). Further, an association between the loss of structural integrity in the DMN key nodes including their white matter connections, and the corresponding functional connectivity, has been has been found in cognitively impaired TBI patients (Bonnelle et al., 2011; Palacios et al., 2013; Sharp et al., 2011) and older healthy subjects (Vidal-Piñeiro et al., 2014). A recent study has indeed demonstrated a significant structure-function correlation in chronic DOC patients, with an increase in global structural damage (i.e. FA in whole brain white matter) related to a reduction in effective connectivity (Bodart et al., 2017). Nevertheless, the structural-functional connectivity relationship has not yet been demonstrated in the brain-injured population in the acute stage of coma.

The present study is a preliminary exploratory study. The previous couple of years spent in analyzing functional connectivity data have resulted in multiple questions regarding the relationship between structural damage and functional dysfunctions in coma patients. This project was executed in the end of my third year, and is not as elaborated as the previous two ones due to time constraints. Nevertheless, the preliminary results presented in this thesis have led to other projects which are currently being executed by our team.

4.3.2 Objectives and hypotheses

The main objective of this study was to investigate the structural integrity, and the structure-function relationship of the PMC (posteromedial) and mPFC (medial prefrontal cortex) sub-regions and their corresponding white matter connections. We expected to find significant structural injury paralleled with a loss of functional connectivity in all comatose patients, irrespective of etiology. However, we hypothesized that the anoxic brain injury patients would primarily show cortical gray matter damage, while TBI patients would mostly exhibit a loss of white matter microstructure within the tract connecting the PMC and mPFC sub-regions.

4.3.3 Methods

4.3.3.1 Participants

From the total number (N = 35) of recruited anoxic BI patients, 6 patients were excluded from this study, 1 due to excessive movement (≥3 mm), 3 due to preprocessing failure (e.g. normalization failure due to ventricular enlargement) and 2 because of low quality (i.e. artefacts) of the acquired images. From the total TBI comatose patients (N=20), 6 patients were excluded, 2 due to excessive movement and 4 due to severe focal brain damage mostly localized in the frontal lobe and thus significantly overlapping with our regions of interest.
Therefore, the final group of patients comprised 29 anoxic (Mean= 51y; STD= 18y; age range= 18-81y) BI injury, and 14 TBI (Mean= 43y; STD= 19y; age range= 18-76y) comatose patients. Thirty four age-matched healthy controls were also included in the analysis (Mean= 50y; STD= 20y; age range= 22-74y).

4.3.3.2 ROI selection

Our cortical gray matter ROIs were selected using the "Willard" functional atlas (Richiardi et al., 2015). This atlas has more gray matter (GM) coverage but significantly overlaps with the original functional atlas published in the article of Shirer and colleagues (2012). More specifically, we chose the three sub-regions of the PMC, and 11 sub-regions of the frontal cortex (i.e. mPFC and anterior cingulate) integrated in the dDMN network, as these were the regions that were most consistently shown to be altered in our comatose patients (and DOC patients in

other studies). The analysis was done using each of these sub-regions separately, and using the total mean values, averaged separately for the PMC and the mPFC region.

The white matter ROI was taken from the atlas published by Figley and colleagues (2015), which is based on an fMRI guided DTI tractography between PMC and mPFC nodes of the dDMN network integrated in the functional atlas published by Shirer and colleagues (2012). Their analysis resulted in a group probability map, more conservative than the raw connection counts, because it reflected the requirement of at least 25% of all subjects having overlapping streamlines (between these two nodes) that are in exactly the same spatial location (in order to eliminate biologically spurious or unlikely tracts). We avoided additional conservative thresholding, due to the inclusion of acquired brain injury patients in which spatial normalization is not always as successful as in healthy controls. The original WM ROI was separated into left and right ROIs, to compare the groups in total and lateralized WM changes. As it may be seen in Figure 1, the WM tract largely overlaps with the cingulum bundle, so for now on, we will refer to this ROI as the cingulum.

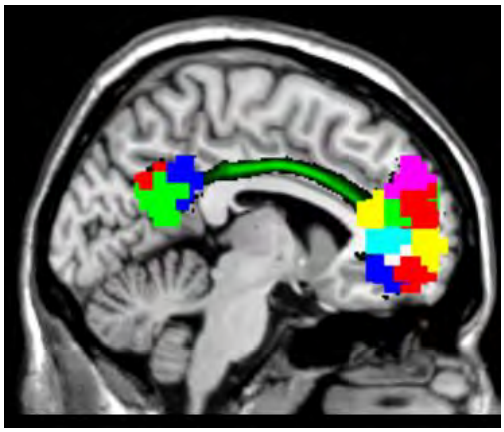

Figure 4.3.4.3.1. Gray matter and white matter ROIs included in our analysis.
The sub-regions are delineated using different colors without any specific significance attached to color nuances.

4.3.3.3 Image processing

4.3.3.3.1 Structural MRI

Gray matter morphometry

Morphometry is the study of the size and the shape of the brain, and is based on standard MRI sequences, such as T1-weighted images (Greve, 2011). There are several metrics that one can

use to test a morphometry-related hypothesis such as gray matter volume, white matter volume or cortical thickness (Greve, 2011). We will specifically focus on voxel-based morphometry (VBM), which enables the investigation of voxel-wise differences in the local grey matter volume/topography without priori information about the location of these possible differences (Good et al., 2001).

Image processing was performed using FSL v5 (www.fmrib.ox.ac.uk/fsl/) and an in-house developed software in Matlab (version 6.5, The MathWorks), with procedures similar to those described previously (Cherubini, Péran, Caltagirone, Sabatini, & Spalletta, 2009; Péran et al., 2009, 2010).

Voxel-based morphometry was performed using the implemented FSL tool FSL-VBM v1.1 (Douaud et al., 2007), an optimized VBM protocol (Good et al., 2001). Briefly, all the T1 images where first brain extracted then segmented into images of gray matter (GM), white matter (WM), and cerebro-spinal fluid (CSF). GM images where then non-linearly registered (Andersson, Jenkinson, & Smith, 2007) to the gray matter ICBM-152 template, concatenated and averaged. The resulting image was then flipped along the x-axis and both images where averaged again creating the first GM template. Second, GM images of all participants where non-linearly registered to this study specific template, and using the same final steps, a second "non-linear" GM template was generated. This "non-linear" template was finally used to register all the GM images. Then, the registered images of all subjects were multiplied by the Jacobian of the warp field in order to introduce a compensation (or "modulation") correction for local expansion or contraction, due to the non-linear component of the spatial transformation. The corrected registered images were then concatenated and smoothed by a Gaussian kernel (sigma = 4mm) to reduce registration imperfections and increase the signal-to-noise ratio. Thus, gray density (GD) images were calculated for each participant.

Diffusion tensor imaging

The preprocessing of the diffusion tensor images was accomplished with FSL implemented tool FDT (FMRIB's Diffusion Toolbox; https://fsl.fmrib.ox.ac.uk/fsl/fslwiki/FDT). The diffusion tensor images were first corrected for distortions caused by eddy currents using the b = 0 volume as reference. A diffusion tensor model was fit at each voxel and two diffusion parameters were extracted, fractional anisotropy (FA) and mean diffusivity (MD), to build two parametric maps. The FA maps were then registered to brain-extracted whole-brain volumes from T1-weighted images using a full affine (correlation ratio cost function) alignment with nearest-neighbor

resampling. The calculated transformation matrix was then applied to the MD maps with identical resampling options. The final results were obtained in calculating the average FA and MD values in the GM and WM regions of interest, described in the previous section.

4.3.3.3.2 Resting-state functional MRI

As in previous studies, functional data were preprocessed using Statistical Parametric Mapping (version SPM 12; http://www.fil.ion.ucl.ac.uk/spm/). The fMRI images were realigned (motion corrected), slice-time corrected, coregistered to each subject's T1-weighted image and normalized to standard stereotaxic anatomical Montreal Neurological Institute (MNI) space (ref). The images were not smoothed in order to minimize the spillage of the signal of the neighboring ROIs. T1-weighted images were segmented to compute gray matter, white matter and cerebro-spinal fluid images.

Rs-fMRI data was further analyzed using the CONN toolbox (v.16a; http://www.nitrc.org/projects/conn; Whitfield-Gabrieli & Nieto-Castanon, 2012). In order to reduce the motion effects on our data, we only included subjects characterized by motion parameters smaller than 3 mm translation and 3° rotation. We have also performed ART outlier detection & scrubbing, as an additional preprocessing step to identify rapid scan-wise movement (global-signal scan-to-scan Z-value=5, and a composite subject-motion signal mm-value = 0.9mm). Non-neuronal sources of noise were estimated and removed using the CompCor method (Behzadi et al., 2007) integrated in the CONN toolbox. Principal components of the signals from the white matter and the CSF voxels (using normalized T1 segmented masks), alongside the motion parameters (estimated during realignment) and between-scan motion outliers (ART toolbox), were removed with regression. Finally, a temporal band-pass filter was applied to the residual blood oxygen level–dependent (BOLD) time course in order to obtain a low-frequency range of 0.01 to 0.1 Hz.

4.3.3.4 Statistical analysis

The Mann-Whitney U test was conducted to investigate the differences in functional connectivity (i.e. Pearson's r) and structural integrity (i.e. VBM - gray matter density, MD, FA) between the coma patient group and the healthy control group. The same test was used to compare the two etiology groups – the anoxic BI and TBI patient sub-groups.

Spearman's correlation analysis was performed to explore the link between the structural integrity and functional connectivity in the total patient group, and two separate etiology groups. All of the above mentioned analyses were performed using the IBM SPSS (IBM SPSS Statistics for Windows, Version 20.0. Armonk, NY: IBM Corp.) statistical package.

4.3.4 Results

4.3.4.1 Structural damage and etiology-related differences in patients

Regional results

The mean diffusivity of the cingulum was significantly higher in the patient group in comparison to the control group (U = 455, p = .005; Figure 4.3.4.3.2).

Further analysis showed that this increase of diffusivity was more present in the TBI group in comparison to the control (U= 64, p< .0001) and anoxic BI (U= 116, p= .024) subjects. Moreover, the loss of structural integrity, primarily seen in TBI patients, seemed to be lateralized with more damage in the right cingulum, indicated by an increase of MD and decrease of FA in this white matter tract (Figure 4.3.4.3.3.). The anoxic patient group showed a significant increase in gray matter VBM values in the PMC region, in comparison to controls (U= 315, p= .014) and traumatic BI patients (U= 120, p= .031) (Figure 4.3.4.3.2).

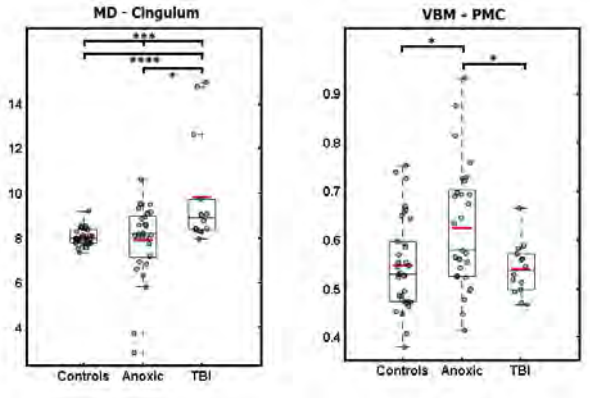

Figure 4.3.4.3.2. Group differences in structural metrics of averaged ROIs.
*The red line presents the mean values of a given metric. The * indicates p<.05, ** p<.01, *** p<.005, **** p<.001. The MD values were multiplied by 10.000 for visualization purposes.*

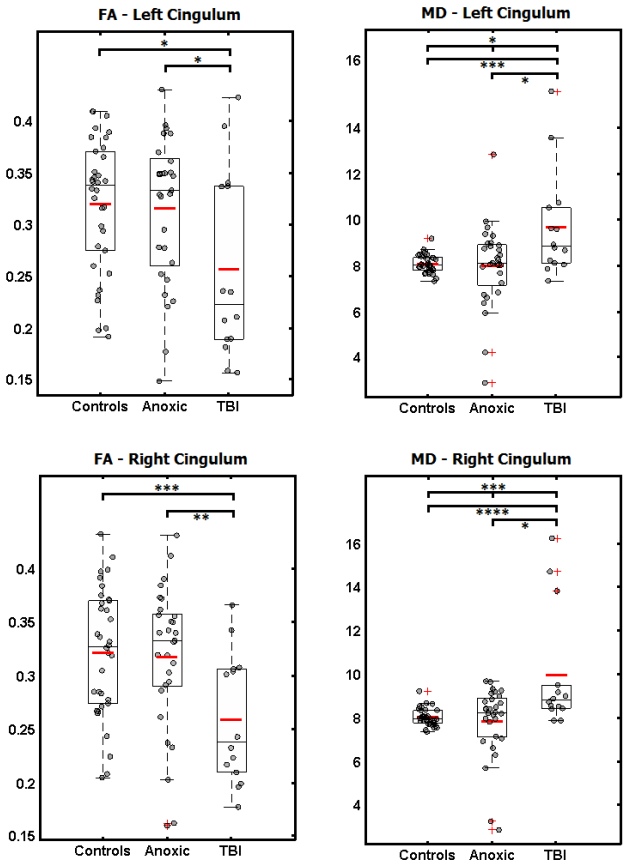

Figure 4.3.4.3.3. Group differences in DTI metrics of the left and right cingulum.
*The red line presents the mean values of a given metric. The * indicates p<.05, ** p<.01, *** p<.005, **** p<.001. The MD values were multiplied by 10.000 for visualization purposes.*

Sub-regional results

The apparent increase in the PMC grey matter density seen in anoxic BI in comparison to controls and TBI patients, was principally located within the PMC 01 and PMC 02 sub-regions. The remaining sub-region of the PMC exhibited an increase in FA only in anoxic patients (Figure 4.3.4.3.4.).

Elevated FA and diminished MD were also shown in several sub-regions of the mPFC in both anoxic and TBI patient groups (Figure 4.3.4.3.4.). However, the increase of the VBM values seemed to be specific to the posteromedial cortex in anoxic brain injury.

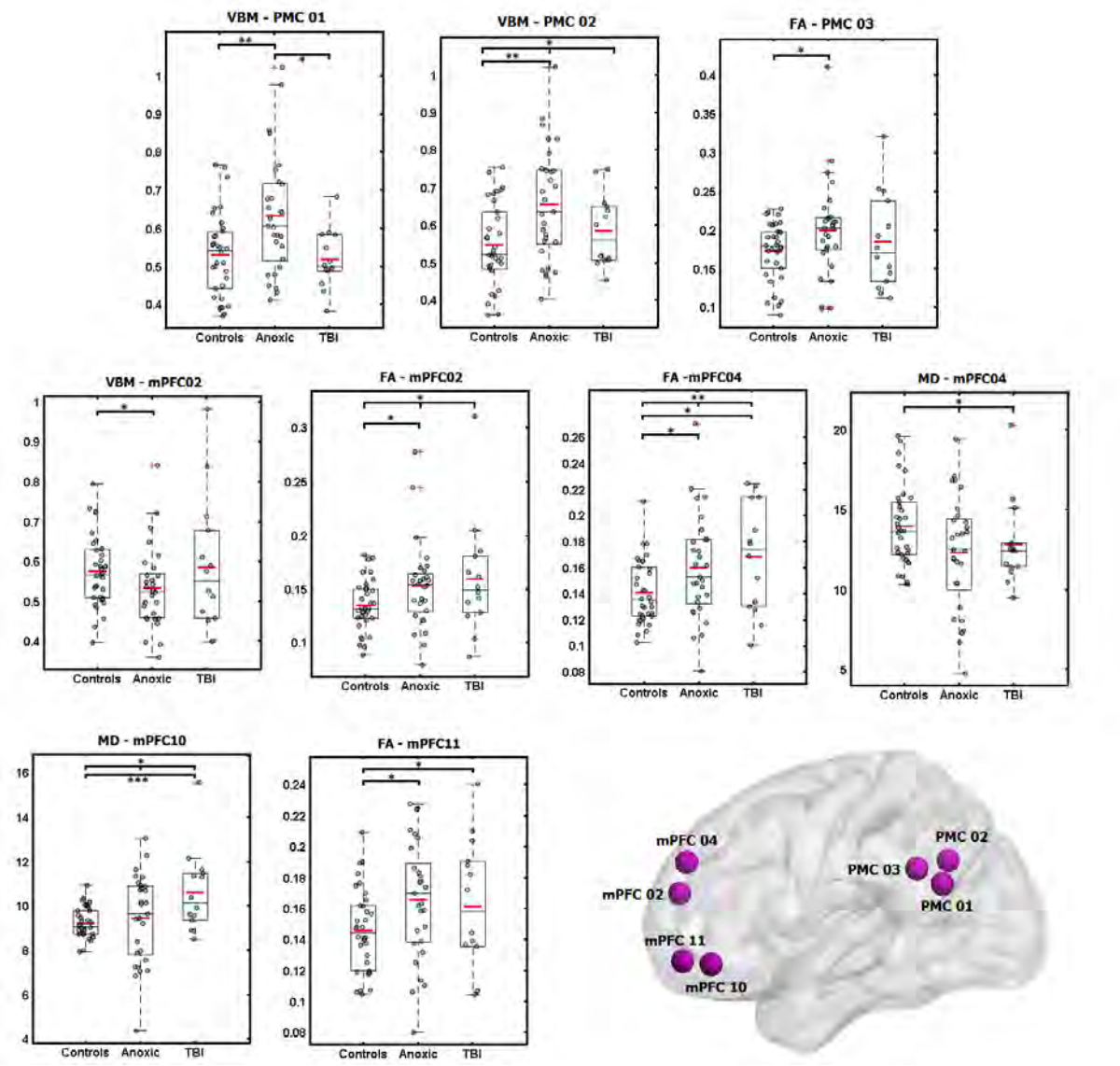

Figure 4.3.4.3.4. Group differences in structural metrics of PMC and mPFC sub-regions.
*The red line presents the mean values of a given metric. The * indicates p<.05, ** p<.01, *** p<.005. The brain image illustrates the anatomical location of center-coordinate spheres of ROIs presented in boxplots. The MD values were multiplied by 10.000 for visualization purposes.*

4.3.4.2 Functional disconnections in the patient group

Figure 4.3.4.3.5. shows the group comparison in mean PMC-mPFC functional connectivity. The FC strength was significantly lower in all patients (U= 89, p< .0001), and in the anoxic (U= 29, p< .0001) and TBI (U= 60, p< .0001) patient group, separately. These results are compatible with the findings from earlier studies presented in this thesis.

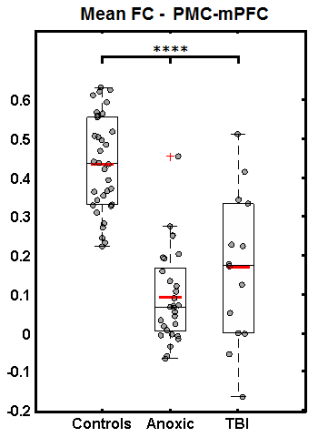

Figure 4.3.4.3.5. Group differences in mean functional connectivity between the entire PMC and the mPFC region. *The red line presents the mean values of a given metric. The **** indicates p<0.001.*

In addition, the FC strength was significantly lower between all PMC and mPFC sub-regions ($p < .001$), except between the mPFC08 and the three sub-regions of the PMC, and the mPFC10 and PMC01 and PMC02. The visual illustration of the strength of FC between individual sub-regions can be seen in Figure 4.3.4.3.6. The direct comparison between the two patient sub-groups did not show any significant differences in the FC strength.

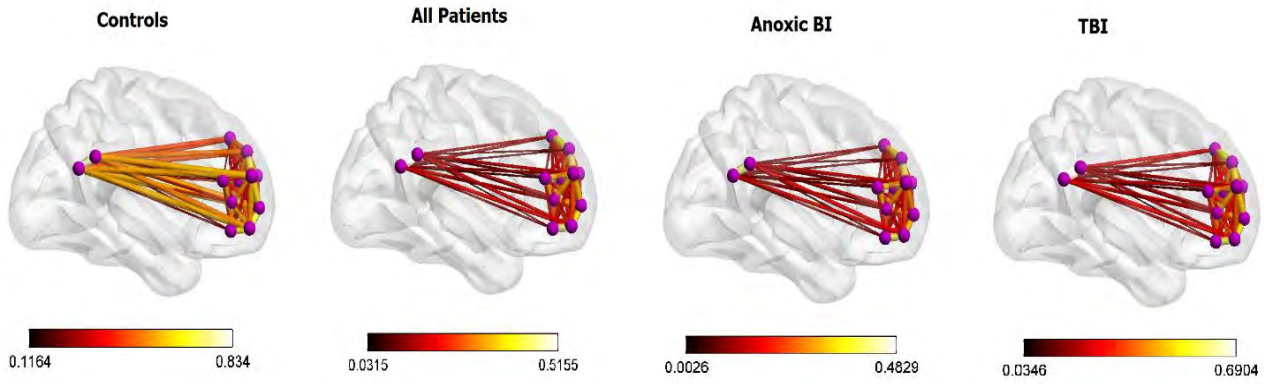

Figure 4.3.4.3.6. Functional connectivity between each of the PMC and mPFC sub-regions in patient and control groups. *The figure shows a significant reduction in fronto-parietal connections in all patients. The color scale shows the functional connectivity strength, ranging from lowest to highest.*

4.3.4.3 Structure-function association in the patient group

The structure-function relationship was investigated using the average values of the entire ROIs in order to ensure the readability of the results.

In the group with all patients (Figure 4.3.4.3.7.), there was a significant positive correlation between the MD of the PMC (r= .433, p= .004) and mPFC (r= .315, p= .040), and the PMC-mPFC functional connectivity. A negative association was indicated between the average posteromedial VBM value and the PMC-mPFC functional connectivity (r= -.352, p= .021). We did not find a significant relationship between the antero-posterior FC and the MD (r= .215, p= .167), FA (r= -.023, p= .884) or VBM values (r= -.180, p= .247) of the cingulum.

There was a significant relationship between the mean diffusivity of the right cingulum and the functional connectivity (r=.367, p=.015), however, the visual inspection of results (Figure 4.3.4.3.7., panel D), indicated that these findings were probably influenced by notable inter-individual variability and outliers. This claim was supported by the lack of significant associations between the MD of the cingulum and the mPFC-PMC FC in the etiology sub-groups.

In the anoxic BI group, a significant negative association was found for the VBM values of the PMC (r= -.504, p= .005) and the mPFC-PMC FC. Our findings also indicated a positive association between the MD of the entire PMC (r= .521, p= .004), mPFC (r= .404, p= .030), and the antero-posterior functional connectivity.

There were no significant structure-functional associations in the TBI group, which could be due to small number of patients with traumatic brain injury (N= 14).

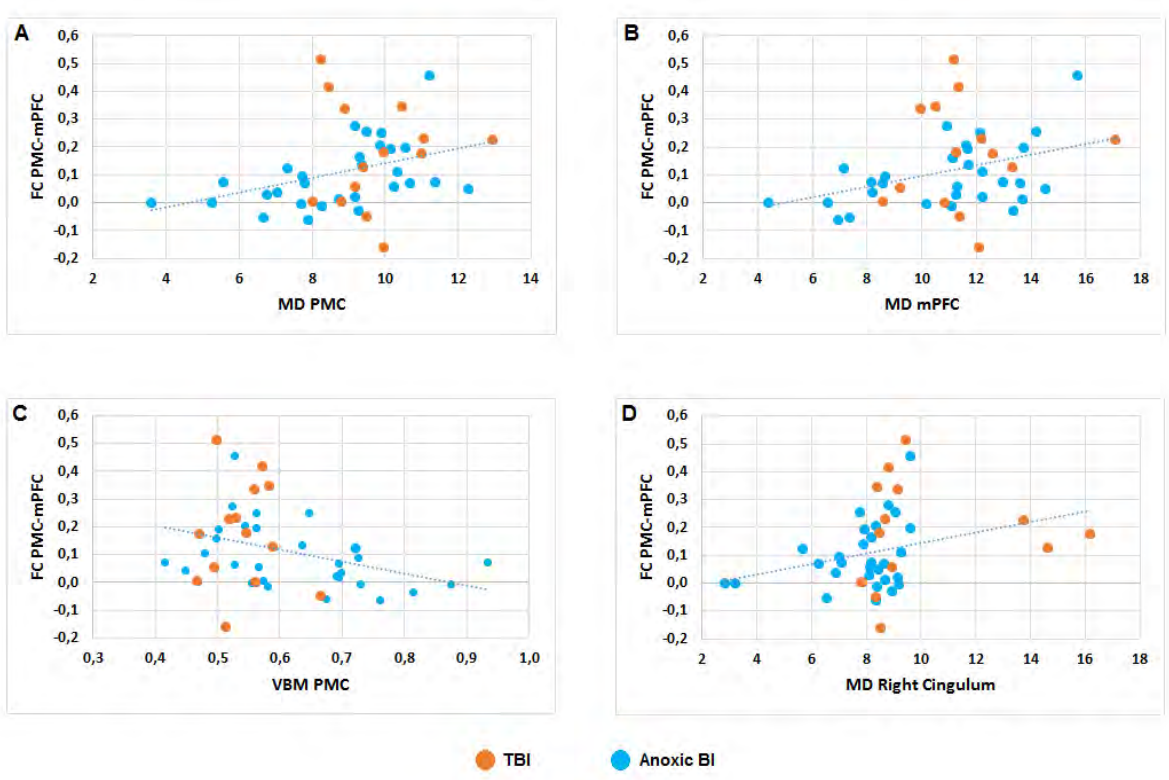

Figure 4.3.4.3.7. Structure-function association in anoxic and traumatic brain injury comatose patients. *The figure presents the mean diffusivity (A) of the PMC and the mPFC (B), the VBM values of the PMC (C) and the MD of the right cingulum (D), plotted against the average PMC-mPFC functional connectivity. The MD values were multiplied by 10.000 for visualization purposes.*

4.3.5 Discussion

4.3.5.1.1 Structural injury and etiology-related pathological mechanisms

In this study, we provide evidence for structural damage in acute stage comatose patients, located in the white matter tract connecting the posteromedial cortex (PMC) and the medial prefrontal cortex, mainly overlapping with the cingulum bundle. An increase in mean diffusivity of the cingulum was present in all patients, and could be indicative of early stage WM inflammation (Alexander et al., 2007). However, an augmentation in MD was significantly more pronounced in traumatic in comparison to anoxic brain injury (Newcombe et al., 2010; Van der Eerden et al., 2014), and it was paralleled with a reduction in fractional anisotropy, suggesting extensive demyelination and widespread axonal loss. Damage to WM integrity is very common in TBI, due to diffuse axonal injury effects on long-distance WM tracts, such as

the cingulum bundle and the corpus callosum (Bonnelle et al., 2011; Palacios et al., 2013; Sharp et al., 2014).

Moreover, the right portion of the cingulum bundle seemed significantly more damaged, suggesting lateralization. This is contrary to some previous studies with DOC patients, indicating left-lateralized grey and white matter atrophy, with higher disruption associated with longer time spent in DOC and discriminative between MCS- and MCS + (Bruno et al., 2011c; Guldenmund et al., 2016; van der Eerden et al., 2014).

In opposed to TBI patients, the anoxic BI group showed predominantly cortical damage (Van der Eerden et al., 2014), as suggested by higher values of VBM in the posteromedial cortex, usually interpreted as an augmentation in gray matter density. However, this in fact may not be indicative of an increase in gray matter volume but possibly of cortical laminar necrosis (i.e. cell death involving cortical layers III and IV, visible in the acute stage, at around 2 weeks post anoxia/ischemia) causing high-signal-intensity features on T1 images, thus resulting in higher VBM values (Choi et al., 2010; Howard et al., 2012; Siskas, Lefkopoulos, Ioannidis, Charitandi, Dimitriadis, 2003; Weiss et al., 2007). Further, our findings suggest that gray matter has greater vulnerability to hypoxia when compared with white matter, particularly in brain regions showing high basal metabolic levels, such as the posteromedial cortex (Howard et al., 2012; Nolan et al., 2010). Also, posterior and anterior cerebral arteries intersect in the medial parietal lobe thus rendering it particularly susceptible to hypoxic/anoxic ischemic injury.

In accordance, diffusion restriction abnormalities (Choi et al., 2010; Hirsch et al., 2014; Ryoo et al., 2015; Youn et al., 2015) and loss of cortical thickness (Silva et al., 2017) in the medial posterior cortex have been found in early stages in cardiac arrest comatose patients, with initial cortical atrophy associated with poor outcome.

Studies with chronic DOC patients (i.e. on average >2y) with mixed etiologies, suggest widespread decrease in gray matter density (assessed with VBM), in particular in the inferior parietal lobe, including the bilateral PMC, the medial and superior frontal lobe and the cingulum (Guldenmund et al., 2016; Juengling, Kassubek, Huppertz, Krause, & Els, 2005). Guldenmund and colleagues (2016) found an association between structural damage and time spent in DOC, and the extent of structural damage that was higher in non-traumatic UWS as compared to MCS, especially in the PMC and ventromedial prefrontal cortex. Therefore, it would be interesting to conduct a longitudinal VBM study with anoxic BI patients, to explore if this initial apparent increase in gray matter density evolves and if these changes are linked to current or future clinical and functional status. Follow-up studies with traumatic brain injury would be equally interesting, as Wallerian degeneration can lead to late complications such as secondary

neuroinflammation and neurodegeneration distal to the initial focal injury (Sharp et al., 2014; Warner et al., 2010).

In contrary to the changes seen in the posteromedial cortex, there seemed to be a complex pattern of decrease/increase of all structural parameters in the medial prefrontal cortex, not specifically discriminative between the two etiology groups. These results may be due to higher heterogeneity in frontal structural damage in coma patients, especially in TBI subjects, and is therefore difficult to interpret in the light of current results. Nevertheless, the most common pattern of structural changes seemed to be a restriction in diffusion (increase in FA) which could be a consequence of acute (ischemic, traumatic) lesions in our coma patients.

4.3.5.1.2 PMC-mPFC structure-function relationship

The functional connectivity was significantly lower for almost all pairwise links included in the analysis, indicating a complete dissolution of PCC-mPFC FC, as frequently shown in disorders of consciousness (Hannawi et al., 2015; Norton et al.; Koenig et al., 2014; Silva et al., 2015). There results suggest that changes in PMC-mPFC function may be directly related to the abolition of consciousness, while structural changes depend more on etiology that is differences in pathology mechanisms associated with various brain injuries.

Our findings implied that a restriction in PMC and mPFC gray matter diffusivity and abnormal PMC gray matter intensity interfere with efficient postero-anterior functional communication, indicating that both structural and functional integrity need to be preserved for consciousness to emerge. This is in accordance with studies showing correlation between mPFC-PMC connectivity and GM integrity (Segall et al., 2012), with posterior midline GM atrophy associated with reduced DMN functional connectivity (Vidal-Piñeiro et al., 2014).

Surprisingly, our findings did not imply codependence between the structural integrity of the cingulum and resting-state FC, as usually shown in healthy subjects (Figley et al., 2015; Greicius et al. 2009; van den Heuvel et al., 2009; Honey et al., 2009; Khalsa et al., 2014) and patients with chronic DOC (Bodart et al., 2017).

However, our anoxic brain injury patients did not have extensive damage of the cingulum, which could have been the underlying cause of the absence of a significant structure-function relationship.

Further, previous studies have identified paralleled DMN structure-function disruption in traumatic brain injury, also associated with worse cognitive functioning (Bonnelle et al., 2011;

Palacios et al., 2013; Sharp et al., 2014), which is in contrast to our findings. Nevertheless, it must be noted that we did not include a large sample of traumatic brain injury patients in our study, which may have led to insufficient power to detect small but important effects.

4.3.5.1.3 Conclusions

To our knowledge, this is the first study to explore brain structure-function relationship in coma patients using multimodal neuroimaging. Our findings implied a significant loss of structural integrity in acute comatose patients, with primarily white matter injury (i.e. cingulum) in TBI, and posteromedial gray matter damage in the anoxic BI group. A major reduction in the functional connectivity between PMC and mPFC was shown for all patients, irrespective of etiology. Furthermore, significant function-structure correlations found in comatose patients suggested that both structural and functional integrity need to be preserved for consciousness to emerge.

Given that we found a decrease in the WM mean diffusivity in all patients, further studies should calculate the axial (AD) and radial (RD) diffusivity, in complement to MD, to explore potential etiology differences in the pathological mechanisms related to structural damage (demyelination – increase in RD vs. primary axonal damage – decrease in AD).

Future multimodal longitudinal studies with such an integrative approach should investigate the evolution of the function-structure relationship and its relevance for long-term outcome prediction. Further studies should conduct voxel-wise structural and functional analysis, as we have shown some sub-regional differences within our functionally defined PMC and mPFC ROIs. A recent meta-analysis showed that hub nodes of the structural (and functional) connectome are much more likely to be pathologically lesioned by a wide-range of brain disorders in comparison to non-hub regions (Crossley et al., 2014). Therefore, it would be interesting to explore the relationship between densely functionally connected voxels (identified in healthy subjects) and the corresponding gray matter volume (i.e. VBM). Also, the WM microstructure should be investigated in more detail, with either voxel-wise or multiple-ROI analysis along the antero-posterior tract in order to precisely locate the damage reflected in our findings.

Finally, it would be of interest to include more regions from the dDMN and other resting-state networks, such as the salience and executive control network, and their corresponding WM connections, to investigate if these changes and their structure-functional association are specific to or expand beyond the default mode network.

4.3.5.1.4 Limitations

This study has several limitations. We did not find significant structure-functional associations when conducting separate analysis with TBI patients, which could be due to small number of patients with traumatic brain injury (N=14) included in our study. The insufficient number of patients was partially influenced by subject exclusion due to focal lesions overlapping with regions of interest, and segmentation failure. The p-values were not corrected for multiple comparisons, as this was a preliminary study conducted for exploratory purposes, however, all p-values are fully reported and open to interpretation. Finally, more advanced analysis should be done (e.g. regression analysis) to fully explore the causal relationship between the structure and function.

5 Chapter V - General discussion and future perspectives

The overall findings of this thesis suggest a major disruption of functional connectivity and significant topological reorganization in high-order resting state networks in the acute stage of coma. Severe functional disconnections were particularly pronounced in the posteromedial cortex, a functionally heterogeneous brain region, primarily associated with the default mode network. More specifically, the ventral portions of the precuneus and the posterior cingulate cortex were hypoconnected with other regions from the DMN (Study 2), most consistently with the mPFC, irrespective of coma etiology (Study 1). In contrast, the dorsal PCC appeared to be implicated in global brain dynamics, as suggested by a significant reduction in centrality and inter-modular connectivity in this region (Study 2). These findings are in line with research showing strong intra-modular coupling between the ventral PCC/PreCu and other DMN regions, in opposed to a more transitional connectivity found in the dorsal PCC, serving to integrate and coordinate the activity across multiple (resting-state) networks.

The functional organization in coma patients appeared to be dedifferentiated, as highlighted in a complex pattern of decrease and increase of brain region connectivity and centrality pertaining to high-level resting-state networks. The "hyper-connectivity/-centrality" (Study 1 and 2) could be a consequence of compensatory brain plastic processes possibly reflecting resilient connections engaging residual critical neural resources, otherwise normally distributed through efficient brain network connections, here disrupted by brain injury, resulting in impaired conscious processing.

The global "randomization" and the fronto-parietal disconnections, implied in this thesis (Study 2), suit connectionist theories of consciousness (presented in the introduction) which accentuate the importance of complexity that is simultaneous differentiation and integration of brain function in the emergence of consciousness.

Further, in the healthy brain long-range connections between segregated areas are supported by the integrative properties of highly connected hub nodes, most commonly identified in the posteromedial and prefrontal brain regions (in healthy subjects). These regions were individually disrupted (i.e. structural damage) and mutually disconnected (i.e. functional connectivity) in our coma patients. Interestingly, the long-range antero-posterior functional disconnection was demonstrated in all of the studies in this thesis (and is compatible with

previous research), irrespective of the applied methodology. These findings are very encouraging given that the reproducibility of results, despite differences between methodological approaches, is the first step towards the development of clinically applicable diagnostic/prognostic markers.

In fact, higher functional connectivity between the ventral PCC and PreCu and the medial frontal regions was significantly related to better neurological recovery, registered 90 days after the initial inclusion of patients, aiming towards potential clinical applicability of neuroimaging in prognosis.

Furthermore, the long-range PMC-mPFC functional disconnection was coupled with significant structural damage in the corresponding gray matter and white matter connections (Study 3), implying that damaged structural integrity is linked to disruption in brain function. Nevertheless, the directionality of this relationship will have to be investigated in further studies, in order to determine if structural brain injury directly leads to functional disconnections. In addition, this analysis should be extended to voxel-wise analysis, necessary to fully explore the structural/functional differentiation of brain damage association with DOC. Future studies should also explore if the structural and functional disruption found in these metabolically expensive and topologically central regions (i.e. PMC) is related to greater vulnerability, or symptomatology which arises once the damage propagates to these highly connected hub nodes. Nonetheless, the identification of either of these mechanisms (i.e. vulnerability and symptomatology) could lead to network-based treatments which aim to restore normal wide-brain functioning through remediation of specific brain hubs.

Finally, it is important to note that a better understanding of etiology differences may prove to be essential in early prediction and understanding of patient's outcomes, as we have shown some significant functional and structural differences between traumatic and anoxic brain injury. This was reflected in a higher prevalence of hyperconnected voxels and white matter structural damage in TBI in opposed to more notable functional disconnection and posteromedial gray matter injury in anoxic BI.

The combination of behavioral clinical assessment with complementary measures derived from brain structure (i.e. DWI/DTI; gray matter volume), brain metabolism (i.e. PET; markers of neuroinflamation) and functional connectivity (i.e. fMRI, EEG), may further increase the accuracy of prognosis prediction in the acute stage. Also, multimodal studies in a research setting could help us better understand the interaction between brain changes observed on different levels, and establish if one modality could be used as a proxy for another in patients who are incompatible for some type of neuroimaging due to a critical clinical state, extensive

brain damage or metallic implants. In fact, our team is currently working on a multimodal neuroimaging protocol which will hopefully lead to new insights regarding consciousness abolition and recovery.

However, the multimodal approach leads to an ever increasing volume and complexity of acquired data, imposing new challenges associated with "big data".

The graph theoretical methodology is well suited for analyzing and integrating results in this context, although, there are still some methodological barriers that need to be overcome in order to fully exploit the possibilities of this approach. For example, traumatic brain injury is associated with heterogeneous brain damage which interferes with node definition, which needs to be exact for each of the subjects included in the graph analysis. Thus, the selection of nodes of interest is not straightforward in TBI, especially when there is a significant spatial overlap with a focal lesion. This was one of the main reasons why we did not include this sub-population of coma patients in our second study. Furthermore, it would be interesting to do the analysis using weighted correlation matrices, as both weak and strong functional connections can give valuable insight into the pathological mechanisms in coma. Also, graph metrics could be calculated separately for positive and negative functional connections, in order to specifically explore the inter-network anticorrelations, which are particularly interesting in the context of RSNs and disorders of consciousness. The continuing collaboration with the "graph theory" team in Grenoble will surely lead to fruitful research and some more interesting results.

Future research should be longitudinal, with repeated MRI scanning, during the acute stage of coma and recovery, in order pinpoint the brain mechanisms related to emergence of conscious awareness. This was initially planned for the original study protocol, however, this idea couldn't be executed to high mortality rate of patients and logistical difficulties associated with prolonged care for patients with disorders of consciousness.

In fact, one of the most important lessons this thesis project has taught me is how to balance the methodological rigor and the clinical practicability, keeping in mind the best interest of patients and yet trying to find the right research approach to deliver reliable and timely results.

Finally, the behavioral assessment (CRS-R) of neurological outcome should be repeated multiple times within a short time interval, as the validity of testing results significantly impacts our ability to find reliable neuroimaging biomarkers. Even though standardized behavioral testing is considered today as the gold-standard for the diagnosis of disorders of consciousness, it poses many limits (as discussed in the introduction), and should be combined with brain imaging data in order to more reliably probe the residual capacity for conscious processing.

Diagnostic and prognostic errors carry particular moral risks in the case of disorders of consciousness and can have important implications for medical decision-making, such as the choice of therapy, concern for family members and the decision to withhold/withdraw life-sustaining treatment.

The main contribution of this thesis in the context of previous research is evidence for: a) a complex pattern of functional disconnection within the PMC (hypo- vs. hyper-connectivity; correlation vs. anticorrelation); ii) significant reorganization in high-order resting-state networks reflective of dedifferentiation and reduced brain complexity; iii) etiology-related differences in functional/structural brain damage in the acute stage of coma; iv) significant association between structural damage and functional disconnection; v) and predictive value of PMC functional disconnections in relation to 3-month neurological outcome.

In conclusion, the analysis of resting-state functional connectivity and structural integrity in the acute stage of coma implies significant heterogeneity in brain function and structure of coma patients irrespectively of their apparent behavioral homogeneity. As such, these findings hold significant promise towards development of neuroimaging markers for prognostication and early identification of patients who would benefit from novel therapies (i.e. pharmacological, brain stimulation) aiming to restore and promote adaptive cerebral plasticity leading to eventual reemergence of consciousness and neurological recovery.

6 Appendices

6.1 Paper I

NeuroImage: Clinical 15 (2017) 315–324

Contents lists available at ScienceDirect

NeuroImage: Clinical

journal homepage: www.elsevier.com/locate/ynicl

Neural signature of coma revealed by posteromedial cortex connection density analysis

Briguita Malagurski[a], Patrice Péran[a], Benjamine Sarton[b], Beatrice Riu[b], Leslie Gonzalez[b], Fanny Vardon-Bounes[c], Thierry Seguin[c], Thomas Geeraerts[d], Olivier Fourcade[d], Francesco de Pasquale[e], Stein Silva[a,b,*]

[a] Toulouse NeuroImaging Center, Université de Toulouse, Inserm, UPS, France
[b] Critical Care Unit, University Teaching Hospital of Purpan, Place du Dr Baylac, F-31059 Toulouse Cedex 9, France
[c] Critical Care Unit, University Teaching Hospital of Rangueil, F-31060 Toulouse Cedex 9, France
[d] Neurocritical Care Unit, University Teaching Hospital of Purpan, Place du Dr Baylac, F-31059 Toulouse Cedex 9, France
[e] ITAB, Department of Neuroscience Imaging and Clinical Science, G. D'Annunzio University, Chieti, Italy

ARTICLE INFO

Keywords:
Acute brain injury
Coma
Connection density
Prognosis
Resting state

ABSTRACT

Posteromedial cortex (PMC) is a highly segregated and dynamic core, which appears to play a critical role in internally/externally directed cognitive processes, including conscious awareness. Nevertheless, neuroimaging studies on acquired disorders of consciousness, have traditionally explored PMC as a homogenous and indivisible structure. We suggest that a fine-grained description of intrinsic PMC topology during coma, could expand our understanding about how this cortical hub contributes to consciousness generation and maintain, and could permit the identification of specific markers related to brain injury mechanism and useful for neurological prognostication.

To explore this, we used a recently developed voxel-based unbiased approach, named functional connectivity density (CD). We compared 27 comatose patients (15 traumatic and 12 anoxic), to 14 age-matched healthy controls. The patients' outcome was assessed 3 months later using Coma Recovery Scale-Revised (CRS-R).

A complex pattern of decreased and increased connections was observed, suggesting a network imbalance between internal/external processing systems, within PMC during coma. The number of PMC voxels with hypo-CD positive correlation showed a significant negative association with the CRS-R score, notwithstanding aetiology. Traumatic injury specifically appeared to be associated with a greater prevalence of hyper-connected (negative correlation) voxels, which was inversely associated with patient neurological outcome. A logistic regression model using the number of hypo-CD positive and hyper-CD negative correlations, accurately permitted patient's outcome prediction (AUC = 0.906, 95%IC = 0.795–1). These points might reflect adaptive plasticity mechanism and pave the way for innovative prognosis and therapeutics methods.

1. Introduction

Over the last few years, the posteromedial cortex (PMC) has received an increasing amount of attention. In fact, this architectonically discrete region, has been recognized as a critical site integrating an important range of multimodal information (Dehaene and Changeux, 2011). Actually, this highly dynamic functional core seems to participate in multiple transitional connectivity networks seemingly playing a critical role in internally/externally directed high-level cognition (Cavanna and Trimble, 2006; Leech and Sharp, 2014). In particular, converging data from physiological, pharmacological (Heine et al., 2012a, 2012b) and pathological models (Hannawi et al., 2015), suggest the implication of PMC and its long-range functional connections in conscious processing. For example, in pathological conditions, patients with disorders of consciousness (DOC) consistently demonstrated a reduced activity (He et al., 2014; Silva et al., 2010; Tsai et al., 2014) or diminished connectivity between this posterior brain structure and other cortical hubs (Hannawi et al., 2015; Vanhaudenhuyse et al.,

Abbreviations: BI, brain injury; BOLD, blood oxygen level–dependent; CRS-R, Coma Recovery Scale–Revised; DOC, disorders of consciousness; DMN, default-mode network; mPFC, medial prefrontal cortex; CDN, connection density based on negative correlation; PCC, posterior cingulate cortex; CDP, connection density based on positive correlation; PMC, posteromedial cortex; PreCu, precuneus; TBI, traumatic brain injury

* Corresponding author at: Critical Care Unit, Toulouse NeuroImaging Center, Inserm, CHU Purpan, 31059 Toulouse Cedex 3, France.
E-mail addresses: silvastein@me.com, silva.s@chu-toulouse.fr (S. Silva).

http://dx.doi.org/10.1016/j.nicl.2017.03.017
Received 25 October 2016; Received in revised form 27 February 2017; Accepted 28 March 2017
Available online 06 May 2017

2010; Qin et al., 2015; Wu et al., 2015), in particular the medial prefrontal cortex (mPFC) (Lant et al., 2016; Silva et al., 2015).

Interestingly, a growing body of literature on animal and human studies, suggests a significant heterogeneity in cytoarchitectonic (Vogt and Laureys, 2005; Vogt et al., 2006), structural (Parvizi et al., 2006; Zhang et al., 2014) and functional connectivity maps characterizing different sub-region of the PMC (Bzdok et al., 2015; Zhang and Li, 2013). Recent studies highlighted that the "metastable" functional connectivity detected in this region follows a complex ventral/dorsal-anterior/posterior gradient, partially overlapped across anatomically defined sub-regions (i.e. Precuneus (PreCu) and Posterior Cingulate Cortex(PCC)) (Bzdok et al., 2015; Cauda et al., 2010; Margulies et al., 2009; Zhang and Li, 2013). Nevertheless, it must be noted that the DOC neuroimaging literature traditionally explored PMC as a homogenous structure and failed to describe such a functional segregation in pathological conditions (Laureys et al., 1999; Norton et al., 2012; Silva et al., 2010; Vanhaudenhuyse et al., 2010). This important issue is probably due to seed-based approaches that are currently used in this setting to evaluate the functional connectivity among non-parcelled brain regions, by using correlation analyses of spontaneous fluctuations of brain activity in resting state conditions (Hannawi et al., 2015).

Therefore, we suggest that a better understanding of intrinsic PMC functional topology, (Silva et al., 2015) could significantly expand our understanding of how this cortical hub contributes to the generation and the maintenance of conscious awareness and might considerably improve DOC patient's clinical management. To explore this, we used a recently developed voxel-based unbiased approach that does not rely on a priori selection of the seed regions, named functional connectivity density (CD) (Tomasi and Volkow, 2010). This voxel-based method, accurately enables the identification of functional connectivity hubs and permit to specifically investigate within brain regions parcellation, in both healthy and pathological conditions. Thus, we aimed to investigated the functional impact of acute brain injures responsible of coma at the level of PMC and intended to study in this setting: (i) the specific interactions of the PMC anatomical (PCC and PreCu) or functional (ventral/dorsal gradient) sub-regions, with a distant cortical hub (mPFC) in resting state conditions (ii) a complete assessment of the whole range of increase/decrease of both positive/negative, i.e. corresponding to positive/negative correlation, connection patterns that could theoretically be detected by this approach, (iii) the impact of injury mechanisms (i.e. traumatic or anoxic), on brain functional connectivity patterns (iv) the prognostic value of functional connection density data for neurological recovery.

2. Materials and methods

2.1. Participants

Patients were included from three intensive critical care units affiliated with the University Teaching Hospital (Toulouse, France) between January 2013 and February 2014. We compared 27 patients, 15 with traumatic and 12 with anoxic brain injury, who met the clinical definition of coma (Glasgow Coma Scale score (Teasdale and Jennett, 1974) at the admission to hospital < 8, with motor responses < 6; age range: 19–70 years) to 14 approximately age-matched healthy controls (age range: 22–37 years). Patients underwent rs-fMRI scanning at least 2 days (4 ± 2days) after complete withdrawal of sedation and under normothermic condition. Standardized clinical examination was performed on the day of the scanning using the Glasgow Coma Scale and the Full Outline of Unresponsiveness (Wijdicks et al., 2005) and 3 months later using Coma Recovery Scale-Revised (Schnakers et al., 2008).

2.2. Image acquisition

In all participants, we acquired 11 min resting state fMRI using a 3 T magnetic resonance scanner (Intera Achieva; Philips, Best, the Netherlands). Two hundred and fifty multislice T2*- weighted images were retrieved with a gradient echo-planar sequence using axial slice orientation (37 slices; voxel size: 2 × 2 × 3.5 mm; TR = 2600 ms; TE = 30 ms; flip angle = 90°; FOV = 240 mm). A 3D T1-weighted sequence (in-plane resolution 1 × 1 × 1 mm, 170 contiguous slices) was also acquired in the same session, which was later used for visual assessment of the structural integrity of the PMC.

2.3. Pre-processing

The rs-fMRI data was preprocessed using SPM 8 (http://www.fil.ion.ucl.ac.uk/spm/) and CONN toolbox ver. 13f (http://www.nitrc.org/projects/conn) (Whitfield-Gabrieli and Nieto-Castanon, 2012). In order to reduce the motion effects on our data, we only included subjects characterized by motion parameters smaller than 3 mm translation and 3° rotation. First, the echo-planar images were realigned (motion corrected), slice-time corrected and normalized to the Montreal Neurological Institute echo-planar imaging template. Second, non-neuronal sources of noise were estimated and removed using the anatomical CompCor method (aCompCor) integrated in the CONN toolbox. Principal components of the signals from the white matter and the CSF voxels, alongside the motion parameters estimated during realignment were removed with regression. Finally, a temporal band-pass filter was applied to the residual blood oxygen level–dependent (BOLD) time course in order to obtain a low-frequency range of interest ($0.008\ Hz < f < 0.09\ Hz$).

2.4. Region of interest selection

Using a home-made MATLAB (MATLAB and Statistics Toolbox Release 2011a, The MathWorks Inc., Natick, Massachusetts, United States) script, the BOLD time series was extracted from voxels in two main regions of interest (ROI), the Posterior Medial Cortex and the Medial Prefrontal Cortex, defined by the Automated Anatomical Labeling atlas (Tzourio-Mazoyer et al., 2002) (voxel size 2 × 2 × 2 mm). The PMC (size = 12,862 voxels) consisted of the Precuneus L/R (size = 11,222 voxels) and the Posterior Cingulate Cortex L/R (size = 1640 voxels), and the mPFC (size = 13,389 voxels) comprised the Frontal Superior Medial L/R (size = 8373 voxels) and the Anterior Cingulate Cortex L/R (5016 voxels). As preliminary step, T2* mean images were used the extract the mean value of voxels in the PMC region, and a two-sample *t*-test was performed to compare values between the control and the patient group.

Additionally, to investigate if the potential changes in connection density are specific to the PMC-mPFC interactions, we have also included the bilateral Calcarine L/R (size = 7134 voxels; part of the primary visual cortex) as a control region, currently not considered to be relevant for conscious awareness.

2.5. Voxel-based connection density

The data analysis pipeline is presented in Fig. 1.

Pearson correlation coefficients were computed between the BOLD time course of all the possible pairs of voxels from PMC and mPFC. Correlation coefficients were then normalized using Fisher's r-to-z transformation. A subject-specific threshold of $p \leq 0.05$ was applied to each correlation coefficient in order in order to retain only a subset of connections with higher in further analysis. We labelled the obtained connections as positive and negative depending on the sign of the obtained z coefficients and we treated them separately. Importantly, to avoid the artificial induction of negative correlations (anticorrelations) by the global signal regression (Murphy et al., 2009; Weissenbacher et al., 2009) we adopted the CompCor method in the preprocessing step, which has been reported as a reliable approach for the exploration of both positive and negative correlations (Chai et al., 2012, 2014).

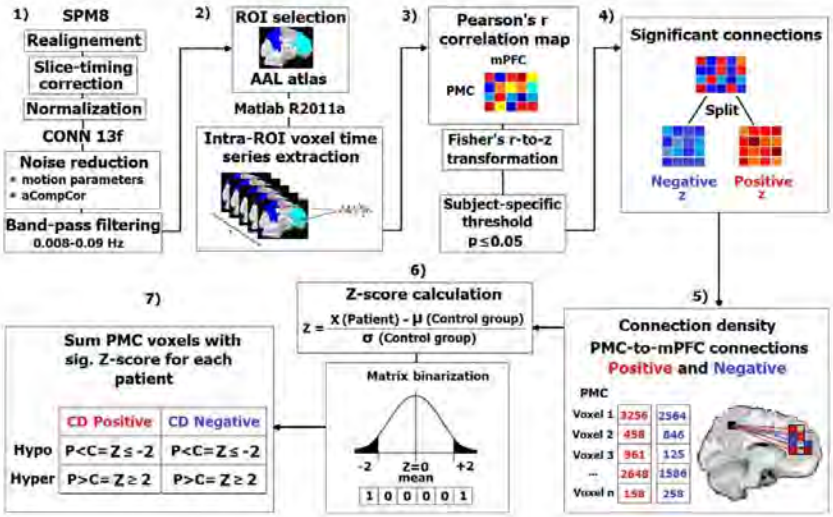

Fig. 1. Overview of the data analysis pipeline. 1) First, the rs-fMRI data was pre-processed using SPM8 and CONN13f, respectively. 2) Using a home-made MATLAB script, the BOLD time series was extracted from voxels in two main regions of interest then used in 3) calculation of Pearson correlation coefficients between the BOLD time course of all the possible pairs of voxels from PMC and mPFC. Then, a subject-specific threshold of $p \leq 0.05$ was applied to include only the significant connections in further analysis. 4) The obtained significant connections were split on positive and negative (based on the sign of the normalized z coefficients), binarized and used to 5) obtain the density of connection between PMC and mPFC voxels. 6) A Z-score was calculated for each single PMC voxel as explained in the figure. 7) Voxels with a sig. Z score were summed and characterized as hypo/hyper-CDP and hypo/hyper-CDN as presented in the figure.

The resulting z coefficients were binarized and then summed to obtain the density of connections between every voxel belonging to PMC and every voxel within the mPFC. These would represent the number of significant positive and negative connections from PMC to mPFC. The number of significant connections obtained for a single PMC voxel was then used to compute a Z-score for every voxel in the patient group using the mean (M) and the standard deviation (SD) of the healthy control group. This will represent the significant deviation of each voxel from the corresponding control.

Thus, the number of PMC voxels with a Z-score higher or equal to 2SD or less or equal to − 2SD (for positive and negative connections) were counted for each patient individually and further used to investigate the changes (significant deviations) in functional connectivity between the PMC to the mPFC. The same analysis was repeated for the control pathway (i.e. representing the connections between the bilateral Calcarine and the mPFC).

Furthermore, in order to facilitate the discussion of our results (Fig. 1), a significant decrease (Patients < Controls, Z-score ≤ − 2) in connection densities is designated as "hypo" connection density or *hypo-CDP* and *hypo-CDN*, for positive and negative correlation based connection densities, respectively. The opposite - increase in connection densities (Patients > Controls, Z-score ≥ 2) is denoted by "hyper" connection density e.g. *hyper-CDP* and *hyper-CDN* for positive and negative correlation based connections, respectively.

Lastly, to allow an easier description of our findings and to test our hypothesis on the differences in functional connectivity changes between the PreCu and PCC, we present the results from these two ROIs separately.

2.6. Spatial homogeneity

In addition to the individual results, we were interested in the spatial similarity (overlap) of these changes between patients within groups (intra-group) and between different coma aetiology groups (inter-group). This allowed us to investigate if these changes were spatially scattered thus highly heterogeneous between subjects or if they were organized in functional clusters shared among multiple participants within/between the two aetiology groups.

The intra-group spatial congruity of single voxel Z-score results was explored at two thresholds: a criteria of 33% and 67% was used to define the total number of disconnected voxels spatially shared between 1/3 and 2/3 of the patient group, respectively. This was explored in the group with all the patients and with two coma aetiology groups separately.

To explore the inter-group similarity, we have calculated the Jaccard similarity coefficient (index) to further test the spatial overlap in connectivity changes between these two groups. The Jaccard index (JI) is defined as the intersection divided by the union of the number of voxels representing significant changes in PMC-mPFC connection density in given groups. The values of JI range from 0 (0%), indicating no overlap, to 1 (100%) suggesting full spatial overlap.

2.7. Statistical analysis

We have conducted the Mann-Whitney *U* test to investigate the differences in PMC-to-mPFC connection density changes between the PreCu and PCC. The same test was used to compare the changes in functional connectivity between our two coma aetiology groups – traumatic and anoxic brain injury patients. This analysis was also repeated for the control pathways. The resulting *p* values were corrected for multiple comparison using a false discovery rate (FDR $p = 0.05$).

We have also calculated the effect size for the Mann-Whitney *U* test by dividing the z value (test statistic) by the square root of N (sample size). This is analogous to Cohen's d for parametric group testing.

Spearman's correlation analysis was performed to explore the link between the number of PMC voxels with significant changes in connection density and the CRS-R score. The same correlation analysis was done to test the association between the connection density changes in the control pathway - Calcarine-mPFC - and the CRS-R

score. The resulting p values were corrected for multiple comparison using a false discovery rate (FDR $p = 0.05$).

Additionally, in order to explore the non-linear association between the outcome and the significant changes in PMC-mPFC connection density, and thus the predictive value of these changes in relation to recovery, we have conducted the binary/logistic regression analysis. Patients were divided into two outcome groups (based on the CRS-R score): good outcome - comprising patients who had recovered or progressed to minimally conscious state (MCS) (N = 12); and the bad outcome – incorporating patients with unresponsive wakefulness syndrome/vegetative state (UWS/VS) (N = 15). This analysis was not done separately for the two aetiologies due to small sample size.

All of the above mentioned analyses were performed using the IBM SPSS (IBM SPSS Statistics for Windows, Version 20.0. Armonk, NY: IBM Corp.) statistical package.

3. Results

3.1. Induced functional topological changes in the PMC

3.1.1. Anatomical sub-regions — precuneus and posterior cingulate cortex

In Fig. 2 we report the induced changes in functional connectivity of the entire PMC and the differences between its anatomical sub-regions, the PreCu and PCC, in the patient group compared to controls. The changes in connection density are presented as the percentage of voxels more or less connected within a given region/sub-region in order to take into account the differences in size (total number of voxels) of different ROIs.

The Mann-Whitney U test with percentage-wise results showed that the PCC exhibited significantly more voxels with both hypo-CDP (U = 202, $p = 0.004$; Fig. 3.A.1.) in comparison to PreCu, with a medium effect size ($r = 0.38$), which is in accordance to previous research. The latter showed a tendency toward a higher number of voxels with hyper-CDP (Fig. 3.A.2) in comparison to PCC, but these results were not statistically significant (U = 261, $p = 0.074$; small effect size ($r = 0.24$)). PCC did not significantly differ from PreCu in hyper-CDN (U = 248, $p = 0.044$; small effect size ($r = 0.27$) after the multiple comparison correction ($p > 0.004$; FDR corr.).

No significant differences were observed in the number of voxels with hypo-CDN between the PCC and the PreCu (U = 256.5, $p = 0.055$; small effect size $r = 0.26$)), which is not unexpected given that these changes were barely present in both sub-regions (Fig. 3.A.3).

3.1.2. Functional sub-regions — ventro/dorsal segregation of the PMC

In order to investigate the spatial architecture of the observed changes in the density of connections, in Fig. 4 we report the spatial topography of the obtained connections. The figure represents the summed changes in functional connectivity in the entire patient group. The individual spatial topography maps of these changes (with aetiology and prognostic information) are presented in the Supp. Fig. 1 and Supp. Fig. 2.

It can be noted that: (i) the ventral PCC and the ventral PreCu seemed to form a functional cluster of hypo-CDP voxels (Fig. 4.A), (ii) the hyper-CDP voxels were primarily located in the dorsal PreCu and a part of the dorsal PCC (Fig. 4.B.), alongside a portion of the ventral PCC (Fig. 4.B.), (iii) the hyper-CDN voxels seemed to be widespread, suggesting high inter-individual variability, and covered large portions of both PMC sub-regions (Fig. 4.D), including almost the entire PCC (97% for the entire patient group, see Table 1), (iv) finally, the hypo-CDN PMC voxels were barely present and mostly found in the posterior ventral PreCu (Fig. 4.C).

The spatial topography of our results indicated a possible significant spatial overlap between voxels with hypo-CDP and hyper-CDN which lead us to calculate the exact number of these intersecting voxels. Thus,

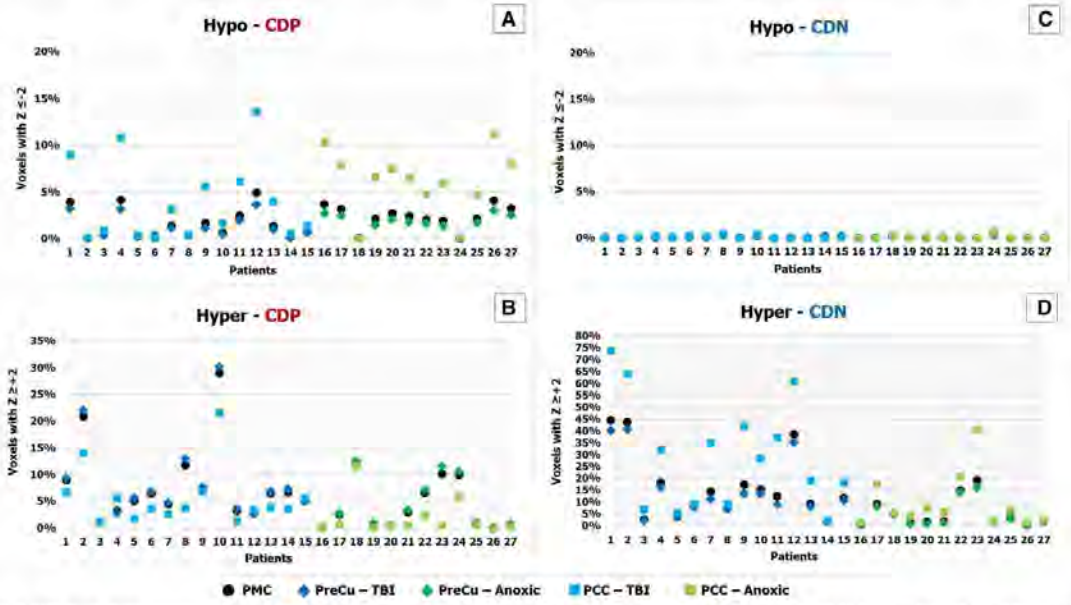

Fig. 2. PMC (PreCu/PCC) connection density Z-score results for individual patients. Patients exhibit a significant number of hypo-CDP (panel A), hyper-CDP (panel B) and hyper-CDN (panel D) in comparison with the control group. There seem to be some differences depending on the coma aetiology. The x axis represent the number of patients (each patient is coded with the same number in all four panels: A, B, C, D). The y axis reflects the percentage of voxels with a sig. Z-score ($-2 \leq Z \geq +2$) of the total number of voxels in the PMC (12,862 voxels) and the PreCu (11,222 voxels) and PCC (1640 voxels) separately. The changes in PreCu and PCC are presented separately for two coma aetiologies using different colours - dark blue/light blue for TBI and dark green/light green for anoxic BI.

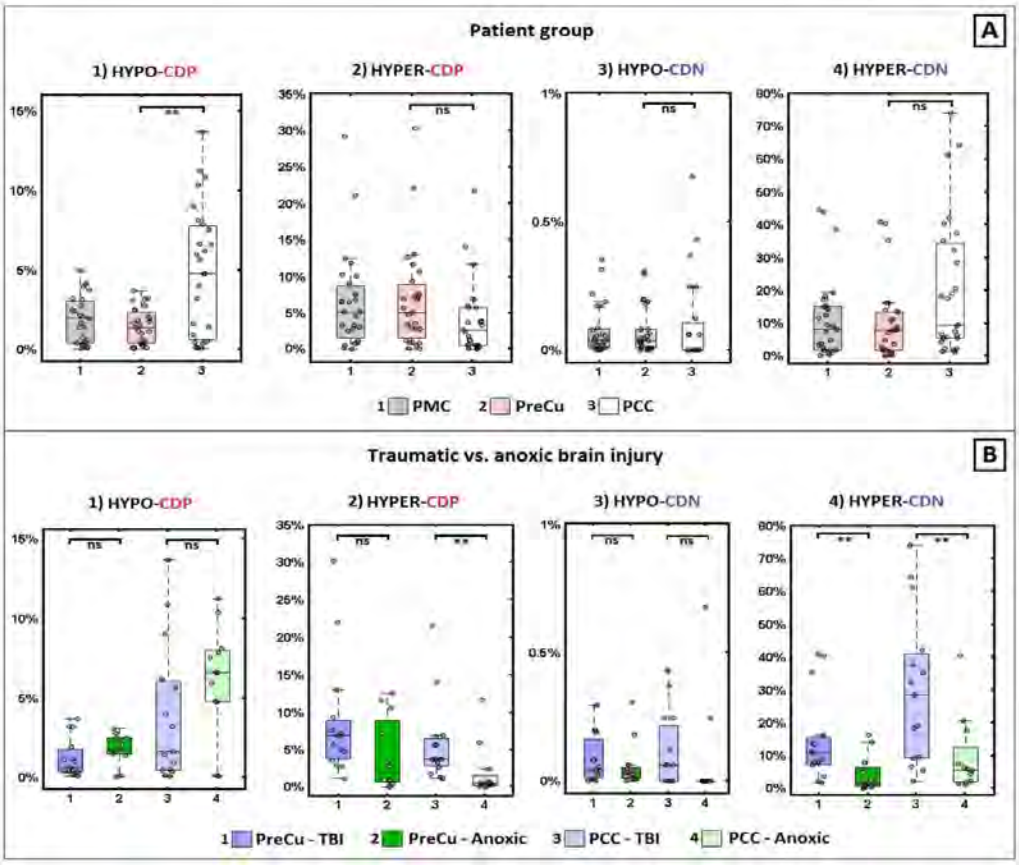

Fig. 3. Differences in changes in connection density between PreCu and PCC and between traumatic and anoxic brain injury. Panel A) PCC showed significantly more hypo-CDP (sub-panel 1) in comparison with the PreCu. Panel B) Traumatic BI patients had more hyper-CDP (sub-panel 2) within the PCC and hyper-CDN voxels in both PreCu and PCC (sub-panel 4) in comparison to anoxic BI patients; Boxplots represent medians with interquartile range and whiskers signify minimum and maximum values (excluding the outliers) (*$p < 0.05$, (**$p < 0.005$, ns: nonsignificant).

our calculation demonstrated a complete overlap of these two types of disconnections, which was equivalent to almost the total number of hypo-CDP voxels (1048 voxels or 11% of summed hypo-CDP and hyper-CDN voxels; see Table 1.) in the entire patient group. However, these changes were not homogeneous and were characterized by important inter-individual differences (SD = 155.3), as demonstrated in the Supp. Table 1.

3.2. Control pathways — Calcarine-mPFC

The changes in connection density are fully presented in the Supp. Fig. 3. The results showed only a small percentage of Calcarine hypo-CDP voxels representing reduced connectivity between this region and the mPFC (median = 0.04%, min = 0, max = 0.7%) in patients. The same result was found for the hypo-CDN voxels (median = 0, min = 0, max = 0.2%). Nevertheless, hyper-CDN and hyper-CDP voxels were present in this control pathways (median = 22%, min = 0.08%, max = 63% and median = 4%, min = 0.04%, max = 22%, respectively).

3.3. Impact of brain injury mechanisms

3.3.1. PMC-mPFC connection density changes

The impact of the patients' aetiology on the observed changes reported in Fig. 3.B. In accordance with the single-subject level (Fig. 2), the group-level statistical analysis showed significant differences between the two aetiologies in the percentage of PMC voxels with hyper-CDN ($U = 32$, $p = 0.004$) with large effect size ($r = 0.55$). There were no significant difference in hypo-CDP ($U = 63$, $p = 0.200$; small effect size ($r = 0.25$)), hyper-CDP ($U = 49$, $p = 0.045$, FDR correction $p < 0.005$; medium effect size ($r = 0.39$)) and hypo-CDN voxels ($U = 66$, $p = 0.249$, small effect size ($r = 0.23$)). These differences were reflected in a significantly higher percentage of hyper-CDN voxels in both PreCu ($U = 32$, $p = 0.004$) and PCC ($U = 33.5$, $p = 0.005$) in TBI in comparison to the anoxic patient group (Fig. 3.B.4). These differences were associated with large effect size in both cases (PreCu, $r = 0.55$; PCC, $r = 0.53$). Additionally, the results showed a higher percentage of hyper-CDP voxels in the PCC sub-region in the TBI group ($U = 27$, $p = 0.001$; Fig. 3.B.2.) with large effect size ($r = 0.59$), which was not reflected in the comparison done using the total percentage of PMC hyper-PCD voxels ($p > 0.005$, FDR corr.).

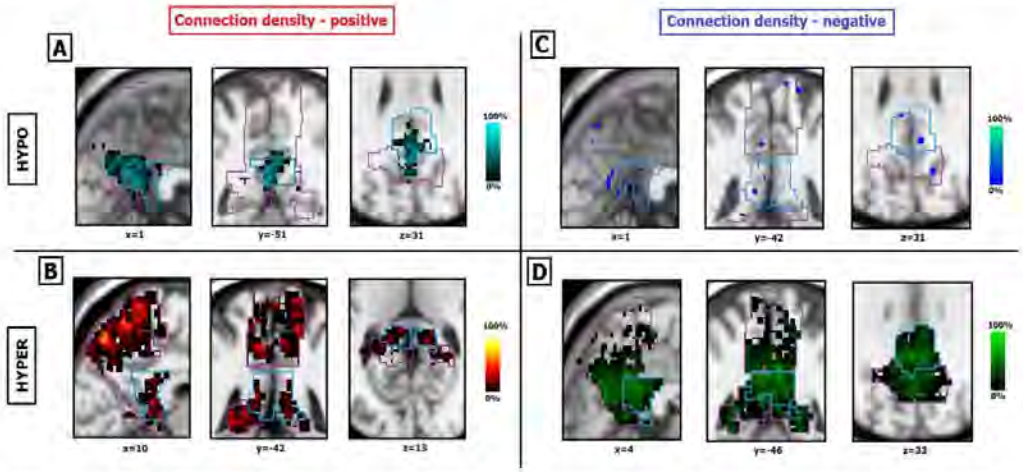

Fig. 4. Spatial maps of changes in PMC-to-mPFC connection density in the patient group. Patients seem to show significant hypo-CDP changes in the ventral portions of both PreCu and PCC (panel A). Hyper-CDP voxels are more specific to the dorsal sub-regions of the PreCu and PCC, and slightly border on the ventral PCC (panel B). Hypo-CDN changes are barely noticeable (panel C), and hyper-CDN voxels seem wide-spread and highly heterogeneous between patients (panel D). Individual results of patients are summed and presented in a single image; Purple and blue outlines reflect the borders of the anatomical PreCu and PCC respectively. Gradient bars (%) reflect the percentage of patients sharing the same voxel with a sig. Z-score (hypo/hyper CDP/CDN) at given anatomical location (spatial homogeneity).

Table 1
Spatial homogeneity of changes in PMC connection density in the patient group. Threshold – at least 33% or 67% of subjects spatially share the same voxel with sig. Z-score. The percentages present the proportion of voxels with significant Z-score out of the total number of voxels in PMC spatially shared between patients.

Group		Hypo-CDP	Hyper-CDP	Hyper-CDN
Patients	No threshold	8% (1054)	51% (6599)	68% (8803)
N = 27	≥ 33%	3% (347)	3% (396)	9% (1138)
	≥ 67%	0% (7)	0% (9)	0% (5)
TBI	No threshold	8% (1011)	46% (5866)	67% (8668)
N = 15	≥ 33%	2% (217)	7% (942)	23% (2959)
	≥ 67%	0% (1)	0.4% (51)	0.8% (102)
ANOXIC	No threshold	6% (730)	29% (3740)	33% (4305)
N = 12	≥ 33%	4% (473)	2% (244)	3% (339)
	≥ 67%	1% (143)	0% (3)	0% (6)

There were no significant differences between these two groups in the hyper-PCD in the PreCu sub-region (U = 50, $p = 0.053$; medium effect size ($r = 0.38$)), hypo-CDP in PreCu (U = 64, $p = 0.213$; small effect size ($r = 0.24$)) and PCC (U = 60, $p = 0.148$; small effect size ($r = 0.28$)), hypo-CDN in PreCu (U = 73, $p = 0.417$), small effect size ($r = 0.16$) and PCC (U = 62, $p = 0.118$; medium effect size ($r = 0.30$)).

3.3.2. Connection density changes in control pathways

Additionally, we wanted to test if the hyper-CDP and hyper-CDP voxels, found in the control pathways, were more specific to one of the aetiologies. The group-level statistical analysis showed a significantly higher percentage of Calcarine-mPFC hyper-CDP ((U = 37, $p = 0.009$; large effect size ($r = 0.5$)), and hyper-CDN voxels ((U = 33, $p = 0.004$; large effect size ($r = 0.54$)) in traumatic in comparison to anoxic brain injury patients (Supp. Figs. 3, 4).

3.4. Spatial homogeneity

The intra-group spatial similarity in voxels with changes in connection density are presented in Table 1. The hypo-CDN voxels were not included in the analysis, because there were no significant differences between the control and patient group. The results are reported without threshold and with the threshold of 33% and 67% of patients having the same voxel changes.

First, there seemed to be a lower spatial congruity in the entire group of patients, as opposed to the groups of same aetiology (Table 1). It can be observed, that even though there is spatial similarity between 1/3 of patients in the disconnected voxels, this number seems very low when considering 2/3 of the patient group.

Second, in comparison with traumatic patients, anoxic brain injury patients seem to have a slightly higher spatial homogeneity in PMC voxels with hypo-CDP. Third, TBI patients showed a higher intra-group similarity in hyper-CDP and hyper-CDN in comparison to anoxic patients. The latter changes were present even at the threshold of 67%, meaning that > 2/3 of patients were spatially sharing voxels with hyper negative connection density. The spatial homogeneity for separate aetiologies is presented in Fig. 5 with a threshold of 33% of patients needing to have the same hypo-CDP and hyper-CDN changes. An overlap between these two types of disconnection was additionally calculated for each subgroup showing an overlap of 1005 voxels in the TBI group (SD = 194; 10% of hypo-CDP/hyper-CDN voxels), and 665 voxels (SD = 67.6; 13% of hypo-CDP/hyper-CDN voxels) in the anoxic group.

The Jaccard index showed a similarity of 65% for hypo-CDP, 46% for hyper-CDP and 47% for hyper-CDN spatial maps between traumatic and anoxic BI patients. The similarity between the spatial maps of anoxic BI and the spatial maps of all patients (including TBI) was 69% for hypo-CDP, 57% for hyper-CDP and 49% for hyper-CDN voxel results. Finally, the comparison between the TBI and the group of all patients, suggested a similarity of 96% for hypo-CDP, 89% for hyper-CDP and 98% for hyper-CDN spatial maps. These results, along the spatial homogeneity results within different sub-groups, indicates that the results are more spatially heterogeneous and more widely distributed in the TBI group in comparison to the anoxic groups, further confirming differences in the pathological processes.

3.5. Prognostic value

3.5.1. Spearman correlation analysis with PMC-mPFC voxels

The number of PMC voxels with hypo-CDP showed a significant

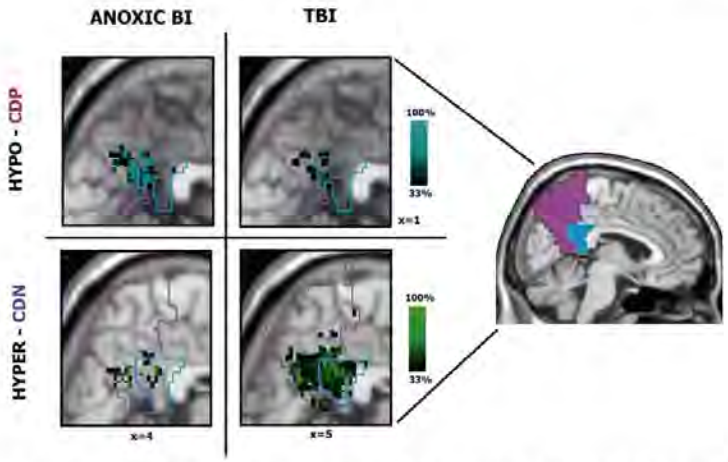

Fig. 5. Intra-group spatial homogeneity differences between the traumatic and anoxic brain injury patients (threshold 33%). Anoxic BI patients show a higher intra-group similarity in hypo-CDP in comparison to TBI patients, while TBI patients show a higher spatial congruity in hyper-CDN voxels. Purple and blue outlines reflect the borders of the anatomical PreCu and PCC respectively. Gradient bars (%) reflect the percentage of patients sharing the same voxel with a sig. Z-score (hypo/hyper CDP/CDN) at given anatomical location. The minimum spatial homogeneity is set to at least 33% of patients in a given group.

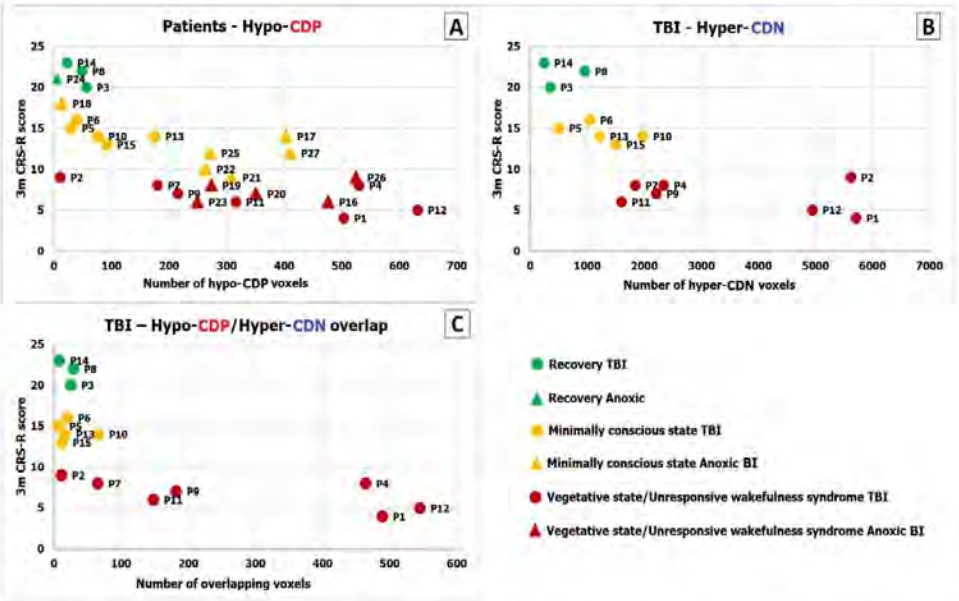

Fig. 6. The prognostic value of changes in PMC-to-mPFC connection density. Panel A) There was a sig. Negative link between the number of PMC voxels with hypo-CDP and the patient outcome ($r_s = -0.72$; $p = 0.00002$); Panel B) TBI patients showed a significant negative association between the number of voxels with hypo-CDP ($r_s = -0.80$; $p = 0.0004$; panel A), hyper-CDN and the CRS-R score ($r_s = -0.86$; $p = 0.00005$); Panel C) In TBI patients, there was highly significant negative association between the number of spatially overlapped hypo-CDP and hyper-CDN voxels and the 3-month outcome ($r_s = -0.73$, $p = 0.002$; Fig. 6.C). The x axis represents the 3-month CRS-R score, the y axis represent the number of voxels with changes in connection density.

negative association with the CRS-R score assessed 3 months after the coma onset ($r_s = -0.72$, $p = 0.00002$), indicating that if a patient had a higher number PMC voxels with hypo-CDP he was less likely to recover (Fig. 6.A). We did not find a significant correlation between hyper-CDP ($r_s = 0.29$, $p = 0.14$) and hyper-CDN ($r_s = -0.35$, $p = 0.07$) voxels and the CRS-R score for the entire patient group. The number of voxels with hypo-CDN was not included in the analysis, because there were no significant differences between the control and patient group.

At the aetiology level, it is worth noting that in the traumatic brain injury group, we found a highly significant link between number of hypo-CDP voxels ($r_s = -0.80$, $p = 0.0004$) and the CRS-R score (Fig. 6.A). Interestingly, a highly statistically relevant association was found between the number of hyper-CDN voxels and the CRS-R score

($r_s = -0.86$, $p = 0.00005$). Therefore, TBI patients with a high number of hypo-CDP and hyper-CDN PMC voxels had less chance for recovery 3 months after the initial fMRI scan (Fig. 6.B). The analysis in the anoxic group did not show a significant association between the CRS-R score and the hyper-CDP ($r_s = 0.43$, $p = 0.16$), hyper-CDN ($r_s = 0.20$, $p = 0.54$) nor the hypo-CDP voxels ($r_s = -0.38$, $p = 0.22$). However, this result should be interpreted in caution due to small sample size of anoxic BI patients.

Additionally, given the significant spatial overlap between voxels with hypo-CDP and hyper-CDP voxels, and the significance of these voxels in relation to the neurological recovery in TBI patients, we performed the same analysis on overlapping voxels. The results showed the same highly significant negative association between the number of spatially overlapping hypo-CDP and hyper-CDN voxels and the 3-month outcome ($r_s = -0.73$, $p = 0.002$; Fig. 6.C).

3.5.2. Spearman correlation analysis with the control pathway voxels

The Spearman correlation analysis did not show any significant association between the CRS-R score assessed 3 months after the coma onset and any of the number of voxels with significant connection density changes in the Calcarine-mPFC control pathways (FDR $p > 0.05$). This was true for the entire group of patients and for the anoxic and traumatic BI groups separately.

3.5.3. Logistic regression analysis with PMC-mPFC voxels

A logistic regression analysis was conducted to ascertain the effects of the number of hypo-CDP, hyper-CDN and hyper-CDP PMC voxels on the likelihood that the patients had a good outcome (recovery and MCS) or bad outcome (UWS/VS). Due to significant collinearity between the hyper-CDP and hyper-NCD ($r = -0.91$), two models were tested, the first including hypo-CDP and hyper-CDP and the second hypo-CDP and hyper-CDN as independent/predictor variables.

The first model was significant (chi square = 10.204, $p = 0.006$ with df = 2), however the number of hyper-CDP voxels did not significantly contribute to the prediction (Wald, $p = 0.296$). Thus, we decided to keep the second model, where both predictors had a significant effect on the outcome.

The full model against the constant only model was statistically significant, suggesting that the predictors as a set reliably distinguished between patients with good and bad outcome (chi square = 16.701, $p < 0.001$ with df = 2). The model explained 62% (Nagelkerke's R^2) of the variance in outcome, and correctly classified 78% of cases (sensitivity – 80%; specificity – 75%). The Wald criterion demonstrated that both variables, hypo-CDP ($p = 0.02$) and hyper-CDN ($p = 0.044$) had a weak but significant contribution to prediction. Increase in both predictors was associated with decreased likelihood of good outcome. Accordingly, Exp (B) indicates that the for every extra unit (number of voxels) of hypo-CDP and hyper-NCD, the odds of recovery decrease by a factor of 0.988 and 0.999, respectively, all other factor being equal.

4. Discussion

Our findings demonstrate that a comparative analysis of voxel-wise connection density disruptions between the PMC and the mPFC, might constitute a reliable and fine-grained study approach, permitting to accurately address the brain functional network changes, which are critically related to consciousness abolition during coma. Crucially, built upon statistical analysis at a single subject level - a necessary condition to make reliable inferences in individual patients - this voxel-wise connection density approach, enabled the description of a novel PMC/mPFC dysconnectional taxonomy, permitting the identification of specific markers related to brain injury mechanism and useful for neuroprognostication. The current study, confirms and expands previous finding through seed-based analysis method (Silva et al., 2015), and permits: (i) a precise topological description of the PMC sub-regions (ventral PreCu and the PCC) who seems implicated in the consciousness impairment observed in this setting, (ii) identification of useful and accurate neuroimaging biomarker for prognostication in this setting, as the number of PMC voxels with hypo-CDP to mPFC, had significant predictive value in relation to patients neurological outcome assessed 3 months after the coma onset in the current study. It is worth noting that such adaptive changes, characterized by a reduction of CDP, were rarely observed in the control pathway (Calcarine/mPFC). Crucially, the number of voxels with any significant connection density changes within this control pathway, was not correlated with patient's neurological outcome. These points strongly support the critical role of PMC/mPFC functional connections in consciousness emergence, and consolidate the specific use of PMC/mPFC functional connectivity to predict coma patient's neurological outcome.

Our data strongly support the concept of a significant structural and functional PMC heterogeneity, which could be implicated in the "tuning" of the whole-brain metastable status (Hellyer et al., 2015). Furthermore, our results are in line with the hypothesis of a dysfunctional mesocircuit (Schiff, 2010) in DOC patients, build upon anterior and posterior critical disruption of neural communication. For example, tract-tracing studies conducted in non-human primates (Vogt et al., 2005) and diffusion tensor tractography in humans (Hagmann et al., 2008) have clearly identified structural connections between dorsal PCC to the mPFC along the cingulum bundle (Greicius et al., 2009). Interestingly, structural injuries within this tract have been described as related to neurological outcome of severely brain injured patients (Fernández-Espejo et al., 2012).

Furthermore, our findings suggest a higher prevalence of hypo-CDP voxels in comatose patients, specifically located in the ventral subdivision of both the PCC and the PreCu. This result seems compatible with the findings of the rs-fMRI study of Silva et al. (2015), suggesting stronger functional connectivity between PCC-centred seed and the mPFC in patient who eventually recovered. However, our voxel-wise connection density method further elucidated the importance of the total number of PMC voxels in prediction of patient's outcome and allowed us to explore the intra-regional topological changes in connectivity which is not possible in seed-based analysis. Additionally, previous resting-state fMRI (Bzdok et al., 2015; Cauda et al., 2010; Margulies et al., 2009; Vogt et al., 2006; Zhang and Li, 2013), and DTI studies (Zhang et.al., 2014) indicate that both these PMC subregions are densely connected to other brain regions that participate to DMN network and appears to be implicated in internally directed cognition (i.e. self-referential information processing, social cognition, mind-wandering, episodic memory retrieval) (Andrews-Hanna et al., 2010; Cavanna and Trimble, 2006; Fox et al., 2015; Leech and Sharp, 2014). In contrast with this hypo-CDP restricted to ventral parts of PreCu/PCC, we demonstrated that dorsal PreCu and anterior dorsal (and a part of ventral) PCC, encompasses specific voxels with hyper-CDP in coma patients. These dorsal PMC structures are known to support and connect to other regions involved in externally directed cognitive processes (Margulies et al., 2009; Zhang and Li, 2013) such as spatially-guided behaviour, visual/motor mental imagery (Cavanna and Trimble, 2006), control of attentional focus (Leech and Sharp, 2014) and high-level sensorimotor functions (Balestrini et al., 2015; Herbet et al., 2015). Overall, the observed rostro-caudal functional segregation between increase and decrease of CDP, seems in line with the hypothesis of the central role played by an imbalance between internal and external awareness systems in the genesis of consciousness disorders (Demertzi et al., 2013; Di Perri et al., 2014; He et al., 2014). Actually, as described in chronic DOC patients (He et al., 2014), this imbalance could reflect overcompensation in the external network due to the loss of input from internal self-networks.

Additionally, we sought for functional signatures of the brain injury mechanisms that were responsible of coma. Regarding, the hypo-CDP voxels, our findings indicate that within the PMC, hypo-CDP voxels were slightly more pronounced in anoxic patients (although not statistically significant), probably representing a neural underpinning

of the overall worse prognosis of this group (Horsting et al., 2015; Koenig et al., 2014). Furthermore, in line with recent studies, suggesting that hyperconnectivity patterns are a common network response to traumatic brain injury (Bharath et al., 2015; Hillary et al., 2014, 2015; Stevens et al., 2012) we observed that hyper-CDP (in the PCC subregion) and hyper-CDN voxels were more frequently detected in the traumatic group. This was true for the PMC-mPFC connectivity patterns, but also for the control pathway, representing connections between the Calcarine and the mPFC.

We hypothesize that the higher prevalence of hyperconnectivity patterns in this group could be the consequence of compensatory brain plastic processes (Di Perri et al., 2014) possibly reflecting resilient connections massively disrupted, but not totally interrupted by traumatic brain injury (i.e. diffuse axonal injury). These resilient connections might have engaged residual critical neural resources, otherwise normally distributed through efficient brain network connections, here disrupted by brain injury, resulting in impaired conscious processing (Hillary et al., 2015). Furthermore, these brain network signature of acute brain injury mechanisms was confirmed by spatial homogeneity analysis (thresholding and Jaccard index), which indicated higher spatial similarity of identified changes in voxel connection density between subjects with same aetiologies in comparison to the whole patient group. However, despite higher intra-group similarity, these changes seemed more spatially scatted in the TBI patients group in comparison to anoxic patients, which is in accordance with the heterogeneity of brain lesion found in this group of patients.

Finally, it is worth noting, that we specifically observed in the traumatic brain injury group, that the loss long-range connection density of positive correlations (hypo-CDP) between the PMC and the mPFC, was balanced with a spatially overlapping increase of negative coactivation (hyper-CDN). The total amount of the later was associated to patient recovery and could depict maladaptive brain plasticity processes. We hypothesize that this potentially compensatory increase of negative connection density may indicate some aberrant inhibitory processes or competitive mechanisms of information processing (Fox et al., 2009, 2012; Gee et al., 2011; Gopinath et al., 2015; Liu et al., 2015), resulting in the breakdown of more efficient network organization (i.e. PMC hypo-CDP). This is further supported by the unfavourable outcome of our patients with a higher number of overlapping PMC voxels with decreased positive connections but yet increased negative connections with mPFC.

Interestingly, the same hyper-CDP and hyper-CDN patterns in the control pathways were not associated with the outcome in TBI patients. This result indicates that despite of the more global pattern of these changes, the increase of negative connection density seems maladaptive only when present in regions critical to conscious processing.

There are several limitations in this study. First the number of patients is relatively small and our results need to be validated in larger cohorts. Second, we performed a study of density of connections between each PMC voxel and all of the MPFC voxels, aiming to explore in detail, the topology and the functional characteristics of the connections established from PMC which was assumed homogeneous. Therefore, future studies should also address the functional segregation and heterogeneity within mPFC in this setting. In future studies, brain damage in the form of lesions in traumatic brain injury should be assessed in the pre-processing step, as though not properly treated lesions can potentially give rise to artificially induced connectivity.

In summary, a complex pattern of decreased and increased connections was observed, and the topography of these changes, seemed to be in agreement with the hypothesis of network imbalance between internal/external processing systems, within PMC during acquired disorders of consciousness. We report a significant link between the PMC (ventral parts of both the PCC and PreCu) and the mPFC functional connectivity and patient recovery. Actually, the number of PMC voxels with hypo-CDP showed a significant negative association with the CRS-R score and a "negative" predictive value in relation to good outcome assessed 3 months after the coma onset, notwithstanding aetiology. Additionally, traumatic brain injury specifically appeared to be associated with a greater prevalence of hyperconnected positively and negatively correlated voxels, and the total amount of latter, was inversely associated with patient neurological outcome. This point might reflect a maladaptive plasticity mechanism through a resilient functional network and an inefficient redistribution of remaining resources and pave the way for innovative prognosis and therapeutics methods in this challenging setting.

Supplementary data to this article can be found online at http://dx.doi.org/10.1016/j.nicl.2017.03.017.

Funding

This study was supported by "Association des Traumatisés du Crâne et de la Face" (2014-A3); "Institut des Sciences du Cerveau de Toulouse" (2016-21); "Institut National de la Santé et de la Recherche Médicale" (2016-DEVIN). The funding sources had no role in the study design, data collection, data analysis, data interpretation, or writing of this report.

Acknowledgements

The authors thank the technicians and engineers of the Neurocampus & Brain Imaging Center of Purpan (Helene Gros, Nathalie Vayssiere) and the medical staff of the Critical Care Units of the University Teaching Hospital of Toulouse (Helene Vinour, Veronique Ramonda, David Rousset, Edith Horcastagnou, Clement Delmas, Caroline Viendel) for their active participation in the MRI studies in comatose patients.

References

Andrews-Hanna, J.R., Reidler, J.S., Sepulcre, J., Poulin, R., Buckner, R.L., 2010. Functional-anatomic fractionation of the Brain's default network. Neuron 65, 550–562. http://dx.doi.org/10.1016/j.neuron.2010.02.005.

Balestrini, S., Francione, S., Mai, R., Castana, L., Casaceli, G., Marino, D., Provinciali, L., Cardinale, F., Tassi, L., 2015. Multimodal responses induced by cortical stimulation of the parietal lobe: a stereo-electroencephalography study. Brain 138, 2596–2607. http://dx.doi.org/10.1093/brain/awv187.

Bharath, R.D., Munivenkatappa, A., Gohel, S., Panda, R., Saini, J., Rajeswaran, J., Shukla, D., Bhagavatula, I.D., Biswal, B.B., 2015. Recovery of resting brain connectivity ensuing mild traumatic brain injury. Front. Hum. Neurosci. 9, 513. http://dx.doi.org/10.3389/fnhum.2015.00513.

Bzdok, D., Heeger, A., Langner, R., Laird, A.R., Fox, P.T., Palomero-Gallagher, N., Vogt, B.A., Zilles, K., Eickhoff, S.B., 2015. Subspecialization in the human posterior medial cortex. NeuroImage 106, 55–71. http://dx.doi.org/10.1016/j.neuroimage.2014.11.009.

Cauda, F., Geminiani, G., D'Agata, F., Sacco, K., Duca, S., Bagshaw, A.P., Cavanna, A.E., 2010. Functional connectivity of the posteromedial cortex. PLoS One 5, 1–11. http://dx.doi.org/10.1371/journal.pone.0013107.

Cavanna, A.E., Trimble, M.R., 2006. The precuneus: a review of its functional anatomy and behavioural correlates. Brain 129, 564–583. http://dx.doi.org/10.1093/brain/awl004.

Chai, X.J., Castañán, A.N., Öngür, D., Whitfield-Gabrieli, S., 2012. Anticorrelations in resting state networks without global signal regression. NeuroImage 59, 1420–1428. http://dx.doi.org/10.1016/j.neuroimage.2011.08.048.

Chai, X.J., Ofen, N., Gabrieli, J.D.E., Whitfield-Gabrieli, S., 2014. Selective development of anticorrelated networks in the intrinsic functional organization of the human brain. J. Cogn. Neurosci. 26, 501–513. http://dx.doi.org/10.1162/jocn_a_00517.

Dehaene, S., Changeux, J.P., 2011. Experimental and theoretical approaches to conscious processing. Neuron 70, 200–227. http://dx.doi.org/10.1016/j.neuron.2011.03.018.

Demertzi, A., Vanhaudenhuyse, A., Bredart, S., Heine, L., Perri, C. Di, Laureys, S., Brédart, S., di Perri, C., 2013. Looking for the self in pathological unconsciousness. Front. Hum. Neurosci. 7, 1–6. http://dx.doi.org/10.3389/fnhum.2013.00538.

Di Perri, C., Heine, L., Amico, E., Soddu, A., Laureys, S., Demertzi, A., 2014. Technology-based assessment in patients with disorders of consciousness. Ann. Ist. Super. Sanita 50, 209–220. http://dx.doi.org/10.4415/ANN.14.03.03.

Fernández-Espejo, D., Soddu, A., Cruse, D., Palacios, E.M., Junque, C., Vanhaudenhuyse, A., Rivas, E., Newcombe, V., Menon, D.K., Pickard, J.D., Laureys, S., Owen, A.M., 2012. A role for the default mode network in the bases of disorders of consciousness. Ann. Neurol. 72, 335–343. http://dx.doi.org/10.1002/ana.23635.

Fox, M.D., Zhang, D., Snyder, A.Z., Raichle, M.E., 2009. The global signal and observed anticorrelated resting state brain networks. J. Neurophysiol. 101, 3270–3283. http://dx.doi.org/10.1152/jn.90777.2008.

Fox, M.D., Buckner, R.L., White, M.P., Greicius, M.D., Pascual-Leone, A., 2012. Efficacy of transcranial magnetic stimulation targets for depression is related to intrinsic functional connectivity with the subgenual cingulate. Biol. Psychiatry 72, 595–603. http://dx.doi.org/10.1016/j.biopsych.2012.04.028.

Fox, K.C.R., Spreng, R.N., Ellamil, M., Andrews-Hanna, J.R., Christoff, K., 2015. The wandering brain: meta-analysis of functional neuroimaging studies of mind-wandering and related spontaneous thought processes. NeuroImage. http://dx.doi.org/10.1016/j.neuroimage.2015.02.039.

Gee, D.G., Biswal, B.B., Kelly, C., Stark, D.E., Margulies, D.S., Shehzad, Z., Uddin, L.Q., Klein, D.F., Banich, M.T., Xavier, F., 2011. Processing Among the Cerebral Hemispheres. 54. pp. 517–527. http://dx.doi.org/10.1016/j.neuroimage.2010.05.073.Low.

Gopinath, K., Krishnamurthy, V., Cabanban, R., Crosson, B.A., 2015. Hubs of anticorrelation in high-resolution resting-state functional connectivity network architecture. Brain Connect XX, 1–9. http://dx.doi.org/10.1089/brain.2014.0323.

Greicius, M.D., Supekar, K., Menon, V., Dougherty, R.F., 2009. Resting-state functional connectivity reflects structural connectivity in the default mode network. Cereb. Cortex 19, 72–78. http://dx.doi.org/10.1093/cercor/bhn059.

Hagmann, P., Cammoun, L., Gigandet, X., Meuli, R., Honey, C.J., Van Wedeen, J., Sporns, O., 2008. Mapping the structural core of human cerebral cortex. PLoS Biol. 6, 1479–1493. http://dx.doi.org/10.1371/journal.pbio.0060159.

Hannawi, Y., Lindquist, M.A., Caffo, B.S., Sair, H.I., Stevens, R.D., 2015. Resting brain activity in disorders of consciousness: a systematic review and meta-analysis. Neurology 84, 1272–1280. http://dx.doi.org/10.1212/WNL.0000000000001404.

He, J.H., Yang, Y., Zhang, Y., Qiu, S.Y., Zhou, Z.Y., Dang, Y.Y., Dai, Y.W., Liu, Y.J., Xu, R.X., 2014. Hyperactive external awareness against hypoactive internal awareness in disorders of consciousness using resting-state functional MRI: highlighting the involvement of visuo-motor modulation. NMR Biomed. 27, 880–886. http://dx.doi.org/10.1002/nbm.3130.

Heine, L., Soddu, A., Gomez, F., Vanhaudenhuyse, A., Tshibanda, L., Thonnard, M., Charland-Verville, V., Kirsch, M., Laureys, S., Demertzi, A., 2012a. Resting state networks and consciousness alterations of multiple resting state network connectivity in physiological, pharmacological, and pathological consciousness states. Front. Psychol. 3, 1–12. http://dx.doi.org/10.3389/fpsyg.2012.00295.

Heine, L., Soddu, A., Gómez, F., Vanhaudenhuyse, A., Tshibanda, L., Thonnard, M., Charland-Verville, V., Kirsch, M., Laureys, S., Demertzi, A., 2012b. Resting state networks and consciousness: alterations of multiple resting state network connectivity in physiological, pharmacological, and pathological consciousness states. Front. Psychol. 3, 295. http://dx.doi.org/10.3389/fpsyg.2012.00295.

Hellyer, X.P.J., Scott, G., Shanahan, X.M., Sharp, D.J., Leech, X.R., 2015. Cognitive Flexibility through Metastable Neural Dynamics is Disrupted by Damage to the Structural Connectome. 35. pp. 9050–9063. http://dx.doi.org/10.1523/JNEUROSCI.4648-14.2015.

Herbet, G., Lafargue, G., Duffau, H., 2015. The dorsal cingulate cortex as a critical gateway in the network supporting conscious awareness. Brain awv381. http://dx.doi.org/10.1093/brain/awv381.

Hillary, F.G., Rajtmajer, S.M., Roman, C.A., Medaglia, J.D., Slocomb-Dluzen, J.E., Calhoun, V.D., Good, D.C., Wylie, G.R., 2014. The rich get richer: brain injury elicits hyperconnectivity in core subnetworks. PLoS One 9. http://dx.doi.org/10.1371/journal.pone.0104021.

Hillary, F.G., Roman, C.A., Venkatesan, U., Rajtmajer, S.M., Bajo, R., Castellanos, N.D., 2015. Hyperconnectivity is a fundamental response to neurological disruption. Neuropsychology 29, 59–75. http://dx.doi.org/10.1037/neu0000110.

Horsting, M.W., Franken, M.D., Meulenbelt, J., van Klei, W.A., de Lange, D.W., 2015. The etiology and outcome of non-traumatic coma in critical care: a systematic review. BMC Anesthesiol. 15, 65. http://dx.doi.org/10.1186/s12871-015-0041-9.

Koenig, M.A., Holt, J.L., Ernst, T., Buchthal, S.D., Nakagawa, K., Stenger, V.A., Chang, L., 2014. MRI default mode network connectivity is associated with functional outcome after cardiopulmonary arrest. Neurocrit. Care. 20, 348–357. http://dx.doi.org/10.1007/s12028-014-9953-3.

Lant, N.D., Gonzalez-Lara, L.E., Owen, A.M., Fernández-Espejo, D., 2016. Relationship between the anterior forebrain mesocircuit and the default mode network in the structural bases of disorders of consciousness. NeuroImage Clin. 10, 27–35. http://dx.doi.org/10.1016/j.nicl.2015.11.004.

Laureys, S., Goldman, S., Phillips, C., et al., 1999. Impaired effective cortical connectivity in vegetative state: preliminary investigation using PET. NeuroImage 9 (4), 377–382.

Leech, R., Sharp, D.J., 2014. The role of the posterior cingulate cortex in cognition and disease. Brain 137, 12–32. http://dx.doi.org/10.1093/brain/awt162.

Liu, Y., Huang, L., Li, M., Zhou, Z., Hu, D., 2015. Anticorrelated networks in resting-state fMRI-BOLD data. Biomed. Mater. Eng. 26 (Suppl. 1), S1201–S1211. http://dx.doi.org/10.3233/BME-151417.

Margulies, D.S., Vincent, J.L., Kelly, C., Lohmann, G., Uddin, L.Q., Biswal, B.B., Villringer, A., Castellanos, F.X., Milham, M.P., Petrides, M., 2009. Precuneus shares intrinsic functional architecture in humans and monkeys. Proc. Natl. Acad. Sci. U. S. A. 106, 20069–20074. http://dx.doi.org/10.1073/pnas.0905314106.

Murphy, K., Birn, R.M., Handwerker, D.A., Jones, T.B., Bandettini, P.A., 2009. The impact of global signal regression on resting state correlations: are anti-correlated networks introduced? NeuroImage 44, 893–905. http://dx.doi.org/10.1016/j.neuroimage.2008.09.036.

Norton, L., Hutchison, R.M., Young, G.B., Lee, D.H., Sharpe, M.D., Mirsattari, S.M., 2012. Disruptions of functional connectivity in the default mode network of comatose patients. Neurology 78, 175–181. http://dx.doi.org/10.1212/WNL.0b013e31823fcd61.

Parvizi, J., Van Hoesen, G.W., Buckwalter, J., Damasio, A., 2006. Neural connections of the posteromedial cortex in the macaque. Proc. Natl. Acad. Sci. U. S. A. 103, 1563–1568. http://dx.doi.org/10.1073/pnas.0507729103.

Qin, P., Wu, X., Huang, Z., Duncan, N.W., Tang, W., Wolff, A., Hu, J., Gao, L., Jin, Y., Wu, X., Zhang, J., Lu, L., Wu, C., Qu, X., Mao, Y., Weng, X., Zhang, J., Northoff, G., 2015. How are different neural networks related to consciousness? Ann. Neurol. 78, 594–605. http://dx.doi.org/10.1002/ana.24479.

Schiff, N.D., 2010. Recovery of consciousness after brain injury: a mesocircuit hypothesis. Trends Neurosci. 33 (1), 1–9. http://dx.doi.org/10.1016/j.tins.2009.11.002.

Schnakers, C., Majerus, S., Giacino, J., Vanhaudenhuyse, A., Bruno, M.-A., Boly, M., Moonen, G., Damas, P., Lambermont, B., Lamy, M., Damas, F., Ventura, M., Laureys, S., 2008. A French validation study of the Coma Recovery Scale-Revised (CRS-R). Brain Inj. 22, 786–792. http://dx.doi.org/10.1080/02699050802403557.

Silva, S., Alacoque, X., Fourcade, O., Samii, K., Marque, P., Woods, R., Mazziotta, J., Chollet, F., Loubinoux, I., 2010. Wakefulness and loss of awareness — brain and brainstem interaction in the vegetative state. Neurology 74, 313–320. http://dx.doi.org/10.1212/WNL.0b013e3181cbcd96.

Silva, S., De Pasquale, F., Vuillaume, C., Riu, B., Loubinoux, I., Geeraerts, T., Seguin, T., Bounes, V., Fourcade, O., Demonet, J.F., Peran, P., 2015. Disruption of posteromedial large-scale neural communication predicts recovery from coma. Neurology 85, 2036–2044. http://dx.doi.org/10.1212/WNL.0000000000002196.

Stevens, M.C., Lovejoy, D., Kim, J., Oakes, H., Kureshi, I., Witt, S.T., 2012. Multiple resting state network functional connectivity abnormalities in mild traumatic brain injury. Brain Imaging Behav. 6, 293–318. http://dx.doi.org/10.1007/s11682-012-9157-4.

Teasdale, G., Jennett, B., 1974. Assessment of coma and impaired consciousness. A practical scale. Lancet 304, 81–84. http://dx.doi.org/10.1016/S0140-6736(74)91639-0.

Tomasi, D., Volkow, N.D., 2010. Functional Connectivity Density Mapping. pp. 107. http://dx.doi.org/10.1073/pnas.1001414107.

Tsai, Y.H., Yuan, R., Huang, Y.C., Yeh, M.Y., Lin, C.P., Biswal, B.B., 2014. Disruption of brain connectivity in acute stroke patients with early impairment in consciousness. Front. Psychol. 4, 1–10. http://dx.doi.org/10.3389/fpsyg.2013.00956.

Tzourio-Mazoyer, N., Landeau, B., Papathanassiou, D., Crivello, F., Etard, O., Delcroix, N., Mazoyer, B., Joliot, M., 2002. Automated anatomical labeling of activations in SPM using a macroscopic anatomical parcellation of the MNI MRI single-subject brain. NeuroImage 15, 273–289. http://dx.doi.org/10.1006/nimg.2001.0978.

Vanhaudenhuyse, A., Noirhomme, Q., Tshibanda, L.J.F., Bruno, M.A., Boveroux, P., Schnakers, C., Soddu, A., Perlbarg, V., Ledoux, D., Brichant, J.F., Moonen, G., Maquet, P., Greicius, M.D., Laureys, S., Boly, M., 2010. Default network connectivity reflects the level of consciousness in non-communicative brain-damaged patients. Brain 133, 161–171. http://dx.doi.org/10.1093/brain/awp313.

Vogt, B.A., Laureys, S., 2005. Posterior cingulate, precuneal and retrosplenial cortices: cytology and components of the neural network correlates of consciousness. Prog. Brain Res. http://dx.doi.org/10.1016/S0079-6123(05)50015-3.

Vogt, B.A., Vogt, L., Farber, N.B., Bush, G., 2005. Architecture and neurocytology of monkey cingulate gyrus. J. Comp. Neurol. 239, 218–239. http://dx.doi.org/10.1002/cne.20512.

Vogt, B.A., Vogt, L., Laureys, S., 2006. Cytology and functionally correlated circuits of human posterior cingulate areas. NeuroImage 29, 452–466. http://dx.doi.org/10.1016/j.neuroimage.2005.07.048.

Weissenbacher, A., Kasess, C., Gerstl, F., Lanzenberger, R., Moser, E., Windischberger, C., 2009. Correlations and anticorrelations in resting-state functional connectivity MRI: a quantitative comparison of preprocessing strategies. NeuroImage 47, 1408–1416. http://dx.doi.org/10.1016/j.neuroimage.2009.05.005.

Whitfield-Gabrieli, S., Nieto-Castanon, A., 2012. Conn: a functional connectivity toolbox for correlated and anticorrelated brain networks. Brain Connect. 2, 125–141. http://dx.doi.org/10.1089/brain.2012.0073.

Wijdicks, E.F.M., Bamlet, W.R., Maramattom, B.V., Manno, E.M., McClelland, R.L., 2005. Validation of a new coma scale: the FOUR score. Ann. Neurol. 58, 585–593. http://dx.doi.org/10.1002/ana.20611.

Wu, X., Zou, Q., Hu, J., Tang, W., Mao, Y., Gao, L., Zhu, J., Jin, Y., Wu, X., Lu, L., Zhang, Y., Zhang, Y., Dai, Z., Gao, J.-H., Weng, X., Zhou, L., Northoff, G., Giacino, J.T., He, Y., Yang, Y., 2015. Intrinsic functional connectivity patterns predict consciousness level and recovery outcome in acquired brain injury. J. Neurosci. 35, 12932–12946. http://dx.doi.org/10.1523/JNEUROSCI.0415-15.2015.

Zhang, S., Li, C.-S.R., 2013. Functional connectivity mapping of the human precuneus by resting state fMRI. NeuroImage 59, 3548–3562. http://dx.doi.org/10.1016/j.neuroimage.2011.11.023.Functional.

Zhang, Y., Fan, L., Zhang, Y., Wang, J., Zhu, M., Zhang, Y., Yu, C., Jiang, T., 2014. Connectivity-based parcellation of the human posteromedial cortex. Cereb. Cortex 24, 719–727. http://dx.doi.org/10.1093/cercor/bhs353.

6.2 Appendices for Chapter I

Table 6.2.1. EEG studies with the graph theoretical approach

Author	Modality	Type of DOC	Etiology	Delay injury/imaging	Delay inclusion/ outcome	Outcome assessment	Reported outcome	Findings
Coma								
Beudel et al. (2014)	19-channel EEG	56 coma	56 CA	≤ 5 days	6 months	CPC	27 patients died (CPC=5); 19 normal (CPC=1), 8 mild (CPC=2), 1 modest (CPC=3), 1 severe (CPC=4) cerebral dysfunction.	Survivors showed significantly more nodes and connections, higher CPL, lower CC and SWI then non-survivors.
Chronic DOC								
Chennu et al. (2014)	High-density resting-state EEG	13 UWS; 19 MCS	23 TBI; 9 anoxia	3 - 154 months	/	/		Reduced CC, and PC (less hubs), increased CPL, and lacking long-distance connections, in the alpha band in DOC compared to healthy controls. Patients had higher CC and PC in delta and theta bands. More modular structure similarity between patients in delta and theta bands in opposed to the alpha band in controls. Metrics of alpha network efficiency correlated with the degree of behavioral awareness.
Chennu et al. (2017)	High-density EEG, PET	23 UWS; 17 MCS -; 49 MCS+; 11 EMCS; 4 LIS	51 TBI ; 53 Non-TBI;	9 - 7387 days	1 year	GOS-E	39 positive outcome; 22 negative outcome	Positive outcome patients had diminished delta-band connectivity in central and parietal areas, and higher modularity and CC in delta networks.

CPC - Cerebral performance category; GOS-E – Glasgow Outcome Scale Extended; CA – cardiac arrest; CC – clustering coefficient; CPL – characteristic path length; PC – participation coefficient; LE – local efficiency; SWI – small-world index.

6.3 Appendices for Chapter IV

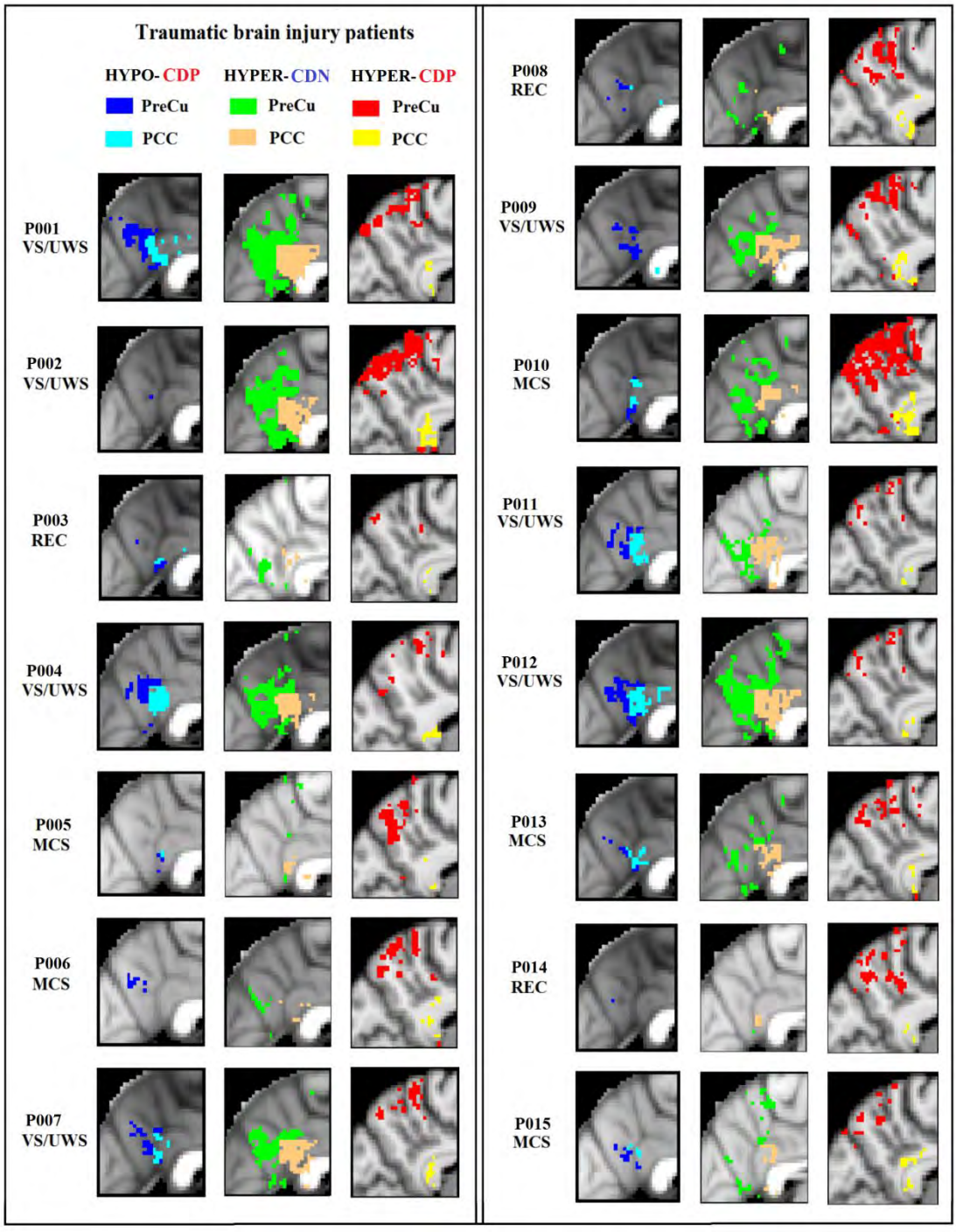

Figure 6.3.1. Individual traumatic brain injury patients' connection density spatial maps.
The spatial maps are presented separately for each patient. The changes in connection density are presented separately for hypo-CDP, hyper-CDP and hyper-CDN and the two anatomical PMC sub-regions – PreCu and PCC. The patients' outcome is marked beneath the patients' code – REC – Recovery, MCS – Minimally conscious state; VS/UWS – Vegetative state/Unresponsive wakefulness syndrome.

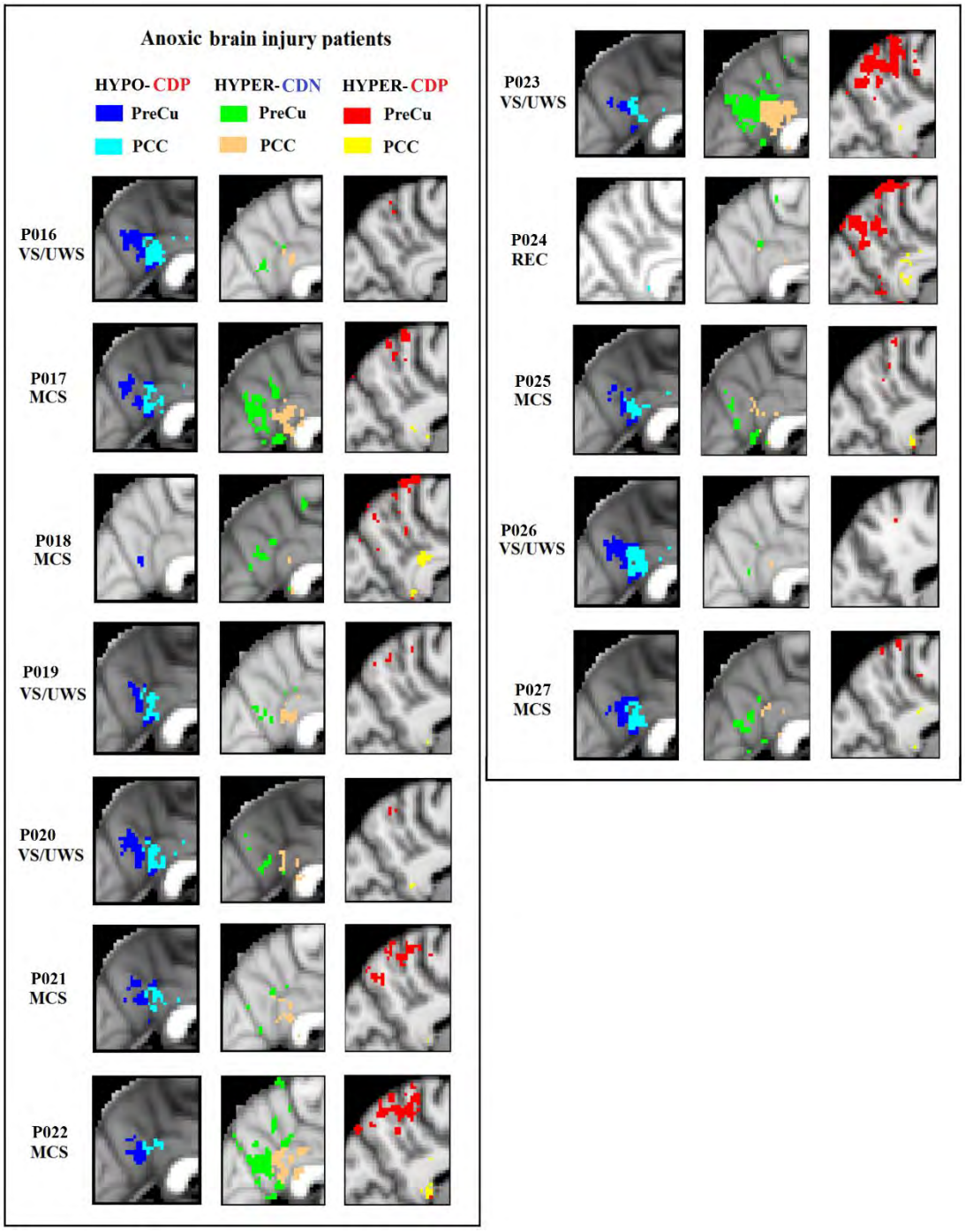

Figure 6.3.2. Individual anoxic brain injury patients' connection density spatial maps.
The spatial maps are presented separately for each patient. The changes in connection density are presented separately for hypo-CDP, hyper-CDP and hyper-CDN and the two anatomical PMC sub-regions – PreCu and PCC. The patients' outcome is marked beneath the patients' code – REC – Recovery, MCS – Minimally conscious state; VS/UWS – Vegetative state/Unresponsive wakefulness syndrome.

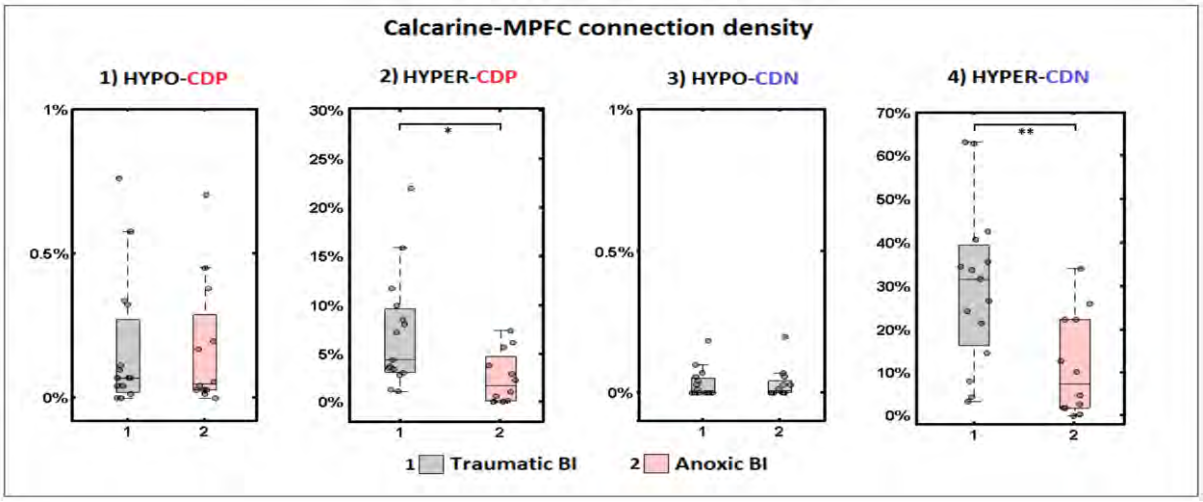

Figure 6.3.3. Differences in Calcarine-mPFC connection density changes between traumatic and anoxic brain injury.
*TBI patients showed significantly more Calcarine-mPFC hyper-CDP (sub-panel 2) and hyper-CDN voxels (sub-panel 4) in comparison with the anoxic BI patients. Boxplots represent medians with interquartile range and whiskers signify minimum and maximum values (excluding the outliers) (*p < .05, (**p < .005, ns: nonsignificant).*

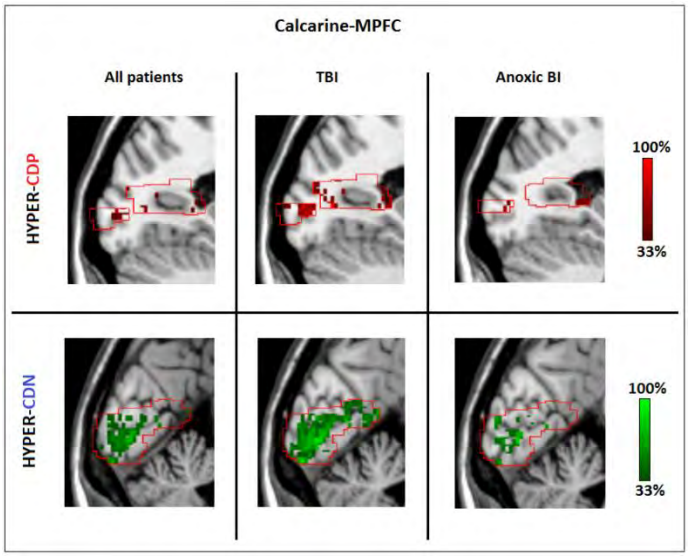

Figure 6.3.4. Connection density changes in the Calcarine-mPFC control pathway (threshold 33%).
TBI patients show more widespread changes and a higher spatial congruity in hyper-CDN and hyper-CDP voxels in comparison to anoxic BI. Gradient bars (%) reflects the percentage of patients sharing the same voxel with a sig. Z-score (hyper CDP/CDN) at given anatomical location within the Calcarine. The minimum spatial homogeneity is set to at least 33% of patients in a given group.

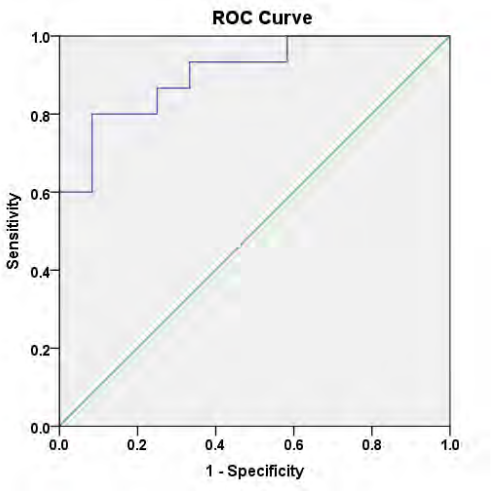

Sensitivity	Specificity	Successfully classified	PPV	NPV	AUC	95% CI	Std. error
80%	75%	77.8%	80%	75%	0.906	0.795-1.00	0.056

Figure 6.3.5. Logistic regression model.
The graph presents true positive (sensitivity) on the vertical axis and true negative (1-specificity) on the horizontal axis. The area under the ROC curve (AUC) ranges from 0.5 to 1.00 with larger values indicative of a better fit. The area under the curve is 0.906 with 95% confidence interval (0.795-1.00). Also, the AUC is significantly different from 0.5 (50/50 chance) with p-value=0.000 suggesting that the logistic regression classifies the group significantly better than by chance. PPV – positive predictive value; NPV – negative predictive value; AUC – area under the curve; CI – confidence interval; Std. error – standard error.

Table 6.3.1. Individual patient results – the total number of hypo/hyper-CDP and hypo/hyper-CDN voxels for PMC (Panel A), PreCu (Panel B) and PCC (Panel B).
The overlapping hypo-CDP and hyper-CDN voxels are presented only for PMC (Panel A). Number of voxels per region: PMC - 12862 voxels, PreCu - 11222 voxels, PCC - 1640 voxels. Abbreviations: TBI – traumatic brain injury, ANOXIC – anoxic brain injury; N – number of voxels with significant Z-score. REC – Recovery, MCS – Minimally conscious state; VS/UWS – Vegetative state/Unresponsive wakefulness syndrome.

A) Individual patient results - PMC results

Patient	Etiology	CRS-R score	Outcome	Hypo-CDP voxels (N)	Hypo-CDN voxels (N)	Hyper-CDP voxels (N)	Hyper-CDN Voxels (N)	Hypo-CDP /Hyper-CDN overlap (N)
Patient 1	TBI	4	VS	504.00	6.00	1150.00	5716.00	489
Patient 2	TBI	9	VS	11.00	.00	2689.00	5620.00	11
Patient 3	TBI	20	REC	57.00	2.00	146.00	354.00	25
Patient 4	TBI	8	VS	530.00	7.00	413.00	2343.00	464
Patient 5	TBI	15	MCS	30.00	10.00	653.00	505.00	7
Patient 6	TBI	16	MCS	39.00	8.00	824.00	1052.00	20
Patient 7	TBI	8	VS	180.00	11.00	575.00	1843.00	65
Patient 8	TBI	22	REC	49.00	40.00	1508.00	958.00	29
Patient 9	TBI	7	VS	215.00	4.00	961.00	2212.00	182
Patient 10	TBI	14	MCS	76.00	28.00	3727.00	1980.00	66
Patient 11	TBI	6	VS	316.00	.00	414.00	1604.00	148
Patient 12	TBI	5	VS	632.00	5.00	360.00	4948.00	545

Patient 13	TBI	14	MCS	175.00	1.00	825.00	1221.00	17
Patient 14	TBI	23	REC	23.00	22.00	866.00	244.00	8
Patient 15	TBI	13	MCS	91.00	22.00	653.00	1507.00	12
Patient 16	Anoxic	6	VS	476.00	1.00	12.00	72.00	22
Patient 17	Anoxic	14	MCS	403.00	2.00	319.00	1184.00	190
Patient 18	Anoxic	18	MCS	13.00	24.00	1586.00	643.00	7
Patient 19	Anoxic	8	VS	273.00	3.00	106.00	159.00	40
Patient 20	Anoxic	7	VS	351.00	4.00	62.00	222.00	78
Patient 21	Anoxic	9	MCS	308.00	4.00	382.00	246.00	47
Patient 22	Anoxic	10	MCS	263.00	5.00	838.00	1917.00	133
Patient 23	Anoxic	6	VS	249.00	1.00	1305.00	2483.00	202
Patient 24	Anoxic	21	REC	5.00	45.00	1279.00	221.00	3
Patient 25	Anoxic	12	MCS	271.00	.00	111.00	437.00	52
Patient 26	Anoxic	9	VS	525.00	1.00	1.00	43.00	25
Patient 27	Anoxic	12	MCS	410.00	7.00	96.00	232.00	72

B) Individual patient results - Precuneus results

Patient	Etiology	CRS-R score	Outcome	Hypo-CDP voxels (N)	Hypo-CDN voxels (N)	Hyper-CDP voxels (N)	Hyper-CDN voxels (N)
Patient 1	TBI	4	VS	357.00	6.00	1040.00	4507.00
Patient 2	TBI	9	VS	9.00	.00	2460.00	4571.00
Patient 3	TBI	20	REC	42.00	1.00	127.00	244.00
Patient 4	TBI	8	VS	353.00	3.00	321.00	1816.00
Patient 5	TBI	15	MCS	24.00	9.00	625.00	415.00
Patient 6	TBI	16	MCS	38.00	4.00	764.00	901.00
Patient 7	TBI	8	VS	128.00	9.00	532.00	1268.00
Patient 8	TBI	22	REC	42.00	33.00	1447.00	801.00
Patient 9	TBI	7	VS	123.00	4.00	849.00	1523.00
Patient 10	TBI	14	MCS	50.00	22.00	3374.00	1514.00
Patient 11	TBI	6	VS	215.00	.00	393.00	993.00
Patient 12	TBI	5	VS	409.00	5.00	306.00	3949.00
Patient 13	TBI	14	MCS	110.00	1.00	763.00	908.00
Patient 14	TBI	23	REC	15.00	22.00	806.00	206.00
Patient 15	TBI	13	MCS	68.00	21.00	561.00	1206.00
Patient 16	Anoxic	6	VS	307.00	1.00	10.00	47.00
Patient 17	Anoxic	14	MCS	275.00	2.00	307.00	896.00
Patient 18	Anoxic	18	MCS	12.00	20.00	1396.00	553.00
Patient 19	Anoxic	8	VS	165.00	3.00	105.00	86.00
Patient 20	Anoxic	7	VS	228.00	4.00	56.00	99.00
Patient 21	Anoxic	9	MCS	201.00	4.00	374.00	150.00
Patient 22	Anoxic	10	MCS	185.00	5.00	799.00	1580.00
Patient 23	Anoxic	6	VS	152.00	1.00	1296.00	1821.00
Patient 24	Anoxic	21	REC	3.00	34.00	1182.00	189.00
Patient 25	Anoxic	12	MCS	194.00	.00	102.00	332.00
Patient 26	Anoxic	9	VS	342.00	1.00	1.00	20.00
Patient 27	Anoxic	12	MCS	278.00	7.00	91.00	193.00

C) Individual patient results - PCC results

Patient	Etiology	CRS-R score	Outcome	Hypo-CDP voxels (N)	Hypo-CDN voxels (N)	Hyper-CDP voxels (N)	Hyper-CDN voxels (N)
Patient 1	TBI	4	VS	147.00	.00	110.00	1209.00

Patient 2	TBI	9	VS	2.00	.00	229.00	1049.00
Patient 3	TBI	20	REC	15.00	1.00	19.00	110.00
Patient 4	TBI	8	VS	177.00	4.00	92.00	527.00
Patient 5	TBI	15	MCS	6.00	1.00	28.00	90.00
Patient 6	TBI	16	MCS	1.00	4.00	60.00	151.00
Patient 7	TBI	8	VS	52.00	2.00	43.00	575.00
Patient 8	TBI	22	REC	7.00	7.00	61.00	157.00
Patient 9	TBI	7	VS	92.00	.00	112.00	689.00
Patient 10	TBI	14	MCS	26.00	6.00	353.00	466.00
Patient 11	TBI	6	VS	101.00	.00	21.00	611.00
Patient 12	TBI	5	VS	223.00	.00	54.00	999.00
Patient 13	TBI	14	MCS	65.00	.00	62.00	313.00
Patient 14	TBI	23	REC	8.00	.00	60.00	38.00
Patient 15	TBI	13	MCS	23.00	1.00	92.00	301.00
Patient 16	Anoxic	6	VS	169.00	.00	2.00	25.00
Patient 17	Anoxic	14	MCS	128.00	.00	12.00	288.00
Patient 18	Anoxic	18	MCS	1.00	4.00	190.00	90.00
Patient 19	Anoxic	8	VS	108.00	.00	1.00	73.00
Patient 20	Anoxic	7	VS	123.00	.00	6.00	123.00
Patient 21	Anoxic	9	MCS	107.00	.00	8.00	96.00
Patient 22	Anoxic	10	MCS	78.00	.00	39.00	337.00
Patient 23	Anoxic	6	VS	97.00	.00	9.00	662.00
Patient 24	Anoxic	21	REC	2.00	11.00	97.00	32.00
Patient 25	Anoxic	12	MCS	77.00	.00	9.00	105.00
Patient 26	Anoxic	9	VS	183.00	.00	.00	23.00
Patient 27	Anoxic	12	MCS	132.00	.00	5.00	39.00

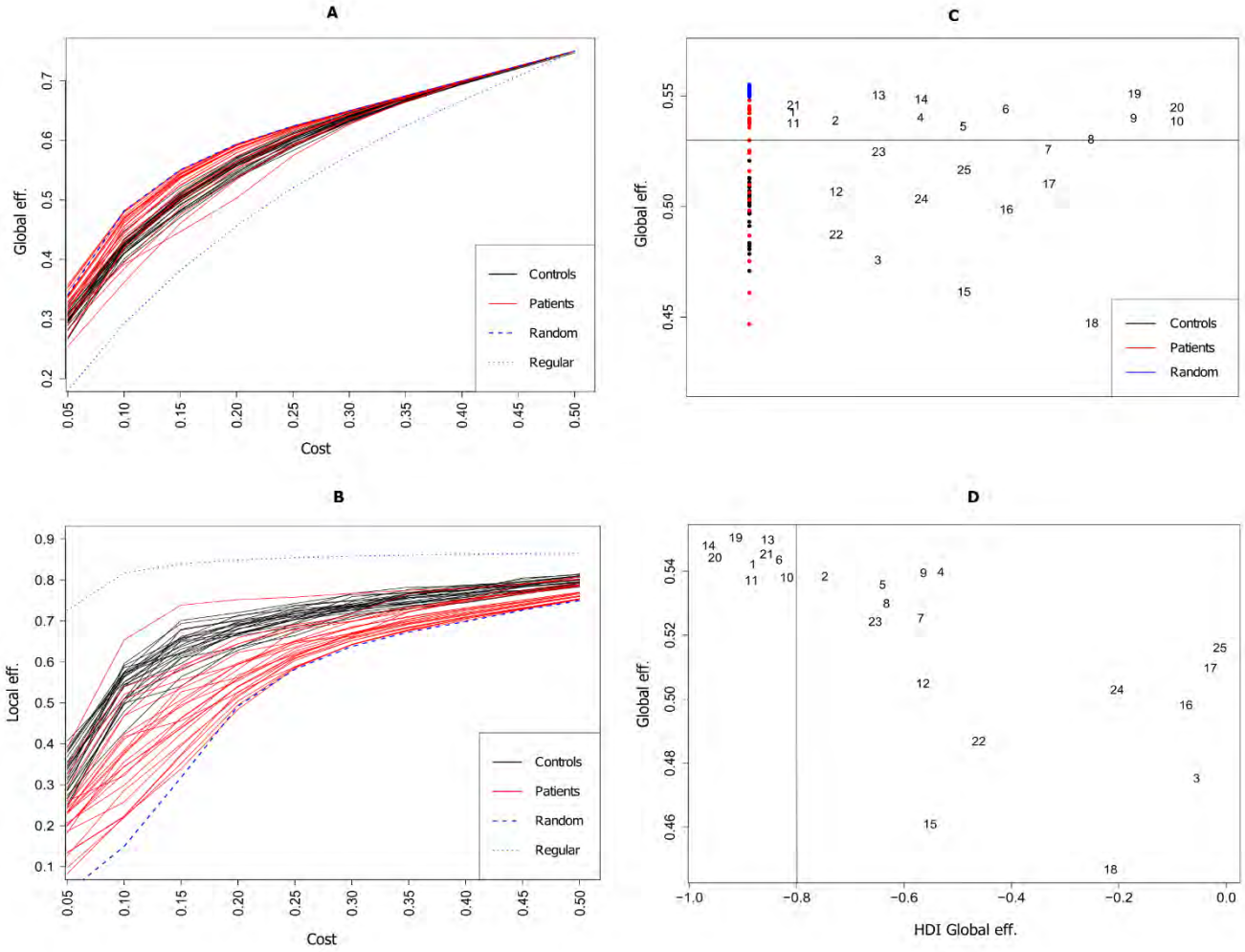

Figure 6.3.6. Global topology in controls and patients – evidence of randomization.
A) Global efficiency (GE) in controls and patients in comparison to regular and random networks, at multiple connection density thresholds (5-50%, increment 5%). B) Clustering in controls and patients in comparison to regular and random networks, at multiple connection density thresholds (5-50%, increment 5%). C) GE in controls and patients in comparison to random networks at the 15% connection density threshold. A sub-group of patients seems to have a GE more similar to random networks than to other subjects. D) Hub disruption index (HDI) calculated using GE (axis x) differentiates three sub-groups of patients (15% cost). Patients with a HDI GE smaller than -0.8 have also show a high GE (axis y) present in random networks.

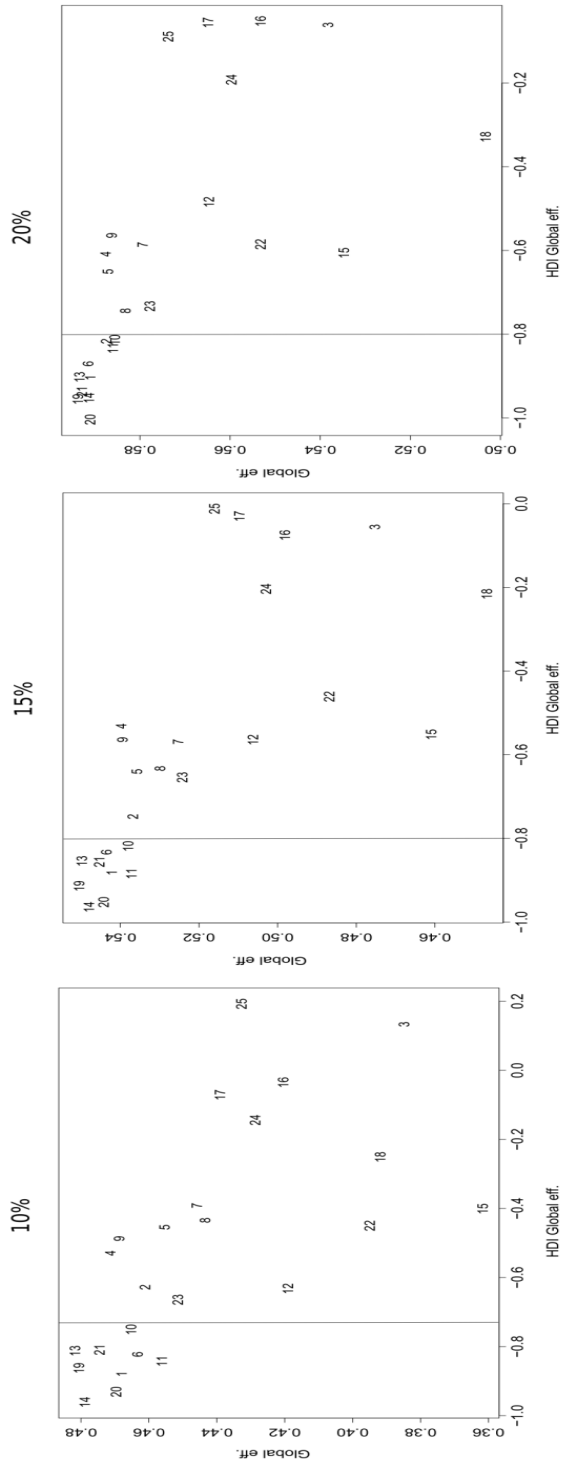

Figure 6.3.7. Global efficiency (axis y) and HDI GE (axis x) at multiple thresholds (10-20%).
Hub disruption index (HDI) calculated using GE (axis x) differentiates three sub-groups of patients at all thresholds. The sub-group of patients most similar to random networks has a HDI GE lower than ~-0.8, at all three connection density thresholds.

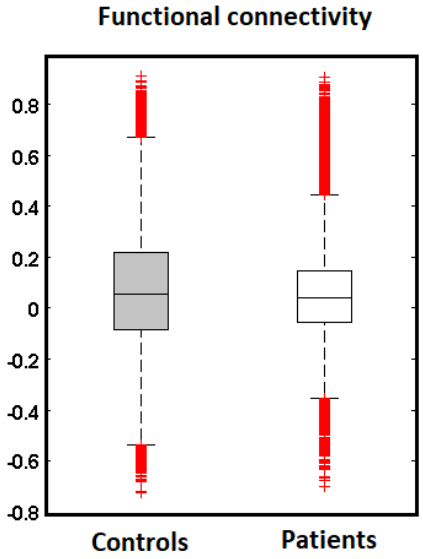

Figure 6.3.8. Functional connectivity (Pearson's r) over all pairs of nodes, in controls and patients. *Boxplots represent medians with interquartile range and whiskers signify minimum and maximum values (excluding outliers).*

Table 6.3.2. MNI center-mass coordinates of each of the nodes used in the analysis. *The AAL atlas was used to define the anatomical names of nodes.*

MNI Coordinates			RSN_region	AAL_atlas_region
-18	40	38	dDMN_1	Frontal_Sup_L
0	54	18	dDMN_2	Frontal_Sup_Medial_L_R
-4	46	16	dDMN_3	Cingulum_Ant_L
-6	52	32	dDMN_4	Frontal_Sup_Medial_L
-2	42	4	dDMN_5	Cingulum_Ant_L_2
-6	60	2	dDMN_6	Frontal_Sup_Medial_L_2
2	46	-2	dDMN_7	Frontal_Med_Orb_R
0	36	16	dDMN_8	Cingulum_Ant_L_R
-14	58	18	dDMN_9	Frontal_Sup_L_2
-4	40	12	dDMN_10	Cingulum_Ant_L_3
-2	54	-10	dDMN_11	Frontal_Med_Orb_L
-48	-70	32	dDMN_12	Angular_L
18	36	46	dDMN_13	Frontal_Sup_R
-2	-58	22	dDMN_14	PreCuneus_L_R
2	-60	32	dDMN_15	PreCu_L_R_2
-2	-46	30	dDMN_16	Cingulum_Post_L_R
0	-18	34	dDMN_17	Cingulum_Mid_L_R
50	-64	30	dDMN_18	Angular_R
-2	-10	2	dDMN_19	Thalamus_L_R
-24	-30	-14	dDMN_20	ParaHippocampal_L

26	-24	-18	dDMN_21	ParaHippocampal_R
-14	-60	14	vDMN_1	Calcarine_L
-26	8	52	vDMN_2	Frontal_Mid_L
-30	-40	-16	vDMN_3	Fusiform_L
-38	-82	30	vDMN_4	Occipital_Mid_L
12	-54	10	vDMN_5	Precuneus_R/Lingual_R
0	-50	52	vDMN_6	PreCuneus_L_R
8	-62	56	vDMN_7	PreCuneus_R
-10	-68	54	vDMN_8	PreCuneus_L
2	-58	44	vDMN_9	PreCuneus_R_2
24	30	36	vDMN_10	Frontal_Mid_R
22	14	48	vDMN_11	Frontal_Mid_R_2
28	-36	-20	vDMN_12	Fusiform_R
42	-74	28	vDMN_13	Occipital_Mid_R
38	18	48	RECN_1	Frontal_Mid_R
44	28	28	RECN_2	Frontal_Inf_Tri_R
26	26	48	RECN_3	Frontal_Sup_R
34	30	40	RECN_4	Frontal_Mid_R_2
36	52	0	RECN_5	Frontal_Mid_Orb_R
48	-60	40	RECN_6	Angular_R
38	-62	52	RECN_7	Angular_R_2
48	-46	46	RECN_8	Parietal_Inf_R
4	36	44	RECN_9	Frontal_Sup_Medial_R
-42	-68	-42	RECN_10	Cerebelum_Crus2_L
-32	-74	-48	RECN_11	Cerebelum_Crus2_L_2
-30	-70	-34	RECN_12	Cerebelum_Crus1_L
-14	-86	-32	RECN_13	Cerebelum_Crus2_L_3
-8	32	40	LECN_1	Frontal_Sup_Medial_L
-42	18	42	LECN_2	Frontal_Mid_L
-24	20	54	LECN_3	Frontal_Sup_L
-32	28	44	LECN_4	Frontal_Mid_L_2
-42	44	-4	LECN_5	Frontal_Inf_Orb_L
-44	-66	40	LECN_6	Angular_L
-48	-52	48	LECN_7	Parietal_Inf_L
-34	-70	48	LECN_8	Parietal Inf_L_2
-60	-44	-14	LECN_9	Temporal_Inf_L
34	-70	-44	LECN_10	Cerebelum_Crus2_R
-32	44	20	SAL_1	Frontal_Mid_L
-42	12	-4	SAL_2	Insula_L
-8	10	62	SAL_3	Supp_Motor_Area_L
-2	26	30	SAL_4	Cingulum_Ant_L
-2	2	62	SAL_5	Supp_Motor_Area_L_2
-2	20	46	SAL_6	Supp_Motor_Area_L_3
-2	12	44	SAL_7	Cingulum_Mid_L
12	8	62	SAL_8	Supp_Motor_Area_R
26	44	26	SAL_9	Frontal_Mid_R
40	14	-2	SAL_10	Insula_R

-36	-56	-34	SAL_11	Cerebelum_Crus1_L
34	-60	-32	SAL_12	Cerebelum_Crus1_R
-40	34	28	P.SAL_1	Frontal_Inf_Tri_L/Frontal_Mid_L
-60	-34	36	P.SAL_2	SupraMarginal_L
-58	-44	36	P.SAL_3	SupraMarginal_L_2
-8	-54	60	P.SAL_4	Precuneus_L
12	-30	44	P.SAL_5	Cingulum_Mid_R
26	-44	70	P.SAL_6	Postcentral_R
14	-54	66	P.SAL_7	Parietal_Sup_R
58	-30	34	P.SAL_8	SupraMarginal_R
58	-40	36	P.SAL_9	SupraMarginal_R_2
-14	-24	4	P.SAL_10	Thalamus_L_post
-34	-44	-38	P.SAL_11	Cerebelum_Crus1_L
-38	-16	-6	P.SAL_12	Insula_L_post
38	-8	-10	P.SAL_13	Insula_R_post

Table 6.3.3. Exclusion criteria.
Nine patients were excluded due to HDI global efficiency < -0.8 or/and low functional connectivity. The functional connection density was calculated by setting a threshold of the correlation coefficients (Pearson's r) > 0.2 and calculating the density of remaining connections within each of the individual matrices. All patients with a connection density <10% were excluded from further analysis.

Patients	Functional_connection_density	HDI_Global_efficiency	Randomness
Subject_001	0.08	-0.88	random
Subject_002	0.10	-0.75	non-random
Subject_003	0.35	-0.05	non-random
Subject_004	0.11	-0.53	non-random
Subject_005	0.12	-0.64	non-random
Subject_006	0.09	-0.83	random
Subject_007	.17	-0.57	non-random
Subject_008	0.14	-0.63	non-random
Subject_009	0.11	-0.56	non-random
Subject_010	0.13	-0.82	random
Subject_011	0.24	-0.88	random
Subject_012	0.28	-0.56	non-random
Subject_013	0.05	-0.85	random
Subject_014	0.06	-0.96	random
Subject_015	0.44	-0.55	non-random
Subject_016	0.34	-0.07	non-random
Subject_017	0.23	-0.03	non-random
Subject_018	0.30	-0.22	non-random
Subject_019	0.06	-0.91	random
Subject_020	0.08	-0.95	random
Subject_021	0.04	-0.86	random
Subject_022	0.17	-0.46	non-random
Subject_023	0.13	-0.65	non-random
Subject_024	0.25	-0.20	non-random
Subject_025	0.18	-0.01	non-random

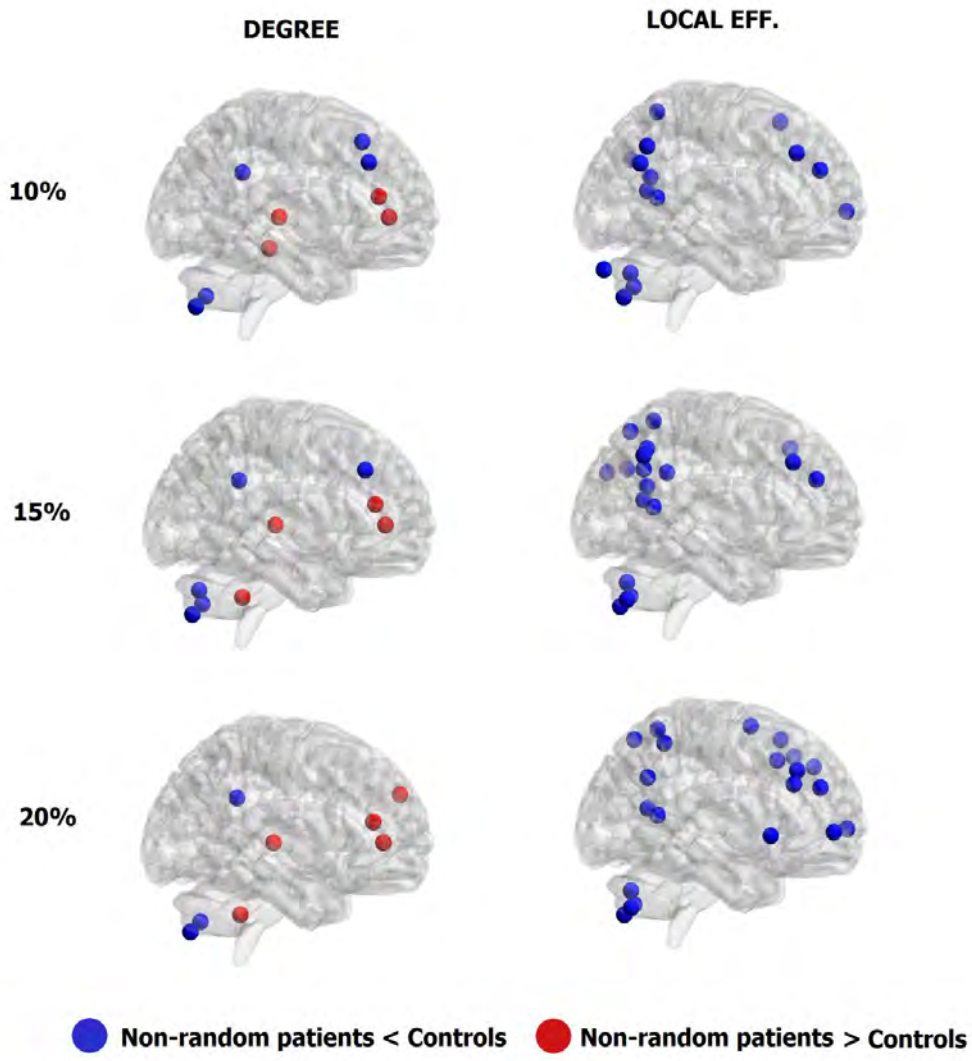

Figure 6.3.9. Nodal topology in non-random patients at different connection density thresholds.
The figures show nodal metric results found to be significantly different between patients and controls – degree and local efficiency. P>C – Values found to be significantly higher in patients in comparison to controls; P<C – values found to be significantly lower in patients versus controls.

7 References

Achard, S., Delon-Martin, C., Vértes, P. E., Renard, F., Schenck, M., Schneider, F., … Bullmore, E. T. (2012). Hubs of brain functional networks are radically reorganized in comatose patients. *Proceedings of the National Academy of Sciences of the United States of America*, *109*(50), 20608–13. http://doi.org/10.1073/pnas.1208933109

Achard, S., Salvador, R., Whitcher, B., Sucklig, J., & Bullmore, E. (2006). A Resilient, Low-Frequency, Small-World Human Brain Functional Network with Highly Connected Association Cortical Hubs. *Journal of Neuroscience*, *26*(1), 63–72. http://doi.org/10.1523/JNEUROSCI.3874-05.2006

Adams, J. H., Graham, D. I., & Jennett, B. (2000). The neuropathology of the vegetative state after an acute brain insult. *Brain*, *123*, 1327–1338. http://doi.org/10.1093/brain/123.7.1327

Alexander, A. L., Lee, J. E., Lazar, M., & Field, A. S. (2007). Diffusion tensor imaging of the brain. *Neurotherapeutics : The Journal of the American Society for Experimental NeuroTherapeutics*, *4*(3), 316–29. http://doi.org/10.1016/j.nurt.2007.05.011

Alexander-Bloch, A. F., Gogtay, N., Meunier, D., Birn, R., Clasen, L., Lalonde, F., … Bullmore, E. T. (2010). Disrupted Modularity and Local Connectivity of Brain Functional Networks in Childhood-Onset Schizophrenia. *Frontiers in Systems Neuroscience*, *4*. http://doi.org/10.3389/fnsys.2010.00147

Alstott, J., Breakspear, M., Hagmann, P., Cammoun, L., & Sporns, O. (2009). Modeling the impact of lesions in the human brain. *PLoS Computational Biology*, *5*(6). http://doi.org/10.1371/journal.pcbi.1000408

Amico, E., Marinazzo, D., Di Perri, C., Heine, L., Annen, J., Martial, C., … Goñi, J. (2017). Mapping the functional connectome traits of levels of consciousness. *NeuroImage*, *148*(November 2016), 201–211. http://doi.org/10.1016/j.neuroimage.2017.01.020

Andersson, J. L. R., Jenkinson, M., & Smith, S. (2007). *Non-linear registration, aka spatial normalisation. FMRIB Technial Report TR07JA2. Oxford Centre for Functional Magnetic Resonance Imaging of the Brain, Department of Clinical Neurology, Oxford University, Oxford, UK*.

Andrews-Hanna, J. R., Reidler, J. S., Sepulcre, J., Poulin, R., & Buckner, R. L. (2010). Functional-Anatomic Fractionation of the Brain's Default Network. *Neuron*, *65*(4), 550–562. http://doi.org/10.1016/j.neuron.2010.02.005

Andrews-Hanna, J., Smallwood, J., & Spreng, R. (2014). The default network and self-generated thought: component processes, dynamic control, and clinical relevance. *Ann N Y Acad Sci, 1316*(1), 29–52. http://doi.org/10.1111/nyas.12360.The

Annen, J., Heine, L., Ziegler, E., Frasso, G., Bahri, M., Di Perri, C., … Laureys, S. (2016). Function–structure connectivity in patients with severe brain injury as measured by MRI-

DWI and FDG-PET. *Human Brain Mapping*, *37*(11), 3707–3720. http://doi.org/10.1002/hbm.23269

Aston-Jones, G., Chen, S., Zhu, Y., & Oshinsky, M. L. (2001). A neural circuit for circadian regulation of arousal. *Nature Neuroscience*, *4*(7), 732–738. http://doi.org/10.1038/89522

Baars, B. J. (1988). A cognitive theory of consciousness. Cambridge University Press, Cambridge, MA.

Balestrini, S., Francione, S., Mai, R., Castana, L., Casaceli, G., Marino, D., … Tassi, L. (2015). Multimodal responses induced by cortical stimulation of the parietal lobe: A stereo-electroencephalography study. *Brain*, *138*(9), 2596–2607. http://doi.org/10.1093/brain/awv187

Barttfeld, P., Uhrig, L., Sitt, J. D., Sigman, M., Jarraya, B., & Dehaene, S. (2015). Signature of consciousness in the dynamics of resting-state brain activity. *Proceedings of the National Academy of Sciences*, *112*(3), 887–892. http://doi.org/10.1073/pnas.1418031112

Bassett, D. S., & Bullmore, E. T. (2009). Human brain networks in health and disease. *Current Opinion in Neurology*, *22*(4), 340–347. http://doi.org/10.1097/WCO.0b013e32832d93dd

Bassett, D. S., Nelson, B. G., Mueller, B. A., Camchong, J., & Lim, K. O. (2012). Altered resting state complexity in schizophrenia. *NeuroImage*, *59*(3), 2196–2207. http://doi.org/10.1016/j.neuroimage.2011.10.002

Beckmann, C. F., DeLuca, M., Devlin, J. T., & Smith, S. M. (2005). Investigations into resting-state connectivity using independent component analysis. *Philosophical Transactions of the Royal Society of London - Series B: Biological Sciences*, *360*(1457), 1001–1013. http://doi.org/10.1098/rstb.2005.1634

Behzadi, Y., Restom, K., Liau, J., & Liu, T. T. (2007). A component based noise correction method (CompCor) for BOLD and perfusion based fMRI. *NeuroImage*, *37*(1), 90–101. http://doi.org/10.1016/j.neuroimage.2007.04.042

Beudel, M., Tjepkema-Cloostermans, M. C., Boersma, J. H., & van Putten, M. J. A. M. (2014). Small-world characteristics of EEG patterns in post-anoxic encephalopathy. *Frontiers in Neurology*, *5 JUN*(June), 1–9. http://doi.org/10.3389/fneur.2014.00097

Bharath, R. D., Munivenkatappa, A., Gohel, S., Panda, R., Saini, J., Rajeswaran, J., … Biswal, B. B. (2015). Recovery of resting brain connectivity ensuing mild traumatic brain injury. *Frontiers in Human Neuroscience*, *9*(September), 513. http://doi.org/10.3389/fnhum.2015.00513

Biswal, B., Yetkin, F. Z., Haughton, V. M., Hyde, J. S. (1995). Functional connectivity in the motor cortex of resting human brain using. *Magn Reson Med*, *34*(9), 537–541. http://doi.org/10.1002/mrm.1910340409

Bodart, O., Amico, E., Gomez, F., Casali, A. G., Wannez, S., Heine, L., … Gosseries, O. (2017). Global structural integrity and effective connectivity in patients with disorders of consciousness. *Brain Stimulation, 10*(2), 6–13. http://doi.org/10.1016/j.brs.2017.11.006

Bodien, Y. G., & Giacino, J. T. (2016). Challenges and Pitfalls Associated with Diagnostic and Prognostic Applications of Functional Neuroimaging in Disorders of Consciousness. *The Open Neuroimaging Journal*, *10*(Suppl-1, M2), 23–31. http://doi.org/10.2174/1874440001610010023

Bonnelle, V., Ham, T. E., Leech, R., Kinnunen, K. M., Mehta, M. A., Greenwood, R. J., & Sharp, D. J. (2012). Salience network integrity predicts default mode network function after traumatic brain injury. *Proceedings of the National Academy of Sciences of the United States of America*, *109*(12), 4690–5. http://doi.org/10.1073/pnas.1113455109

Bonnelle, V., Leech, R., Kinnunen, K. M., Ham, T. E., Beckmann, C. F., De Boissezon, X., … Sharp, D. J. (2011). Default Mode Network Connectivity Predicts Sustained Attention Deficits after Traumatic Brain Injury. *Journal of Neuroscience*, *31*(38), 13442–13451. http://doi.org/10.1523/JNEUROSCI.1163-11.2011

Bruno, M. A., Fernández-Espejo, D., Lehembre, R., Tshibanda, L., Vanhaudenhuyse, A., Gosseries, O., … Soddu, A. (2011c). Multimodal neuroimaging in patients with disorders of consciousness showing "functional hemispherectomy." *Progress in Brain Research*, *193*, 323–333. http://doi.org/10.1016/B978-0-444-53839-0.00021-1

Bruno, M. A., Ledoux, D., Lambermont, B., Damas, F., Schnakers, C., Vanhaudenhuyse, A., … Laureys, S. (2011b). Comparison of the full outline of unresponsiveness and Glasgow Liege Scale/Glasgow Coma Scale in an intensive care unit population. *Neurocritical Care*, *15*(3), 447–453. http://doi.org/10.1007/s12028-011-9547-2

Bruno, M. A., Vanhaudenhuyse, A., Thibaut, A., Moonen, G., & Laureys, S. (2011a). From unresponsive wakefulness to minimally conscious PLUS and functional locked-in syndromes: Recent advances in our understanding of disorders of consciousness. *Journal of Neurology*, *258*(7), 1373–1384. http://doi.org/10.1007/s00415-011-6114-x

Buckner, R. L. (2013). The cerebellum and cognitive function: 25 years of insight from anatomy and neuroimaging. *Neuron*. http://doi.org/10.1016/j.neuron.2013.10.044

Buckner, R. L., Andrews-Hanna, J. R., & Schacter, D. L. (2008). The brain's default network: Anatomy, function, and relevance to disease. *Annals of the New York Academy of Sciences*, *1124*, 1–38. http://doi.org/10.1196/annals.1440.011

Bullmore, E. T., & Bassett, D. S. (2011). Brain Graphs: Graphical Models of the Human Brain Connectome. *Annual Review of Clinical Psychology*, *7*(1), 113–140. http://doi.org/10.1146/annurev-clinpsy-040510-143934

Bullmore, E., & Sporns, O. (2009). Complex brain networks: graph theoretical analysis of structural and functional systems. *Nature Publishing Group*, *10*(3), 186–198. http://doi.org/10.1038/nrn2575

Bullmore, E., & Sporns, O. (2012). The economy of brain network organization. *Nature Reviews Neuroscience*, *13*(MAY), 336–349. http://doi.org/10.1038/nrn3214

Bzdok, D., Heeger, A., Langner, R., Laird, A. R., Fox, P. T., Palomero-Gallagher, N., … Eickhoff, S. B. (2015). Subspecialization in the human posterior medial cortex. *NeuroImage*, *106*, 55–71. http://doi.org/10.1016/j.neuroimage.2014.11.009

Calhoun, V. D., Lawrie, S. M., Mourao-Miranda, J., & Stephan, K. E. (2017). Prediction of Individual Differences from Neuroimaging Data. *NeuroImage*, *145*, 135–136. http://doi.org/10.1016/j.neuroimage.2016.12.012

Casali, A. G., Gosseries, O., Rosanova, M., Boly, M., Sarasso, S., Casali, K. R., … Massimini, M. (2013). A Theoretically Based Index of Consciousness Independent of Sensory Processing and Behavior. *Science Translational Medicine*, *5*(198), 198ra105-198ra105. http://doi.org/10.1126/scitranslmed.3006294

Casarotto, S., Comanducci, A., Rosanova, M., Sarasso, S., Fecchio, M., Napolitani, M., … Massimini, M. (2016). Stratification of unresponsive patients by an independently validated index of brain complexity. *Annals of Neurology*, *80*(5), 718–729. http://doi.org/10.1002/ana.24779

Castellanos, N. P., Leyva, I., Buldú, J. M., Bajo, R., Paúl, N., Cuesta, P., … del-Pozo, F. (2011). Principles of recovery from traumatic brain injury: Reorganization of functional networks. *NeuroImage*, *55*(3), 1189–1199. http://doi.org/10.1016/j.neuroimage.2010.12.046

Cauda, F., Geminiani, G., D'Agata, F., Sacco, K., Duca, S., Bagshaw, A. P., & Cavanna, A. E. (2010). Functional connectivity of the posteromedial cortex. *PLoS ONE*, *5*(9), 1–11. http://doi.org/10.1371/journal.pone.0013107

Cauda, F., Micon, B. M., Sacco, K., Duca, S., D'Agata, F., Geminiani, G., & Canavero, S. (2009). Disrupted intrinsic functional connectivity in the vegetative state. *Journal of Neurology, Neurosurgery, and Psychiatry*, *80*(4), 429–431. http://doi.org/10.1136/jnnp.2007.142349

Cavaliere, C., Aiello, M., Di Perri, C., Amico, E., Martial, C., Thibaut, A., … Soddu, A. (2016). Functional Connectivity Substrates for tDCS Response in Minimally Conscious State Patients. *Frontiers in Cellular Neuroscience*, *10*. http://doi.org/10.3389/fncel.2016.00257

Cavaliere, C., Aiello, M., Di Perri, C., Fernandez-Espejo, D., Owen, A. M., & Soddu, A. (2015). Diffusion tensor imaging and white matter abnormalities in patients with disorders of consciousness. *Frontiers in Human Neuroscience*, *8*(January), 6–12. http://doi.org/10.3389/fnhum.2014.01028

Cavanna, A. E., & Nani, A. (2014). *Consciousness: Theories in neuroscience and philosophy of mind*. Springer-Verlag Berlin Heidelberg. http://doi.org/10.1007/978-3-662-44088-9

Cavanna, A. E., & Trimble, M. R. (2006). The precuneus: A review of its functional anatomy and behavioural correlates. *Brain*, *129*(3), 564–583. http://doi.org/10.1093/brain/awl004

Cha, J., Jo, H. J., Gibson, W. S., & Lee, J.-M. (2017). Functional organization of the human posterior cingulate cortex, revealed by multiple connectivity-based parcellation methods. *Human Brain Mapping*, *38*(6), 2808–2818. http://doi.org/10.1002/hbm.23570

Chai, X. J., Castañán, A. N., Öngür, D., & Whitfield-Gabrieli, S. (2012). Anticorrelations in resting state networks without global signal regression. *NeuroImage*, *59*(2), 1420–1428. http://doi.org/10.1016/j.neuroimage.2011.08.048

Chai, X. J., Ofen, N., Gabrieli, J. D. E., & Whitfield-Gabrieli, S. (2014). Selective Development of Anticorrelated Networks in the Intrinsic Functional Organization of the Human Brain. *Journal of Cognitive Neuroscience*, *26*(3), 501–513. http://doi.org/10.1162/jocn_a_00517

Chang, C., & Glover, G. H. (2009). Effects of model-based physiological noise correction on default mode network anti-correlations and correlations. *NeuroImage*, *47*(4), 1448–1459. http://doi.org/10.1016/j.neuroimage.2009.05.012

Chang, C., & Glover, G. H. (2010). Time-frequency dynamics of resting-state brain connectivity measured with fMRI. *NeuroImage*, *50*(1), 81–98. http://doi.org/10.1016/j.neuroimage.2009.12.011

Chaudhary, U., Xia, B., Silvoni, S., Cohen, L. G., & Birbaumer, N. (2017). Brain–Computer Interface–Based Communication in the Completely Locked-In State. *PLoS Biology*, *15*(1), 1–25. http://doi.org/10.1371/journal.pbio.1002593

Chen, J. E., Glover, G. H., Greicius, M. D., & Chang, C. (2017). Dissociated patterns of anti-correlations with dorsal and ventral default-mode networks at rest. *Human Brain Mapping*, *38*(5), 2454–2465. http://doi.org/10.1002/hbm.23532

Chennu, S., Annen, J., Wannez, S., Thibaut, A., Chatelle, C., Cassol, H., … Laureys, S. (2017). Brain networks predict metabolism, diagnosis and prognosis at the bedside in disorders of consciousness. *Brain*, *140*(8), 2120–2132. http://doi.org/10.1093/brain/awx163

Chennu, S., Finoia, P., Kamau, E., Allanson, J., Williams, G. B., Monti, M. M., … Bekinschtein, T. A. (2014). Spectral Signatures of Reorganised Brain Networks in Disorders of Consciousness. *PLoS Computational Biology*, *10*(10). http://doi.org/10.1371/journal.pcbi.1003887

Cherubini, A., Péran, P., Caltagirone, C., Sabatini, U., & Spalletta, G. (2009). Aging of subcortical nuclei: Microstructural, mineralization and atrophy modifications measured in vivo using MRI. *NeuroImage*, *48*(1), 29–36. http://doi.org/10.1016/j.neuroimage.2009.06.035

Choi, S. P., Park, K. N., Park, H. K., Kim, J. Y., Youn, C. S., Ahn, K. J., & Yim, H. W. (2010). Diffusion-weighted magnetic resonance imaging for predicting the clinical outcome of comatose survivors after cardiac arrest: a cohort study. *Critical Care (London, England)*, *14*(1), R17. http://doi.org/10.1186/cc8874

Cole, D. M., Smith, S. M., & Beckmann, C. F. (2010). Advances and pitfalls in the analysis and interpretation of resting-state FMRI data. *Frontiers in Systems Neuroscience*, *4*(April), 1–15. http://doi.org/10.3389/fnsys.2010.00008

Coleman, N. L., Brieva, J. L., & Crowfoot, E. (2008). Prediction of death after withdrawal of life-sustaining treatments. *Critical Care and Resuscitation : Journal of the Australasian Academy of Critical Care Medicine*, *10*(4), 278–284.

Collin, G., Sporns, O., Mandl, R. C. W., & Van Den Heuvel, M. P. (2014). Structural and functional aspects relating to cost and benefit of rich club organization in the human cerebral cortex. *Cerebral Cortex*, *24*(9), 2258–2267. http://doi.org/10.1093/cercor/bht064

Cortese, M., Riganello, F., Arcuri, F., Pugliese, M., Lucca, L., Dolce, G., & Sannita, W. (2015). Coma recovery scale-r: variability in the disorder of consciousness. *BMC Neurology*, *15*(1), 186. http://doi.org/10.1186/s12883-015-0455-5

Crick, F., & A, C. K. (2003). Framework for Consciousness. *Nat Neurosci*, *6*(2), 119–126. http://doi.org/10.1038/nn0203-119

Crone, J. S., Ladurner, G., Höller, Y., Golaszewski, S., Trinka, E., & Kronbichler, M. (2011). Deactivation of the default mode network as a marker of impaired consciousness: An fmri study. *PLoS ONE*, *6*(10). http://doi.org/10.1371/journal.pone.0026373

Crone, J. S., Soddu, A., Höller, Y., Vanhaudenhuyse, A., Schurz, M., Bergmann, J. J. J., … Kronbichler, M. (2014). Altered network properties of the fronto-parietal network and the thalamus in impaired consciousness. *NeuroImage: Clinical*, *4*, 240–248. http://doi.org/10.1016/j.nicl.2013.12.005

Crossley, N. A., Mechelli, A., Scott, J., Carletti, F., Fox, P. T., Mcguire, P., & Bullmore, E. T. (2014). The hubs of the human connectome are generally implicated in the anatomy of brain disorders. *Brain*, *137*(8), 2382–2395. http://doi.org/10.1093/brain/awu132

Cullen, N.K., Weisz, K. (2010). Cognitive correlates with functional outcome after anoxic brain injury: A case-controlled comparison with traumatic brain injury. *Archives of Physical Medicine and Rehabilitation*, *91*(10), e6. http://doi.org/10.3109/02699052.2010.531691

Cullen, N. K., Crescini, C., & Bayley, M. T. (2009). Rehabilitation Outcomes After Anoxic Brain Injury: A Case-Controlled Comparison With Traumatic Brain Injury. *PM and R*, *1*(12), 1069–1076. http://doi.org/10.1016/j.pmrj.2009.09.013

Cullen, N. K., Park, Y.-G., & Bayley, M. T. (2008). Functional recovery following traumatic vs non-traumatic brain injury: a case-controlled study. *Brain Injury*, *22*(13–14), 1013–20. http://doi.org/10.1080/02699050802530581

Gosseries, O., Vanhaudenhuyse, A., Bruno, M., Demertzi, A., Schnakers, C., Boly, M., … Laureys, S. (2011). Disorders of Consciousness: Coma, Vegetative and Minimally Conscious States. In Cvetkovic, D., & Cosic, I. *States of consciousness : experimental*

insights into meditation, waking, sleep, and dreams. *Frontiers collection,* http://doi.org/10.1007/978-3-642-18047-7

Damoiseaux, J. S., Rombouts, S. A. R. B., Barkhof, F., Scheltens, P., Stam, C. J., Smith, S. M., & Beckmann, C. F. (2006). Consistent resting-state networks across healthy subjects. *Proceedings of the National Academy of Sciences*, *103*(37), 13848–13853. http://doi.org/10.1073/pnas.0601417103

Dehaene, S., & Changeux, J. P. (2011). Experimental and Theoretical Approaches to Conscious Processing. *Neuron*, *70*(2), 200–227. http://doi.org/10.1016/j.neuron.2011.03.018

Dehaene, S., & Naccache, L. (2001). Towards a cognitive neuroscience of consciousness: Basic evidence and a workspace framework. *Cognition*. http://doi.org/10.1016/S0010-0277(00)00123-2

Dehaene, S., Changeux, J. P., & Naccache, L. (2011). The global neuronal workspace model of conscious access: From neuronal architectures to clinical applications. *Research and Perspectives in Neurosciences*, *18*, 55–84. http://doi.org/10.1007/978-3-642-18015-6_4

Demertzi, A., Antonopoulos, G., Heine, L., Voss, H. U., Crone, J. S., De Los Angeles, C., … Laureys, S. (2015). Intrinsic functional connectivity differentiates minimally conscious from unresponsive patients. *Brain*, *138*(9), 2619–2631. http://doi.org/10.1093/brain/awv169

Demertzi, A., Gomez, F., Crone, J. S., Vanhaudenhuyse, A., Tshibanda, L., Noirhomme, Q., … Soddu, A. (2014). Multiple fMRI system-level baseline connectivity is disrupted in patients with consciousness alterations. *Cortex*, *52*(1), 35–46. http://doi.org/10.1016/j.cortex.2013.11.005

Demertzi, A., Sitt, J. D., Sarasso, S., & Pinxten, W. (2017). Measuring states of pathological (un)consciousness: research dimensions, clinical applications, and ethics. *Neuroscience of Consciousness*, *3*(1). http://doi.org/10.1093/nc/nix010

Demertzi, A., Soddu, A., & Laureys, S. (2013). Consciousness supporting networks. *Current Opinion in Neurobiology*, *23,* 239–244. http://doi.org/10.1016/j.conb.2012.12.003

Di Perri, C., Bahri, M. A., Amico, E., Thibaut, A., Heine, L., Antonopoulos, G., … Laureys, S. (2016). Neural correlates of consciousness in patients who have emerged from a minimally conscious state: A cross-sectional multimodal imaging study. *The Lancet Neurology*, *15*(8), 830–842. http://doi.org/10.1016/S1474-4422(16)00111-3

Di Perri, C., Heine, L., Amico, E., Soddu, A., Laureys, S., & Demertzi, A. (2014). Technology-based assessment in patients with disorders of consciousness. *Annali dell'Istituto Superiore Di Sanita*, *50*(3), 209–220. http://doi.org/10.4415/ANN_14_03_03

Dinkel, J., Drier, A., Khalilzadeh, O., Perlbarg, V., Czernecki, V., Gupta, R., … Stevens, R. D. (2014). Long-Term White Matter Changes after Severe Traumatic Brain Injury: A 5-

Year Prospective Cohort. *AJNR: American Journal of Neuroradiology*, *35*(1), 23–29. http://doi.org/10.3174/ajnr.A3616

Douaud, G., Smith, S., Jenkinson, M., Behrens, T., Johansen-Berg, H., Vickers, J., … James, A. (2007). Anatomically related grey and white matter abnormalities in adolescent-onset schizophrenia. *Brain*, *130*(9), 2375–2386. http://doi.org/10.1093/brain/awm184

Dubois, J., & Adolphs, R. (2016). Building a Science of Individual Differences from fMRI. *Trends in Cognitive Sciences*, *20*(6), 425–443. http://doi.org/10.1016/j.tics.2016.03.014

Estraneo, A., Moretta, P., Loreto, V., Lanzillo, B., Santoro, L., & Trojano, L. (2010). Late recovery after traumatic, anoxic, or hemorrhagic long-lasting vegetative state. *Neurology*, *75*(3), 239–245. http://doi.org/10.1212/WNL.0b013e3181e8e8cc

Fallani, F. D. V., Richiardi, J., Chavez, M., & Achard, S. (2014). Graph analysis of functional brain networks: practical issues in translational neuroscience. *Phil Trans Royal Society B: Biological Sciences*, *369*(1653). http://doi.org/10.1098/rstb.2013.0521

Faugeras, F., Rohaut, B., Valente, M., Sitt, J., Demeret, S., & Bolgert, F. (2017). Survival and consciousness recovery are better in the minimally conscious state than in the vegetative state. *Brain Injury*, *0*(0), 1–6. http://doi.org/10.1080/02699052.2017.1364421

Feldman, H., Yeatman, J., Lee, E., Barde, L., & Gaman-Bean, S. (2010). Diffusion Tensor Imaging: A review for Pediatric Researchers and Clinicians. *J Dev Behav Pediatr*, *31*(4), 346–356. http://doi.org/10.1097/DBP.0b013e3181dcaa8b.Diffusion

Fernández-Espejo, D., Soddu, A., Cruse, D., Palacios, E. M., Junque, C., Vanhaudenhuyse, A., … Owen, A. M. (2012). A role for the default mode network in the bases of disorders of consciousness. *Annals of Neurology*, *72*(3), 335–343. http://doi.org/10.1002/ana.23635

Figley, T. D., Bhullar, N., Courtney, S. M., & Figley, C. R. (2015). Probabilistic atlases of default mode, executive control and salience network white matter tracts: an fMRI-guided diffusion tensor imaging and tractography study. *Frontiers in Human Neuroscience*, *9*(November), 1–20. http://doi.org/10.3389/fnhum.2015.00585

Fornito, A., Zalesky, A., & Breakspear, M. (2013). Graph analysis of the human connectome: Promise, progress, and pitfalls. *NeuroImage*, *80*, 426–444. http://doi.org/10.1016/j.neuroimage.2013.04.087

Fornito, A., Zalesky, A., & Breakspear, M. (2015). The connectomics of brain disorders. *Nature Reviews Neuroscience*, *16*(3), 159–172. http://doi.org/10.1038/nrn3901

Fornito, A., Zalesky, A., & Bullmore, E. (2016). Fundamentals of brain network analysis. *Fundamentals of Brain Network Analysis.* Retrieved from http://ovidsp.ovid.com/ovidweb.cgi?T=JS&PAGE=reference&D=psyc12&NEWS=N&AN=2016-10843-000

Fornito. (2010). Network scaling effects in graph analytic studies of human resting-state fMRI data. *Frontiers in Systems Neuroscience*. http://doi.org/10.3389/fnsys.2010.00022

Fox, K. C. R., Spreng, R. N., Ellamil, M., Andrews-Hanna, J. R., & Christoff, K. (2015). The wandering brain: Meta-analysis of functional neuroimaging studies of mind-wandering and related spontaneous thought processes. *NeuroImage*. http://doi.org/10.1016/j.neuroimage.2015.02.039

Fox, M. D., & Greicius, M. (2010). Clinical applications of resting state functional connectivity. *Frontiers in Systems Neuroscience*, *4*(June), 19. http://doi.org/10.3389/fnsys.2010.00019

Fox, M. D., Zhang, D., Snyder, A. Z., & Raichle, M. E. (2009). The Global Signal and Observed Anticorrelated Resting State Brain Networks. *Journal of Neurophysiology*, *101*(6), 3270–3283. http://doi.org/10.1152/jn.90777.2008

Fransson, P. (2005). Spontaneous low-frequency BOLD signal fluctuations: An fMRI investigation of the resting-state default mode of brain function hypothesis. *Human Brain Mapping*, *26*(1), 15–29. http://doi.org/10.1002/hbm.20113

Galanaud, D., Perlbarg, V., Gupta, R., Stevens, R. D., Sanchez, P., Tollard, E., … Puybasset, L. (2012). Assessment of White Matter Injury and Outcome in Severe Brain Trauma. *Anesthesiology*, *117*(6), 1300–1310. http://doi.org/10.1097/ALN.0b013e3182755558

Gee, D. G., Biswal, B. B., Kelly, C., Stark, D. E., Margulies, D. S., Shehzad, Z., … Xavier, F. (2011). Processing among the Cerebral Hemispheres, *Neuroimage*, *54*(1), 517–527. http://doi.org/10.1016/j.neuroimage.2010.05.073.Low

Giacino, J. T., & Kalmar, K. (1997). The Vegetative and Minimally Conscious States: A Comparison of Clinical Features and Functional Outcome. *Journal of Head Trauma Rehabilitation*, *12*(4), 36–51. http://doi.org/10.1097/00001199-199708000-00005

Giacino, J. T., Ashwal, S., Childs, N., Cranford, R., Jennett, B., & Katz, D. I. (2002). The minimally conscious state, *Neurology, 58*, 349-353.

Giacino, J. T., Fins, J. J., Laureys, S., & Schiff, N. D. (2014). Disorders of consciousness after acquired brain injury: the state of the science. *Nature Reviews Neurology Neurology*, *10*(2), 99–114. http://doi.org/10.1038/nrneurol.2013.279

Giacino, J. T., Kalmar, K., & Whyte, J. (2004). The JFK Coma Recovery Scale-Revised: Measurement characteristics and diagnostic utility. *Archives of Physical Medicine and Rehabilitation*, *85*(12), 2020–2029. http://doi.org/10.1016/j.apmr.2004.02.033

Good, C. D., Johnsrude, I. S., Ashburner, J., Henson, R. N., Friston, K. J., & Frackowiak, R. S. (2001). A voxel-based morphometric study of ageing in 465 normal adult human brains. *NeuroImage*, *14*(1 Pt 1), 21–36. http://doi.org/10.1006/nimg.2001.0786

Gopinath, K., Krishnamurthy, V., Cabanban, R., & Crosson, B. A. (2015). Hubs of Anticorrelation in High-Resolution Resting-State Functional Connectivity Network Architecture. *Brain Connectivity, 5*(5), 267–275. http://doi.org/10.1089/brain.2014.0323

Gore, J. C. (2003). Principles and practice of functional MRI of the human brain. *Journal of Clinical Investigation*, *112*(1), 4–9. http://doi.org/10.1172/JCI200319010.Conventional

Gosseries, O., Zasler, N. D., & Laureys, S. (2014). Recent advances in disorders of consciousness: Focus on the diagnosis. *Brain Injury*, *28*(9), 1141–50. http://doi.org/10.3109/02699052.2014.920522

Greer, D., & Wu, O. (2017). Neuroimaging in Cardiac Arrest Prognostication. *Seminars in Neurology*, *37*(1), 066–074. http://doi.org/10.1055/s-0036-1594253

Greicius, M. D., & Menon, V. (2004). Default-Mode Activity during a Passive Sensory Task: Uncoupled from Deactivation but Impacting Activation. *Journal of Cognitive Neuroscience*, *16*(9), 1484–1492. http://doi.org/10.1162/0898929042568532

Greicius, M. D., Krasnow, B., Reiss, A. L., & Menon, V. (2003). Functional connectivity in the resting brain: a network analysis of the default mode hypothesis. *Proceedings of the National Academy of Sciences*, *100*(1), 253–258. http://doi.org/10.1073/pnas.0135058100

Greicius, M. D., Supekar, K., Menon, V., & Dougherty, R. F. (2009). Resting-state functional connectivity reflects structural connectivity in the default mode network. *Cerebral Cortex*, *19*(1), 72–78. http://doi.org/10.1093/cercor/bhn059

Greve, D. N. (2011). An Absolute Beginner's Guide to Surface- and Voxel-based Morphometric Analysis. *Proceedings of the International Society for Magnetic Resonance in Medicine*, *i*, 1–7.

Guldenmund, P., Soddu, A., Baquero, K., Vanhaudenhuyse, A., Bruno, M.-A., Gosseries, O., & Laureys, S. (2016). Structural brain injury in patients with disorders of consciousness: A voxel-based morphometry study. *Brain Injury*, *30*(3), 343–352. http://doi.org/10.3109/02699052.2015.1118765

Haenggi, M., Z'Graggen, W. J., & Wiest, R. (2014). Prognostic Markers for Coma and Disorders of Consciousness. *Epileptologie*, *31*, 68–72.

Hagmann, P., Cammoun, L., Gigandet, X., Meuli, R., Honey, C. J., Van Wedeen, J., & Sporns, O. (2008). Mapping the structural core of human cerebral cortex. *PLoS Biology*, *6*(7), 1479–1493. http://doi.org/10.1371/journal.pbio.0060159

Hagmann, P., Jonasson, L., Maeder, P., Thiran, J.-P., Wedeen, V. J., & Meuli, R. (2006). Understanding Diffusion MR Imaging Techniques: From Scalar Diffusion-weighted Imaging to Diffusion Tensor Imaging and Beyond. *RadioGraphics*, *26*(suppl_1), S205–S223. http://doi.org/10.1148/rg.26si065510

Hannawi, Y., Lindquist, M. A., Caffo, B. S., Sair, H. I., & Stevens, R. D. (2015). Resting brain activity in disorders of consciousness: a systematic review and meta-analysis. *Neurology*, *84*(12), 1272–1280. http://doi.org/10.1212/WNL.0000000000001404; 10.1212/WNL.0000000000001404

He, J. H., Cui, Y., Song, M., Yang, Y., Dang, Y. Y., Jiang, T. Z., & Xu, R. X. (2015). Decreased functional connectivity between the mediodorsal thalamus and default mode network in patients with disorders of consciousness. *Acta Neurologica Scandinavica*, *131*(3), 145–151. http://doi.org/10.1111/ane.12299

He, J. H., Yang, Y., Zhang, Y., Qiu, S. Y., Zhou, Z. Y., Dang, Y. Y., … Xu, R. X. (2014). Hyperactive external awareness against hypoactive internal awareness in disorders of consciousness using resting-state functional MRI: Highlighting the involvement of visuo-motor modulation. *NMR in Biomedicine*, *27*(8), 880–886. http://doi.org/10.1002/nbm.3130

Heine, L., Demertzi, A., Laureys, S., & Gosseries, O. (2015). Consciousness: And Disorders of Consciousness. In *Brain Mapping: An Encyclopedic Reference* (Vol. 3, pp. 1067–1073). http://doi.org/10.1016/B978-0-12-397025-1.00133-0

Heine, L., Soddu, A., Gómez, F., Vanhaudenhuyse, A., Tshibanda, L., Thonnard, M., … Demertzi, A. (2012). Resting state networks and consciousness Alterations of multiple resting state network connectivity in physiological, pharmacological, and pathological consciousness states. *Frontiers in Psychology*, *3*(AUG), 1–12. http://doi.org/10.3389/fpsyg.2012.00295

Hellyer, P. J., Scott, G., Shanahan, M., Sharp, D. J., & Leech, R. (2015). Cognitive Flexibility through Metastable Neural Dynamics Is Disrupted by Damage to the Structural Connectome. *Journal of Neuroscience*, *35*(24), 9050–9063. http://doi.org/10.1523/JNEUROSCI.4648-14.2015

Herbet, G., Lafargue, G., & Duffau, H. (2015). The dorsal cingulate cortex as a critical gateway in the network supporting conscious awareness. *Brain*, awv381. http://doi.org/10.1093/brain/awv381

Herbet, G., Lafargue, G., de Champfleur, N. M., Moritz-Gasser, S., le Bars, E., Bonnetblanc, F., & Duffau, H. (2014). Disrupting posterior cingulate connectivity disconnects consciousness from the external environment. *Neuropsychologia*, *56*(1), 239–244. http://doi.org/10.1016/j.neuropsychologia.2014.01.020

Herculano-Houzel, S. (2012). The remarkable, yet not extraordinary, human brain as a scaled-up primate brain and its associated cost. *Proceedings of the National Academy of Sciences*, *109*(Supplement_1), 10661–10668. http://doi.org/10.1073/pnas.1201895109

Hillary, F. G., Rajtmajer, S. M., Roman, C. A., Medaglia, J. D., Slocomb-Dluzen, J. E., Calhoun, V. D., … Wylie, G. R. (2014). The rich get richer: Brain injury elicits hyperconnectivity in core subnetworks. *PLoS ONE*, *9*(8). http://doi.org/10.1371/journal.pone.0104021

Hillary, F. G., Roman, C. A., Venkatesan, U., Rajtmajer, S. M., Bajo, R., & Castellanos, N. D. (2015). Hyperconnectivity is a fundamental response to neurological disruption. *Neuropsychology*, *29*(1), 59–75. http://doi.org/10.1037/neu0000110

Hirsch, K. G., Mlynash, M., Jansen, S., Persoon, S., Eyngorn, I., Krasnokutsky, M. V., … Fischbein, N. J. (2014). Prognostic Value of A Qualitative Brain MRI Scoring System After Cardiac Arrest. *Journal of Neuroimaging*, *25*(3), 430–437. http://doi.org/10.1111/jon.12143

Hirschberg, R., & Giacino, J. T. (2011). The Vegetative and Minimally Conscious States: Diagnosis, Prognosis and Treatment. *Neurologic Clinics*, *29*(4), 773–786. http://doi.org/10.1016/j.ncl.2011.07.009

Honey, C. J., Sporns, O., Cammoun, L., Gigandet, X., Thiran, J. P., Meuli, R., & Hagmann, P. (2009). Predicting human resting-state functional connectivity from structural connectivity. *Proceedings of the National Academy of Sciences of the United States of America*, *106*(6), 2035–40. http://doi.org/10.1073/pnas.0811168106

Horn, A., Ostwald, D., Reisert, M., & Blankenburg, F. (2014). The structural-functional connectome and the default mode network of the human brain. *NeuroImage*, *102*(P1), 142–151. http://doi.org/10.1016/j.neuroimage.2013.09.069

Horsting, M. W., Franken, M. D., Meulenbelt, J., van Klei, W. A., & de Lange, D. W. (2015). The etiology and outcome of non-traumatic coma in critical care: a systematic review. *BMC Anesthesiology*, *15*(1), 65. http://doi.org/10.1186/s12871-015-0041-9

Howard, R. S., Holmes, P. A., Siddiqui, A., Treacher, D., Tsiropoulos, I., & Koutroumanidis, M. (2012). Hypoxic-ischaemic brain injury: Imaging and neurophysiology abnormalities related to outcome. *QJM*, *105*(6), 551–561. http://doi.org/10.1093/qjmed/hcs016

Huang, Z., Dai, R., Wu, X., Yang, Z., Liu, D., Hu, J., … Northoff, G. (2014). The self and its resting state in consciousness: An investigation of the vegetative state. *Human Brain Mapping*, *35*(5), 1997–2008. http://doi.org/10.1002/hbm.22308

Hudetz, A. G., Liu, X., & Pillay, S. (2015). Dynamic Repertoire of Intrinsic Brain States Is Reduced in Propofol-Induced Unconsciousness. *Brain Connectivity*, *5*(1), 10–22. http://doi.org/10.1089/brain.2014.0230

Juengling, F. D., Kassubek, J., Huppertz, H.-J., Krause, T., & Els, T. (2005). Separating functional and structural damage in persistent vegetative state using combined voxel-based analysis of 3-D MRI and FDG-PET. *Journal of the Neurological Sciences*, *228*(2), 179–184. http://doi.org/10.1016/j.jns.2004.11.052

Keller, C. J., Bickel, S., Honey, C. J., Groppe, D. M., Entz, L., Craddock, R. C., … Mehta, A. D. (2013). Neurophysiological Investigation of Spontaneous Correlated and Anticorrelated Fluctuations of the BOLD Signal. *Journal of Neuroscience*, *33*(15), 6333–6342. http://doi.org/10.1523/JNEUROSCI.4837-12.2013

Khalsa, S., Mayhew, S. D., Chechlacz, M., Bagary, M., & Bagshaw, A. P. (2014). The structural and functional connectivity of the posterior cingulate cortex: Comparison between deterministic and probabilistic tractography for the investigation of structure-function relationships. *NeuroImage*, *102*(P1), 118–127. http://doi.org/10.1016/j.neuroimage.2013.12.022

Kim, Y. W., Kim, H. S., An, Y.-S., & Im, S. H. (2010). Voxel-based statistical analysis of cerebral glucose metabolism in patients with permanent vegetative state after acquired brain injury. *Chinese Medical Journal*, *123*(20), 2853–2857. http://doi.org/10.3760/cma.j.issn.0366-6999.2010.20.020

Kirsch, M., Guldenmund, P., Ali Bahri, M., Demertzi, A., Baquero, K., Heine, L., … Laureys, S. (2017). Sedation of Patients With Disorders of Consciousness During Neuroimaging: Effects on Resting State Functional Brain Connectivity. *Anesthesia and Analgesia*, *124*(2), 588–598. http://doi.org/10.1213/ANE.0000000000001721

Koch, C., Massimini, M., Boly, M., & Tononi, G. (2016). Neural correlates of consciousness: progress and problems. *Nature Reviews Neuroscience*, *17*(5), 307–321. http://doi.org/10.1038/nrn.2016.22

Koenig, M. A., Holt, J. L., Ernst, T., Buchthal, S. D., Nakagawa, K., Stenger, V. A., & Chang, L. (2014). MRI default mode network connectivity is associated with functional outcome after cardiopulmonary arrest. *Neurocritical Care*, *20*(3), 348–57. http://doi.org/10.1007/s12028-014-9953-3

Kondziella, D., Fisher, P. M., Larsen, V. A., Hauerberg, J., Fabricius, M., Møller, K., & Knudsen, G. M. (2017). Functional MRI for Assessment of the Default Mode Network in Acute Brain Injury. *Neurocritical Care*, 1–6. http://doi.org/10.1007/s12028-017-0407-6

Laird, A. R., Fox, P. M., Eickhoff, S. B., Turner, J. A., Ray, K. L., McKay, D. R., … Fox, P. T. (2011). Behavioral Interpretations of Intrinsic Connectivity Networks. *Journal of Cognitive Neuroscience*, *23*(12), 4022–4037. http://doi.org/10.1162/jocn_a_00077

Lant, N. D., Gonzalez-Lara, L. E., Owen, A. M., & Fernández-Espejo, D. (2016). Relationship between the anterior forebrain mesocircuit and the default mode network in the structural bases of disorders of consciousness. *NeuroImage: Clinical*, *10*, 27–35. http://doi.org/10.1016/j.nicl.2015.11.004

Latora, V., & Marchiori, M. (2001). Efficient Behavior of Small World Networks. *Physical Review Letters*, *87*, 198701. http://doi.org/10.1103/PhysRevLett.87.198701

Laureys, S. (2005). The neural correlate of (un) awareness: lessons from the vegetative state. *Trends in Cognitive Sciences*, *9*(12), 556–559. http://doi.org/10.1016/j.tics.2005.10.010

Laureys, S., & Schiff, N. D. (2012). Coma and consciousness: Paradigms (re)framed by neuroimaging. *NeuroImage*, *61*(2), 478–491. http://doi.org/10.1016/j.neuroimage.2011.12.041

Laureys, S., Celesia, G. G., Cohadon, F., Lavrijsen, J., León-carrión, J., Sannita, W. G., … Dolce, G. (2010). Unresponsive wakefulness syndrome : a new name for the vegetative state or apallic syndrome. *BMC Medicine*, *8*(1), 68. http://doi.org/10.1186/1741-7015-8-68

Laureys, S., Faymonville, M. E., Luxen, A., Lamy, M., Franck, G., & Maquet, P. (2000). Restoration of thalamocortical connectivity after recovery from persistent vegetative state. *Lancet*, *355*(9217), 1790–1791. http://doi.org/10.1016/S0140-6736(00)02271-6

Laureys, S., Owen, A. M., & Schiff, N. D. (2004). Brain function in coma, vegetative state, and related disorders. *Lancet Neurology*. http://doi.org/10.1016/S1474-4422(04)00852-X

Laureys, S., Majerus, S., & Moonen, G. (2002). Assessing consciousness in critically ill patients. In: Vincent, J.L. (ed), Yearbook of intensive care and emergency medicine. Springer.

Lee, M. H., Smyser, C. D., & Shimony, J. S. (2013). Resting-State fMRI: A Review of Methods and Clinical Applications. *American Journal of Neuroradiology*, *34*(10), 1866–1872. http://doi.org/10.3174/ajnr.A3263

Leech, R., & Sharp, D. J. (2014). The role of the posterior cingulate cortex in cognition and disease. *Brain*, *137*(1), 12–32. http://doi.org/10.1093/brain/awt162

Leech, R., Braga, R., & Sharp, D. J. (2012). Echoes of the brain within the posterior cingulate cortex. *The Journal of Neuroscience : The Official Journal of the Society for Neuroscience*, *32*(1), 215–222. http://doi.org/10.1523/JNEUROSCI.3689-11.2012

Siskas, N., Lefkopoulos, A., Ioannidis, I., Charitandi, A., Dimitriadis, A.S. (2003). Cortical laminar necrosis in brain infarcts: serial MRI. *Neuroradiology*, *45*(5), 283–8. http://doi.org/10.1007/s00234-002-0887-7

Lin, J. S. (2000). Brain structures and mechanisms involved in the control of cortical activation and wakefulness, with emphasis on the posterior hypothalamus and histaminergic neurons. *Sleep Medicine Reviews*. http://doi.org/10.1053/smrv.2000.0116

Liu, X., Li, J., Gao, J., Zhou, Z., Meng, F., Pan, G., & Luo, B. (2017). Association of medial prefrontal cortex connectivity with consciousness level and its outcome in patients with acquired brain injury. *Journal of Clinical Neuroscience*. http://doi.org/10.1016/j.jocn.2017.04.015

Liu, X., Ward, B. D., Binder, J. R., Li, S. J., & Hudetz, A. G. (2014). Scale-free functional connectivity of the brain is maintained in anesthetized healthy participants but not in patients with unresponsive wakefulness syndrome. *PLoS ONE*, *9*(3). http://doi.org/10.1371/journal.pone.0092182

Liu, Y., Huang, L., Li, M., Zhou, Z., & Hu, D. (2015). Anticorrelated networks in resting-state fMRI-BOLD data. *Bio-Medical Materials and Engineering*, *26 Suppl 1*, S1201-11. http://doi.org/10.3233/BME-151417

Liu, Y., Liang, M., Zhou, Y., He, Y., Hao, Y., Song, M., … Jiang, T. (2008). Disrupted small-world networks in schizophrenia. *Brain*, *131*(4), 945–961. http://doi.org/10.1093/brain/awn018

Luauté, J., Maucort-Boulch, D., Tell, L., Quelard, F., Sarraf, T., Iwaz, J., … Fischer, C. (2010). Long-term outcomes of chronic minimally conscious and vegetative states. *Neurology*, *75*(3), 246–252. http://doi.org/10.1212/WNL.0b013e3181e8e8df

Luauté, J., Morlet, D., & Mattout, J. (2015). BCI in patients with disorders of consciousness: Clinical perspectives. *Annals of Physical and Rehabilitation Medicine*, *58*(1), 29–34. http://doi.org/10.1016/j.rehab.2014.09.015

Luyt, C.-E., Galanaud, D., Perlbarg, V., Vanhaudenhuyse, A., Stevens, R. D., Gupta, R., … Puybasset, L. (2012). Diffusion Tensor Imaging to Predict Long-term Outcome after Cardiac Arrest. *Anesthesiology*, *117*(6), 1311–1321. http://doi.org/10.1097/ALN.0b013e318275148c

Malagurski, B., Péran, P., Sarton, B., Riu, B., Gonzalez, L., Vardon-Bounes, F., … Silva, S. (2017). Neural signature of coma revealed by posteromedial cortex connection density analysis. *NeuroImage: Clinical*, *15*(February), 315–324. http://doi.org/10.1016/j.nicl.2017.03.017

Margulies, D. S., Vincent, J. L., Kelly, C., Lohmann, G., Uddin, L. Q., Biswal, B. B., … Petrides, M. (2009). Precuneus shares intrinsic functional architecture in humans and monkeys. *Proceedings of the National Academy of Sciences of the United States of America*, *106*(47), 20069–20074. http://doi.org/10.1073/pnas.0905314106

Mazoyer, B., Zago, L., Mellet, E., Bricogne, S., Etard, O., Houdé, O., … Tzourio-Mazoyer, N. (2001). Cortical networks for working memory and executive functions sustain the conscious resting state in man. *Brain Research Bulletin*, *54*(3), 287–298. http://doi.org/10.1016/S0361-9230(00)00437-8

Mckee, A. C., & Daneshvar, D. H. (2015). The neuropathology of traumatic brain injury. *Handbook of Clinical Neurology*, *127*, 45–66. http://doi.org/10.1016/B978-0-444-52892-6.00004-0

Mechelli, A., Price, C. J., Friston, K. J., & Ashburner, J. (2005). Voxel-based morphometry of the human brain: methods and applications. *Current Medical …*, *1*(2), 105–113. http://doi.org/10.2174/1573405054038726

Menon, V. (2015). *Salience Network*. *Brain Mapping: An Encyclopedic Reference* (Vol. 2). Elsevier Inc. http://doi.org/10.1016/B978-0-12-397025-1.00052-X

Menon, V., & Uddin, L. Q. (2010). Saliency, switching, attention and control: a network model of insula function. *Brain Structure and Function*, 1–13. http://doi.org/10.1007/s00429-010-0262-0

Meskaldji, D. E., Fischi-Gomez, E., Griffa, A., Hagmann, P., Morgenthaler, S., & Thiran, J. P. (2013). Comparing connectomes across subjects and populations at different scales. *NeuroImage*, *80*, 416–425. http://doi.org/10.1016/j.neuroimage.2013.04.084

Monti, M. M., Vanhaudenhuyse, A., Coleman, M. R., Boly, M., Pickard, J. D., Tshibanda, L., … Laureys, S. (2010). Willful modulation of brain activity in disorders of consciousness. *The New England Journal of Medicine*, *362*(7), 579–89. http://doi.org/10.1056/NEJMoa0905370

Mori, S., & Zhang, J. (2006). Principles of Diffusion Tensor Imaging and Its Applications to Basic Neuroscience Research. *Neuron*, *51*(5), 527–539. http://doi.org/10.1016/j.neuron.2006.08.012

Murphy, K., Birn, R. M., Handwerker, D. A., Jones, T. B., & Bandettini, P. A. (2009). The impact of global signal regression on resting state correlations: Are anti-correlated

networks introduced? *NeuroImage*, *44*(3), 893–905. http://doi.org/10.1016/j.neuroimage.2008.09.036

Nakamura, T., Hillary, F. G., & Biswal, B. B. (2009). Resting network plasticity following brain injury. *PLoS ONE*, *4*(12). http://doi.org/10.1371/journal.pone.0008220

Newcombe, V. F. J., Williams, G. B., Scoffings, D., Cross, J., Carpenter, T. A., Pickard, J. D., & Menon, D. K. (2010). Aetiological differences in neuroanatomy of the vegetative state: insights from diffusion tensor imaging and functional implications. *Journal of Neurology, Neurosurgery & Psychiatry*, *81*(5), 552–561. http://doi.org/10.1136/jnnp.2009.196246

Nolan, J. P., Neumar, R. W., Adrie, C., Aibiki, M., Berg, R. A., Bbttiger, B. W., … Hoek, T. Vanden. (2010). Post-cardiac arrest syndrome : Epidemiology , pathophysiology , treatment , and prognostication : A Scientific Statement from the International Liaison Committee on Resuscitation ; the American Heart Association Emergency Cardiovascular Care Committee ; t. *International Emergency Nursing*, *18*(1), 8–28. http://doi.org/10.1016/j.ienj.2009.07.001

Norton, L., Hutchison, R. M., Young, G. B., Lee, D. H., Sharpe, M. D., & Mirsattari, S. M. (2012). Disruptions of functional connectivity in the default mode network of comatose patients. *Neurology*, *78*(3), 175–181. http://doi.org/10.1212/WNL.0b013e31823fcd61

O'Donnell, L. J., & Westin, C. F. (2011). An introduction to diffusion tensor image analysis. *Neurosurgery Clinics of North America*, *22*(2), 185–viii. http://doi.org/10.1016/j.nec.2010.12.004

Ogawa, S., Lee, T. M., Kay, A. R., & Tank, D. W. (1990). Brain magnetic resonance imaging with contrast dependent on blood oxygenation. *Proceedings of the National Academy of Sciences of the United States of America*, *87*(24), 9868–72. http://doi.org/10.1073/pnas.87.24.9868

Orringer, D. A., Vago, D. R., & Golby, A. J. (2012). Clinical applications and future directions of functional MRI. *Seminars in Neurology*, *32*(4), 466–475. http://doi.org/10.1055/s-0032-1331816

Ovadia-Caro, S., Nir, Y., Soddu, A., Ramot, M., Hesselmann, G., Vanhaudenhuyse, A., … Malach, R. (2012). Reduction in inter-hemispheric connectivity in disorders of consciousness. *PLoS ONE*, *7*(5). http://doi.org/10.1371/journal.pone.0037238

Palacios, E. M., Sala-Llonch, R., Junque, C., Roig, T., Tormos, J. M., Bargallo, N., & Vendrell, P. (2013). Resting-state functional magnetic resonance imaging activity and connectivity and cognitive outcome in traumatic brain injury. *JAMA Neurology*, *70*(7), 845–51. http://doi.org/10.1001/jamaneurol.2013.38

Parente, F., Frascarelli, M., Mirigliani, A., Di Fabio, F., Biondi, M., & Colosimo, A. (2017). Negative functional brain networks. *Brain Imaging and Behavior*. doi: 10.1007/s11682-017-9715-x. [Epub ahead of print]

Parvizi, J. (2003). Neuroanatomical correlates of brainstem coma. *Brain*, *126*(7), 1524–1536. http://doi.org/10.1093/brain/awg166

Parvizi, J., Van Hoesen, G. W., Buckwalter, J., & Damasio, A. (2006). Neural connections of the posteromedial cortex in the macaque. *Proceedings of the National Academy of Sciences of the United States of America*, *103*(5), 1563–8. http://doi.org/10.1073/pnas.0507729103

Péran, P., Cherubini, A., Assogna, F., Piras, F., Quattrocchi, C., Peppe, A., … Sabatini, U. (2010). Magnetic resonance imaging markers of Parkinson's disease nigrostriatal signature. *Brain*, *133*(11), 3423–3433. http://doi.org/10.1093/brain/awq212

Péran, P., Cherubini, A., Luccichenti, G., Hagberg, G., Démonet, J. F., Rascol, O., … Sabatini, U. (2009). Volume and iron content in basal ganglia and thalamus. *Human Brain Mapping*, *30*(8), 2667–2675. http://doi.org/10.1002/hbm.20698

Perlbarg, V., Puybasset, L., Tollard, E., Lehéricy, S., Benali, H., & Galanaud, D. (2009). Relation between brain lesion location and clinical outcome in patients with severe traumatic brain injury: A diffusion tensor imaging study using voxel-based approaches. *Human Brain Mapping*, *30*(12), 3924–3933. http://doi.org/10.1002/hbm.20817

Peterson, A., Cruse, D., Naci, L., Weijer, C., & Owen, A. M. (2015). Risk, diagnostic error, and the clinical science of consciousness. *NeuroImage: Clinical*. http://doi.org/10.1016/j.nicl.2015.02.008

Poldrack, R. A. (2007). Region of interest analysis for fMRI. *Social Cognitive and Affective Neuroscience*, *2*(1), 67–70. http://doi.org/10.1093/scan/nsm006

Popa, D., Popescu, A. T., & Pare, D. (2009). Contrasting Activity Profile of Two Distributed Cortical Networks as a Function of Attentional Demands. *Journal of Neuroscience*, *29*(4), 1191–1201. http://doi.org/10.1523/JNEUROSCI.4867-08.2009

Posner, J. B., Plum, F., & Saper, C. (2007). *Plum and Posner's Diagnosis of Estupor and Coma*. *Neurology* (Vol. 1). http://doi.org/10.1002/1521-3773(20010316)40:6<9823::AID-ANIE9823>3.3.CO;2-C

Prim, R. C. (1957). Shortest Connection Networks And Some Generalizations. *Bell System Technical Journal*, *36*(6), 1389–1401. http://doi.org/10.1002/j.1538-7305.1957.tb01515.x

Qin, P., Wu, X., Huang, Z., Duncan, N. W., Tang, W., Wolff, A., … Northoff, G. (2015). How are different neural networks related to consciousness? *Annals of Neurology*, *78*(4), 594–605. http://doi.org/10.1002/ana.24479

Raichle, M. E. (2015). The Brain's Default Mode Network. *Annual Review of Neuroscience*, *38*(1), 433–447. http://doi.org/10.1146/annurev-neuro-071013-014030

Raichle, M. E., MacLeod, A. M., Snyder, A. Z., Powers, W. J., Gusnard, D. A., & Shulman, G. L. (2001). A default mode of brain function. *Proceedings of the National Academy of*

Sciences of the United States of America, *98*(2), 676–82. http://doi.org/10.1073/pnas.98.2.676

Richiardi, J., Altmann, A., Milazzo, A.-C., Chang, C., Chakravarty, M. M., Banaschewski, T., … Jonas, R. (2015). BRAIN NETWORKS. Correlated gene expression supports synchronous activity in brain networks. *Science (New York, N.Y.)*, *348*(6240), 1241–1244. http://doi.org/10.1126/science.1255905

Roquet, D., Foucher, J. R., Froehlig, P., Renard, F., Pottecher, J., Besancenot, H., … Kremer, S. (2016). Resting-state networks distinguish locked-in from vegetative state patients. *NeuroImage: Clinical*, *12*, 16–22. http://doi.org/10.1016/j.nicl.2016.06.003

Rosazza, C., & Minati, L. (2011). Resting-state brain networks: Literature review and clinical applications. *Neurological Sciences*, *32*(5), 773–785. http://doi.org/10.1007/s10072-011-0636-y

Rosazza, C., Andronache, A., Sattin, D., Bruzzone, M. G., Marotta, G., Nigri, A., … Minati, L. (2016). Multimodal study of default-mode network integrity in disorders of consciousness. *Annals of Neurology*, *79*(5), 841–853. http://doi.org/10.1002/ana.24634

Rubinov, M., & Sporns, O. (2010). Complex network measures of brain connectivity: Uses and interpretations. *NeuroImage*, *52*(3), 1059–1069. http://doi.org/10.1016/j.neuroimage.2009.10.003

Ryoo, S. M., Jeon, S.-B., Sohn, C. H., Ahn, S., Han, C., Lee, B. K., … Kim, W. Y. (2015). Predicting Outcome With Diffusion-Weighted Imaging in Cardiac Arrest Patients Receiving Hypothermia Therapy. *Critical Care Medicine*, *43*(11), 2370–2377. http://doi.org/10.1097/CCM.0000000000001263

Sair, H. I., Hannawi, Y., Li, S., Kornbluth, J., Demertzi, A., Di Perri, C., … Stevens, R. D. (2017). Early Functional Connectome Integrity and 1-Year Recovery in Comatose Survivors of Cardiac Arrest. *Radiology*, (October), 162161. doi:10.1148/radiol.2017162161. [Epub ahead of print]

Satoru Hayasaka; Paul J. Laurienti. (2011). Comparison of Characteristics between Region- and Voxel-Based Network Analyses in Resting-State fMRI Data. *NeuroImage*, *18*(11), 499–508. http://doi.org/10.1016/j.str.2010.08.012.Structure

Schiff, N. D. (2010). Recovery of consciousness after brain injury: a mesocircuit hypothesis. *Trends in Neurosciences*, 33(1), 1-9. doi: 10.1016/j.tins.2009.11.002.

Schiff, N. D. (2008). Central thalamic contributions to arousal regulation and neurological disorders of consciousness. *Ann N Y Acad Sci,1129,* 105-18. doi: 10.1196/annals.1417.029.

Schiff, N. D., Giacino, J. T., Kalmar, K., Victor, J. D., Baker, K., Gerber, M., … Rezai, A. R. (2007). Behavioural improvements with thalamic stimulation after severe traumatic brain injury. *Nature*, *448*(7153), 600–603. http://doi.org/10.1038/nature06041

Schnakers, C., Majerus, S., & Laureys, S. (2004). Diagnosis and investigation of altered states of consciousness. *Reanimation*, *13*(5), 368–375. http://doi.org/10.1016/j.reaurg.2004.03.019

Schnakers, C., Majerus, S., Giacino, J., Vanhaudenhuyse, A., Bruno, M.-A. A., Boly, M., … Laureys, S. (2008). A French validation study of the Coma Recovery Scale-Revised (CRS-R). *Brain Injury*, *22*(10), 786–792. http://doi.org/10.1080/02699050802403557

Schnakers, C., Vanhaudenhuyse, A., Giacino, J., Ventura, M., Boly, M., Majerus, S., … Laureys, S. (2009). Diagnostic accuracy of the vegetative and minimally conscious state: Clinical consensus versus standardized neurobehavioral assessment. *BMC Neurology*, *9*(1), 35. http://doi.org/10.1186/1471-2377-9-35

Seel, R. T., Sherer, M., Whyte, J., Katz, D. I., Giacino, J. T., Rosenbaum, A. M., … Zasler, N. (2010). Assessment scales for disorders of consciousness: Evidence-based recommendations for clinical practice and research. In *Archives of Physical Medicine and Rehabilitation*, *91*(12), 1795-813. doi: 10.1016/j.apmr.2010.07.218.

Seeley, W. W., Crawford, R. K., Zhou, J., Miller, B. L., & Greicius, M. D. (2009). Neurodegenerative Diseases Target Large-Scale Human Brain Networks. *Neuron*, *62*(1), 42–52. http://doi.org/10.1016/j.neuron.2009.03.024

Segall, J. M., Allen, E. A., Jung, R. E., Erhardt, E. B., Arja, S. K., Kiehl, K., & Calhoun, V. D. (2012). Correspondence between structure and function in the human brain at rest. *Frontiers in Neuroinformatics*, *27,* 6:10. doi: 10.3389/fninf.2012.00010.

Sharp, D. J., Beckmann, C. F., Greenwood, R., Kinnunen, K. M., Bonnelle, V., De Boissezon, X., … Leech, R. (2011). Default mode network functional and structural connectivity after traumatic brain injury. *Brain*, *134*(8), 2233–2247. http://doi.org/10.1093/brain/awr175

Sharp, D. J., Scott, G., & Leech, R. (2014). Network dysfunction after traumatic brain injury. *Nat Rev Neurol*, *10*(3), 156–166. http://doi.org/10.1038/nrneurol.2014.15

Shirer, W. R., Ryali, S., Rykhlevskaia, E., Menon, V., & Greicius, M. D. (2012). Decoding subject-driven cognitive states with whole-brain connectivity patterns. *Cerebral Cortex*, *22*(1), 158–165. http://doi.org/10.1093/cercor/bhr099

Siclari, F., Baird, B., Perogamvros, L., Bernardi, G., LaRocque, J. J., Riedner, B., … Tononi, G. (2017). The neural correlates of dreaming. *Nature Neuroscience*, *20*(6), 872–878. http://doi.org/10.1038/nn.4545

Sidaros, A., Engberg, A. W., Sidaros, K., Liptrot, M. G., Herning, M., Petersen, P., … Rostrup, E. (2008). Diffusion tensor imaging during recovery from severe traumatic brain injury and relation to clinical outcome: A longitudinal study. *Brain*, *131*(2), 559–572. http://doi.org/10.1093/brain/awm294

Siero, J. C. W., Bhogal, A., & Jansma, J. M. (2013). Blood oxygenation level-dependent/functional magnetic resonance imaging: Underpinnings, practice, and perspectives. *PET Clinics*, *8*(3), 329–344. http://doi.org/10.1016/j.cpet.2013.04.003

Silva, S., Alacoque, X., Fourcade, O., Samii, K., Marque, P., Woods, R., … Loubinoux, I. (2010). Wakefulness and loss of awareness: Brain and brainstem interaction in the vegetative state. *Neurology*, *74*(4), 313–320. http://doi.org/10.1212/WNL.0b013e3181cbcd96

Silva, S., De Pasquale, F., Vuillaume, C., Riu, B., Loubinoux, I., Geeraerts, T., … Peran, P. (2015). Disruption of posteromedial large-scale neural communication predicts recovery from coma. *Neurology*, *85*(23), 2036–2044. http://doi.org/10.1212/WNL.0000000000002196

Silva, S., Peran, P., Kerhuel, L., Malagurski, B., Chauveau, N., Bataille, B., … Puybasset, L. (2017). Brain Gray Matter MRI Morphometry for Neuroprognostication After Cardiac Arrest. *Critical Care Medicine*, *45*(8), e763–e771. http://doi.org/10.1097/CCM.0000000000002379

Skudlarski, P., Jagannathan, K., Calhoun, V. D., Hampson, M., Skudlarska, B. A., & Pearlson, G. (2008). Measuring brain connectivity: Diffusion tensor imaging validates resting state temporal correlations. *NeuroImage*, *43*(3), 554–561. http://doi.org/10.1016/j.neuroimage.2008.07.063

Smith, S. M., Fox, P. T., Miller, K. L., Glahn, D. C., Fox, P. M., Mackay, C. E., … Beckmann, C. F. (2009). Correspondence of the brain's functional architecture during activation and rest. *Proceedings of the National Academy of Sciences*, *106*(31), 13040–13045. http://doi.org/10.1073/pnas.0905267106

Soares, J. M., Marques, P., Alves, V., & Sousa, N. (2013). A hitchhiker's guide to diffusion tensor imaging. *Frontiers in Neuroscience*, *12, 7:31. doi: 10.3389/fnins.2013.00031.*

Soddu, A., Gómez, F., Heine, L., Di Perri, C., Bahri, M. A., Voss, H. U., … Laureys, S. (2016). Correlation between resting state fMRI total neuronal activity and PET metabolism in healthy controls and patients with disorders of consciousness. *Brain and Behavior*, *6*(1), 1–15. http://doi.org/10.1002/brb3.424

Soddu, A., Vanhaudenhuyse, A., Demertzi, A., Bruno, M.-A., Tshibanda, L., Di, H., … Noirhomme, Q. (2011). Resting state activity in patients with disorders of consciousness. *Functional Neurology*, *26*(1), 37–43.

Soddu, A., Vanhaudenhuyse, A., Bahri, M. A., Bruno, M. A., Boly, M., Demertzi, A., … Noirhomme, Q. (2012). Identifying the default-mode component in spatial IC analyses of patients with disorders of consciousness. *Human Brain Mapping, 33*(4), 778–796. http://doi.org/10.1002/hbm.21249

Sokolov, A. A., Miall, R. C., & Ivry, R. B. (2017). The Cerebellum: Adaptive Prediction for Movement and Cognition. *Trends in Cognitive Sciences, 21*(5), 313-332. doi: 10.1016/j.tics.2017.02.005.

Spreng, R. N., & Andrews-Hanna, J. R. (2015). The Default Network and Social Cognition. *In Brain Mapping: An Encyclopedic Reference* (pp. 165–169). http://doi.org/10.1016/B978-0-12-397025-1.00173-1

Stam, C. J. (2014). Modern network science of neurological disorders. *Nature Reviews Neuroscience*, *15*(10), 683–695. http://doi.org/10.1038/nrn3801

Stanley, M. L., Moussa, M. N., Paolini, B. M., Lyday, R. G., Burdette, J. H., & Laurienti, P. J. (2013). Defining nodes in complex brain networks. *Frontiers in Computational Neuroscience*, *7*(November), 169. http://doi.org/10.3389/fncom.2013.00169

Stevens, M. C., Lovejoy, D., Kim, J., Oakes, H., Kureshi, I., & Witt, S. T. (2012). Multiple resting state network functional connectivity abnormalities in mild traumatic brain injury. *Brain Imaging and Behavior*, *6*(2), 293–318. http://doi.org/10.1007/s11682-012-9157-4

Stevens, R. D., & Hannawi, Y. (2016). Coma Prognostication: Looks That Count. *Critical Care Medicine*, *44*(12), 2292–2293. http://doi.org/10.1097/CCM.0000000000002039

Tagliazucchi, E., Chialvo, D. R., Siniatchkin, M., Amico, E., Brichant, J.-F., Bonhomme, V., … Laureys, S. (2016). Large-scale signatures of unconsciousness are consistent with a departure from critical dynamics. *Journal of The Royal Society Interface*, *13*(114), 20151027. http://doi.org/10.1098/rsif.2015.1027

Teasdale, G., & Jennett, B. (1974). ASSESSMENT OF COMA AND IMPAIRED CONSCIOUSNESS. A Practical Scale. *The Lancet*, *304*(7872), 81–84. http://doi.org/10.1016/S0140-6736(74)91639-0

Teasdale, G., Maas, A., Lecky, F., Manley, G., Stocchetti, N., & Murray, G. (2014). The Glasgow Coma Scale at 40 years: Standing the test of time. *The Lancet Neurology*, *13*(8), 844–854. http://doi.org/10.1016/S1474-4422(14)70120-6

The Multi-Society Task Force on PVS. (1994). Medical aspects of the persistent vegetative state. *The New England Journal of Medicine*, *330*(21), 1499–1508. http://doi.org/10.1056/NEJM199405263302107

Thibaut, A., Bruno, M. A., Chatelle, C., Gosseries, O., Vanhaudenhuyse, A., Demertzi, A., … Laureys, S. (2012). Metabolic activity in external and internal awareness networks in severely brain-damaged patients. *Journal of Rehabilitation Medicine*, *44*(6), 487–494. http://doi.org/10.2340/16501977-0940

Thibaut, A., Bruno, M.-A., Ledoux, D., Demertzi, A., & Laureys, S. (2014). tDCS in patients with disorders of consciousness: sham-controlled randomized double-blind study. *Neurology*, *82*(13), 1112–1118. http://doi.org/10.1212/WNL.0000000000000260

Thibaut, A., Di Perri, C., Chatelle, C., Bruno, M. A., Bahri, M. A., Wannez, S., … Laureys, S. (2015). Clinical response to tDCS depends on residual brain metabolism and grey matter integrity in patients with minimally conscious state. *Brain Stimulation*, *8*(6), 1116–1123. http://doi.org/10.1016/j.brs.2015.07.024

Thibaut, A., Wannez, S., Donneau, A. F., Chatelle, C., Gosseries, O., Bruno, M. A., & Laureys, S. (2017). Controlled clinical trial of repeated prefrontal tDCS in patients with chronic minimally conscious state. *Brain Injury*, *31*(4), 466–474. http://doi.org/10.1080/02699052.2016.1274776

Toga, A. W., Thompson, P. M., Mori, S., Amunts, K., & Zilles, K. (2006). Towards multimodal atlases of the human brain. *Nature Reviews Neuroscience*, *7*(12), 952–966. http://doi.org/10.1038/nrn2012

Tomaiuolo, F., Cecchetti, L., Gibson, R. M., Logi, F., Owen, A. M., Malasoma, F., … Ricciardi, E. (2016). Progression from Vegetative to Minimally Conscious State Is Associated with Changes in Brain Neural Response to Passive Tasks: A Longitudinal Single-Case Functional MRI Study. *Journal of the International Neuropsychological Society*, *22*(6), 620-30. http://doi.org/10.1017/S1355617716000485

Tomasi, D., & Volkow, N. D. (2010). Functional connectivity density mapping. *Proceedings of the National Academy of Sciences*, *107*(21), 9885–9890. http://doi.org/10.1073/pnas.1001414107

Tomasi, D., & Volkow, N. D. (2011). Functional connectivity hubs in the human brain. *NeuroImage*, *57*(3), 908–917. http://doi.org/10.1016/j.neuroimage.2011.05.024

Tononi, G. (1998). Consciousness and Complexity. *Science*, *282*(5395), 1846–1851. http://doi.org/10.1126/science.282.5395.1846

Tononi, G. (2004). An information integration theory of consciousness. *BMC Neuroscience*, *5*(1), 42. http://doi.org/10.1186/1471-2202-5-42

Tononi, G., & Koch, C. (2008). The neural correlates of consciousness: An update. *Annals of the New York Academy of Sciences*, *1124*, 239-61. doi: 10.1196/annals.1440.004.

Tononi, G., & Koch, C. (2015). Consciousness: here, there and everywhere? *Philosophical Transactions of the Royal Society B: Biological Sciences*, *370*(1668), 20140167–20140167. http://doi.org/10.1098/rstb.2014.0167

Tononi, G., Boly, M., Massimini, M., & Koch, C. (2016). Integrated information theory: from consciousness to its physical substrate. *Nature Reviews Neuroscience*, *17*(7), 450–461. http://doi.org/10.1038/nrn.2016.44

Tsai, Y. H., Yuan, R., Huang, Y. C., Yeh, M. Y., Lin, C. P., & Biswal, B. B. (2014). Disruption of brain connectivity in acute stroke patients with early impairment in consciousness. *Frontiers in Psychology*, *4*(JAN), 1–10. http://doi.org/10.3389/fpsyg.2013.00956

Turgeon, A. F., Lauzier, F., Simard, J.-F., Scales, D. C., Burns, K. E. A., Moore, L., … Canadian Critical Care Trials Group. (2011). Mortality associated with withdrawal of life-sustaining therapy for patients with severe traumatic brain injury: a Canadian multicentre cohort study. *CMAJ : Canadian Medical Association Journal = Journal de l'Association Medicale Canadienne*, *183*(14), 1581–8. http://doi.org/10.1503/cmaj.101786

Tzourio-Mazoyer, N., Landeau, B., Papathanassiou, D., Crivello, F., Etard, O., Delcroix, N., … Joliot, M. (2002). Automated anatomical labeling of activations in SPM using a macroscopic anatomical parcellation of the MNI MRI single-subject brain. *NeuroImage*, *15*(1), 273–289. http://doi.org/10.1006/nimg.2001.0978

Uddin, L. Q. (2014). Salience processing and insular cortical function and dysfunction. *Nature Reviews Neuroscience*, *16*(1), 55–61. http://doi.org/10.1038/nrn3857

Uddin, L. Q., Kelly, A. M. C., Biswal, B. B., Castellanos, F. X., & Milham, M. P. (2009). Functional Connectivity of Default Mode Network Components: Correlation, Anticorrelation, and Causality. *Human Brain Mapping*, *30*(2), 625–637. http://doi.org/10.1002/hbm.20531

van den Heuvel, M. P., & Hulshoff Pol, H. E. (2010). Exploring the brain network: A review on resting-state fMRI functional connectivity. *European Neuropsychopharmacology*, *20*(8), 519–534. http://doi.org/10.1016/j.euroneuro.2010.03.008

van den Heuvel, M. P., & Sporns, O. (2011). Rich-club organization of the human connectome. *The Journal of Neuroscience*, *31*(44), 15775–15786. http://doi.org/10.1523/JNEUROSCI.3539-11.2011

van den Heuvel, M. P., & Sporns, O. (2013). Network hubs in the human brain. *Trends in Cognitive Sciences*, *17*(12), 683–696. http://doi.org/10.1016/j.tics.2013.09.012

van den Heuvel, M. P., de Lange, S. C., Zalesky, A., Seguin, C., Yeo, B. T. T., & Schmidt, R. (2017). Proportional thresholding in resting-state fMRI functional connectivity networks and consequences for patient-control connectome studies: Issues and recommendations. *NeuroImage*, *152*(December 2016), 437–449. http://doi.org/10.1016/j.neuroimage.2017.02.005

van den Heuvel, M. P., Mandl, R. C. W., Kahn, R. S., & Hulshoff Pol, H. E. (2009). Functionally linked resting-state networks reflect the underlying structural connectivity architecture of the human brain. *Human Brain Mapping*, *30*(10), 3127–3141. http://doi.org/10.1002/hbm.20737

van den Heuvel, M., Mandl, R., Luigjes, J., & Hulshoff Pol, H. (2008). Microstructural Organization of the Cingulum Tract and the Level of Default Mode Functional Connectivity. *Journal of Neuroscience*, *28*(43), 10844–10851. http://doi.org/10.1523/JNEUROSCI.2964-08.2008

van der Eerden, A. W., Khalilzadeh, O., Perlbarg, V., Dinkel, J., Sanchez, P., Vos, P. E., … Puybasset, L. (2014). White matter changes in comatose survivors of anoxic ischemic encephalopathy and traumatic brain injury: comparative diffusion-tensor imaging study. *Radiology*, *270*(2), 506–16. http://doi.org/10.1148/radiol.13122720

Van Dijk, K. R. A., Hedden, T., Venkataraman, A., Evans, K. C., Lazar, S. W., & Buckner, R. L. (2010). Intrinsic Functional Connectivity As a Tool For Human Connectomics: Theory, Properties, and Optimization. *Journal of Neurophysiology*, *103*(1), 297–321. http://doi.org/10.1152/jn.00783.2009

van Erp, W. S., Lavrijsen, J. C. M., Vos, P. E., Bor, H., Laureys, S., & Koopmans, R. T. C. M. (2015). The vegetative state: Prevalence, misdiagnosis, and treatment limitations. *Journal of the American Medical Directors Association*, *16*(1), 85.e9-85.e14. http://doi.org/10.1016/j.jamda.2014.10.014

Van Oort, E. S. B., van Cappellen van Walsum, A. M., & Norris, D. G. (2014). An investigation into the functional and structural connectivity of the Default Mode Network. *NeuroImage*, *90*, 381–389. http://doi.org/10.1016/j.neuroimage.2013.12.051

van Wijk, B. C. M., Stam, C. J., & Daffertshofer, A. (2010). Comparing brain networks of different size and connectivity density using graph theory. *PLoS ONE*, *5*(10). http://doi.org/10.1371/journal.pone.0013701

Vanhaudenhuyse, A., Noirhomme, Q., Tshibanda, L. J. F., Bruno, M. A., Boveroux, P., Schnakers, C., … Boly, M. (2010). Default network connectivity reflects the level of consciousness in non-communicative brain-damaged patients. *Brain*, *133*(1), 161–171. http://doi.org/10.1093/brain/awp313

Varotto, G., Fazio, P., Rossi Sebastiano, D., Avanzini, G., Franceschetti, S., & Panzica, F. (2012). Music and emotion: An EEG connectivity study in patients with disorders of consciousness. *Proceedings of the Annual International Conference of the IEEE Engineering in Medicine and Biology Society, EMBS*, 5206–5209. http://doi.org/10.1109/EMBC.2012.6347167

Vidal-Piñeiro, D., Valls-Pedret, C., Fernández-Cabello, S., Arenaza-Urquijo, E. M., Sala-Llonch, R., Solana, E., … Bartrés-Faz, D. (2014). Decreased Default Mode Network connectivity correlates with age-associated structural and cognitive changes. *Frontiers in Aging Neuroscience*, *6*(September), 1–17. http://doi.org/10.3389/fnagi.2014.00256

Vogt, B. A., & Laureys, S. (2005). Posterior cingulate, precuneal and retrosplenial cortices: Cytology and components of the neural network correlates of consciousness. *Progress in Brain Research*, *150*, 205-217. http://doi.org/10.1016/S0079-6123(05)50015-3

Vogt, B. A., Vogt, L., & Laureys, S. (2006). Cytology and functionally correlated circuits of human posterior cingulate areas. *NeuroImage*, *29*(2), 452–466. http://doi.org/10.1016/j.neuroimage.2005.07.048

Voss, H. U., Ulu, A. M., Dyke, J. P., Watts, R., Kobylarz, E. J., Mccandliss, B. D., … Schiff, N. D. (2006). Possible axonal regrowth in late recovery from the minimally conscious state, *116*(7), 2005–2011. http://doi.org/10.1172/JCI27021.Related

Wang, F., Di, H., Hu, X., Jing, S., Thibaut, A., Di Perri, C., … Laureys, S. (2015). Cerebral response to subject's own name showed high prognostic value in traumatic vegetative state. *BMC Medicine*, *13*(1), 83. http://doi.org/10.1186/s12916-015-0330-7

Wang, J. (2010). Graph-based network analysis of resting-state functional MRI. *Frontiers in Systems Neuroscience*, *4*(June), 16. http://doi.org/10.3389/fnsys.2010.00016

Wang, Z., Dai, Z., Gong, G., Zhou, C., & He, Y. (2014). Understanding structural-functional relationships in the human brain: a large-scale network perspective. *Neuroscientist*, *21*(3), 290–305. http://doi.org/10.1177/1073858414537560

Wannez, S., Heine, L., Thonnard, M., Gosseries, O., & Laureys, S. (2017). The repetition of behavioral assessments in diagnosis of disorders of consciousness. *Annals of Neurology*, *81*(6), 883–889. http://doi.org/10.1002/ana.24962

Warner, M. A., Youn, T. S., Davis, T., Chandra, A., Marquez de la Plata, C., Moore, C., … Diaz-Arrastia, R. (2010). Regionally Selective Atrophy After Traumatic Axonal Injury. *Archives of Neurology, 67*(11). http://doi.org/10.1001/archneurol.2010.149

Watts, D., & Strogatz, S. (1998). Collective dynamics of "small-world" networks. *Nature*, *393*(6684), 440–442. http://doi.org/10.1038/30918

Weijer, C., Bruni, T., Gofton, T., Young, G. B., Norton, L., Peterson, A., & Owen, A. M. (2016). Ethical considerations in functional magnetic resonance imaging research in acutely comatose patients. *Brain*, *139*(1), 292–299. http://doi.org/10.1093/brain/awv272

Weiss, N., Galanaud, D., Carpentier, A., Naccache, L., & Puybasset, L. (2007). Clinical review : Prognostic value of magnetic resonance imaging in acute brain injury and coma, *Crit Care, 11(5): 230.* http://doi.org/10.1186/cc6107

Weissenbacher, A., Kasess, C., Gerstl, F., Lanzenberger, R., Moser, E., & Windischberger, C. (2009). Correlations and anticorrelations in resting-state functional connectivity MRI: A quantitative comparison of preprocessing strategies. *NeuroImage*, *47*(4), 1408–1416. http://doi.org/10.1016/j.neuroimage.2009.05.005

Weng, L., Xie, Q., Zhao, L., Zhang, R., Ma, Q., Wang, J., … Huang, R. (2017). Abnormal structural connectivity between the basal ganglia, thalamus, and frontal cortex in patients with disorders of consciousness. *Cortex*, *90*(March), 71–87. http://doi.org/10.1016/j.cortex.2017.02.011

Whitfield-Gabrieli, S., & Nieto-Castanon, A. (2012). Conn: A Functional Connectivity Toolbox for Correlated and Anticorrelated Brain Networks. *Brain Connectivity*, *2*(3), 125–141. http://doi.org/10.1089/brain.2012.0073

Wijdicks, E. F. M. (2001). The diagnosis of brain death. *New England Journal of Medicine*, *344*(16), 1215–1221. http://doi.org/10.1056/NEJM200104193441606

Wijdicks, E. F. M., Bamlet, W. R., Maramattom, B. V., Manno, E. M., & McClelland, R. L. (2005). Validation of a new coma scale: The FOUR score. *Annals of Neurology*, *58*(4), 585–593. http://doi.org/10.1002/ana.20611

Wu, K., Taki, Y., Sato, K., Sassa, Y., Inoue, K., Goto, R., … Fukuda, H. (2011). The overlapping community structure of structural brain network in young healthy individuals. *PLoS ONE*, *6*(5). http://doi.org/10.1371/journal.pone.0019608

Wu, X., Zou, Q., Hu, J., Tang, W., Mao, Y., Gao, L., … Yang, Y. (2015). Intrinsic Functional Connectivity Patterns Predict Consciousness Level and Recovery Outcome in Acquired Brain Injury. *The Journal of Neuroscience : The Official Journal of the Society for Neuroscience*, *35*(37), 12932–46. http://doi.org/10.1523/JNEUROSCI.0415-15.2015

Wu, X., Zhang, J., Cui, Z., Tang, W., Shao, C., Hu, J., …, & He, Y. (2016). White matter deficits underlie the loss of consciousness level and predict recovery outcome in disorders of consciousness. https://arxiv.org/abs/1611.08310

Xia, M., Wang, J., & He, Y. (2013). BrainNet Viewer: A Network Visualization Tool for Human Brain Connectomics. *PLoS ONE*, *8*(7). http://doi.org/10.1371/journal.pone.0068910

Yao, S., Song, J., Gao, L., Yan, Y., Huang, C., Ding, H., … Xu, G. (2015). Thalamocortical Sensorimotor Circuit Damage Associated with Disorders of Consciousness for Diffuse Axonal Injury Patients. *Journal of the Neurological Sciences*, *356*(1–2), 168–174. http://doi.org/10.1016/j.jns.2015.06.044

Yeo, S. S., Chang, P. H., & Jang, S. H. (2013). The Ascending Reticular Activating System from Pontine Reticular Formation to the Thalamus in the Human Brain. *Frontiers in Human Neuroscience*, *7*. http://doi.org/10.3389/fnhum.2013.00416

Youn, C. S., Park, K. N., Kim, J. Y., Callaway, C. W., Choi, S. P., Rittenberger, J. C., … Kim, Y. M. (2015). Repeated diffusion weighted imaging in comatose cardiac arrest patients with therapeutic hypothermia. *Resuscitation*, *96*, 1–8. http://doi.org/10.1016/j.resuscitation.2015.06.029

Yu, C., Zhou, Y., Liu, Y., Jiang, T., Dong, H., Zhang, Y., & Walter, M. (2011). Functional segregation of the human cingulate cortex is confirmed by functional connectivity based neuroanatomical parcellation. *NeuroImage*, *54*(4), 2571–2581. http://doi.org/10.1016/j.neuroimage.2010.11.018

Zalesky, A., Fornito, A., Harding, I. H., Cocchi, L., Yücel, M., Pantelis, C., & Bullmore, E. T. (2010). Whole-brain anatomical networks: Does the choice of nodes matter? *NeuroImage*, *50*(3), 970–983. http://doi.org/10.1016/j.neuroimage.2009.12.027

Zhang, H., Dai, R., Qin, P., Tang, W., Hu, J., Weng, X., … Northoff, G. (2017). Posterior cingulate cross- hemispheric functional connectivity predicts the level of consciousness in traumatic brain injury. *Scientific Reports*, (February), 1–9. http://doi.org/10.1038/s41598-017-00392-5

Zhang, S., & Li, C.S. (2012). Functional connectivity mapping of the human precuneus by resting state fMRI. *NeuroImage*, *59*(4), 3548–3562. http://doi.org/10.1016/j.neuroimage.2011.11.023.Functional

Zhang, S., Ide, J. S., & Li, C. S. R. (2012). Resting-state functional connectivity of the medial superior frontal cortex. *Cerebral Cortex*, *22*(1), 99–111. http://doi.org/10.1093/cercor/bhr088

Zhang, Y., Fan, L., Zhang, Y., Wang, J., Zhu, M., Zhang, Y., … Jiang, T. (2014). Connectivity-based parcellation of the human posteromedial cortex. *Cerebral Cortex*, *24*(3), 719–727. http://doi.org/10.1093/cercor/bhs353

Zheng, Z. S., Reggente, N., Lutkenhoff, E., Owen, A. M., & Monti, M. M. (2017). Disentangling disorders of consciousness: Insights from diffusion tensor imaging and machine learning. *Human Brain Mapping*, *38*(1), 431–443. http://doi.org/10.1002/hbm.23370